Forschungszentrum Karlsruhe

in der Helmholtz-Gemeinschaft

Wissenschaftliche Berichte

FZKA 7466

EURATOM
EC 7th Framework Program

Collaborative Project "Redox Phenomena Controlling Systems"

1st Annual Workshop Proceedings

Gunnar Buckau (KIT-INE)
Bernhard Kienzler (KIT-INE)
Lara Duro (Amphos 21)
Mireia Grivé (Amphos 21)
Vanessa Montoya (Amphos 21)

Forschungszentrum Karlsruhe GmbH, Karlsruhe

2009

FOREWORD

The present document is the proceedings of the 1st Annual Workshop of the Euratom FP7 Collaborative Project RECOSY (Redox Phenomena Controlling System). The Workshop was hosted by AMPHOS (Amphos 21), and held in Barcelona 10th – 12th February 2009. The project started April 2008 and has four years duration. It has 32 Contractors and presently 4 Associated Groups. Annual workshops bring together, Contractors, Associated Groups and external interested groups. The present proceedings will be followed by three additional proceedings corresponding to the forthcoming annual workshops to be held in 2010, 2011 and 2012, respectively. The 2nd Annual Workshop will be held in Larnaca 16th – 19th March 2010, hosted by University Cyprus.

The proceedings serve several purposes. The key purpose is to document and make available to a broad scientific community the outcome of the RECOSY project. For this purpose, a considerable part of the project activity reporting is done through the proceedings, together with the outcome of topical sessions, a large number of scientific-technical contributions and two additional contributions on a specific area of project activities. Additional purposes are to ensure ongoing documentation of the outcome of the project, promote systematic scientific-technical development throughout the project, and to allow thorough review of the progress of the project.

The proceedings give only very brief information about the project structure and the different activities around the project, such training measures and dissemination of knowledge. Such exhaustive information about the project can be found under www.recosy.eu

TABLE OF CONTENTS

THE PROJECT

The EURATOM 7th EC Framework Program Collaborative Project REdox phenomena Controlling SYstems (RECOSY) started in April 2008 and extends over 4 years. Main objectives of RECOSY are the sound understanding of redox phenomena controlling the long-term release/retention of radionuclides in nuclear waste disposal and providing tools to apply the result to Performance Assessment/Safety Case, training of next generation, and documentation and communication of the results. To this aim, the project set up a consortium of 32 Contractors and presently 4 Associated Groups. The consortium includes key European Research Institutes, Universities, National Waste Management Agencies and SMEs from 13 EURATOM signatory states, Russia, Korea and one European Joint Research Centre. The ReCosy concept is innovative in the scientific approach to the redox phenomena. It includes i) advanced analytical tools, ii) investigations of processes responsible for redox control (thermodynamically and kinetically controlled processes, surface reactions and microbial processes, ..), iii) provision of required data on redox controlling processes, and iv) response to disturbances in disposal systems. The work program is structured along six RTD workpackages (WP1-6). They cover near-field and far field aspects as well as all relevant host-rocks considered in Europe. In WP1, the scientific state-of-the-art and its application to Performance Assessment/Safety Case is documented and regularly up-dated. WP2 focused on development of redox determination methods. WP3 focuses on redox response of defined and near-natural systems. WP4 studied the redox reactions of radionuclides. WP5 focuses on Redox processes in radionuclide transport and WP6 are dealing with the redox reactions affecting the spent fuel source-term. Specific workpackages on knowledge management, education and training (WP7) and administrative management issues (WP8) are also included in the project

The present proceedings document the outcome of the 1st Annual Project Workshop and give an overview of the outcome of the 1st project year.

THE FIRST ANNUAL WORKSHOP

The 1st Annual Project Workshop was held in Barcelona 10th – 12th February 2009. The Workshop was hosted by AMPHOS. There were 72 attendees at the workshop, representing Contractors, Associated Groups, the European Commission, the End-User Consultancy Group, and project external organizations. The workshop was organized in three days of oral presentations around the project, a poster session, a topical session and additional talks.

Objectives

The Workshop combines different activities and meetings with the following objectives:

- Informing about the scientific progress
- Informing about the administrative status
- Informing/agreeing upon forthcoming reporting
- Discussing various topics of interest
- Informing about and discuss training
- Agreeing upon the forthcoming work program

Emphasis was on scientific-technical topics with administrative issues kept to the minimum necessary.

RTD sessions

Individual RTD workpackages meetings were held in parallel during the annual workshop. The respective workpackage leaders presented a summary of the work conducted so far within their respective RTDC's. Next to an overview of the achievements within the respective WP, scientific highlights were presented. The following presentations were given within the project

WP2 session:

- J. Cortot, E. Lambert, A. Cheikh Ibrahim, M. Etienne, M. Perdicakis Investigations with a view to developing an amperometric device for the determination of the redox potential
- C. Tournassat, J-M. Greneche, E. Gaucher, L. Charlet, and I. Ignatiadis. Probing the highly redox reactive mineral reservoirs in a clayey formation.
- M. Altmaier, V. Neck, J. Runke, D. Fellhauer, Th. Fanghänel. Quantification of the redox potential for the reduction of Np(V) to colloidal Np(IV) in aqueous solution (pH 5 - 10)
- B. Grambow, C. Bailly, C. Landesman, S. Ribet. Redox state determination in hyperalkaline solutions by speciation of selenium
- E. Marosits, B. Kuczewski. Influence of iodine species on electrochemical redox potential measurements in aqueous samples and on the determination of total iodine content by ICP-OES and ICP-MS

- B. P. Bischofer, S. Hagemann, C. Hühne, D. Schönwiese, T. Scharge. Influence of Chloride Concentrations on the Signal of Redox Electrode and on UV/VIS-Spectroscopic Determination of Fe Species

- D. Steinbrück. Development of multiparametric optical sensing for environmental applications.

- E. Krawczyk-Bärsch. Studies on oxygen concentrations in uranium contaminated biofilms: Comparing electrochemical and fiber-optic sensors-collaboration with UPPC

WP3 session:

The workpackage leader (Laurent Charlet) presented a summary of the Deliverable 3.1: Synthesis and characterization of Solids

- D. Arcos, J. Salas, L. Duro, I. Rojo, J. de Pablo. Incorporation of ReDucing Capacity concept (RDC) in reactive transport models.

- K. Pedersen, J. Arlinger, L. Rabe, S. Eriksson, L. Hallbeck. The effect from microorganismson the redox state of laboratory and natural systems

- M. J. Gimeno, L. F. Auqué, P. Acero, J. B. Gómez. General characterisation of the redox systems in the Swedish candidate sites for deep disposal of Nuclear Waste Disposal.

- L. Charlet. Incorporation of Se and Fe into calcite and reactivity of Fe(II)-rich calcite

WP4 session

- J. Tits, X. Gaona, E. Wieland. Influence of the oxidation state on the neptunium uptake by calcium silicate hydrates and cement.

- N. Evans, R. Hallam, S. Aldridge, P. Warwick and N. Bryan. Effect of Anthropogenic Organics on the Fate of Technetium in a UK Intermediate-Level Nuclear Waste Repository.

- N. Bryan. Contribution of The University of Manchester

- E. Krawczyk-Bärsch. First reporting of the scientific-technical outcome of WP 4.2: Effects of microorganisms on redox behavior of radionuclides

WP5 session

- K. Lázár, Z. Máthé, M. Földvári. Tracing Fe^{2+} / Fe^{3+} redox transition in clay minerals of Boda Siltstone by means of Mössbauer spectroscopy

- S. Antoniou, F. Papanicolaou, I. Pashalidis. Redox Processes Controlling the Fate of Sulfate and Uranium in a Phosphogypsum Stack

- S. Salminen, J. Suksi. University of Helsinki Activities

- S. Kalmykov, O. Batuk. Lomonosov Moscow State University activities

WP6 session

- D.H. Wegen, Corrosion of spent fuel in presence of corroding iron.

- D.H. Wegen, A. Seibert, S. Stumpf, T. Gouder, D. Bosbach, J. Römer, E. Soballa, Fuel corrosion studies on thin film model systems.

- P. Carbol, P. Fors, High burn-up UO_2 fuel corrosion under reducing conditions.

- M. Trummer, O. Roth, A. Puranen, S. Nilsson, M. Jonsson. Combined effect of metallic and rare earth doping on the oxidative dissolution of UO_2

- B. Kienzler, A. Loida. Reductive Trapping of Actinides in Container Corrosion Products during Spent Fuel Corrosion

- D. Cui, V. Rondinella, C. Kuetahyali, M. Amme, T. Wiss, D. Grolimund, E. Wieland C. Borca and K. Spahiu. The reductive immobilization of 237Np and 239Pu on iron canister under repository conditions.

- D. Dobrev, P. Brůha, A. Vokál, The effect of Iron corrosion on conditions inside waste packages,

Poster presentations

The following posters were presented during the 1st annual Workshop

- S. Antonious, F. Papanicolaou, I. Pashalidis. Redox Processes Controlling the Fate of Sulfate and Uranium in a Phosphogypsum Stack

- P. Ivanov, L. Abrahamsen, A. Pitois, N. Bryan, G. Bozhikov, O.Maslov, S. Dmitriev , Nick Evans, P. Warwick. Actinide Behaviour In Humic Acid Bentonite Ternary Systems At Trace Concentrations

- Rojo, F. Clarens, J. de Pablo, M. Grivé, L. Duro, D. Arcos. Redox buffer capacity of pyrrhotite.

- M. Grivé, L. Duro, O. Riba, V. Montoya. Redox Uranium behaviour under hyperalkaline conditions

- X. Gaona, J. Tits, E. Wieland. Interaction of Np(IV/V) with cement phases under controlled redox conditions: setting-up of the system and preliminary results

- N. Evans, R. Hallam, S. Aldridge, P. Warwick and N. Bryan, Complexation of Tc(IV) with Gluconate at High pH

- M. Trummer, O. Roth, A. Puranen, S. Nilsson, M. Jonsson. Effects of solid state alterations on the redox reactivity of UO_2

- P. Coombs, K. Bateman, J.M West, D. Wagner, G. Turner, A.E. Milodowski. A Lacinsca, H. Harrison, D.J. Noy. Influence of biofilms on transport of fluids in subsurface granitic environments – Some mineralogical and petrographical observations of materials from column experiments

Topical session

The Topical Sessions aim at covering the key areas of redox determination methods along with the project. The Topical Session focuses on the scientific state-of-the-art and the present status of Electrochemical techniques for Redox state determination. It also provides a brief overview of optical methods.

Presentations within this topic were:

- Marcus Altmaier. Critical evaluation of the Questionnaire on Redox measurement techniques

- Michael Kumke. Presentation on optical methods

- Igniatadis. Redox measurements in clay

- M. J.Gimeno. Redox measurements in crystalline rocks

- M. Caceci. Electrochemical sensors: a critical look at hardware and physics

Additional presentations

Additional presentations were given on topics of general interest, especially the context of the present project within the Euratom FP7 program on geologic disposal. The additional presentations serve different purposes: i) they give opportunity to incorporate issues of interest for the project but not directly dealt with within the project, ii) the invited lecturers provide complementary views to the project, iii) they are useful ways of identifying opportunities of collaboration with other groups and iv) they give opportunity to other running initiatives to interact with the project in a more pro-active manner.

The additional presentations given during the 1st Annual Workshop were:

- Scott Altmann. B-2 Cell concept
- Gaetano di Bartolo. Euratom FP7/DG Research act. in Fission: Latest developments

Structure of the proceedings

The proceedings are divided into the following sections:

- WP activity overviews, with summaries of the Research, Technology and Development Components
- Individual Scientific and Technical Contributions, containing reviewed scientific and technical manuscripts

Scientific-technical contributions submitted by Contractors were reviewed by the EUCG members (End-User Consultancy Group).

SUMMARY OF WP ACTIVITIES

WORKPACKAGE 2: DEVELOPMENT OF REDOX DETERMINATION METHODS

D. Steinbrück[1], M.U. Kumke[1], M. Altmaier[2], V. Neck[2], D. Fellhauer[2], J. Runke[2], Bernd Grambow[3], Catherine Landesman[3], Solange Ribet[3], Evelyn Krawczyk-Bärsch[4], Michel Perdicakis[5], BRGM[6], GRS[7], TUG[8]

[1]Institute of Chemistry, University of Potsdam, Karl-Liebknechtstr. 24-25, 14476 Potsdam, Germany

[2] Institut für Nukleare Entsorgung, KIT, Campus Nord, Herrmann-von-Helmholtz-Platz 1, 76344 Eggenstein-Leopoldshafen, Germany

[3] SUBATECH (Ecole des Mines, University of Nantes, IN2P3/CNRS (FRANCE)

[4]Forschungszentrum Dresden-Rossendorf, Germany

[5]Laboratoire de Chimie Physique et Microbiologie pour l'Environnement

Nancy-Université, CNRS -54600 VILLERS-LES-NANCY France

[6]Environnement Industriel et Procédés Innovants, BRGM, 3 avenue Claude Guillemin, 6009, 45 060, Orléans Cedex 2, France

[7]Gesellschaft für Anlagen und Reaktorsicherheit (GRS) mbH, (GER)

[8]Graz University of Technology, Technikerstrasse 4, 8010 Graz, Austria

Introduction

The objective of WP2 is the development and testing of redox determination methods using different type of electrodes as well as optodes (optical sensors) in order to provide a broad and solid scientific-technical basis for the application of such. In combination with chemical analysis and associated thermodynamic modeling the redox state of systems (relevant for nuclear waste repositories) is assessed. The overall goals are (i) redox determination methods specifically designed for environmental applications, and (ii) a broader information base for interpretation of system conditions.

The first point reflects the limitations of existing determination methods and models (and new developments) due to poisoning of electrode material, diffusion potentials in electrode bridges, drift through catalytic reactions on electrode material, drift through changes in electrolytes via diffusion, analytical difficulties in determining concentrations of redox sensitive system components or state of involved solids/minerals, and insufficient/inadequate thermodynamic data for calculation of the redox state.

Work performed by partners

Within ReCosy **KIT-INE** will establish the thermodynamic basis for the determination of system redox states based on the distribution of actinide and technetium species. In the experimental and modeling approach the formation of colloids will be included as well. In order to have a broader basis of thermodynamic data, the system redox state is varied by aeration and addition of hydroquinone. Moreover, in the investigations high salinity conditions (brines) are included.

In the first year KIT-INE focused on the quantification of the redox potential for the reduction of Np(V) in non-complexing aqueous solutions at pH 5 – 10.

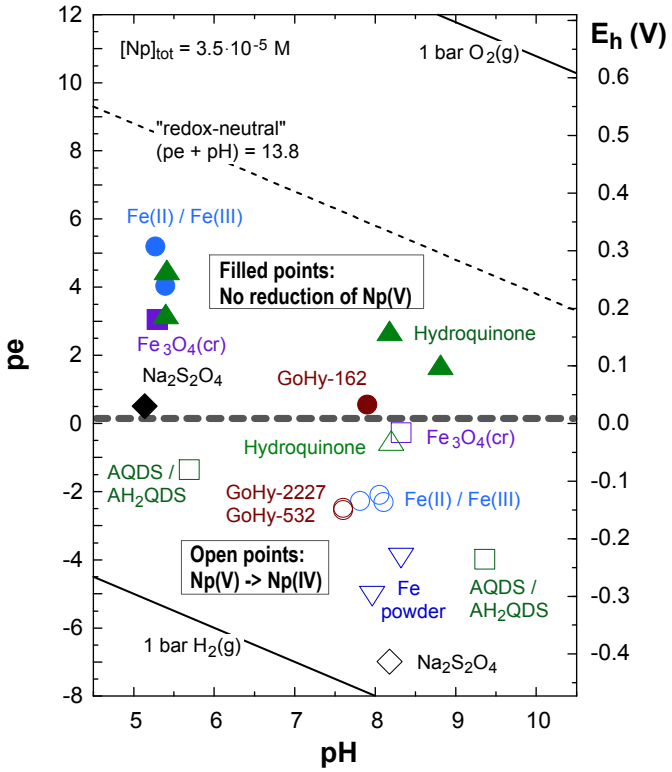

***Figure 1**: Experimental studies on the reduction of Np(V) in 0.1 M NaCl and in dilute Gorleben groundwaters (GoHy). In the systems shown as open symbols Np(V) is reduced to colloidal Np(IV), in the systems shown as filled symbols Np(V) is not reduced within the time of investigation (≥ 100 days).*

The reduction of $3.5 \cdot 10^{-5}$ M Np(V) solutions is studied in the pH range 5 - 10 in non-complexing 0.1 M NaCl solutions under Ar atmosphere. To cover a wide range of chemically different reducing systems, the redox behaviour of Np(V) was studied in numerous homogeneous solutions and heterogeneous suspensions containing 1 - 2 mM additions of $Na_2S_2O_4$, Fe(II)/Fe(III) buffers (10:1), metallic iron powder, magnetite Fe_3O_4(cr), hydroquinone and sodium anthraquinone / anthrahydroquinone disulfonate (AQDS/AH_2QDS) redox buffers. The reduction process was monitored as a function of time (up to 100 - 300 days) by the decrease of the aqueous Np(V) concentration determined after removal of colloidal Np(IV) particles by 10 kD ultrafiltration. The experimental results indicate that the redox potential of $E_h = 0.01 \pm 0.02$ V (pe = 0.15 ±

0.35) is a general border for the reduction of NpO_2^+(aq). Regardless of the reducing agent and whether the system is homogeneous or heterogeneous, Np(V) is found to be stable at $E_h \geq 0.03$ V (pe ≥ 0.5) and reduced to Np(IV) at $E_h \leq - 0.01$ V (pe ≤ - 0.2). The more negative the redox potential the faster is the reduction.

The focus of work of **ARMINES** conducted in the ReCosy framework is the development of a methodology for redox determination in hyperalkaline systems based on Se speciation. Induced redox state perturbation is achieved by aeration, addition of nitrate or of hydroquinone. In the first year, the thermodynamic calculations and preparatory work has been done in preparation for detailed measurements in the forthcoming project years.

Selenium is a redox sensitive element existing in aqueous solutions in the redox states –II (organic and inorganic forms), IV and VI and in the solid state as well as Se(0). Laboratory experiments show that even at high Se concentrations over a wide range of pH the Pt electrode is completely insensitive to the relative abundance of dissolved Se(VI) and Se(IV) (Liu, 2007, Runnells and Lindberg, 1990). Hence, Se speciation cannot be deduced directly form Eh measurements with Pt electrodes and geochemical equilibrium calculations. This indicates that under certain conditions the Pt electrode measured Eh does not correspond to a "master variable" of the redox system. This clearly points to the need of direct measurement of solution speciation to assess the redox state relevant for Se speciation. For this purpose, advanced analytical techniques for Se speciation are indispensable.

A full review of the chemical thermodynamics of selenium in aqueous/solid systems has recently been presented by the NEA-TDB project (Olin et al., 2005). However, no thermodynamic data were proposed for ion pairs of the form $CaSeO_3$(aq). Using literature data on $CaSeO_3$(aq) large variability of stability constants is invoked which has been studied in the present project by a sensitivity study. This study shows that the stability fields of SeO_3^{-2} and $CaSeO_3$(aq) are about overlapping for the selected conditions and depending on the stability constant the stability field of Se(IV) could be enlarged relative to the situation of not considering $CaSeO_3$(aq). Considering that the stability constant for the ion pair is rather uncertain, it is important to assess, to which degree these uncertainties affect the ability to use solution speciation methods to deduce the redox state of the solution. Figure 3 shows the effect of varying the formation constant for $CaSeO_3$ on the calculated stability field boundary between Se(0) and Se(IV). In the range studied the uncertainty in log K values amount to an uncertainty of 30 mV in the stability field boundary.

Solution speciation in hyperalkaline solution will further be complicated by the formation of polyselenide species such as Se_2^{-2} Se_3^{-2}, Se_4^{-2} with stability fields These ions have formal oxidation states between 0 and –II. Obviously, polymer formation depends on total Se concentration in solution, hence experiments of redox state determination needs to be done as a function of total Se concentration to assess the influence of these species.

Also polymer species play a large role under alkaline conditions and the presence of polymer species will strongly reduce the stability field for Se(0, triclinic). First calculations indicate that, in the interesting hyperalkaline pH range between pH 11 and 13, no Se(0, triclinic) will be formed. Even further reduced is the probability to

form monoclinic Se(0). Nevertheless, considering all uncertainties, Se(0) analyses by stolid state techniques is still necessary.

Solution species for Se(IV) and Se(VI) can easily be distinguished simultaneously using ion chromatography. Quantifications limits in our laboratory were lower than 10^{-6} M, and about 20 times lower detection limits can be achieved by coupling ion chromatography with ICP-MS. in hyperalkaline solutions. In contrast, Se(-II) can best be analysed using polarographic techniques, using a hanging mercury drop electrode. The detection limit is 10^{-7} M. Methods for analysing polyselenides in solution have not yet been developed in our laboratory. This will be done in the next year. The idea is to use in a first step UV identification at large total Se concentrations (about 10^{-4}M) concentration, calibrate in a second step the ion chromatography with this identified species and couple finally ion chromatography with a fraction collector and analyse of collected fractions by collision cell ICP/MS. This should allow detection limits as low as $5 \cdot 10^{-8}$ M. Upper limits of total Se concentrations in hyperalkaline solutions are in the range of 10^{-3} M governed by the potential formation of $CaSeO_3$(s). In this concentration range Se(0) is present under certain redox conditions and Se(0)/Se(-II) or Se(0)/Se(IV) might be encountered as redox couple indicating the solution redox state.

Se(0) cannot be detected in solution but requires redox sensitive solid state analytical techniques such as XPS. This technique works in presence of solid phases (cement phases) but it might as well work, if Se(0) is present in colloidal form. In the latter case, colloids must be separated by ultrafiltration and the Se-redox state on the filter residues shall be analysed. Ultrafiltration will be done in the inert gas box and transfer of the sample from the inert gas box to the XPS will be done in specially designed transfer-equipment, allowing no access of air to the samples. Some further uncertainties in the determined redox potential arise from the contribution of surface energy as a function of particle size to the Gibbs free energy of formation of Se(0). In the literature, various stability constants for solid Se(0) are given. Se(0) exists in trigonal ($\Delta°G_f$=0) or monoclinic form ($\Delta°G_f$=1.281±0.184 kJ/mol, thermodynamic data from Olin et al. 2005). These uncertainties results in uncertainties for the Se(0)/Se(-II) of only 6 mV on the expected equilibrium potential.

At **BRGM** Pt, Au and glassy carbon microelectrodes for E_h determination are tested on different laboratory systems (Callovo-Oxfordian clay stone and/or clay paste, different redox relevant minerals found in natural clay). The investigations include induced perturbations by aeration, variation of H_2 partial pressure, nitrate plume and addition of redox sensitive radio nuclides. The reliability, time-response behavior and lifetime of electrodes will be investigated, including electrode interface characterization by MET, SEM, FTIR and XPS.

The redox transformations of COX claystone samples under oxidizing perturbation were investigated, e.g., using Mössbauer spectrometry. The investigated samples had different oxidation histories ranging from no oxidation (transport from field to laboratory under liquid N_2, experiments carried out in a glove box) to massive air oxidation. Pyrite and Fe(II) carbonates are found to oxidise very slowly or not at all when the samples are brought into contact with the atmosphere. In contrast, iron associated with clay minerals exhibits very fast oxidation kinetics, which is in full agreement with the high redox reactivity of Fe(II) adsorbed on smectite. An important consequence of the present results concerns sorption and diffusion experiments

involving redox-sensitive species. Given the reactivity of part of the Fe(II) associated with clay minerals, special care must be taken during the transport and preparation of COX samples to ensure that the full redox reactivity of the formation is taken into account during subsequent experiments.

On the other hand, particular equipment has been set up and a methodology has been developed and/or adapted for the investigation, including the design of various specific electrodes and the use of diverse electrochemical techniques, in order to explore the electrochemical kinetics of the COX system in contact with different plausible redox perturbations (e.g. redox sensitive radio nuclides, nitrate plume, contact with atmosphere before the closure of the system, H_2 perturbation). Material under investigation included massive and/or paste claystone rock samples (COX) as well as individual mineral contributors to the redox reactivity already identified in the media, provided we could met the necessary conductivity limits (e.g. pyrite, clay paste, Fe(II) clays included chlorite, sorbed Fe(II) on various surfaces, sphalerite,..).

The future work will consist in relating the observations of the changes in certain key electrochemical parameters of the working electrodes (part of the conventional triplet of the electrochemical cell) to the presence of: i) finely ground COX materials, ii) ions (H^+, Cl^-, SO_4^{2-}, Fe^{2+} and Fe^{3+}, I^-, Se(VI), Se(IV)…) and iii) gases (O_2, CO_2, H_2, H_2S), in different situations, both natural and induced. The continuous electrochemical measurements (e.g., open circuit potential, cyclic voltammetry, electrochemical impedance spectroscopy) will serve to identify, monitor and compare the electrochemical reactions and kinetics occurring during immersion, both in solution and on the surface of all these specific electrodes. The electrochemical behaviour of these electrodes will be compared to those of known inert and unattackable electrodes (Pt, Au, glassy carbon) positioned in the same operating conditions. Consequently, the evolution of the redox conditions in the host rock of the deep repository will be predicted.

CNRS/LCPME evaluates an amperometric method for the in-situ determination of the redox potential by the quantitative determination of the components of a redox couple using ultramicroelectrodes.

During the first year of the project, the CNRS/LCPME activities consisted in: i) the voltammetric characterization of compounds that will be used in WP3 and WP4 to provoke redox disturbances (i.e. soluble species of selenium and iodide as well as oxygen/oxygen peroxide mixtures) as well as of minor electroactive constituents of Callovo-Oxfordian argillite porewater (Fe) or NaCl brines (I, Fe) that are potential internals indicators of the redox state, ii) investigations in order to perform redox potential determinations in saturated NaCl brines and Bure Callovo-Oxfordian argillite porewater, iii) an extensive bibliographic research on redox couples that could be used as potentiometric indicators.

For the moment, our investigations have been limited to the I_2/I^- and Fe(III)/Fe(II) couples in chloride media and to the oxygen/oxygen peroxide mixtures in various conditions. The experiments have been performed using classic platinum rotating disc electrodes (Pt RDEs) in diluted solutions in order to evaluate the detection limits of these species by traditional means.

The voltammetric oxidation of iodide in chloride media shows two successive waves because of the oxidation of I_2 formed at the electrode surface into ICl or ICl_2^-.

This fact could be a mean for the identification of I^- in a complex medium. In neutral as well as in acidic 1 M KCl media iodide can be easily detected at 2 10^{-6} M. Concerning the Fe^{2+} oxidation, if high scan rates are not used its detection is not easy, even at pH 3, because of the formation of insoluble Fe(III) species that passivate the electrodes surface. If rapid electrochemistry is performed the voltammogram shape is not favourable for quantitative determinations. The use of ultramicroelectrodes (UMEs) should significantly improve these results. On the one hand, the detection limit of iodide could be improved and, on the other hand, UMEs are well appropriate for rapid scans or pulsed methods and the voltammograms shape remains sigmoidal for a wide range of scan rates (the smaller the electrode the wider the range).

Hydrogen peroxide is an interesting oxidizing agent because the oxidation of a species by H_2O_2 or oxygen involves exactly the same electrons/protons ratio, however, only the addition of H_2O_2 can be easily controlled. Moreover, the reduction product of H_2O_2 is water that neither pollutes the reaction medium nor modifies its ionic strength. We attempted to detect H_2O_2 at low concentration in the presence of oxygen and in deaerated solutions, in various media (pure deionised water, chloride and sulphate media) using Pt UMEs as well as Pt and Au classic RDEs. Hydrogen peroxide is a compound that is just as well oxidizable as reducible. Therefore, its voltammetric curves exhibit an anodic and a cathodic wave that are separated by variable potential differences that depend on the medium. The cathodic wave of H_2O_2 is very close to that of dissolved oxygen and the two signals cannot be distinguished from each other. In any case, as the electrochemical kinetics is slow, potentials are without thermodynamic meaning. (i) In pure water (Pt UME) the anodic and the cathodic wave are separated by about 300 mV. The voltammetric curves are well defined until concentrations as low as 5 10^{-5} M. For lower concentrations the signal becomes peakshape but H_2O_2 remains detectable until 10^{-5} M. The addition in the solution of HCO_3^- or $H_2PO_4^-$ shifts progressively the H_2O_2 oxidation to more negative potentials. In the presence of 0.3 M HCO_3^- the voltammograms show the existence of a strong exchange current between the oxidation and the reduction waves of H_2O_2. (ii) In sulphate medium (Pt classic RDE) the voltammetric curves are very similar to those in pure water. The detection limit is about 10^{-4} M. (iii) In chloride medium (Pt classic RDE) the separation between the anodic and the cathodic wave is wider (about 400 mV); the detection limit is the same (10^{-4} M) but the voltammetric curves are strongly distorted. (iv) The voltammograms plotted using the Au classic RDE are complex because of the formation of electroactive gold oxides. In any case, if small quantities of hydrogen peroxide remain in the solution after a redox disturbance, it will be detected easily by its anodic wave instead of the anodic one. The determination of the detection limits in sulphate and chloride medium using UMEs remains to be done

In case of NaCl brines exceeding care must be taken to ensure that all the glassware and the electrodes are extremely clean otherwise electroactive species that were strongly sorbed on surfaces, perhaps for several years in the contact with the brine, gradually pass into solution and give voltammetric signals. (i) Preliminary experiments have been performed with a classic platinum RDE (2 mm diameter permanently sealed in Teflon) in three concentrated NaCl, 1 M, 4.27 M and saturated (~ 4.43 M), using ferrocene dimethanol, dissolved oxygen and iron(III) as the electroactive species. The limiting current for ferrocene dimethanol diminishes by a factor of about 1.5 when passing from 1 M NaCl to the saturated NaCl medium. Therefore, CNRS/LCPME does not expect strong changes in the detection limits. On the other hand, the voltammetric signal for dissolved oxygen is reduced by a factor of about 5.5. This fact is due to the

diminishing of the oxygen solubility. (ii) In unbuffered NaCl saturated solutions and without pH control, iron(III) can be easily detected until its concentration is reduced down to 10^{-5} M. Therefore, its detection limit could be improved significantly by optimization and the use of UMEs. (iii) UMEs are usually fabricated by sealing platinum microwires into glass capillaries. The capillaries serve as the insulator and the body of the electrodes. Surprisingly, CNRS/LCPME finds that UMEs, which perfectly work in low concentrated solutions, once immersed in the saturated NaCl brine (without the addition of any electroactive species), provide voltammograms that exhibit intense signals that completely hinder any measurement. Moreover, CNRS/LCPME noticed that these signals varied with the nature of the glass capillaries. Therefore, CNRS/LCPME tested commercial UMEs and home made ones made of Pyrex glass and two soft glasses from different origins; the results are quite different: virtually each electrode has its own voltammogram.

In the literature concerning voltammetry in brines such a phenomenon is not reported yet, but it is well known that glasses are corroded in concentrated saline solutions and within an ion exchange process some of the constituents of the glass are concentrated on its surface. If these constituents are electroactive (i.e. iron oxides) one can easily understand the signals provided by the voltammograms in NaCl brines without the addition of electroactive species. In view of these results, the meaning of potentiometric measurements performed in brines with platinum electrodes sealed in glass needed to be re-evaluated.

CNRS/LCPME prepared UMEs by sealing platinum microwires into quartz capillaries under a laser beam. With this tool ferrocene dimethanol has been easily detected at concentrations in the 10^{-5} M range in the saturated brine. Nevertheless, after a 12 hours immersion of the UME in the brine, its electrochemical behaviour became very similar to that exhibited by specimens prepared in glass. UMEs prepared by moulding a platinum microwire in an epoxy resin work very well is diluted solutions but not in concentrated brines. There are several other possibilities for preparing satisfactory UMEs that are listed by the ease with which they can be implemented and used: i) by moulding a platinum microwire in a polyester resin (brines are stored in tanks made of polyester resin), ii) by sealing platinum microwires into quartz suprasil capillaries (purity of 99.99999 % can be achieved), iii) construction of a wall-jet ultramicroelectrochemical cell.

Synthetic COx porewater has been prepared according to the recipe provided by BRGM. Both classic platinum RDE and platinum UMEs seems to work quite satisfactory in the non-deaerated porewater. A device for allowing the deaeration of the medium without entraining the dissolved carbonates is under construction.

As a security measure, if the direct potential determination failed, a long list of redox couples, which are susceptible to be added in the system as redox indicators, has been established. This list covers a wide range of potential. Most of the selected redox couples are proposed in the literature as mediators for experiments of scanning electrochemical microscopy; therefore, in principle, their electrochemical kinetics is rapid. The next step is to examine if there are no chemical reactions (other than redox ones) between the redox indicators the constituents of the media that will be checked.

Since measurement of E_h with normal platinum electrodes is difficult in saline environments because the half cell potentials of the reference electrodes are altered by

variable liquid junction potentials, **GRS** develops a fiber-optics based determination method of the Fe(II)/Fe(III) redox couple. The Fe(II)/Fe(III) system is believed to be a very important redox couple in aqueous solutions. In the experiments the salinity is varied up to saturated brines and the influence of temperature is determined for 25°C < T < 60°C. Moreover, the thermodynamic basis for interpretation of the system redox state based on the concentrations/activities of different iron species will be developed (including aqueous Fe(III) chloro, hydroxo and mixed chlorohydroxo complexes in saline solutions). In addition, the correlation between redox electrode signal, Fe(II)/Fe(III) ratio and background salt concentrations will be investigated by systematic variation of the specified variables.

For the speciation of iron by UV/VIS spectroscopy insufficient data in saline solutions are available. Consequently, first the influence of saline solutions on the UV/VIS detection of Fe(II) and Fe(III) has to be characterized. For the quantitative detection of Fe(II) by UV/VIS spectroscopy the German DIN-method (DIN 38406 Part 1, 1983) using phenanthroline was selected. The advantages of this method are its fast sample preparation and the high stability of the Fe(II)-phenanthroline complex. A complex of phenanthroline formed with Fe(III) in Fe(II)/Fe(III) mixed solutions does not disturb the Fe(II) determination as long as the ratio Fe(II)/Fe(III) is greater than 0.1. In this case a masking with fluoride is necessary. For the quantitative determination of Fe(III) the complexation with potassium thiocyanate (KSCN) was chosen. The advantages of this method are again the fast sample preparation and the lack of disturbance due to the presence of Fe(II). However, disadvantages of the thiocyanate method are i) the quick decomposition of the complex, so that the samples have to be prepared directly before the measurement and ii) the relatively low sensitivity in the detection of the thiocyanate complex. Since for the detection of the Fe(II) and Fe(III) concentrations in natural systems a spectrometer equipped with a 5 m long flow cell (which should result in a 5000 fold increase of absorption) those difficulties can be circumvented. However, the absorption band of the Fe(III)-thiocyanate complex is completely superimposed by the absorption band of the Fe(II)-phenanthroline complex. Therefore, simultaneous analysis of Fe(III)/Fe(II) is not possible using phenanthroline as indicator for Fe(II).

Several series of experiments have been conducted in order to assess the performance of the platinum redox electrode in saline solutions. The measurements of the redox potential in concentrated chloride solutions show a salinity effect of 30 mV to 43 mV deviation near saturation. Depending on the regarded system or if the equilibrium of the regarded system is located near a boundary of an important stability field, this small deviation can be very significant. Responsible for this salinity effect are probably both, the reference electrode and a change in speciation. For a detailed explanation of the observed effects and for the calculation of the Fe^{2+}/Fe^{3+} activities, further Pitzer ion interaction parameters and a consistent set of chloride complex formation constants valid in high saline systems have to be developed.

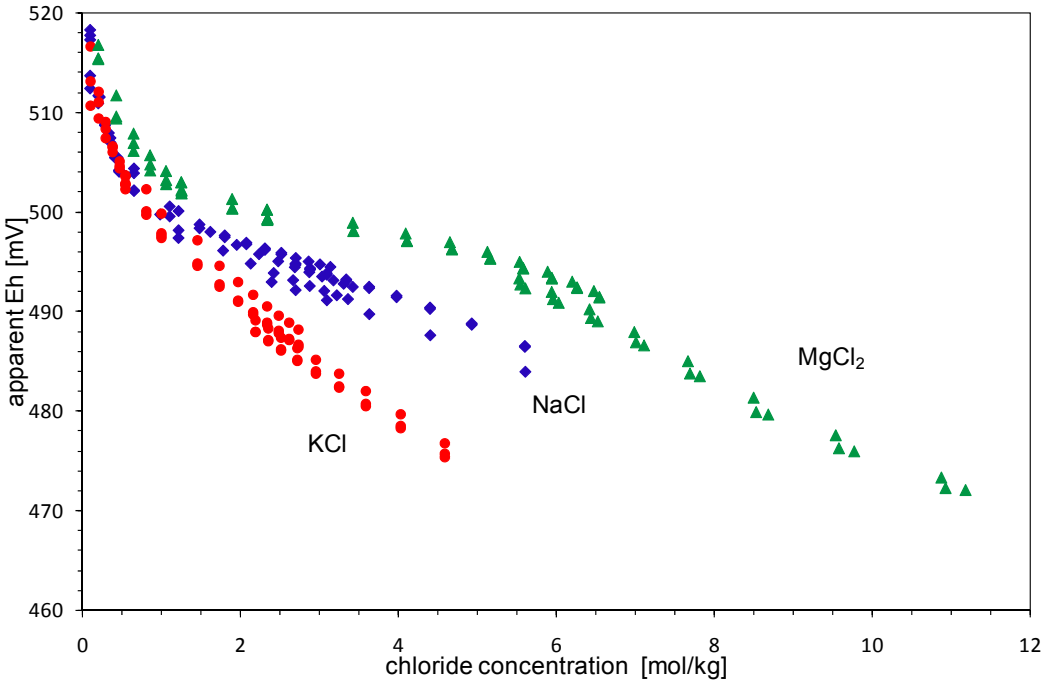

Figure 2 *E_h in relation to chloride concentration of a redox defined system by concentration of Fe(II)/Fe(III) = 1 in 0.01 M $HClO_4$, c(Fe_{tot}) = 10^{-4}M.*

In accordance with theoretical predictions, a change of the Fe(II)/Fe(III) ratio leads to a linear decline with increasing Fe(II)/Fe(III) ratio. But compared to the theoretical slope of 59.16 mV an approximately 15 % reduced slope was observed. E_h measurements with varying H^+-concentrations in concentrated NaCl solutions resulted in an increasing redox potential of about 7 mV per decreasing measured pH unit. No salinity effect is observed for the spectroscopic determination of Fe(II) and Fe_{tot} based phenanthroline in NaCl solutions. For the analysis of Fe(III) with thiocyanate a complex dependency on the salinity was found for 0.1 mol/l SCN, but no effect was seen for higher thiocyanate concentrations (0.5 and 1.0 mol/l SCN).

Final disposal of long-live radioactive waste in geological formations implies the risks of possibly migration of long-live radionuclides and contamination of the surrounding solid (minerals, rocks) and liquid phases. One of these nuclides is iodine I-129 with a half live of $T_{1/2}$= 1.57x10^7 *a*. The dominant species of iodine in aqueous phases is iodide with smaller amounts of iodate and di-iodine. Different studies reported that iodide has in contrast to iodate high mobility and sorbs to mineral phases little or not at all (Couture and Seitz, 1983, Ticknor and Cho (1990), Kaplan et al., 2000). **TUG** develops a redox determination method based on the speciation of iodine using CE-ICP-MS. The outcome is compared with other redox determination methods.

For redox potential measurements TUG used a Hamilton Easycontrol redox electrode (non-refillable, Pt-glass, Ag/AgCl reference system, gel reference electrolyte, ceramic diaphragm).

	Redox calib. standard		3 M KCl		MilliQ#	
	no stirring	*stirring*	*no stirring*	*stirring*	*no stirring*	*stirring*
Reproducibility*	± 2 mV	± 2 mV	± 30 mV	± 15 mV	± 60 mV	± 20 mV
Equilibrium time*	< 5 min	< 5 min	> 60 min	30-60 min	>> 60 min	30-60 min

#Long-term storage in MilliQ increases the equilibrium time (wrong conditioning), but a wrong conditioned electrode can be regenerated with 3 M KCl solution.

First measurements of solutions containing iodate or iodide (5 ppm in 0,1 M $NaClO_4$) showed equilibrium times of about 30 minutes and although adding $Na_2S_2O_3$ to the iodide-solution caused as expected a decrease of redox potential, the long equilibrium times for the open stirred iodide-solutions let us query how much iodide get lost in the form of di-iodine. Another issue TUG addressed is the visible loss (~ 5 %) of the gel electrolyte after only 5 weeks-handling, which questions the suitability of this electrode for our applications.

The reliability of iodide and iodate measurements on ICP-OES (Spectro Ciros Vision EOP) (wavelength: 178.276 nm) was tested under different circumstances. The following first observations were made: 1. For iodide and iodate solutions in combination with wash solution HNO_3, sample vials glass or PP (polypropylene), ion strength with or without 0.1 M $NaClO_4$ it was found that: (i) Significant differences between the signals of iodide and iodate solutions with same iodine concentrations (iodide > iodate up to 50 %), (ii) difference between solutions with and without $NaClO_4$ (up to %), (iii) difference between same solutions in glass and in PP bottle, (glass > PP up to 70 %), and (iv) pump tube ruptured several times. 2. For iodide and iodate solutions in combination with wash solution 0.1 M $HClO_4$, sample vials glass or PS (polystyrol), ion strength with or without 0.1 M $NaClO_4$ it was found that: (i) There were no significant differences between iodide and iodate solutions with same iodine concentrations (< 5 %), (ii) there were no significant differences between solutions in glass and solutions in polystyrol vials (< 5 %), and (iii) storage of iodide solutions causes an increase of the signal (~ 2-5 %, maybe development of di-iodine with higher excitation efficiency).

TUG started testing several methods known from literature und own developments for the iodine speciation with respect to reliability. The methods are CE-ICP-MS, IC-ICP-MS/OES as an online or offline technique as well as chemical separation by volatilisation of iodine.

In recent years, a range of microsensor studies were carried out to measure in situ microbial activities and microbial metabolic processes in biofilms. But investigations of the influence of toxic heavy metals on the metabolic activity of biofilms using microelectrodes are sparse. **FZD** develops methods for redox potential (Eh) and dissolved oxygen (O_2) concentration measurements using microsensors (Clark type design) in biofilms. The depth profiles provide information on geochemical heterogeneities in the biofilms, which in turn influence the oxidation state of the redox sensitive radionuclides in the respective system. Moreover, FZD tests TRLFS of

uranium(IV) species and LIPAS techniques in small compartments and for its applicability in biofilms.

Notwithstanding their importance as essential micronutrients, heavy metals are toxic to micro-organisms at higher concentration because of their adversary binding to enzymes and DNA (Schmidt et al., 2005). Despite the importance of microbial responses to toxic heavy metals in environmentally relevant concentrations, there is little information on this issue. A study of the impact of Zn and Ni on microbial benthic communities was conducted by Viret et al.,(2006) estimating the oxygen consumption on the basis of microsensor profiles. In a recent study, the metabolic response of stable multispecies biofilms on the stress factor uranium, for the first time was studied by electrochemical oxygen microsensors (Krawczyk-Bärsch, et al. 2008). The studied biofilms were grown in the laboratory biofilm reactors at the air/liquid interface and exposed to uranium in ecologically relevant concentrations ($1x10^{-5}$ and $1x10^{-6}$ M), e.g., in seepage water of Schlema/Saxony, Germany. The microsensor profile measurements in the stable multispecies biofilms exposed to uranium showed that the oxygen concentration decreased faster with increasing biofilm depth compared to the uranium free biofilms. The fast decrease in the oxygen concentrations in the biofilm profiles showed that the bacteria in the top region of the biofilms, i.e., the metabolically most active biofilm zone, battle the toxic effects of aqueous uranium with an increased respiratory activity. This increased respiratory activity results in oxygen depleted zones closer to the biofilm/air interface which may trigger uranium redox processes, since suitable redox partners, e.g., extracellular polymeric substance (EPS) and other organics (e.g., metabolites), are sufficiently available in the biofilm porewaters. Such redox reactions may lead to precipitation of uranium (IV) solids and consequently to a removal of uranium from the aqueous phase.

Within the framework of ReCosy first comparative investigations of electrochemical and fiber-optic sensors were performed in collaboration with the University Potsdam (UP). Fiber-optic sensor measurements in biofilms have some advantages compared to those made by electro-chemical microelectrodes. As described by Beyenal fiber-optic sensors are immune to environmental changes in pH, salinity, and ionic strength and immune to interference from moisture, carbon dioxide, methane, and other substances (Beyenal et al., 2000). A range of fiber-optic sensor studies were carried out to measure in situ geochemical gradients in biofilms (Ganesh and Radhakrishnan, 2008, Klimant, et al. 1997, Kohls and Scheper, 2000). To our knowledge optical sensors applied to biofilm samples exposed to heavy metals are so far not reported in the literature. In our first collaboration with the UP we compared the oxygen concentration profiles obtained by electrochemical and optical microsensors, respectively. Oxygen concentration profiles were measured in the biofilms by electrochemical microsensors of the Clark design (Unisense, Denmark). These Clark-type oxygen microsensors are generally used for microbial ecology studies and contain a guard electrode (Revsbech, 1989, Revsbech, 2005). They have a tip diameter of 10 µm, a stirring sensitivity of <1–2%, and a response time of <1 s. The used multispecies biofilms were cultivated in the laboratory under non-sterile conditions in different biofilm reactors. One biofilm reactor was adjusted to a uranium concentration of ($1x10^{-5}$ M), which is typical for uranium contaminated sites. The data achieved from both sensor methods are directly comparable. Fiber-optic sensor measurements showed high concentrations of oxygen over the total thickness of the biofilms, which were not in contact with uranium. In contrast, biofilms exposed to uranium revealed a much lower oxygen concentration in the bottom parts of the biofilm. Already at a depth of

approximately 400 µm no oxygen was detectable. The comparative studies revealed that depending on the existing environmental conditions during the measurements a decision for the appropriate method is possible. However, further developments, e.g. miniaturization of the sensor equipments, are needed and aimed for within ReCosy.

UPPC develops fiber-optical detection schemes for the in-situ monitoring of redox relevant parameters, such as oxygen and pH. In order to adapt optical sensing different combinations of polymers (as support materials for reporter dyes), optical fibers and luminescence probes were tested. Adaptation to the specific in-situ measurement conditions like high ionic strength or aging of the polymer matrix (e.g., due to "poising" caused by matrix constituents) as well as method parameters (excitation conditions, dye, modulation frequency etc.) is work in progress. In case of fiber-based optical sensing for oxygen the fundamental technical parameters are defined and miniaturization of the optical set-up is finished. Using a miniaturized fiber probe (tip diameter 10 µm) a successful test of depth-resolved oxygen detection in biofilms was carried out in collaboration with FZD (*vide supra*). The next step will be the development of an advanced optical detection system for trace amounts of oxygen.

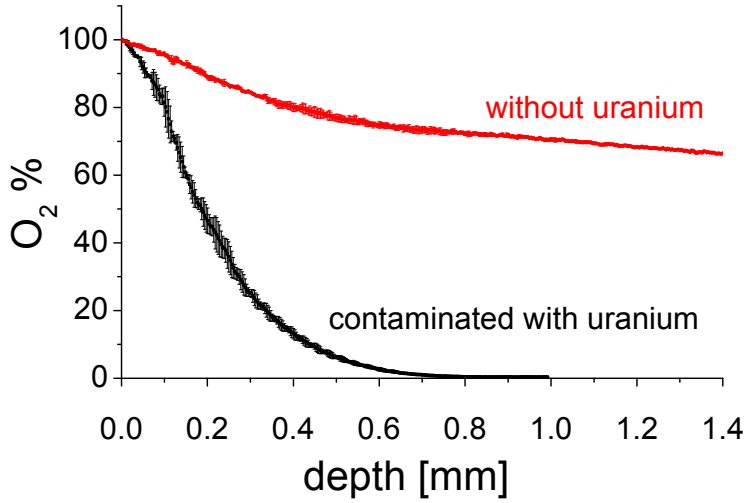

Figure 3: *Oxygen depth profile of a biofilm in the absence and presence of uranium*

Different fluorescence probes for fiber-based pH monitoring were tested with respect to the accessible pH range, the selectivity, and the sensitivity, respectively. A promising fluorescence probe for pH sensing is 2',7'-Bis(2-carboxyethyl)-5(6)-carboxyfluorescein (BCECF) because the emission spectrum as well as the fluorescence decay time are dependent on the pH. BCECF can be used in a fairly large pH range ($2 < pH < 8$) since in its spectral characteristics BCECF shows two inflection points. The basic spectroscopic characterization with respect to spectral distribution and intensity as a function of pH and the pH dependence of the fluorescence decay time under various excitation conditions.

For the implementation in optodes the immobilisation of probes in polymer materials is the crucial step. In the case of pH probes the dye should stay within the polymer (no bleeding) and at the same time the polymer matrix should be permeable for

water (or at least for protons). Different polymers were tested to this respect and work is still in progress to finalize this issue. Because fluorescence decay times of BCECF are only a few nanoseconds, a novel design of the detection electonics needs to be implemented. Currently, MHz modulation frequencies are tested for their applicability in a two-frequency phase modulation detection scheme. After successful implementation a joined micro optode for simultaneous detection of oxygen and pH is planned.

References

Beyenal, H, Lewandowski, Z, Yakymyshyn, C, Lemley B., Wehri, J. (2000) Fiber-Optic Microsensors to Measure Backscattered Light Intensity in Biofilms. Applied Optics, 39, 3408-3412.

Couture, R. A., Seitz, M. N. G.(1983) Sorption of anions of iodine by iron oxides and kaolinite. Nuclear and Chem. Waste Management, 4, 301-306

Ganesh, A.B. and Radhakrishnan, T.K. (2008) Fiber-optic sensors for the estimation of oxygen gradients within biofilms on metals. Optics and Lasers in Engineering, 46, 321-327.

Kaplan, D. I., Serne, R. J., Parker, D. E., Kutnyakov, I. V. (2000) Iodide Sorption to Subsurface Sediments and Illitic Minerals. Environmental Sciences and Technology, 34, 399-405

Klimant, I., Holst G., Kuhl M. (1997) A Simple Fiberoptic Sensor to Detect the Penetration of Microsensors Into Sediments and Other Biogeochemical Systems. American Society of Limnology and Oceanography, 42, 1638–1643

Kohls, O., Scheper Th. (2000) Setup of a fiber optical oxygen multisensor-system and its applications in biotechnology. Sensors Actuators B, 70, 121–30.

Krawczyk-Bärsch, E., Grossmanna K., Arnold T., Hofmann S. ,Wobus A. (2008) Influence of uranium (VI) on the metabolic activity of stable multispecies biofilms studied by oxygen microsensors and fluorescence microscopy Geochimica et Cosmochimica Acta, 72, 5251–5265.

Liu X. (2007). Rétention du Séléniure sur la Pyrite en Milieu Réducteur. Nantes, University of Nantes. PhD

Olin A., Noläng B, Öhman, L.O, Osadchii, E., Rosén E (2005): Chemical thermodynamics of selenium, Amsterdam, Elsevier.

Revsbech, N.P. (1989) An Oxygen Microsensor with a Guard Cathode. American Society of Limnology and Oceanography. 34, 474–478.

Revsbech, N.P. (2005) Analysis of microbial communities with electrochemical microsensors and microscale biosensors. Methods Enzymol. 397, 147–166.

Runnells D.D., Lindberg R.D.: (1990) Selenium in aqueous solutions: The impossibility of obtaining a meaningful Eh using a platinum electrode, with implications for modeling of natural waters. Geology, 18, 212 – 215

Schmidt A., Haferburg G., Sineriz M., Merten D., Büchel G., Kothe E.(2005) Heavy metal resistance mechanisms in actinobacteria for survival in AMD contaminated soils Chemie der Erde – Geochemistry, 65, 131–144.

Ticknor, K. V., Cho, Y. H.: J. (1990) Interaction of iodide and iodate with granitic fracture-filling minerals. Journal of Radioanalytical and Nuclear Chemistry, 40, 75-90

Viret H., Pringault O., Duran R. (2006) Impact of zinc and nickel on oxygen consumption of benthic microbial communities assessed with microsensors. Science of The Total Environment, 367, 302– 311.

WORK PACKAGE 3: REDOX RESPONSE OF DEFINED AND NEAR NATURAL SYSTEMS

Laurent Charlet
(CNRS)-Laboratoire de Géophysique Interne et tectonophysique LGIT- (UMR 5559)
Rue de la Piscine, 1381
38041/19 Grenoble
France

Introduction

The "Redox processes of defined and near-natural system" WP3 group has in Year 1 performed work on (i) Field data, (ii) Field samples, (iii) Microbiology, (iv) Sorption experiments, (v) Redox experiments and (vi) Conceptual Model. This work is summarized below.

Work performed by partners

Field data

Uni Cyprus (Partner 20) has sampled and characterized a phosphogypsum stack. Stack fluid sampling, pH, EC and Eh measurements and chemical analysis were performed Eh (Pt) electrode calibration and Eh measurements of Stack and laboratory solutions. Stack solutions were sampled from the existing boreholes and pH, EC, Eh, composition (main constituents) and the uranium content determined. Compilation of measurements will be presented in Year 2.

Uni. Zaragoza (Partner 17) and **Geopoint AB** (Partner 26) have collected data and started their analysis for two crystalline field sites located in Sweden, in the vicinity of power plants and radioactive waste repositories, namely Forsmark (site A) and Laxemar-Aspö (site B) sites.

A general description of the redox characteristics and methodologies in the two Swedish sites characterisation program related to the redox parameters in crystalline system has been done, from 0 to -1500 meters below sea level. The geology in Site A is dominated by granites and granodiorites and granite and quartz-monzodiorite in Site B. Rocks are 1.9 to 1.8 Ga old. Thin sections of 300 fractures have been sampled, and the mineralogy of open fractures is dominated by calcite, chlorite and pyrite. At shallow depths, hematite is present.

Hydrochemistry results from the mixing of old (>50 ka) meteoric, glacial and saline waters with more recent (>4.5 ka) meteoric waters as shown by Cl and $d^{18}O$ data. The deep waters are therefore Na-Ca-Cl-SO4 type saline (>10 g/L TDS) waters, while shallow waters are Na-HCO3 type dilute (<3.5 g/L TDS) waters. pH is controlled by calcite equilibrium (7.2<pH<8.6). Calcite precipitation has a clear marine signature.

Redox potential decreases with increasing pH. It is found in the -143—281 mV range (site A) and -210 to -310 mV range (site B). It has been measured by 3 electrodes (Pt, Au and Carbon Glass). Fe(II), Mn(II) and NH_4^+ concentrations are equal to (or are below) 2, 0.5 and 0.1 mg/L, respectively, down to depths of 600 m.b.s.l. S(-II) concentrations are usually low, although they can reach 0.84 and 2.5 mg/L at site A and B, respectively.

Field sample characterization

II-HAS (Partner 19) investigates the reduction driven retention in clay rock redox gradients. Samples were collected from 3 sites. The effects of redox disturbances occurring in natural conditions were analysed by monitoring the change in the Fe^{2+}/Fe^{3+} ratio in dependence to depth (i.e. weathering). Four series of samples collected from different boreholes were analysed by Mössbauer spectroscopy with respect to the change of Fe^{2+}/Fe^{3+} ratio in them. The raw spectra, indicative of the presence of Fe(II) into chlorite were produced. Further analysis of the data will be performed in Year 2.

KIT-INE (Partner 1) has characterized clay samples originating from Oxfordian argillite (447 m depth, borehole EST 104). Synchrotron based carbon K-edge and Fe L-edge XANES scanning transmission X-ray microscopy (STXM) and FT-IR microspectroscopy was used to identify under high spatial resolution the distribution of organic matter and iron oxidation states using principal component and cluster analysis. The results show an organic functionality difference depending on mineral association. After radiation of 1.7GGy under helium atmosphere the same rock sample area was investigated for radiation damage. Radiation damage of natural organic matter is independent of the mineral association comparably low with 20–30% total oxygen mass loss and 13–18% total carbon mass loss. This result indicates a rather low sensitivity of the Callovo-Oxfordian organic matter independent of clay type to high radiation doses under helium atmosphere. A critical dose dc of 2.5GGy and an optical density (OD) after infinite radiation of 54% of the initial OD was calculated under room temperature conditions. C(1s) XANES show a clear increase in C=C bonds more pronounced in the initially lower aromatic illite–MLM associated organics. These results suggest a combination of the formation of C=C bond due to crosslinking via polymerization and mass loss due to bond breaking (scissioning) to appear in parallel on the organic macromolecules upon irradiation. Fe L2,3-edge data is still under evaluation and publication in preparation.

Microbiology

MICANS AB (Partner 24) has worked in the Äspö hard rock laboratory with pilot tests of how microbial cultures of sulphate reducing bacteria influence the redox potential in the culture media. Site investigation data on the relation of microbial numbers and redox have been evaluated. Field experiments in the Äspö tunnel have generated data on the relation between sulphide, ferrous iron and microbes. Sulfate

reducing bacteria was demonstrated to be an important component for the measured redox state in the studied deep groundwater. The inverse relationship between Fe(II) and S(-II) concentrations indirect evidence of FeS precipitation will be further investigated. Mn(II) concentration increases with increasing Eh, which remains to be explained. Pressure resistant in situ microelectrodes for pH and redox have been developed for up-coming field work in the Äspö hard rock laboratory tunnel environment. Experiments with increasing H_2 and S(-II) concentrations are underway.

Uni Utrecht (Partner 22) performed batch experiments with lepidocrocite and U(VI) suspensions to which different amounts of S(-II) were added. Addition of S(-II) was used to mimic the activity of sulfate reducing bacteria in this stage of the study. X-ray absorption spectroscopy at the ROBL beamline at the ESRF was used to analyze samples from this study (ESRF proposal EC 279). The Kd for the partitioning of U(VI) between solution and iron oxide decreases by about 2 orders of magnitude upon complete or partial conversion of iron oxide (lepidocrocite) into FeS due to the reaction with S(-II). The decrease in Kd occurs when 0-20% of the initial Fe(III) are reduced to Fe(II). Further reduction of Fe(III) has no effect on Kd. This indicates that the transformation of iron oxide into FeS occurs at the mineral surface and that the transformation at the surface is sufficient to cause the drop of Kd values. When the initial S(-II) to Fe(III) ratios are below 10% practically no reduction of U(VI) is observed. This implies that reduction of Fe(III) can outcompete U(VI) as an oxidant for S(-II) and that the products of the reaction of iron oxides with S(-II) do not necessarily act as effective reductants for U(VI).

Sorption experiments

The WP 3 Leader has completed the Deliverable 3.1 in due time. This deliverable lists all pure solids to be used in WP3, their synthesis procedure and characterization (XRD, BET, SEM, Mössbauer spectroscopy).

TUG (Partner 14) studied the feasibility study for the determination of iodine sorbed on clay minerals by NAA at Johannes Gutenberg Universität Mainz, Institut für Kernchemie, Research reactor TRIGA Mainz. The absolute limit of detection is 1 µg Iodine. All tools for a complete iodine mass balance, both in the liquid and in the solid phase are now available. The maximum amount of clay mineral paste is 10 g, in case of high sodium or chlorine content the LOD increases due to the higher Compton continuum.

CNRS (Partner 16) studied and model Fe(II) adsorption/surface precipitation on calcite, and initiated macroscopic and spectroscopic reactivity of calcite towards Se(IV). The surface reactivity of calcite with respect to Fe(II) was modelled with a surface complexation model. The results showed that Fe(II) binds to calcite (i) by surface adsorption and (ii) by co-precipitation forming a mixed Fe/Ca carbonate phase. Co-precipitation kinetics of Fe(II) into calcite could be fitted to first order kinetics with respect to the solid concentration. Incorporation was clearly detected in sorption experiments conducted for more than 15 h. After this time, it was not possible to recover all of the added Fe(II) using strong Fe(II) ligands, such as ferrozine or

phenanthroline, contrasting to the results of shorter equilibration time. Dissolution of the Fe(II)-equilibrated calcite with carbonic acid allowed complete recovery of the Fe(II) revealing that a ferrous calcite solid solution had formed with a Fe(II) to calcium molar ratio close to 0.4%. Sorption isotherms displayed two uptake mechanisms for Fe(II) sorption on calcite: (i) Langmuir-type adsorption at low metal coverage and (ii) co-precipitation at high metal surface concentrations. The adsorption-precipitation model successfully described our data. In contrast, a straightforward surface complexation model describing sorption of Fe(II) to a single adsorption site $>CO_3Fe^+$ could not reproduce the isotherm data. Consideration of the additional surface reaction, $>CO_3H° + FeCO_3° = >CO_3FeCO_3H°$, with a log K of 7.4 was necessary. The nature of ferrous complexes at the calcite surface has still to be confirmed by spectroscopic methods but they propose that the adsorbed ferrous carbonate species $>CO_3FeCO_3H°$ is a likely precursor in the formation of the $Fe/CaCO_3$ surface precipitate, which forms after a long exposure of dissolved Fe(II) to calcite under anaerobic conditions. They propose that Fe(II) is progressively incorporated in the calcite lattice, where it is no longer susceptible to oxidation.

Redox experiments

INE (Partner 1) has investigated the U(VI) reaction with synthetic 50-300 nm wide magnetite particles, using XPS spectroscopy. Results show the formation of 1.5 nm wide UO_2 nanoparticles, possibly linked to small Fe colloids/clusters.

Amphos (Partner 7) has carried out a bibliographic review on the role of pyrrhotite and mackinawite (FeS minerals) in buffering the redox state in natural systems. In reference to environmental conditions and mineral species, the bibliographical review clearly shows that the most of the reported experiments (evaluating kinetics mechanisms of Fe-S and Fe(II)-oxy-hydroxides alteration) are very specific (pyrite, mainly). The factors affecting pyrite and pyrrhotite oxidation are similar, but pyrrhotite has not been too much analyzed. In this way, these experiments will be an important advance in the understanding of the effects on the groundwater redox control of these non-stoichiometric compounds.

CTM (Partner 3) has investigated the reducing capacity of pyrrhotite (FeSx). Two different kinds of experiments have been carried out with natural pyrrhotite using $NaClO_4$ as non-complexing media. 1) Thermodynamic studies to study the redox buffer capacity and the response to external pH perturbations under anoxic conditions (N_2 saturated). 2) Kinetic experiments to determine the oxygen uptake rate and capacity at room temperature with a solution equilibrated with synthetic air (no carbonates present). Preliminary results suggest that natural pyrrhotite have limited buffer capacity. Pyrrhotite buffer capacity can be related to the system Fe(II)/FeS (am). At room temperature initially air saturated, the oxygen uptake rate is higher than pyrrhotite dissolution ($r_{o2,\ uptake} \sim 8 \cdot 10^{-10}$ mol m^{-2} s^{-1} , $r_{diss,Fe} \sim 10 \cdot 10^{-11}$ mol m^{-2} s^{-1}). Preliminary results show no significant differences between gold and platinum electrodes indicating reproducible measurements, however more studies are needed to understand the kinetic response of both electrodes.

BRGM (Partner 2) developed and adapted specific equipment for the study, including the design of natural or modified argillite and pyrite electrodes and the use of electrochemical methods for investigating the electrode/solution interface. Cox argillite was therefore necessary to make electrodes. First, argillite was fully characterised and then used as it is, after machining of samples in different forms directly starting from an original sample. Argillite was also used as finely grounded and mixed with graphite carbon and silicone oil to obtain electrodes with the required conductivity. Clay paste as well as different redox relevant minerals (pyrite) found in natural clay was also used to machine electrodes. The study required the development and adaptation of equipment including the design of specific electrodes and the use of electrochemical methods for investigating the electrode/solution interface. These tools will make it possible to identify and monitor the electrochemical redox reactions that will occur during their immersion, in both in solution (detected using unattackable platinum (Pt) or gold (Au) electrodes) and on the surface of natural or modified argillite electrodes as well as pyrite and glassy carbon electrodes. The global process of redox reactions will be determined and separated into distinct elementary stages. The key factors of each elementary stage and their respective roles will be identified. It will be then possible, for each stage; to differentiate electrochemical reactions occurring in solution or at interfaces, which, when combined, lead to global reactions that rule the electrode/solution system.

CNRS (Partner 16) studied (i) macroscopically and spectroscopically the reactivity of siderite towards Se(IV), (ii) the change in Kd of iron oxides upon partial reduction of iron oxides by S(-II) related to the initiation of sulfate reduction, (iii) the resulting competition between U(VI) and Fe(III) reduction by S(-II) and (iv) evaluated of various electrochemical techniques for the characterization of Callovo-Oxfordian argillite.

Fe^{2+} reactivity (e.g. towards dissolved O_2) at the surface of calcite was shown to vary dramatically as a function of speciation. Adsorbed Fe(II) was highly reactive whereas surface coprecipitated Fe(II) was not reactive at all. Ferrous carbonate mineral (siderite) was found to be highly reactive towards Se(IV). The reaction lead to precipitation of Se° nano clusters, as shown by XANES and EXAFS.

The Kd for the partitioning of U(VI) between solution and iron oxide decreases by about 2 orders of magnitude upon complete or partial conversion of iron oxide (lepidocrocite) into FeS due to the reaction with S(-II). The decrease in Kd occurs when 0-20% of the initial Fe(III) are reduced to Fe(II). Further reduction of Fe(III) has no effect on Kd. This indicates that the transformation of iron oxide into FeS occurs at the mineral surface and that the transformation at the surface is sufficient to cause the drop of Kd values. When the initial S(-II) to Fe(III) ratios are below 10% practically no reduction of U(VI) is observed. This implies that reduction of Fe(III) can outcompete U(VI) as an oxidant for S(-II) and that the products of the reaction of iron oxides with S(-II) do not necessarily act as effective reductants for U(VI)

The electrochemical oxidation of pyrite contained in the Callovo-Oxfordian argillite can be easily pointed out despite the very low amount of FeS_2 (~1%). The identification of another species, that is reducible, is pending. Preliminary Scanning ElectroChemical Microscopy experiments showed that this technique is promising for the further detection of species that diffuse through the pores of the clay

Conceptual Model

Amphos (Partner 7) developed a conceptual model of the reduction capacity in crystalline or clay compacted rocks. Possibility to incorporate this concept in reactive transport codes has been evaluated. The evolution of reduction capacity in natural systems is a complex task, requiring an integrated approach with multisolute reactive transport models. Only in this context, groundwater redox could be accurately estimated. The most realistic approach to reproduce oxidation of Fe-bearing minerals is considering kinetic assumptions. The kinetic rates of dissolution depend on pH, temperature, and reactive surface areas of solid phases. Therefore not only equilibrium, but also kinetic, data on biotite and chrorite dissolution, as well as pyrite, siderite, pyrrhotite, magnetite, hematite and goethite precipitation and/or dissolution must be integrated in the model, as well as their dependence on temperature, reactive surface area and groundwater composition. Recent studies have also shown that the presence of microbes enhances the capacity of the system to buffer redox. In this way, numerical calculations are needed as the most efficient tool to integrate fluid flow, transport of solutes (by advection, dispersion and diffusion), and chemical reactions in equilibrium and/or under kinetic assumptions (acid-base, redox, complexation, dissolution-precipitation of minerals, cationic exchange and adsorption). Due to the intrinsic uncertainties of the numerical models and of hydrogeological evolution of natural systems, additionally to the simulation of different hydrogeological scenarios, a sensitivity analysis of the main hydrochemical parameters will have to be performed.

WORK PACKAGE 4: REDOX REACTIONS OF RADIONUCLIDES

WP 4.1.

Chemical and redox behaviour of the investigated radionuclides in the different systems

Jan Tits
Paul Scherrer Institut, Laboratory for Waste Management, CH-5232 Villigen-PSI, Switzerland
jan.tits@psi.ch

Introduction

The goal of the activities within this work package is to provide fundamental process understanding of the redox behaviour of radionuclides, including the question of equilibrium / disequilibrium with the system redox conditions. The objectives of this work package result from gaps in the knowledge identified from previous projects dealing with redox processes involving radionuclides

The activities within WP4.1 can broadly be divided in three main topics:

1. Interactions of radionuclides with pyrite
2. Interactions of radionuclides with far-field solids
3. Redox processes under hyperalkaline conditions

Work performed by partners

Interactions of radionuclides with pyrite

The work performed within this topic is focused on obtaining a fundamental process understanding of the interaction of iodine, selenium and uranium with pyrite surfaces.

The scientific activities of **CEA** focused on three different tasks:

A bibliographic review upon the reactivity of pyrite and its sorption properties was conducted. This task highlighted the importance to take into account the knowledge of the pyrite reactivity with $O_{2(aq.)}$ and Fe(III), as the main oxidizing species. Even if the pyrite oxidation mechanism is still under debate, its reactivity has to be taken into account prior to any uptake study. Indeed, if no special care is taken to avoid the oxidation of pyrite prior or during the uptake experiments, the observed sorption could

occur rather on the surface of pyrite oxidation products (ferric oxy-hydroxides) than on the sulphide pristine surface. Moreover, sorption and reduction of redox sensitive elements onto pyrite surface have most of the time been observed with the help of both observations of aqueous and surface approaches.

In a second step, CEA finalised their interpretation of previous experiments concerning the uptake of Eu, U and Co onto pyrite surfaces. These results are planned to be published in 2009. They will allow to increase present understanding of the reactivity of U and I towards pyrite. This study was performed in the absence of carbonate, i.e., in physico-chemical conditions somewhat different from the conditions prevailing in deep geological formations. It is known that carbonate can drastically modify the speciation of U and therefore change its reactivity towards pyrite surfaces. On the other hand, carbonate can also be sorbed onto pyrite surfaces and limit the sorption of iodine anionic species.

The activities of **CNRS/LCPME** during the first year comprised essentially preliminary voltammetric and Scanning ElectroChemical Microscopy (SECM) measurements, the fabrication of pyrite ultramicroelectrodes and the interfacing of a vector impedance meter in view of the dielectric characterization of pyrite micrometric particles. Moreover, the basis of a new representation of the redox properties of a species and of its (thermodynamic) reactivity towards another species is currently being developed.

Voltammetric measurements

First, voltammograms have been recorded at a massive pyrite rotating electrode in chloride medium (pH 3) in 1 mM solutions of selenite, selenate, iodine and iodate. The measurement of the corrosion currents allowed us to have an idea about the kinetics of oxidation of FeS_2 by the different oxidizers.

Then pyrite electrodes have been immersed for half an hour in each of the oxidizing solutions rinsed with distilled water and characterized voltammetrically in chloride medium in the absence of the oxidant.

The corrosion current for the I_2-FeS_2 system is very high (comparable with the H^+-Fe system) and the characterization of the reacted pyrite shows several cathodic signals. The kinetics of the electrochemical reduction of IO_3^- is very slow at the pyrite electrode. Moreover, the cathodic barrier is shifted by more than 1 V in the negative direction. However, the characterization of the reacted pyrite shows also several cathodic signals.

When SeO_3^{2-} is present in solution the electro-oxidation of pyrite is easier, probably because of the formation of insoluble $Fe_2(SeO_3)_3$. By reason of the deposit of an insulating species the voltammograms do no show any corrosion current but the characterization of the pyrite electrode after immersion in the selenite solution is quite different from that of pure pyrite. Selenate does not seem to react with pyrite.

SECM measurements

A positive feedback effect is observed when a Pt ultramicroelectrode (UME) is approaching the surface of a pyrite plate (origin: Spain) immersed in a solution containing $Ru(NH_3)_6^{3+}$ as the mediator. It means that the surface of FeS_2 can regenerate $Ru(NH_3)_6^{3+}$ from $Ru(NH_3)_6^{2+}$ which is formed at the UME under reducing potential. Similar experiments are planned with smaller pyrite samples (until to micrometric sized ones) from different origins.

The feasibility of generation-collection experiments with pyrite was tested by applying an oxidizing potential to the pyrite plate to liberate soluble species of iron and sulphur that are reduced at the level of the UME that is held at a reducing potential and scanned over the pyrite surface. Future experiments will focus on the collection of species released at the pyrite surface following the addition of iodine, iodate and selenite in the solution.

Fabrication of pyrite ultramicroelectrodes

Single band UMEs have been constructed by sealing very thin plates of pyrite in an epoxy resin (photograph) in order to benefit by the advantages of UMEs, i.e. voltammetric records in short time, better resolution, reduced ohmic drops…, in further experiments. To our knowledge, the use of band UMEs made of natural minerals has never been reported.

Moreover, multiband pyrite UMEs are in fabrication. This tool will be useful for the in situ monitoring of the reactions of pyrite suspensions with various reagents. Indeed the multi-electrode will be immersed in the reaction medium and the bands will be successively addressed as a function of time. Therefore, sampling and ex situ characterization of pyrite microparticles will be avoided.

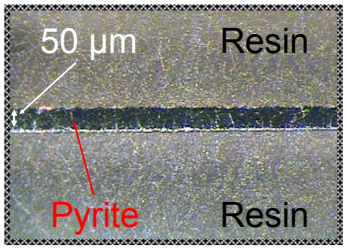

Dielectric measurements

Dielectric measurements in the 0.4-100 MHz range are adequate for in situ characterization of solid/liquid interfaces, the solids being conducting or insulating. The interfaced vector impedance meter has been tested with a model experiment: the oxidation with time of copper microparticles by atmospheric oxygen as a function of the particles sizes. Now similar experiments are in progress on the oxidation of pyrite samples from different origins.

Thermodynamic predictions

The set up of the basis of a new method for representing the evolution of the redox properties of a constant amount of a species as a function of Eh and pH has been completed. (Classic Eh-pH diagrams consider that the concentrations of all soluble species are equal and solid species available at infinite amounts. For example, if one considers a 1 mM iodide solution that is oxidized successively according to the scheme

$I^- \rightarrow I_3^- \rightarrow I_2$ Eh-pH diagrams account for the concentrations of all iodine species to be equal to 1 mM whereas the effective concentrations are 1mM, 0.33 mM and 0.5 mM).

Interactions of radionuclides with far-field solids

The work performed within this topic is focused on obtaining fundamental process understanding of the interaction of redox sensitive radionuclides such as Tc, U, Np and Pu with various far-field minerals.

UMANCH investigates the interactions between surfaces, humic acids (HA) and plutonium in ternary systems, with the aim of predicting the chemistry and solid/solution partition of Pu.

During the FUNMIG FP6 project together with collaborators at the Flerov laboratory, Dubna a new uranium tracer (^{237}U) was developed that allows U chemistry to be studied over a wide range of concentrations. The work has been extended to include the redox sensitive actinide element Pu using the radiotracer ^{237}Pu. HA and U/Pu ternary systems (hematite, bentonite and kaolin) are currently under investigation. As examples, some results for the effect of pH and HA concentration in the ^{237}U(VI)/HA/bentonite ternary system (Figure 1) and the effect of order of addition of system components and sorption kinetics in the Pu(III) and U(VI) HA bentonite ternary systems are shown (Figure 2a and 2b). These results will be described in more detail in a scientific contribution in this volume.

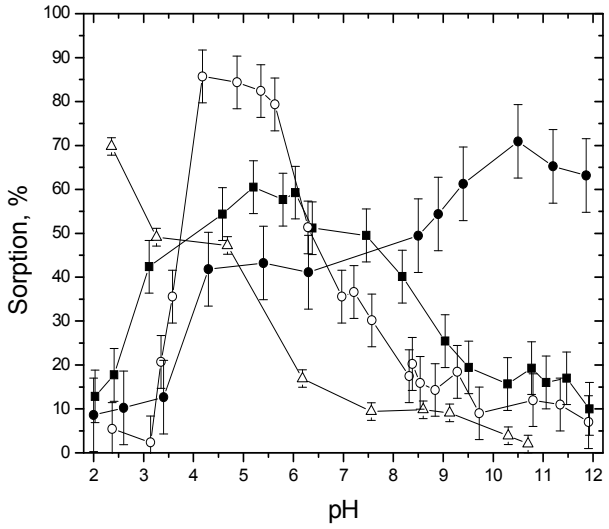

Figure 1: *Effect of pH on U(VI) (10^{-10} M) sorption onto 1 g·L^{-1} bentonite in the absence of HA (○) and in the presence of 100 mg·L^{-1} HA (■) and the sorption of HA on bentonite alone (Δ). Filled circles (●) represent the sorption of U(VI) at a concentration of 1x10^{-4} M on bentonite in the presence of 100 mg·L^{-1} HA.*

The effect of HA on U(VI) sorption on bentonite was studied at a U concentration of 10^{-10} M and a HA concentration of 100 mg·L^{-1}. The distribution of U(VI) between the liquid and solid phase was studied as a function of pH and ionic strength both in the absence and presence of HA. Uranyl sorption on bentonite is

strongly dependent on pH and the presence of HA. In the absence of HA, an enhancement in the uptake with increasing pH was observed, and a sharp sorption edge was found to take place between pH 3.2 and 4.2. The presence of HA slightly increases U(VI) sorption at low pH and curtails it at moderate pH. In the basic pH range for both the presence and absence of HA the sorption of uranium is significantly reduced, due to the formation of soluble uranyl carbonate complexes. The influence of ionic strength on U(VI) and HA uptake by bentonite was investigated in the range 0.01 – 1.0, and while there was an enhancement in the sorption of HA with increasing ionic strength, U(VI) sorption was found to be indifferent to ionic strength both in the absence and presence of HA at I < 1 (data not shown here).

The effect of the addition order of ternary system components and reaction kinetics were investigated at pH=5.0 and ionic strength 0.01 in the U(VI) and Pu(III) systems, and the results are given in Figures 2a and 2b.

In the systems where the uranyl was added to the HA prior to contact with the bentonite, it takes approximately 2-4 days for equilibrium. For the Pu system, there is an initial increase, which is similar to the U data, but this time the amount bound continues to increase with time. In the U(VI)-bentonite binary systems (squares and triangles in Figure 2, before addition of HA), it takes approximately 1 h to reach the point of 50% sorption, but equilibrium (80 – 85 %) is reached after 2-3 days. For both the 1 and 7 day systems, the sorption of U(VI) on bentonite appears to be reversible, i.e. upon addition of HA, there was a gradual decrease over a few days in the amount of uranyl bound to the equilibrium level (the same as the system where HA and U were mixed first).

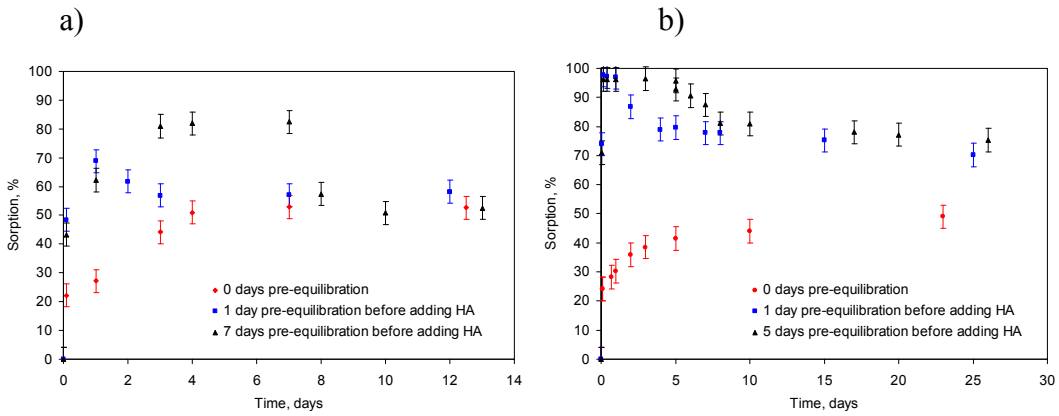

Figure 2 *Effect of the addition order and pre-equilibration time on sorption of (a) U(VI) and (b) Pu(III) onto 1 g·L^{-1} bentonite at pH=5.0 and I=0.01 M.. 100 mg·L^{-1} HA added after: 0 days (●), 1 day (■) and 7 (U) or 5 (Pu) days (▲) after the actinide was put in contact with the bentonite.*

For Pu(III), the behaviour is very different. For the binary ^{237}Pu/bentonite reaction (before addition of HA), sorption is very rapid, with 70-75% sorption within a few minutes and apparent equilibrium (95% sorbed) within a few hours. The U(VI) systems were relatively insensitive to the order of addition, but this is not the case for Pu(III). Following addition of the HA, there is a reduction in the amount of Pu bound, but in both systems the amount sorbed only falls to approximately 75%, significantly higher than for the 0 day system. Hence, on the timescale of a few months, there is significant irreversibility. It is interesting that the 1 and 5 day pre-equilibration systems

behave in the same way following the addition of the HA, i.e., they take 2-3 days for the amount sorbed to fall to approximately 75%. It is tempting to think that the difference is due to the redox properties of Pu(III) (very likely to change oxidation state) and U(VI) (not).

IPL studies the sorption of Pu to natural clays containing natural iron oxide coatings. For the laboratory investigations, samples of a Triassic clay were taken from the Šaltiškiai quarry, an industrial mining site in north Lithuania, . This clay is selected for the engineered barrier of the Lithuanian near surface repository. It is composed of micro-aggregates of clay particles which are cemented by limonite $FeO(OH)\cdot nH_2O$. The fraction <1μm of this clay contains 56-71% of smectite group minerals, 20% of illite and 1 to 9 % of chlorite minerals. X–ray diffraction analyses indicated about 14 % of montmorillonite. The chemical composition of the Šaltiškiai clay is SiO_2 – 45.51%, Al_2O_3 – 13.50%, Fe_2O_3 – 5.17% MgO – 3.00%, CaO- 12.88%, Na_2O – 0.28 %, K_2O – 5.02%, TiO_2 – 0.43%, total S – 0.16%, loss on ignition 13.96%.

A mixture of Pu isotopes was used in the sorption experiments. The oxidation state purity of Pu (IV) stock solution was analyzed by solvent extraction at pH 0.5 using 0.5 M TTA as extractant. Typically 96 ± 3 % of the total plutonium was found in the tetravalent state. The starting concentration of Pu(IV) was approximately $1.10\cdot10^{-9}$ mol/L.

The batch sorption method was used for the sorption studies. Sorption experiments were carried out in polypropylene bottles using 0.1 M $NaNO_3$ solutions, (solid : liquid ratio 1:1000 was used). The pH of the suspensions used in the experiments was adjusted with nitric acid. Repeated washings with fresh portions of the working solution having the desired pH, were performed until the pH remained stable (±0.1 pH units) over the desirable range for 48 hours. Then aliquots of the Pu tracer solution were added to achieve the desired initial concentration. The Pu-containing suspensions were equilibrated for 11 days. The pH was measured before and after sorption experiments under continuous Ar flow. Phase separation was obtained by centrifugation for twenty minutes at 10,000 - 15,000 g. The oxidation state of Pu at different pH values was determined in solid and liquid faces using TTA, HDEHP and DBM solvent extractions. Fractions of Pu(IV), Pu(III+IV), Pu(IV/ hydroxide/oxide polymers), Pu(V) and Pu(VI) were separated. Plutonium in the solution and the solid phases as well as in separated fractions were determined after radiochemical separation using the UTEVA and TRU resins (Eichrom Industries) and the activities were measured by alpha spectrometry. ^{242}Pu was used as tracers in the separation procedure. The preliminary results showed that in some cases the modification and validation of used conventional methods are required. Measurements are in the progress.

Redox processes under hyperalkaline conditions

The work performed within this topic aims to provide an understanding of the redox behaviour of redox-sensitive radionuclides such as Tc, U, Np under hyperalkaline conditions.

ULough has studied the complexation of Tc(IV) with gluconic acid (GLU) under hyperalkaline conditions and the reduction of Tc(VII) in the presence of GLU.

Complexation of Tc(IV) with GLU

Figure 3 shows the effect of increasing GLU concentration on the Tc(IV) solubility. The slope of close to unity indicates that the increase in solubility of Tc is being controlled by the formation of a 1:1 Tc(IV)-GLU complex. This relationship allows the calculation of a conditional stability constant for this complex using the solubility product approach. The conditional stability constant was determined to be; $\beta = 4.0 \times 10^{26}$ or $\log \beta = 26.6 \pm 0.2$.

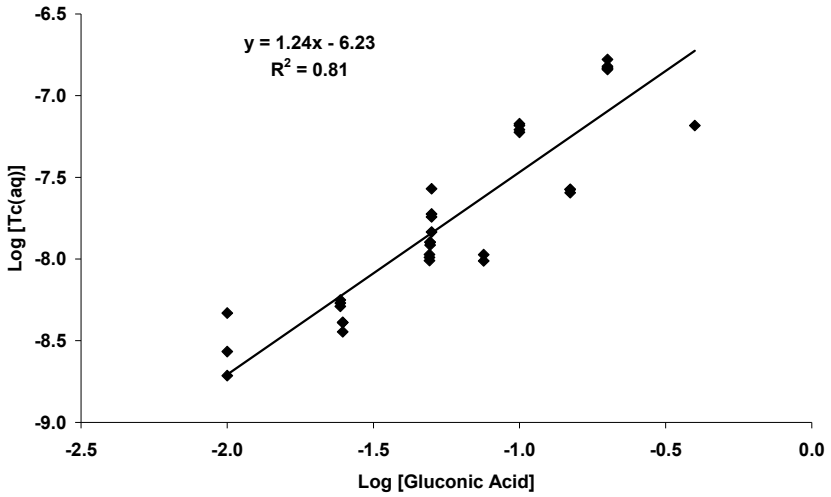

Figure 3: *Effect of concentration of GLU on aqueous technetium concentration above $TcO_2(am)$ at pH 13.3.*

Reduction of Tc(VII) in the presence of GLU.

In the presence of GLU a lowering of the aqueous Technetium concentration took place upon reduction, showing that the ligand did not prevent reduction taking place. If this reduction was to Tc(IV), then the final aqueous concentration of technetium should be the same as that produced by the addition of the same ligands to Tc(IV) solution, i.e. the Tc(IV)-ligand complexes would again be formed, but by two different routes, assuming steady state had been obtained. However, the final Tc solubility in the system where reduction took place in the presence of GLU was higher than when TcO_2 was the starting point (Fig. 4). This indicates that Tc(VII) may not have been reduced to Tc(IV) but an intermediate oxidation state such as Tc(V) complex may have been formed.

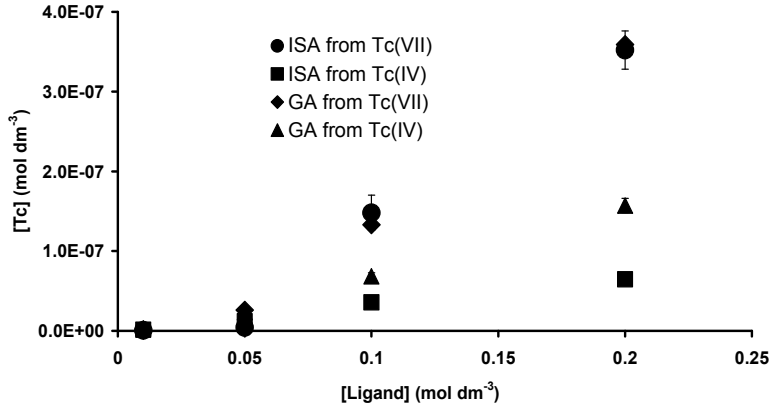

Figure 4: *Comparison of final Tc concentrations in the presence GLU at pH 13.3, starting from TcO_4^- and Tc(IV). Comparison with data in the presence of isosaccharinic acid (ISA)*

Amphos aims to provide an understanding of the redox behaviour of the uranium system under hyperalkaline conditions (pH > 12). The transition between aqueous U(IV) and U(VI) hydroxides at high pH values is an issue of relevance for studies in the presence of cement. To this aim, a combination of UO_2 solubility experiments under well controlled redox conditions will be performed. In order to elucidate the dissolution mechanism, not only the aqueous phase but the solid phase will also be characterized at different stages with spectroscopy techniques (e.g. XANES and XPS).

The objective of Amphos during this first activity period is to focus on the solubility of a synthetic UO_2(am) solid phase at a pH range from 8 to 13 and under highly reducing conditions to prevent oxidation of U(IV).

Synthesis and Characterization of UO_2(am)

UO_2(am) is synthesized following an adaptation of the method reported by (CASAS, 1989). Briefly, an stock solution of uranyl nitrate hexahydrate is firstly acidified and then continuously bubbled with H_2 at atmospheric pressure in the presence of Pd as catalyst to reduce U(VI) to U(IV). The reduction process is monitored both qualitatively, by colour change, and quantitatively by time-resolved laser-induced fluorescence spectrometry (TRLFS), controlling the disappearance of the peak attributed to U(VI). Amorphous UO_2 is precipitated by slow addition of NaOH solution (H_2 saturated and carbonates free) (see Scheme 1). The final product will be characterized by X-ray diffraction (XRD) and X-ray photoelectron spectroscopy (XPS) and transferred to the batch reactor using a glove box to minimise its oxidation.

$$UO_2(NO_3)_2\cdot 6H_2O \xrightarrow[Pd(cat),48h]{H_2(g)} U^{4+} \xrightarrow{NaOH} UO_2(am)$$

Yellow **green** **green**

$$UO_2^{2+} + 4H^+ + 2e^- \Leftrightarrow U^{4+} + H_2O$$

$$\text{Pt mesh} \xrightarrow[I = 0.3\ A,\ 4\text{-}5\ min]{PdCl_2} Pd(0) \xrightarrow[I = 0.3\ A,\ 20\text{-}30\ min]{H_2SO_4,\ 10\%} Pd(cat)$$

Deposition **Activation**

Scheme 1. *Synthetic procedure followed to prepare UO_2(am).*

Solubility experiments

Solubility experiments will be performed from undersaturation direction using an autoclave as a batch reactor (see Figure 5). $NaClO_4$ will be used as background electrolyte at two different ionic strengths (0.2 and 1 M). The pH will be adjusted to different values ranging from 8 to 13 and the Eh value will be measured by a redox combined electrode (Pt electrode). Different methods will be used to maintain the required reducing conditions to avoid oxidation of U(IV). Experiments performed under an H_2 atmosphere (applying a H_2 pressure of 1.5-2 bar) will be compared with parallel experiments using a reducing agent ($NaHSO_3$ or $Na_2S_2O_4$) and the achievement of the desired experimental reducing conditions will be evaluated.

An attempt to continuously monitor the reducing conditions will be made by connecting the autoclave to the Time-resolved Laser-induced Fluorescence Spectrometer (TRLFS) (Figure 5), which would analyse the concentration of U(VI) species.

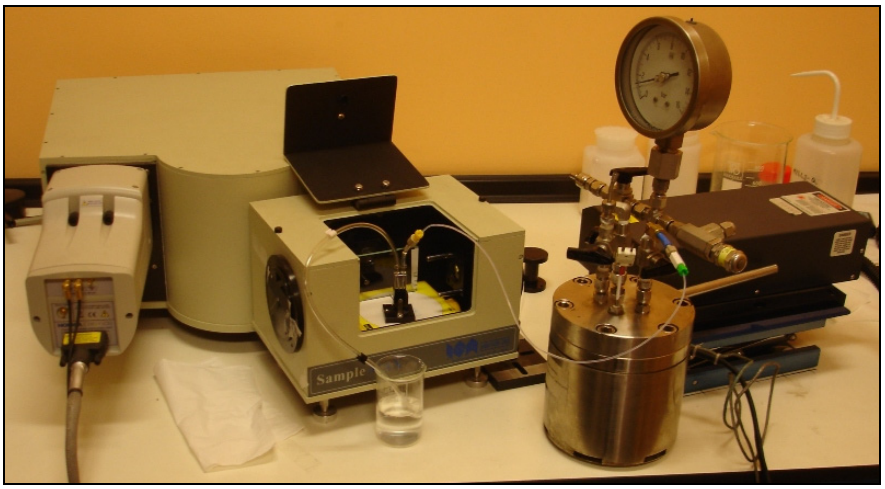

Figure 5*. Autoclave used as a batch reactor to perform the solubility experiments and connected to TRLFS.*

The concentration of uranium in the filtrate will be measured using an Inductively Coupled Plasma Mass Spectrometer (ICP-MS) and the solid phase formed will be characterized by X-ray Absorption Spectra (XANES), XPS, XRD, Infrared Spectroscopy (IR-TF) and Scanning Electron Microscope (SEM).

Subsequent experiments would involve studying uranium solubility in synthetic cementitious groundwater.

The contribution of **PSI** to WP4 is focused on the influence of redox conditions on the immobilization of Neptunium in highly alkaline cementitious environments. In many sorption databases, sorption values for tetravalent actinides such as Np(IV), and Pu(IV) are often estimated based on their chemical analogy with Th(IV), an actinide for which sorption data more easily experimentally accessible. On the other hand, the sorption behaviour of Np(V) is expected to be similar to bi- or trivalent metal cations based on its effective charge of 2.3 (CHOPPIN, 1983). The PSI contribution to WP4 aims at validating both assumptions.

During the first 6 months of WP4, emphasis was mainly put on four topics: 1) Neptunium speciation calculations under hyperalkaline conditions. 2) Development of experimental procedures to control the redox conditions and measure the Np redox state during solubility and sorption experiments. 3) Np solubility tests under anoxic and reducing conditions. 4) Np(V) sorption tests on calcium silicate hydrates (C-S-H) phases, the main sorbing component of hardened cement paste, under anoxic conditions.

Neptunium speciation under hyperalkaline conditions

Speciation calculations were performed for Np under alkaline conditions (10.0<pH<13.3) in the absence of CO_2 using the Nagra-PSI Chemical Thermodynamic Database (HUMMEL et al., 2002) excluding stability constants for the Np(VI) hydroxyl species, $NpO_2(OH)_3^-$ and $NpO_2(OH)_4^{2-}$, for which only limiting values are proposed. Np predominance diagrams show that under anoxic conditions in a glovebox (O_2<2 ppm, no redox control, 500 mV<E_h<600mV versus standard hydrogen electrodes (SHE)), Np is predominantly in the pentavalent state. It appears that the redox speciation depends significantly on the presence of Np solids: Np(IV) becomes the dominating redox species at potentials below roughly 0 mV at [Np] below 10^{-8} M in the absence of $Np(OH)_4$(am) and NpO_2(OH)(fresh), whereas in the presence of these solids, the stability field of Np(IV) moves with ~200 mV to higher potentials and the Np(V) stability field becomes smaller. Np(VI) only becomes dominant at potentials above ~700mV (vs. SHE) under hyperalkaline conditions. Tetravalent Np(IV) becomes the dominant redox state at potentials roughly below 0 mV (vs SHE). The main aqueous Np(V) species under hyperalkaline conditions are NpO_2^+, $NpO_2(OH)$ and $NpO_2(OH)_2^-$.

Development of experimental procedures to control the redox potential and to determine the Np redox state

Hyperalkaline systems set up in a glove box under anoxic conditions (O_2<2 ppm) in the absence of redox buffers exhibit a redox potential (calculated) between +500 mV and +650 mV (vs SHE). The stability field of Np(IV) under hyperalkaline conditions lies below a redox potential of 0 mV. To maintain such low redox potentials

during the course of the sorption experiments, it is planned to use either a chemical reducing agent or a potentiostat. The reducing agent envisaged is Na-dithionite ($Na_2S_2O_4$). Under alkaline conditions, the redox potential in aqueous systems containing dithionite, is controlled by the following reaction:

$$2SO_3^{2-} + 2e^- + 2H_2O \Leftrightarrow S_2O_4^{2-} + 4OH^- \qquad E_H^0 = -1.13 \text{ V}$$

This reducing agent is stable under alkaline conditions and using $[S_2O_4^{2-}]=10^{-3}$ M it maintains the E_h at values (calculated) between -745 mV (vs SHE) at pH=10 and -1220mV (vs SHE) at pH=14. Preliminary stability tests carried out by PSI showed that the presence of $Na_2S_2O_4$ in (C-S-H) suspensions up to concentrations of $2x10^{-3}$ M did not have a significant influence on the Ca and Si solubilities. In a next step it is foreseen to test whether the presence $Na_2S_2O_4$ affects the sorption of tetravalent actinides on C-S-H phases, by comparing Th(IV) sorption in the absence and presence of this reducing agent.

In a second approach controlled redox conditions are established with the help of a potentiostat. All components of the electrolytic cell must be adapted to the alkaline conditions of the experiment. I.e. TFA containers, electrode shafts made of TFA, as well as special leak-free Ag/AgCl reference electrodes to avoid Ag_2O precipitation in the electrode in contact with alkaline solutions

The oxidation state of Np in the aqueous phase is determined by liquid-liquid extraction using Thenoyl-trifluoro acetone (TTA).

Np solubility tests under anoxic and reducing conditions.

In order to allow a proper interpretation of Np sorption data, its solubility and speciation must be known. Though considerable fundamental information is available on the chemical thermodynamics of Np(V), significantly less is known about Np(IV) mainly because measurements of this oxidation state are very difficult due to its sensitiveness to oxygen traces. Moreover the number of experimental investigations of the Np speciation under hyperalkaline conditions is rather limited. Therefore a first phase of the project consists of a series of solubility tests with Np(IV) and Np(V) in various alkaline solutions. Solubility tests from oversaturation were set-up with Np(V) under anoxic conditions in a glovebox (O_2, CO_2 < 2 ppm). The redox state in these experiments was not controlled. In the tests, series of alkaline solutions containing increasing amounts of Np(V) (Np-237) were prepared and equilibrated for 1 day, 30 days and 60 days. Two alkaline solutions were used: 1) an artificial cement pore water (ACW) containing 0.12 M NaOH, 0.18 M KOH, $1.6 \cdot 10^{-3}$ M $Ca(OH)_2$ (pH=13.3), reflecting the pore water composition of a fresh hardened cement paste. 2) a 10^{-4} M $Ca(OH)_2$ solution (pH=10.3) reflecting the pore water composition of a degraded hardened cement paste controlled by the C-S-H solubility. After equilibration, the solutions were sampled, the remaining solution centrifuged for 1 hour at 90'000 g(max) and the supernatant was sampled again. The Np(V)concentration in all the samples was determined using a liquid scintillation counter α/β discrimination capabilities. The results of these solubility tests are shown in Figure 6a and b.

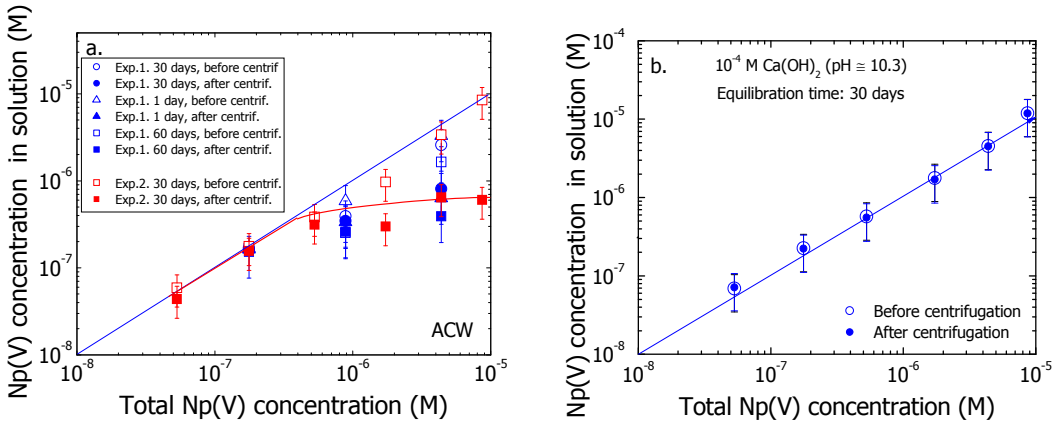

Figure 6: *Np(V) solubility test experiments in ACW at pH=13.3 (a) and in 10^{-4} M $Ca(OH)_2$ at pH=10.3 (b)*

In ACW, Np(V) supernatant concentrations after centrifugation remain constant at a value of $6 \cdot 10^{-7}$ M, independent of the amount of Np(V) added, suggesting that the Np(V) solution concentration is controlled by a solid phase. In the 10^{-4} M $Ca(OH)_2$ solution, no indications for Np(V) precipitation were found in the concentration range between $5 \cdot 10^{-8}$ M to 10^{-4} M. The latter observation is in agreement with thermodynamic calculations. The solubility of NpO_2OH(aged) however, is predicted to be $3.7 \cdot 10^{-6}$ M in ACW; i.e., more than 1 order of magnitude higher than the experimental values. This inconsistency will be investigated in more detail.

Solubility tests with Np(IV) were started as well. In these first experiments, the redox potential is fixed at -100 mV with the help of a potentiostat. Preliminary tests with 10^{-7} and 10-8 M Np seem to indicate that $Np(OH)_4$(am) is the phase controlling Np(IV) solubility at [Np] higher than 10^{-9} M. These tests also point out that colloids play a relevant role in the chemistry of Np(IV) under hyperalkaline conditions. In the second year of the ReCoSy project, complementary solubility tests in the presence of $Na_2S_2O_4$ as a reducing agent, will be carried out. Would you find also appropriate mentioning the first experiments with Np-239.

Np sorption tests

A first series of Np(V) sorption tests on C-S-H phases have been conducted. C-S-H phases with different $CaO:SiO_2$ ratios (0.64, 0.96, 1.6) were synthesized following a procedure described in (TITS et al., 2006). The pH of the resulting suspensions was 10.3, 12.0 and 12.5, respectively. Sorption experiments were performed on the original C-S-H suspensions resulting from the synthesis. These suspensions had a solid : liquid ratio of 1.0 g L^{-1}. Aliquots of an Np(V) (Np-237) stock solution ([Np(V)]=$3.55 \cdot 10^{-4}$ M) in 0.5 M HCl were added to obtain a total Np concentration in the suspensions of 10^{-6} M. After equilibration, phase separation was carried out by centrifugation during 1 hour at 90'000g(max). The first results of these experiments are shown in Figure 7. Np(V) sorption distribution ratios (R_d) were found to be of the order of 10^6 L kg^{-1}. These R_d values are surprisingly high, as the effective charge of the NpO_2^+ cation of 2.3 suggests a sorption behaviour similar to divalent cations with R_d values of the order of 10^3 L kg^{-1}.

This unexpected behaviour will be investigated in more detail during the next reporting period.

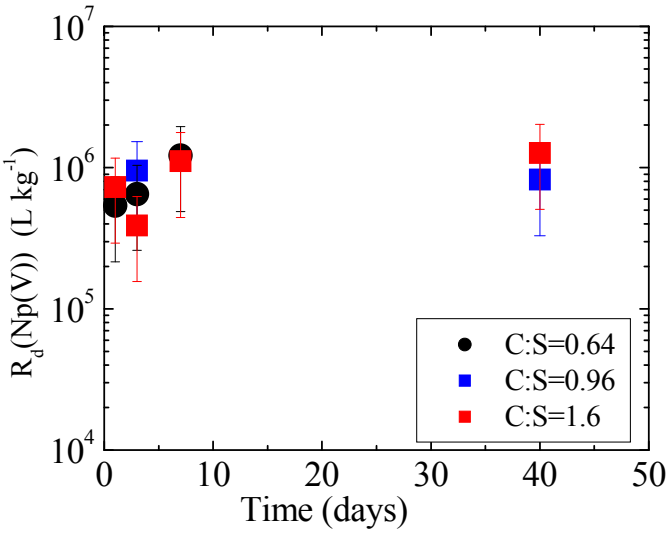

Figure 7: Np(V) sorption kinetics on C-S-H phases with 3 different C:S ratios. The S:L ratio in the experiments was 1.0 g L^{-1}. The total Np(V) concentration was 10^{-6} M.

References

Casas, I., 1989. Estudios Fisico-Quimicos de la disolucion del UO_2, Thesis, Universitat Autònoma de Barcelona, Barcelona, Spain.

Choppin, G. R., 1983. Solution chemistry of actinides. Radiochim. Acta 32, 43-53.

Hummel, W., Berner, U. R., Curti, E., Pearson Jr, F. J., and Thoenen, T., 2002. Nagra-PSI chemical thermodynamic database, version 01/01. Universal Publishers / Upubl.com, New York.

Tits, J., Wieland, E., Müller, C. J., Landesman, C., and Bradbury, M. H., 2006. Strontium binding by calcium silicate hydrates. J. Coll. Interf. Sci. 300, 78-87.

WP 4.2.

Chemical and redox behaviour of the investigated radionuclides in the different systems through microbial mediated processes

Evelyn Krawczyk-Bärsch.
Institute of Radiochemistry,Forschungszentrum Dresden-Rossendorf, Germany (FZD)
E.Krawczyk-Baersch@fzd.de

Introduction

Within WP 4.2 the participating institutes are focusing their work on the study of the microbial impact (IPL) and on the O_2 concentration and uranium redox state in-situ in biofilms with emphasis on biologically mediated redox processes (FZD). The studies are carried out on isolated microorganisms as well as on biofilms. Biofilms are composed of bacteria, fungi, algae, protozoa, exopolymeric substances (EPS), corrosion products and 50–95% water. They are ubiquitous and have to be considered as an important factor in natural biogeochemical processes influencing the redox state of radionuclides. They show a multiplicity of interactions with metals and contribute to metal mobility or immobilization. Once on the surface, the organisms secrete a slimy or glue-like substance (EPS) that allows them to securely anchor themselves on the surface and form connections with other organisms. After attachment, the organisms divide and expand into multicellular communities or microcolonies and create a protective barrier commonly known as a biofilm. At the detachment stage, single mobile cells and cell communities are released from the biofilm. They are transported away with the bulk solution and will attach themselves on other surfaces. Since microbial processes emerge whenever suitable conditions are found, biofilms are influencing the transport behaviour of heavy metals and radionuclides by changing the geochemical parameters (e.g. dissolved oxygen, pH, redox potential), increasing the metabolic and respiratory activity, inducing redox reactions in anoxic zones within the biofilms and finally immobilising toxic heavy metals and radionuclides.

To obtain more detailed information on the effect of microorganisms on the redox behaviour of radionuclides first investigations have been started within WP 4.2.

Work performed by partners

IPL focuses its work within ReCoSy on the study of the microbial impact. Microorganisms from clay and groundwater samples will be isolated, identified and their oxidation ability towards Pu will be investigated. In further studies sorption-desorption of Pu, Tc, Np and Am to various minerals, including nanoparticles, will be studied under oxidizing and reducing conditions. In first experiments soil

microorganisms were brought in contact with mixture of heavy metals (Cr(III), Ni, Fe(III), Cd, Mn) in order to isolate the most tolerant ones. Among all microorganisms fungi were determined as the most metal tolerant microorganisms. They were isolated into pure cultures of *Aspergillus niger, Fusarium sp., Eupenicillium sp., Penicillium oxalicum, Paecilomyces lilacinus* and *Phoma sp.* These fungi were investigated for their tolerance range and their metal accumulation abilities by adding Cr(III), Ni, Fe(III), Cd and Mn in separate experiments into the growth medium with a concentration of 0,1– 20 mM, respectively. The results showed that fungal tolerance towards heavy metals differed depending on metals used. The highest growth inhibition effect was manifested by Cd and Ni, while Mn showed the weakest influence. The most tolerant fungi to most metals were *Aspergillus niger, Penicillium oxalicum* and *Paecilomyces lilacinus,* whereas *Fusarium sp.* was the most sensitive among the tested fungi. Accumulation ability of metal tolerant fungi was tested using Fe(III) and ^{242}Pu. All fungi showed high Fe-accumulation capacity. While growing in the medium with 1mM iron, most fungi accumulated over 90% of Fe in their biomass. Very good accumulation and growth abilities in Fe-supplemented medium were demonstrated by *Paecilomyces lilacinus.* Preliminary investigation of ^{242}Pu accumulation by fungal biomass showed that the all fungi accumulated ^{242}Pu, and among the most effective radionuclide accumulators *Penicillium oxalicum* and *Aspergillus niger* could be mentioned.

***Table 1**: Fe removal from growth medium by growing fungal biomass (Fe added to the medium 1 mM)*

Fungi	pH change, $pH_{initial}$=7,15	Accumulated Fe mg/1 g dry biomass	Fe removed from growth medium, %	Biomass growth (%)*,
Aspergillus niger	-3,48	16,7	82,8	107
Eupenicillium sp.	-2,74	30,7	93	104
Fusarium sp.	-1,31	51	96	77
Paecilomyces lilacinus	-0,92	38,7	98,7	113
Phoma sp.	-0,84	29,4	99,7	76
Penicillium oxalicum	-0,92	20,6	94,8	98

* to compare to the control growth without iron addition)

The focus of **FZD** within ReCosy will be the study of the O_2 concentration and uranium redox state in-situ in biofilms with emphasis on biologically mediated redox processes. Within the framework of ReCosy redox processes in biofilms, grown in-situ in radionuclide contaminated environments, will be studied by oxygen and redox potential microsensors. Measurements of dissolved oxygen by electrochemical microsensors and with fiber-optic sensors combined with confocal laser scanning microscopy (CLSM) are planned as well as studies of the oxidation state of uranium in biofilms by coupling TRLFS with CLSM. First in-situ measurement activities have already taken place in a former uranium mine in Saxony (Germany). Since the mining activities had stopped in 1990, the uranium mine has been partially flooded for

remediation. This resulted in encroaching release of heavy metals and radionuclides as contaminants in acid, sulphate-rich waters. Huge biofilms with a thickness of more than 10 centimetres are currently growing in drainage channels (not flooded so far) under acid conditions and in the presence of uranium concentrations of approximately $1x10^{-4}$ M. Analysis of the amplified 16S rRNA gene fragments were carried out on these biofilms for determination of the microbial diversity. The clone library from the biofilms is dominated by representatives of cyanobacteria and β-Proteobacteria with a fraction of 35 %, respectively and 16 % of γ-Proteobacteria. Cyanobacteria are photoautotrophic. Since they obtain their energy through photosynthesis, we assume that the electric light in the underground will be sufficient for them. *Ferrovum myxofaciens* was determined as the most representative β-Proteobacteria species. These acidophilic bacteria are able to survive in radionuclides contaminated, acid and sulphate-rich waters. Concentration profiles of oxygen were measured in these biofilms in-situ by means of Clark-type electrochemical microsensors (Unisense, Denmark). These oxygen microsensors are generally used for microbial ecology studies and contain a guard electrode. They have a tip diameter of 10 µm, a stirring sensitivity of <1–2%, and a response time of <1 s. The sensors were connected to a picoammeter and fixed in a holder on a motor-driven micromanipulator stage, connected with a motor controller, for a precise small-scale positioning and for automated measurements in 50 µm steps in Z-axis. The motor controller communicated with a PC via the RS-232 serial port. It is controlled from the PC with the program PROFIX (Unisense, Denmark). Due to the heterogeneities of the biofilm, numerous microprofiles were measured at different points of the biofilm. The results revealed a fast decrease of the oxygen concentration in the biofilm profiles as a function of depth. Already at a depth of approximately 2 mm O_2 partial pressure fell below the detection limit (value). It can be assumed that the microorganisms of the biofilm fight the toxic effects of aqueous uranium in a similar way as the biofilms described in Krawczyk-Bärsch et al. (2008). The biofilm community is reacting to the exposition of uranium in environmentally relevant concentrations with an increase of the respiratory activity. The increased metabolic activity of the microorganisms, as a result of an activation of heavy metal resistance mechanisms, will lead to larger anoxic zones (reducing zones) within the biofilms, which may induce redox processes. In these zones uranium (VI) can be reduced to highly insoluble uranium (IV) through abiotic processes. The precipitations of uranium (IV) solids will result in an increased removal of uranium and immobilization of uranium from the solution.

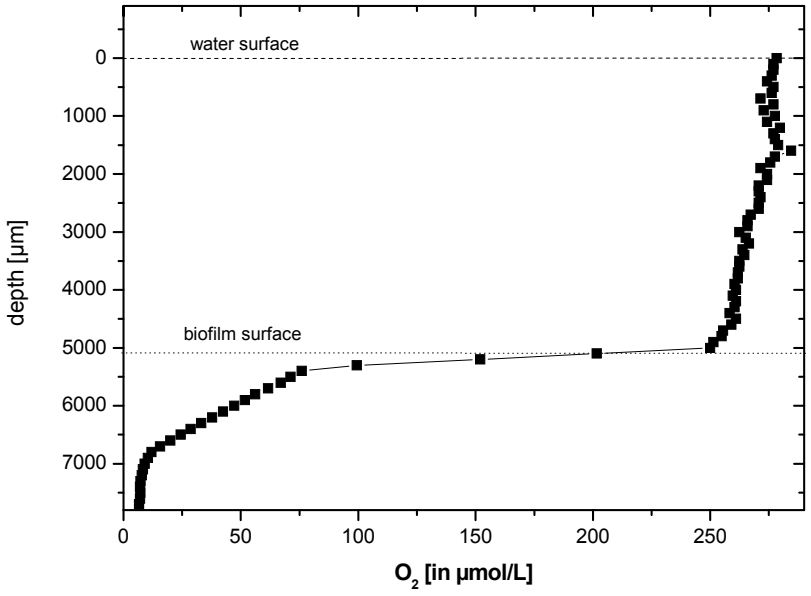

Figure 1: *O_2 concentration profile in a biofilm growing in a drainage channel of a flooded uranium mine in Saxony (Germany) under acid conditions and in the presence of uranium concentrations of approximately $1x10^{-4}$ M. Shown are the averaged oxygen concentrations. The increments of each microelectrode movement during the measurements were 50 µm.*

References

Krawczyk-Bärsch, E. , Grossmann, K., Arnold, T., Hofmann, S., Wobus, A. (2008). Influence of uranium(VI) on the metabolic activity of stable multispecies biofilms studies by oxygen microsensors and fluorescence microscopy. Geochimica et Cosmochimica Acta 72, 5251–5265

WORK PACKAGE 5: REDOX PROCESSES IN RADIONUCLIDE MIGRATION

Juhani Suksi[1], Torsten Schaefer[2], Károly Lázár[3], Ioannis Paschalidis[4], Sebastien Savoye[5], and Stepan Kalmykov[6]

[1] University of Helsinki, Department of Chemistry, Laboratory of Radiochemistry, Finland

[2]KIT-INE, Germany

[3]Institute of Isotopes, HAS, Hungary

[4]University of Cyprus, Department of Chemistry, Cyprus

[5]Atomic Energy Commission, CEA, France

[6] Lomonosov Moscow State University, Russia

Introduction

The objective of WP5 is the determination of redox impact on radionuclide transport. The objective is approached by studying the behavior of relevant redox-sensitive radionuclides in water-rock interaction in different redox-milieux that can be met around planned waste repositories. Radionuclide behavior is studied in carefully controlled laboratory conditions and retrospectively using observations from site, field and natural analogue studies. Investigations are performed in simulated near-field/far-field interface and in far-field conditions at planned repository sites in Finland and Sweden and contaminated sites in Russia and Cyprus. An important tool in our approaches is radionuclide redox-speciation which is carried out with various spectroscopic techniques, wet chemical methods and modeling.

Activities so far have been mainly on preparative measures including reviews of early studies, construction and testing of new experimental designs, sampling campaigns and negotiations of collaborations within and between different WPs. The state-of-the-art of WP5 and future plans were presented by the partners in the 1st ReCoSy AWS in Barcelona. All 1st AWS presentations are available in the ReCoSy home page. Furthermore, a S+T publication has been submitted by II-HAS. WP5 leadership was transferred from CEA to University of Helsinki (UH). In the following a summary of the partners' activities in 2008 is given.

Work performed and to be performed by partners

KIT-INE has conducted batch type experiments to study the sorption of radionuclides during the interaction of Febex bentonite colloids and fracture filling materials from Äspö Hard Rock Laboratory and Grimsel. Experiments have been conducted using a cocktail of radionuclides spiked to Febex bentonite colloids containing natural groundwater from Grimsel. U(VI), Tc(VII) and Np(V) are not colloidal associated in contrast to the tri- and tetravalent radionuclides Th(IV), Pu(IV) and Am(III) which are clearly sorbed to colloids. The last mentioned elements show reversibility kinetics which starts at about 100h after beginning of the experiments. In the case of Np-237 the decrease in concentration could be explained by both sorption to the fracture filling material which should onset much earlier and/or, more likely, by reduction to Np(IV) which is thermodynamically reasonable under the experimental E_h/pH conditions.

Three migration experiments using a bore core from the Äspö HRL equilibrated with Grimsel groundwater to simulate glacial melt water intrusion were conducted. Under a flow velocity of 50µL min^{-1} an unretarded breakthrough both for HTO and Tc(VII) could be observed. For the colloid associated tri- and tetravalent radionuclides, Th, Pu and Am, no breakthrough was detected within the experimental duration, although the groundwater conditions are assumed to be unfavourable for colloid attachment. Np shows a slightly retarded breakthrough exhibiting a distinct tailing which indicates a strong interaction with the fracture material. The reproducibility of the experiments have been proved providing confidence in the experimental set-up. The analysis of the complete set of radionuclides present in the injected cocktail are in progress. Further migration experiments are underway applying near natural flow velocities (~1 mL d^{-1}). Post mortem analysis of the used core will be made after the end of the planned experimental program.

CEA has started investigations on diffusive behaviour of redox sensitive actinides (U) and long-lived fission products (Se, I) through Callovo-Oxfordian (CO_x) argillite samples. This hard-clay rock can be considered as a redox active component according to the presence of the mineralogical buffer defined by FeS_2/FeOOH/$FeCO_3$. Redox impact is studied with diffusion experiments in specifically designed diffusion cell. Special care is given to the aqueous speciation (HPLC, EC and TRLIF). The distribution of each species in the rock, i.e. Se, I and U solid profiles, will be studied using µ-LIBS and EXAFS techniques. The study is divided along with different initial redox states, namely Iodine (I-I and I+V), Selenium (Se+IV and Se+VI) and Uranium (U+VI). Concentration effects of each studied element will allow to determine the effective diffusion coefficient, porosity and Kd in the argillite rock samples. Se and I aqueous speciation representative CO_x porewater (high [SO_4^{2-}] and [Cl^-] measured by IC) has been made and diffusion cell tested for its chemical inertia. Other planned operations are under progress.

UH has continued investigations initiated during FUNMIG. The focus of UH's investigations is in the relationship of past redox-conditions and U behavior. U

immobilization history is studied in water-conducting fractures at Olkiluoto and Forsmark study sites and in Tertiary sediments at Ruprechtov natural analogue study site. A combination of different techniques is used. U series disequilibrium measurements are used to find samples where U has recently (within the last 100 ka) immobilized. Wet chemistry is used to study U oxidation states in immobilized U phases. In practice, U(IV) and U(VI) forms are dissolved simultaneously from sample material in anoxic conditions. Dissolution of U causes some iron dissolution which may disturb original redox-state of U. If U and iron in the solid phase are not in redox equilibrium the dissolved iron may modify the redox-state of U in the solution. This problem is of particular concern. From experimental point of view, fortunately, immobilised U phases are generally loosely bound and can be dissolved with chemically mildly extraction which significantly reduces dissolution of disturbing iron. We have studied the influence anoxic extraction with the mixture of 4.5 M HCl and 0.02 M HF and found in some cases disturbance due to iron. In extractions we use artificial U isotopes as redox-tracers (^{232,233,236}U) in the U(IV) and U(VI) forms to monitor possible changes in redox-conditions. The stability of redox-tracers has been studied by analysing their oxidation states as a function of time. The tracers have kept stable in extraction solution for much longer time than needed for extraction and loading the sample solution in anion exchange chromatographic column for U(IV) and U(VI) separation. U isotopes have been analysed by α-spectrometry. In the second project year investigations on sample disturbances are continued. As a new approach batch type experiments in near-natural anoxic conditions are used to mimic field observations.

II-HAS prepares investigations on the reduction driven retention of I, Tc and U in a redox gradient in clay rock. In the first stage the Boday Claystone samples are selected and analysed from the point of view of the presence and presumable accessibility of ferrous component, as the prospective partner in redox couples playing role in migration of radionuclides. The overwhelming part of the Boda Claystone Formation was formed under oxidative conditions – the existence and occurrence of ferrous component(s) in the samples cannot be expected unconditionally. In the first stage of our studies we analysed in what extent is this condition fulfilled.

Two types of claystone samples are analysed and the Fe^{2+} and Fe^{3+} containing mineral constituents are investigated in them by Mössbauer spectroscopy. In the first case samples from a borehole near to the surface are analysed. In this strata probably some secondary weathering processes have also taken place. Most of the iron is located in hematite, only a minor part of iron was found in ferrous state. These Fe^{2+} ions were located in layered clay minerals (either in chlorite or illite or in montmorrilonite). The second series of studied samples was taken from a deep borehole (1050 m depth). (The minerals in this site probably occur in their original, undisturbed form, without any secondary metamorphoses.) All the iron was found in ferrous state in some of these samples – the respective minerals were chlorite and pyrite.

In summary, both types of samples contain Fe^{2+}, thus both of them can be considered as perspective host media for studying the redox processes taking place in radionuclide migration. This analysis of the Boda Claystone samples is also a part of the work planned in WP3. Further details can be found in the S+T paper in this Appendix.

UCYPRUS performs field and laboratory measurements in phosphogypsum stack solutions of different composition (e.g., pH, salinity, TDS) by means of electrochemical and optical redox sensors. The redox conditions are correlated with the distribution and mobility of redox sensitive radionuclides. During the first project year phosphogypsum and stack fluid samples have been collected from three different sub-areas of the phosphogypsum stack. The solid samples have been investigated by TGA, XRF and XRD regarding their water content and composition. The stack fluids have been analyzed regarding pH, EC, Eh, the main constituents and uranium concentration in solution.

MSU has investigated actinide speciation in samples collected at contaminated sites in Russia to verify the experimental data obtained under well-defined laboratory conditions. New sampling campaign with careful geochemical site characterization including bacteria was carried out in Karachay Lake in summer 2008. The methods included (1) redox speciation of actinides by spectroscopic methods (XPS, XAFS) and membrane extraction, (2) study of possibility of formation of An(IV) eigencolloids by alpha track analysis, TEM, STEM-HAADF, EELS and XAFS and their evolution upon redox transformations, dilution, changes of pH, Eh, ionic strength, interaction with NOM, (3) study of preferential binding of actinides to different colloids by nano-SIMS and their redox speciation by membrane extraction.

WORKPACKAGE 6: REDOX PROCESSES AFFECTING THE SPENT FUEL SOURCE-TERM

Detlef H. Wegen[1*], Paul Carbol[1], Alice Seibert[1], Mats Jonsson[2] et al, Andreas Loida[3] et al., Daqing Cui[4], Antonín Vokál[5] et al.

[1] Institute for Transuranium Elements (DE)

[2] KTH Chemical Science and Engineering, Nuclear Chemistry, Royal Institute of Technology, (SE)

[3] Institut für Nukleare Entsorgung, KIT, Campus Nord, Herrmann-von-Helmholtz-Platz 1, 76344 Eggenstein-Leopoldshafen, Germany

[4]Studsvik Nuclear AB, (SE)

[5] Nuclear Research Institute Řež plc (CZ)

* Corresponding author: Detlef.Wegen@ec.europa.eu

Introduction

The source term from spent fuel dissolution is subject to considerable uncertainties, both with respect to the presence and extent of oxidative dissolution processes of the spent fuel itself and the coupling with processes associated with the iron canister. Related problems to be examined in this work package are the representativeness and reliability of laboratory data with respect to the impact of unavoidable minor concentrations of oxygen also in inert-gas boxes used, the potential reactivity and its outcome of hydrogen from container corrosion in combination with high burn-up spent fuel, possible galvanic coupling of spent fuel and container material and the retention of redox sensitive radionuclides by relevant minerals, especially by steel container corrosion products.

A set of investigations has been conducted with the aim of getting better insight into redox processes determining spent fuel and iron canister corrosion. The investigations include galvanic coupling of spent fuel and waste canister components as well as spent high burn-up fuel corrosion/dissolution under high temperatures and hydrogen pressures.

A specific aspect is the use of uranium thin films allowing coupling with the high-end analytical methods available through the project in order to gain the desired process understanding for uranium dissolution and the relation to redox processes.

Another field of investigation is the corrosion and redox response behaviour of Fe with different pre-treatments and different conditions, including high radiation fields.

In particular, redox-based retention properties of corroded iron phases with respect to dissolved radionuclides are investigated.

Advances within the work packages

Corrosion of spent fuel in presence of corroding Fe

For galvanic coupling experiments ITU has prepared electrodes using the carbon steel ST37-2. Three types with surface areas of 0.13, 0.5 and 2 cm^2 has been prepared and the steel composition was analysed.

Slices from a UO_2 pellet were cut to act as electrodes. Stoichiometric UO_2 has a low electric conductivity at room temperature which results in a high ohmic resistance for UO_2 electrodes. A high ohmic resistance of electrodes in galvanic coupling experiments is a potential source for uncertainties and should be avoided. To achieve this goal the UO_2 was slightly oxidised in a CO/CO_2 gas mixture to approximately $UO_{2.02}$. For further experiments also simfuel electrodes simulating a burn-up of 3% - 8% were prepared. These electrodes have due to their content of metallic inclusions a lower resistivity.

Corrosion of spent fuel in presence of H_2

ITU has started corrosion experiments on the high burn-up structure zone of commercial spent nuclear fuel in presence of 4.1 MPa hydrogen gas pressure. The burn-up at this zone was determined to be 67 MWd/kg HM and the inventory was calculated. Leaching results were obtained for the first 60 days. More details are given below.

Preparation of the autoclave in the hot cell

A 600 cm^3 titanium autoclave (Parr Instruments Co, USA) was modified for work on active material and hot cell manipulation. The entire setup, i.e., the autoclave itself, valves, tubing, magnetic stirrer, was manufactured of quality grade II-weldable titanium (99.3 wt-% Ti, 0.3 wt-% Fe, and trace elements C, N, O and H). To avoid titanium abrasion due to stirring, the Ti-coated magnetic stirrer was placed in a small PEEK cup. Graphite seals and gaskets were used for all connections, to avoid foreign metal surfaces.

The setup was equipped with electrical and mechanical pressure gauges, electrochemical sensors for measurement of oxygen and hydrogen concentrations, possibilities for gas and solution sampling, and with an in-stream Eh-sensor for redox potential measurement during sampling. The setup allows filling, purging and sampling of solutions and gases, without intrusion of external air oxygen into the autoclave, and was certified for H_2-pressures up to 60 bars. A schematic of the setup and a picture of the autoclave are shown in Fig. 1 (a-b).

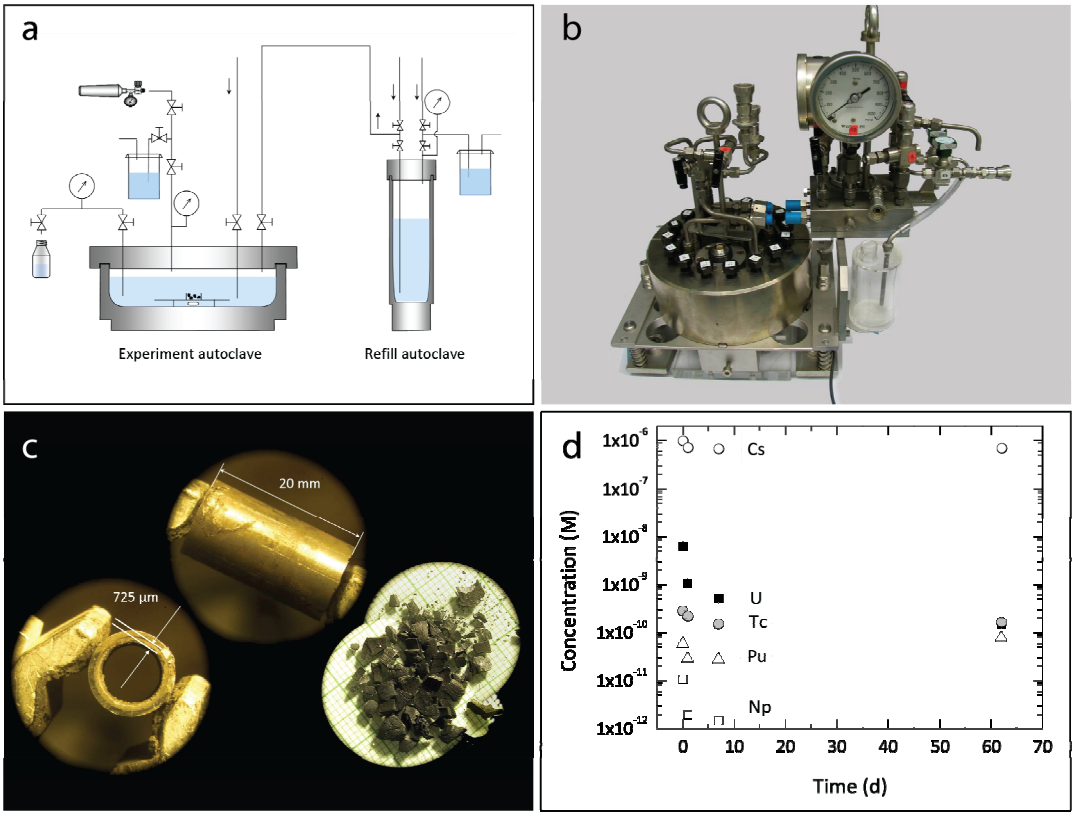

Figure 1: a. *Schematic of the autoclave setup;* ***b.*** *photo of the autoclave, before hot cell introduction;* ***c.*** *photo of the fuel (top: cut segment, left: core drilled fuel, right: rim structure containing fuel fragments);* ***d.*** *concentration of Tc (●), Cs (○), U (■), Np (□) and Pu (Δ) and as a function of corrosion time. Cs errors are within point diameters (±4%), Np errors are large due to the low concentration (estimated to ±100%).*

Preparation and inventory determination of the fuel

A high burn-up UO_2 fuel rod irradiated under normal conditions (without ramping) in a pressurized water reactor to an average burn-up of 59.1 MWd/(kg HM) was used for the experiment. The rod was cut into 20 mm long segments. The segment was drilled with a core drill to separate the centre of the pellet from its radial periphery, in order to single out the rim-structure containing outer part of the fuel, see Fig. 1 (c). The rim containing part was detached from the Zircaloy cladding. The thickness of the rim-containing part resulting from the drilling was 725 µm, while the thickness of the rim-structure was approximately 75-100 µm. The de-cladded fuel fragments (~millimetre-sized) were stored under dry N_2 atmosphere during one year before the start of the corrosion experiment. Of those fragments, 20 pieces, with a total mass of 0.26 gram, were selected for the corrosion study. The surface to volume ratio at the experiment start was approximately 0.2 m^{-1}.

Some fuel fragments were used for total dissolution with subsequent ICP-MS analysis to determine the content of actinides, lanthanides and lighter fission products. The U, Pu and Cs vectors together with the ^{148}Nd and the in-pile history were used as input into the ORIGEN code calculation to obtain the complete fuel inventory. After some iteration it could be settled that the average burn-up for this fuel fraction, of the

outer 750 µm of the 16N03 fuel pin, was 67 MWd/kg HM. The fuel inventory after end of irradiation and on the reference day 2008-07-07 was determined.

Corrosion experiment

The experiment was carried out in a simplified groundwater consisting of 10 mM NaCl (suprapur, Merck) and 2 mM $NaHCO_3$ (suprapur, Merck) dissolved in ultra pure Milli-Q H_2O (>18 MΩ/m, UHQ ELGASTAR). The pH of the initial solution, 8.1, was measured with a combined KCl pH-electrode (WTW SenTic Mic, and WTW pH340/ION analysator). Gas was supplied to the autoclave in welded tubes from a gas bottle. The experiment was run under 4.1 MPa pure H_2 gas (grade 6.0, Linde GmbH) corresponding to 33 mM dissolved H_2.

The initial result is shown in Fig. 1 (d). It can be seen that a pre-oxidised fuel layer was dissolved during the first day. A fast instant release of Cs from the fuel fragments resulted in an instantaneous Cs concentration of $9.7 \cdot 10^{-7}$ M in the first leachate. The subsequent leachates contained lower Cs concentrations as a result of additional filling of the autoclave. The amount of dissolved Cs remained constant at a level of $3.76 \cdot 10^{-7}$ mol during the time period of 7-62 days. On the other hand, the concentration of U in the leachate decreases by a factor of 40, from $6.3 \cdot 10^{-9}$ M to $1.5 \cdot 10^{-10}$ M, during the initial 62 days.

Neptunium was measurable above the detection limit ($1 \cdot 10^{-12}$ M) only during the initial 7 days. The Np concentration is well correlated with the changes in U concentration and the ratio between the concentrations is close to the average inventory of the rim containing fraction of the fuel. Plutonium was congruently dissolved with U at the beginning of the corrosion experiment. The Pu/U ratio in the leachate was close to the Pu/U ratio in the fuel fragments. After this initial dissolution, the almost parallel decrease in Pu and U concentrations indicate a chemical co-reduction of U and Pu. After the co-reduction phase, the Pu concentration passes through a minimum and then starts to increase towards a concentration of $\sim 7 \cdot 10^{-11}$ M. Technetium was found at a relatively stable concentration range between $1 \cdot 10^{-10}$ to $4 \cdot 10^{-10}$ M. It is known that Tc exists in different solid solutions in the fuel, e.g. metal alloy particles, high burn-up structure rim material and in the fuel matrix, and is solubility limited in the system by one of these phases.

Fuel corrosion studies on thin film model systems

ITU has prepared thin films of actinide oxides by sputter deposition from an actinide metal target in the presence of O_2, which can serve as model system for spent nuclear fuel.

In a first step the sputter co-deposition from U and Pd metal targets in presence of O_2 was tested for the production of UO_2/Pd thin films. The variation of the target current (of both targets) and of the O_2 partial pressure provides for the control of the Pd-content of the compound film and the oxidation state of the uranium.

First results for depositions at room temperature clearly show that the sputter technique allows the production of $UO_{2(+x)}$ films with imbedded Pd. Different U/Pd compositions ranging from 2-70 % Pd-content were produced and characterised by X-

ray photoemission spectroscopy (XPS), X-ray diffraction (XRD), Scanning electron microscopy with energy dispersive X-ray emission analysis (SEM-EDX) and AFM. The XPS results provide for the elemental composition (U/Pd ratios) calculated from U-4f and Pd-3d core level lines as well as for the stoichiometry of the uranium oxide (from U-4f and O-1s lines). Films with compositions from UO_2 to UO_{2+x} ($x < 0.33$) were produced. The XPS spectra (Pd-3d levels) also gave rise to the conclusion that the Pd is in an oxidized form. This is ascribed to the sputter deposition process itself as here the thermal quenching of the film constituting atoms on the cold substrate can lead to metastable solid compounds. SEM-EDX analysis of the samples showed, that Pd and U are homogeneously distributed throughout entire film. XRD measurements show for all the UO_2/Pd compound films (≤ 30 % Pd) the typical UO_2 reflexes (cubic fluorite lattice). An increase of the Pd concentration resulted in the decrease of the UO_2 reflex intensity together with a slight shift of $\Delta 2\,\Theta = \sim 0.2$ °, but reflexes, which could be attributed to a metallic Pd-phase, were not detected. Only the sample with the highest Pd concentration highest (~ 70%) showed, instead of the UO_2 related reflexes, only one reflexes ~ 40.3 ° which was attributed to the (420) reflex of Pd metal.

Heating of such mixed UO_2-Pd films resulted in an enhanced diffusion of the film components, which at moderate temperatures (~ 200°C) resulted in the formation of Pd metal agglomerates. These agglomerates were easily identified by SEM-EDX and AFM measurements. Compared to results from literature (Cui et al., 2004) the Pd agglomerates resemble well ε-particles in spent fuel. The film characteristics are reported in detail in the S&T contribution section of the 1st Annual Workshop Proceedings 7th EC FP - Recosy CP 2009 (S. Stumpf et al., "*THIN FILMS AS SPENT FUEL MODELS*").

The investigations showed that the thin film technique is well suitable for the preparation of model systems for spent nuclear fuel. A reproducible production scheme for UO_2/Pd thin film electrodes was set up. In a next step surface corrosion processes will be investigated by electrochemical methods on these electrodes.

Combined effect of metallic inclusions and rare earth doping on the oxidative dissolution of UO_2. Preliminary results.

Mechanistic conclusions are difficult to draw from experiments on spent nuclear fuel, as a result of its inherent complexity. Therefore UO_2 systems with and without additives have been used by KTH to quantitatively and qualitatively elucidate the elementary processes involved. Generally, additives can be classified into two groups according to their solubility in the UO_2 matrix,

1. Elements that build up separate phases due to their low solubility
2. Soluble elements that substitute uranium in the matrix.

In our work, Pd has been used as a model substance for the metallic ε-phase metal particles and Y_2O_3 for elements that substitute uranium.

At KTH experiments with 0.3 wt-% Y_2O_3 and/or 0.1 wt-% Pd have been performed in H_2O_2 (Trummer and Jonsson, 201X) (Figure 2). It can be seen that the dissolution rate at 1 bar H_2 atmosphere is lower than under N_2 atmosphere. For a UO_2

pellet doped with only Pd, the oxidative dissolution rate is higher than for the pure UO_2 pellet, as expected. The pellets doped with Y_2O_3 display a significantly lower dissolution rate under N_2 and H_2 atmosphere. The rationale for this is probably that Y_2O_3 doping of UO_2 alters the redox properties of the matrix.

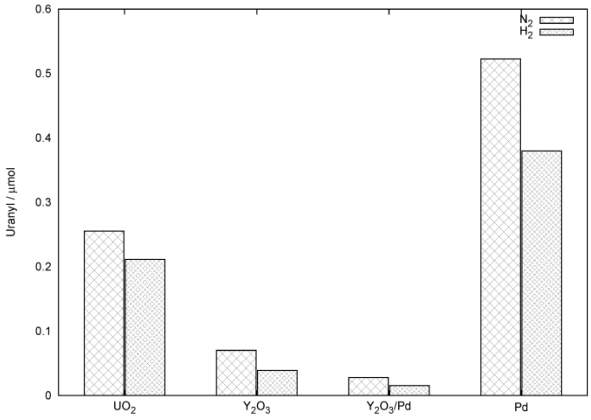

Figure 2: *Uranyl dissolution under N_2 and 1 bar H_2 atmosphere with Y_2O_3 and Pd as additives.*

Reductive Trapping of Actinides in Container Corrosion Products during Spent Fuel Corrosion

With respect to the assessment of the long-term behaviour of the waste form spent nuclear fuel, it is of high importance to study the fuel alteration resulting from the contact with groundwater in presence of Fe based container material, or its corrosion products, respectively. Performance assessment of spent nuclear fuel disposal requires careful quantification of its long-term ability to re-immobilize individual radioelements. This may be achieved either by retention upon the surfaces of the solid phases, which are present in the system, or incorporation in newly formed secondary phases. Related research comprises analyses of the (geo)chemical interactions of spent fuel with aqueous solutions (groundwater, brine), host rocks and near field components.

Various experimental data on the dissolution behaviour of the spent fuel matrix itself and in some cases in presence of container material (initial metallic Fe powder) as well, and the associated releases of radioelements were already obtained by extensive laboratory test programs and reported e.g. in Shoesmith, D.W. (2000), Ferry et al., (2005), Loida et al. (1996). However, only minor amount of knowledge is available on the extent and nature of radionuclide retention immediately after their mobilization from the fuel inventory in the course of long-term corrosion.

Thus, in the frame of this work INE studies the effect of the presence of magnetite (Fe_3O_4), representing the most important container corrosion product on the overall alteration behaviour of high burn-up spent fuel in highly concentrated salt brine, over a long-term period of time. Special attention will be directed on the fate of radionuclides released from the fuel inventory. In this context issues are addressed to the fraction of radionuclides mobilized from the fuel inventory (1) either released into solution, or (2) re-immobilized by various processes upon the surfaces of the solid phases in the system. Processes under consideration are sorption upon the fuel sample itself, upon the magnetite or the vessel wall, or incorporation in the crystal lattice of

newly formed secondary phases. A further question is related on the impact of Fe corrosion products on the dissolution rate of the fuel matrix, because magnetite is known to sorb uranium, the main constituent of spent fuel, at a high extent. This may possibly result in an accelerated dissolution of the fuel matrix ("pump effect").

As an experimental approach, INE investigates the alteration behaviour of a spent fuel pellet (50 MWd/kgHM) in presence of magnetite granulate (Ø about 5 µm) in 5M NaCl brine under anoxic conditions over a "long-term" period of time. We will terminate the related corrosion experiment, which is running presently over totally 9.3 years, where the duration of the last sampling interval will have been reached a duration of about 4.4 years. To determine the reaction progress both, the gas phase and the solution will be analyzed with respect to hydrogen, oxygen and released radionuclides. Special attention will be directed on the retention of radionuclides upon the solid phases. Studies aiming on their identification and characterization will be performed by means of "in-situ" Raman spectroscopy, directly upon the corroded spent fuel sample. The suitability of Raman spectroscopy in particular to study uranium bearing solid phases was recently described by Amme et al. (2002). SEM/EDS-techniques and XRD will be applied for Fe-corrosion products and small particles removed from the fuel surface. To determine the amount of actinides retained on the corroded magnetite in the course of brine contact, a part of it will be dissolved in concentrated nitric acid, and afterwards analyzed radiochemically. Moreover, the amount of radionuclides sorbed upon the surface of the vessel wall will be identified by stripping the vessel with concentrated nitric acid and subsequent radiochemical analyze.

During the initial phase of this project, INE performed general preparations in our hot cells, related to terminate the long-term spent fuel corrosion experiment in presence of magnetite in 5M NaCl solution. This is foreseen within the first half of 2009, when the total corrosion time will have been reached almost 10 years in total. The termination of the experiments will comprise analysis of the released fission gases and radiolysis gases hydrogen and oxygen, radiochemical analysis of the solution with attention on the possible formation of colloids and detailed studies of the solid phases present in the system.

In the frame of preparation solid phase investigations strong emphasis was put on establishing the Raman probe inside of the hot cell, allowing "in-situ" Raman measurements upon the surfaces of the corroded spent fuel sample and the added magnetite as well. The concept is to operate the Raman probe in association with an optical microscope and a micromanipulator. Both equipments are already installed and are used for preparation works with "hot" sample material in the hot cell. Thus, a holder for the Raman probe was designed and fabricated, to enable its fixation with the micromanipulator in such a way that the required Raman measuring conditions will be fulfilled. These comprise that the focusing distance of 17 mm between the sample and the lens of the Raman probe can always be achieved by adjusting the micromanipulator control, and that the angle between the microscope axis and of the Raman probe axis does not deviate significantly from 90°. It has to be assured that the emitted laser spot is fully visible upon the area of interest to be measured by means of the microscope.

To enable the cable connection between the Raman probe inside of the hot cell and the Raman measuring equipment in the service gangway a plug, containing a cable channel was established. The optical fibres were feed through this channel inside the plug. The entrance into the channel was sealed by a tube elbow, accommodating the optical fibres. Additionally, the remaining voidage of this tube elbow was filled with

araldite to avoid the migration of radioactivity outside the hot cell, thus to prevent a contamination of the service gangway in the non radioactive area.

First results from the long-term corrosion experiment with spent fuel pellet in 5M NaCl solution in presence of magnetite are expected in the middle of 2009.

The reductive immobilization of ^{237}Np on iron canister material under repository conditions

In the reporting period ICP-MS, SEM-EDS, and Micro-XAS analysis data were evaluated. The major observations made in this work are:

- Np(V) and Pu(VI) in carbonate containing groundwater solution can be effectively immobilized by iron canister material. Pre-corroded iron surface with Fe_3O_4 layer is more reactive than polished iron surface to immobilize Np(V) and Pu(VI)
- SEM-EDS analysis shows that 7 -8 μm Np rich (>50% Np 10% Si and 20% Fe) layer precipitated on the Fe_3O_4 layer.
- The preliminary result of EXAFS analysis suggests that Np(V) in solution can be, at least partially, reduced to Np(IV) and precipitated on the top of corroded iron surface (with Fe_3O_4).

Detailed information is reported in the S&T contribution section of the 1st Annual Workshop Proceedings 7th EC FP - Recosy CP 2009 (D. Cui et al., "*The reductive immobilization of ^{237}Np and ^{239}Pu on iron canister under repository conditions*").

The effect of iron corrosion on conditions inside waste packages

It is well known that both iron species have a strong influence on spent fuel corrosion rates, no detailed effort was devoted, however, to the effect of iron species on conditions that will evolve inside waste packages, primarily on the effect of iron corrosion on Eh development, which to a great extent controls spent fuel dissolution. The main aim of the work at NRI is to measure Eh in simplified systems simulating the conditions inside waste packages and the effect of iron corrosion on Eh development inside waste packages after ingression of groundwater.

The first system that simulated the environment inside a waste package after the ingression of water consisted of a closed vessel with synthetic bentonite porewater and electrodes and with and without 5 g of iron powder. Synthetic bentonite pore water corresponding to the composition of sodium bentonite Volclay KWK 20-80 of a density of 1600 $kg \cdot m^{-3}$ was prepared. Pt, Au and standard commercial silver chloride RE 403 (Theta 90) electrodes were used for Eh measurements. An electrochemical noise measurement system with three electrodes, two iron electrodes and one reference electrode were used to measure corrosion potentials. Before the electrodes were immersed in the corrosion cell, the cell was purged by nitrogen for 30 minutes. An ECM 8 Electrochemical Multiplexer Analyser with evaluation software ESA 400

Electrochemical Signal Analyser version 2.01 from Gamry Instruments was used to evaluate the results. The experiments were carried at various temperatures controlled by a TDC 2 Temperature Controller with a Watlow series 988 PID control unit.

In the second system, instead of iron powder, 10 carbon steel plates were immersed in approximately 2 l of synthetic bentonite water solution. The corrosion rates were continuously measured by measuring hydrogen evolution through volume changes and by measuring the weight of the carbon steel plates after the experiments. Eh was measured by Pt and Au electrodes. The experiments lasted 30 days. Under these conditions, commercial reference electrodes could not be used because of the significant changes of electrolytes inside the electrodes. A special reference electrode had to be prepared by coating Ag wire with silver chloride.

It was found that the Eh of bentonite water decreases considerably in the system with iron powder after a very short time to values of approximately – 600 mV against standard hydrogen electrode. These low values of Eh in a system with iron did not change over time. The results of the measurements of the corrosion potentials of iron, which represent potentials at which the rates of anodic half-cell reaction of iron corrosion and cathodic half-cell reaction of water reduction will be equal, are significantly affected by a change of Eh. At 50 °C and 60 °C the corrosion potentials of iron are increased significantly in the presence of iron powder, but at 70 °C the corrosion potentials of iron decrease in a system with iron powder over time and increase in the system without iron powder. The decrease of Eh at 50 and 60 °C by adding iron to the system led presumably to a decrease in the rate of anodic reaction so that the corrosion potential settled at a higher value at which the rates of anodic and cathodic reactions will be equal. It appears that at 70 °C an increase of corrosion potentials of electrodes in water without iron is caused by the fact that at this temperature oxygen penetrates more easily to the vessel and more efficient cathodic reactions with oxygen are applied. A decrease of corrosion potentials in the system with iron powder suggests that at 70 °C the rate of anodic reaction increases with temperature and accordingly increases the rate of cathodic reaction.

In the second experimental system 10 carbon steel plates were added in reaction vessel instead of iron powder. In these experiments, the corrosion rates of carbon steel plates were continuously measured using measurements of the amount of hydrogen evolution generated. It was found that the corrosion rate decreased from initial values of approximately 34 μm/yr to values of approximately 1 μm/yr after 10 days of corrosion. The average corrosion rate from the measurements of the weight loss of 10 carbon steel plates after 30 days was 3.7 ± 0.5 μm/yr in the first experiment and 5.2 ± 0.7 μm/yr in the second experiment. Eh decreased during first day of the experiment to values lower than –400 mV, but then started to increase and after several days stabilized at positive values of approximately 200 mV. We assumed that corrosion products covering the electrodes caused this increase. Therefore a special device enabling Eh to be measured discontinuously by pumping a small amount of water from the reaction vessel for measurement with a clean Pt electrode was developed for a second experiment under otherwise the same conditions as in the first experiment. The Eh values obtained by discontinuous measurements with clean electrodes measured after some time of corrosion were much lower than the values obtained with electrodes immersed in the solution. Nevertheless, the results of Eh measured with clean electrodes after some time were higher than the initial values of Eh after measuring in the first days of corrosion. This could be caused by the penetration of oxygen in the closed reaction vessel despite

an overpressure of hydrogen in the vessel. The discontinuous measurements also enabled pH to be measured. It was observed that pH decreased from the initial values of approximately 8.6 to values of approximately 7.3 after 15 days. This is probably caused by hydrolysis of iron ions

It was confirmed that in long-term experiments, iron corrosion products affect continuous measurements of Eh with Pt or Au electrodes in a system with iron, which is manifested by an apparent increase of Eh after the first days of corrosion. But this increase in Eh did not disappear at all if the measurements were performed discontinuously with clean electrodes. This indicates that oxygen could diffuse slowly in reaction vessels. Therefore further experiments are now being prepared using an anaerobic box with a concentration of oxygen below 0.1 ppm. A detailed discussion of the experiments is given in the 1st Annual Workshop Proceedings 7th EC FP - Recosy CP 2009 (D. Dobrev et al., "*THE EFFECT OF IRON CORROSION ON CONDITIONS INSIDE WASTE PACKAGES*").

References

Amme M., Renker B., Schmid B., Feth M.P., Bertagnolli H., Döbelin W. (2002): Raman microspectrometric identification of corrosion products formed on UO_2 nuclear fuel during leaching experiments, J. Nucl. Mater. 306 (2002) 202-212

Cui D., Low J., Sjöstedt C.J., Spahiu K. (2004): On Mo-Ru-Tc-Pd-Rh-Te alloy particles extracted from spent fuel and their leaching behavior under Ar and H_2 atmospheres, Radiochim. Acta 92, 551-555

Ferry C., Poinssot C., Broudique V., Cappelaere C, Desgranges L., Garcia,P., Jegou C., Lovera P., Marimbeau P., Piron J.P., Poulesquen A., Roudil D., Gras J.-M., Bouffioux P. (2005): Synthesis of the Spent Fuel Long-Term Evolution, Rapport CEA-R-6084

Loida A.; Grambow B.; Geckeis H. (1996): Anoxic corrosion of various high burnup spent fuel samples. J. Nucl. Mater. 238, 11-22

Trummer,M, Jonsson, M. (201X), To be published

Shoesmith, D.W. (2000): Fuel corrosion processes under waste disposal conditions, J. Nucl. Mater., 282, 1-31

S + T CONTRIBUTIONS

List of contributions

QUANTIFICATION OF THE REDOX POTENTIAL FOR THE REDUCTION OF Np(V) IN NON-COMPLEXING AQUEOUS SOLUTIONS AT pH 5 - 10

V. Neck[1], M. Altmaier[1], D. Fellhauer[1,2], J. Runke[1], Th. Fanghänel[2]

[1] Institut für Nukleare Entsorgung, KIT, Campus Nord, Herrmann-von-Helmholtz-Platz 1, 76344 Eggenstein-Leopoldshafen, Germany

[2] European Commission, JRC, Institute for Transuranium Elements, Karlsruhe, Germany

* Corresponding authors: marcus.altmaier@kit.edu

Abstract

The reduction of about $3.5 \cdot 10^{-5}$ M Np(V) solutions was investigated in the pH range 5 - 10 in 0.1 M NaCl at 22°C under Ar atmosphere. The results obtained for various reducing systems (homogeneous solutions with inorganic and organic reductants and heterogeneous suspensions containing Fe(II)/Fe(III) precipitates, magnetite Fe_3O_4(cr) or metallic iron powder) indicate that the redox potential of $E_h = 0.01 \pm 0.02$ V (pe = 0.15 ± 0.35) is a general border for the reduction of NpO_2^+(aq). Regardless of the reducing agent and whether the system is homogeneous or heterogeneous, Np(V) is found to be stable at $E_h \geq 0.03$ V (pe ≥ 0.5) and reduced to Np(IV) at $E_h \leq - 0.01$ V (pe ≤ - 0.2). The more negative the redox potential the faster is the reduction. The observed borderline for the reduction of Np(V) is about 0.35 V (6 pe-units) lower than calculated for the redox couple NpO_2^+(aq) / NpO_2(am, hyd) at $[Np]_{tot} = 3.5 \cdot 10^{-5}$ M. It does not refer to the reaction $NpO_2^+ + e^- \Leftrightarrow NpO_2$(am, hyd) but rather to an initial reduction step from NpO_2^+(aq) to $Np(OH)_4$(aq) or small polymers $Np_m(OH)_{4m}$(aq) which agglomerate to colloidal NpO_2(coll, hyd) particles with a high tendency towards sorption on the container walls or solid phases present in heterogeneous systems.

Introduction

In geochemical systems of nuclear waste repositories, the migration behaviour of neptunium depends primarily on its oxidation state, either +V or +IV. Under most conditions Np(V) is highly soluble and mobile whereas Np(IV) is very immobile because of its high tendency towards sorption and the low solubility of $10^{-(9\pm1)}$ M in the near-neutral pH range (Guillaumont et al., 2003). The reduction of Np(V) has been investigated in numerous studies, for instance in site-specific groundwater systems containing the reducing sediments (Lieser et al., 1988), humic substances (Zeh et al., 1999; Artinger et al., 2000) or dissolved iron and iron minerals (Cui and Eriksen, 1996;

Nakata et al., 2002 and 2004). However, the experimental observations are usually described phenomenologically. The goal of the present study is to explore whether there is a well-defined redox potential for the reduction of Np(V) in aqueous solution and to quantify the redox process in terms of thermodynamics. For this purpose we performed a systematic study on the reduction of $3.5 \cdot 10^{-5}$ M Np(V) solutions in the pH range 5 - 10 in non-complexing 0.1 M NaCl solutions under Ar atmosphere. To cover a wide range of chemically different reducing systems, the redox behaviour of Np(V) was studied in homogeneous solutions containing 1 - 2 mM inorganic and organic reductants and also in heterogeneous suspensions containing corresponding amounts of Fe(II)/Fe(III) precipitates, magnetite Fe_3O_4(cr) or metallic iron powder.

Experimental

The investigated neptunium samples with initial Np(V) concentrations in the range [Np(V)] = $(3.5 \pm 0.2) \cdot 10^{-5}$ M were prepared by adding 100 µl of 5.0 - 5.5 mM ^{237}Np(V) stock solutions (pH ≈ 4) to 15 ml 0.1 M NaCl pre-equilibrated with the following reducing agents (p.a. grade chemicals):

- $2 \cdot 10^{-3}$ M $Na_2S_2O_4$ (Merck); homogeneous solutions
- 10^{-3} M hydroquinone (Riedel de Haën); homogeneous solutions
- $1.6 \cdot 10^{-3}$ M sodium anthraquinone/anthrahydroquinone disulfonate; homogeneous solutions (AQDS/AH_2QDS = 3:1); oxidized form from Fluka; partly reduced with $Na_2S_2O_4$ at pH 11
- 20 mg Fe powder (Merck, grain size 10 µm); suspensions in 15 ml 0.1 M NaCl
- 10^{-3} M $FeCl_2$ / 10^{-4} M $FeCl_3$ (Alfa Aesar); Fe(II) dissolved (pH 5) / suspensions of Fe(III) and Fe(II) hydroxide precipitates at pH > 4 and pH > 8, respectively
- 35 mg Fe_3O_4(cr) (Alfa Aesar); suspensions in 15 ml 0.1 M NaCl

The pH values were adjusted with 0.1 M HCl (Merck) and 0.1 M NaOH (carbonate-free, Baker). In several samples pH was fixed at values in the ranges 5 - 6 and 8 - 9 by additions of redox-inert 0.01 M MES and TRIS buffers (Sigma), respectively, because many redox couples vary with pH. All solutions and suspensions were prepared with ultrapure deionized water and purged with Ar before they were used. The samples were prepared in polyethylene vials and stored at 22 ± 2°C in an argon glove box. The reduction process was monitored as a function of time by the decrease of the aqueous Np(V) concentration. After reaction times of 1 - 99 days, partly up to 335 days, the samples were analyzed for pH, E_h and Np concentration.

The Np concentrations were measured after ultrafiltration (Pall Life Sciences, 10 kD) by liquid scintillation counting of the ^{237}Np α-radiation and α/β-discrimination of the counts from the daughter nuclide ^{233}Pa (TriCarb 2500 TR/AB instrument, Canberra-Packard); detection limit: $10^{-8.3}$ M. In some of the samples which showed no or only slight reduction (Np(V) concentrations remaining above 10^{-5} M), the oxidation state of the dissolved Np was additionally confirmed by UV/Vis/NIR absorption spectroscopy using a Cary 5E spectrometer.

The values of pH = - log a_{H^+} (activity scale) were determined with combination pH electrodes (type ROSS, Orion) calibrated against standard buffers (pH 1 - 10, Merck). Redox potentials were measured with a combined Pt and Ag/AgCl reference electrode (Metrohm) calibrated against commercial redox-buffers (220 mV and 640 mV, Merck). The electrode response usually reached a steady reading after 5 - 10 minutes continuous stirring. For solutions containing redox buffers the redox potential is stable within an uncertainty less than ± 5 mV. In other samples the uncertainty is larger, and the reproducibility varies up to ± 30 mV in the 4 - 10 measurements after different time periods. The measured potential is converted into E_h versus the standard hydrogen electrode (SHE) by correction for the potential of the Ag/AgCl reference electrode. The apparent electron activity (pe = - log a_{e^-}) is calculated from E_h = - (RT/F) ln a_{e^-} according to the relation: pe = 16.9·E_h(V) at 25 °C.

Results and discussion

At first, the results obtained in the different redox systems are discussed separately and then all together to achieve a more general understanding of the reduction process Np(V) → Np(IV) in aqueous systems.

Sodium dithionite solutions

In 2 mM $Na_2S_2O_4$ solution at pH = 5.1 and pe = 0.5 ± 0.2 no reduction of Np(V) was observed while in another 2 mM $Na_2S_2O_4$ solution at pH = 8.2 and pe = - 7.1 ± 0.1 the initial Np(V) was completely reduced after one day.

Suspensions of Fe powder and Fe(II)-Fe(III) redox buffers

In all samples containing iron powder or Fe(II)-Fe(III) redox buffers at pH ≈ 8 the redox potentials were very low (pe values in the range - 2 to - 5) and more than 99 % of the Np(V) was reduced after one day. After 3 - 14 days the Np concentration measured after ultrafiltration was at or below the detection limit (log [Np] < - 8.3). In contrast to this, the samples containing 10^{-3} M $FeCl_2$ / 10^{-4} M $FeCl_3$ at pH = 5.3 showed positive E_h values (pe ≈ 4 - 5) and the Np(V) concentration did not decrease within the time of investigation.

AQDS/AH_2QDS redox buffer solutions and Gorleben groundwaters (GoHy)

Anthraquinone/anthrahydroquinone derivates are often used as well-defined model compounds to study the reducing properties of humic or fulvic substances. The redox behaviour of Np(V) in AQDS/AH_2QDS redox buffer solutions may therefore be compared with the results obtained by Zeh et al. (1999) and Artinger et al. (2000) for similar Np(V) concentrations in dilute Gorleben groundwaters where about 50 % of the initial Np(V) is complexed by carbonate and humic acid. In 1.6 mM AQDS/AH_2QDS (3:1) at pH = 9.4 and pe = - 4.0, the initial Np(V) is reduced within one day to a Np(V) concentration of $5 \cdot 10^{-8}$ M. In a corresponding AQDS/AH_2QDS solution at pH = 5.7 and pe = - 1.4 and also in Gorleben groundwaters at pH = 7.6, GoHy-2227 (pe = - 2.47) and GoHy-532 (pe = - 2.54), the reduction process is considerably slower. In GoHy-162 (pH = 7.9, pe = 0.56) no reduction was observed.

Hydroquinone solutions

In three 10^{-3} M hydroquinone solutions at pH 5.4, 8.2 and 8.8 the Np(V) concentration remained constant for 100 days. The redox potentials in these solutions were positive, with mean values of pe = 4.5 ± 0.3, 2.7 ± 0.3 and 1.7 ± 0.1, respectively. In a second set of samples at pH 5.4 (buffered with MES), and pH 8.2 (buffered with TRIS), the redox potentials were considerably lower. At pH = 5.4 and pe = 3.2 ± 0.4, Np(V) was also stable but at pH = 8.2 and pe = - 0.5 ± 0.3 a slow reduction of Np(V) was observed (about 25 % reduction after 100 days). The latter observation was reproduced in a third experiment at pH = 8.2 and pe = - 0.5 ± 0.5 (Fig. 1a). The higher pe values in the first set of samples is possibly due to a slight O_2 contamination that leads to the formation of quinone. According to the redox couple quinone / hydroquinone (with log K° = 23.65 for the reaction $C_6H_4O_2 + 2H^+ + 2e^- \Leftrightarrow C_6H_4(OH)_2$ (Rai et al., 1982)), the quinone concentration at pH = 8.2 and pe = 2.7 is about $1.4 \cdot 10^{-5}$ M (ca. 1 %). We assume that in the second set of samples the exclusion of oxygen was more successful; the quinone concentration calculated for pH = 8.2 and pe = - 0.5 is below 10^{-10} M. The different redox behaviour of Np(V) in 10^{-3} M hydroquinone solutions buffered with TRIS at pH 8.2 shows that not the hydroquinone (in both cases 1 mM) but the redox potential (different pe values) is decisive whether Np(V) is reduced or not.

Magnetite suspensions

The results obtained for magnetite suspensions are complicated by the simultaneous sorption of Np(V) (Nakata et al., 2002 and 2004). In order to minimize sorption of Np(V), we added a relatively small amount of magnetite (35 mg Fe_3O_4(cr) in 15 ml solution; corresponding to 0.01 mole Fe_3O_4(cr) per liter solution) compared to Nakata et al. (2002, 2004) (1 g Fe_3O_4(cr) in 40 - 50 ml solution, corresponding to 0.1 mole Fe_3O_4(cr) per liter solution). Nevertheless 10 - 15 % of the initial Np(V) concentration ([Np(V)]° = $3.4 \cdot 10^{-5}$ M) sorbed on the magnetite. This becomes evident from the comparison of the samples buffered with MES at pH = 5.3 and with TRIS at pH = 8.3 (Fig. 1b). In both samples the Np(V) concentration decreased about 10 % within the first 10 days. However, in the sample at pH = 5.3 and pe = 3.1 ± 0.5, the Np(V) concentration approached a constant level of $3.0 \cdot 10^{-5}$ M, whereas in the sample at pH = 8.3 and pe = - 0.2 ± 0.4, the Np(V) concentration decreased slowly but continuously to lower values. This further decrease of the Np(V) concentration is obviously caused by a very slow reduction to insoluble/sorbed Np(IV). These results indicate that not the presence of solid Fe_3O_4(cr) or the concentration of dissolved Fe^{2+} ions (at pH 8.3 the Fe^{2+} concentration is even lower than at pH 5.3) is decisive for the reduction of Np(V) but the slightly negative redox potential at higher pH. Unfortunately, in previous papers on the reduction and sorption of Np(V) in magnetite suspensions (Cui and Eriksen, 1996; Nakata et al., 2002 and 2004) redox potentials were not reported.

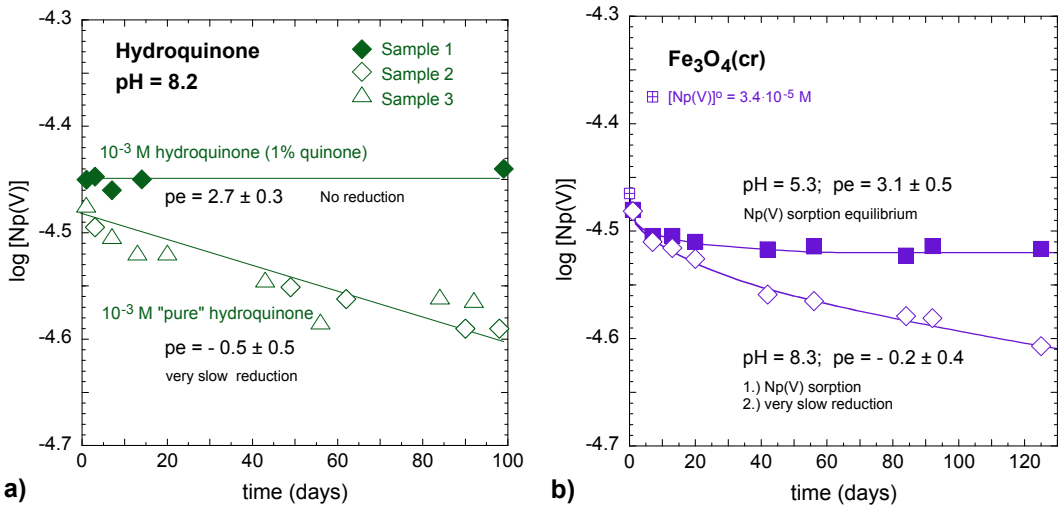

Figure 1: *Experimental studies on the reduction of Np(V), a) in 1mM hydroquinone solutions at pH = 8.2 (buffered with TRIS), b) in magnetite suspensions at pH = 5.3 (buffered with MES) and pH = 8.3 (buffered with TRIS).*

General interpretation of the thermodynamics, kinetics and mechanism of the reduction of Np(V) to Np(IV) in aqueous solutions

The results discussed above are summarized qualitatively in the pe-pH diagram shown in Fig. 2. Samples in which no reduction of Np(V) was observed are plotted as filled symbols, samples in which the initial Np(V) was reduced are plotted as open symbols. The thick dashed line in Fig. 2, at pe = 0.15 ± 0.35 (E_h = 0.01 ± 0.02 V), represents the borderline for the reduction of Np(V) under the given conditions. Reduction of Np(V) occurs in all solutions and suspensions with redox potentials below this line (pe ≤ - 0.2, E_h ≤ - 0.01 V), but not in any system with redox potentials above this line (pe ≥ 0.5, E_h ≥ 0.03 V). This general observation is independent of the reducing agent and whether the system is homogeneous or heterogeneous. Therefore, the observation that Np(V) is reduced in the presence of corroding iron powder or Fe(II)-bearing solid phases like $Fe(OH)_2$(s) or Fe_3O_4(cr) = $Fe^{II}(Fe^{III})_2O_4$(cr) does not necessarily mean that the reduction process is a surface reaction. Under the same redox conditions (pe and pH) in homogeneous solutions, Np(V) is reduced as well. Vice versa, above the borderline of pe = 0.15 ± 0.35, Np(V) is neither reduced by 10^{-3} M Fe^{2+} in solution nor in the investigated Fe_3O_4(cr) suspension at pH 5.

The reaction rate for the reduction of dissolved Np(V) ("pseudo" first order reaction with regard to NpO_2^+) also shows a pronounced dependence on pe. The more negative the redox potential the stronger is the thermodynamic driving force and the faster is the reduction (Table 1). The reduction rate decreases systematically when pe increases from strongly negative values to the borderline at pe = 0.15 ± 0.35. In systems at pe < - 3 the reduction is complete after one day, while in Gorleben groundwaters at pH = 7.6 and pe = - 2.5 and in AQDS/AH_2QDS solutions at pH = 5.7 and pe = - 1.4 the reduction process is considerably slower. In 10^{-3} M hydroquinone solutions at pe = - 0.5 ± 0.5 and the magnetite suspension at pe = - 0.2 ± 0.4, close to the borderline for the reduction of Np(V), the reduction process is extremely slow.

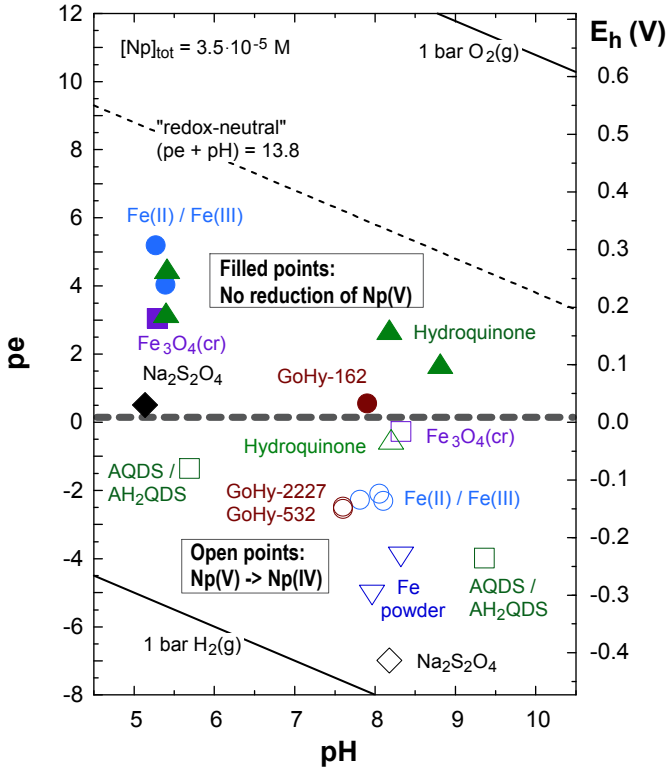

Figure 2: *Experimental studies on the reduction of Np(V) in 0.1 M NaCl (p.w.) and in dilute Gorleben groundwaters (GoHy) (Zeh et al., 1999; Artinger et al., 2000). In the systems shown as open symbols Np(V) is reduced to Np(IV), in the systems shown as filled symbols Np(V) is not reduced within the time of investigation (≥ 100 days).*

Table 1: *Reduction rates (half life times $t_{1/2}$) observed for $3.5 \cdot 10^{-5}$ M Np(V) solutions in various redox systems*

Various redox systems at pH 5 - 9	pe ≥ 0.5	No reduction observed [a]
Fe_3O_4 suspension at pH 8.3	pe = - 0.2 ± 0.4	$t_{1/2}$ = 460 d
1 mM hydroquinone, pH = 8.2	pe = - 0.5 ± 0.5	$t_{1/2}$ ≈ 300 d
2 mM AQDS/AH_2QDS, pH 5.7	pe = - 1.4	$t_{1/2}$ = 12 d [b]
GoHy groundwaters at pH 7.6	pe = - 2.5	$t_{1/2}$ = 2 d / 5 d
2 mM AQDS/AH_2QDS, pH 9.4	pe = - 4.0	$t_{1/2}$ = 0.1 d
Fe powder suspensions pH ≈ 8	pe = - 4.7 ± 0.7	very fast reduction [c]
2 mM $Na_2S_2O_4$, pH 8.2	pe = - 7.1 ± 0.1	very fast reduction [c]

[a] See systems shown in Fig. 2 as filled symbols.
[b] The mean value of seven experiments at initial Np(V) concentrations varying from $1.6 \cdot 10^{-7}$ M to $1.35 \cdot 10^{-4}$ M (Fig. 3) is $t_{1/2}$ = 17 ± 6 days.
[c] The complete reduction of Np(V) after 1 day, with [Np] < 10^{-8} M (detection limit), did not allow to calculate $t_{1/2}$ but only an upper limit of $t_{1/2}$ < 0.1 d.

The observed borderline for the reduction of Np(V) is much lower than predicted by a pe-pH diagram where the equilibrium line (50 % Np(V), 50 % Np(IV)) is calculated for the reaction:

$$NpO_2^+ + e^- \Leftrightarrow NpO_2(am, hyd)$$

with $\log K°_{V\text{-}IVs} = -\log([NpO_2^+]\cdot\gamma_{NpO2}+) + pe = 10.9 \pm 1.5$ (based on data selected in the NEA-TDB (Guillaumont et al., 2003)). For $[Np]_{tot} = 3.5\cdot10^{-5}$ M and pH 5 - 10 in 0.1 M NaCl, i.e., $\log[NpO_2^+] = \log\{[Np]_{tot}/2\} = -4.76$ and $\log\gamma_{NpO2+} = -0.10$ (calculated with the SIT according to Guillaumont et al., 2003), the borderline for the reduction of NpO_2^+(aq) to NpO_2(am, hyd) is calculated to be at pe = 6.0 ± 1.5. Accordingly Np(V) should be reduced in all systems investigated in the present study. However, the experimental results clearly show that the redox potential necessary for the reduction of Np(V) is much lower, about 6 pe-units (0.35 V). This may be explained by the small total amounts of 0.12 mg Np(V) in 15 ml 0.1 M NaCl, for which the reduction does not lead to solid NpO_2(am, hyd) precipitates as for higher Np concentrations but to colloidal oxyhydroxide particles, $Np_mO_p(OH)_{4m-2p}$(coll, hyd), in the following designated as "NpO_2(coll, hyd)". If the observed borderline at pe = 0.15 ± 0.35 is ascribed to an equilibrium between 50 % Np(V) and 50 % colloidal Np(IV) solid particles

$$NpO_2^+ + e^- \Leftrightarrow NpO_2(coll, hyd)$$

an equilibrium constant of $\log K°_{V\text{-}IVcoll} = -\log([NpO_2^+]\cdot\gamma_{NpO2+}) + pe = 5.0 \pm 0.4$ is obtained. This interpretation, i.e., treating NpO_2(coll, hyd) as small solid particles with a higher molar Gibbs energy than solid NpO_2(am, hyd) (c.f., discussion in Neck et al., 2007), implies that the pe value necessary for the reduction of Np(V) depends on the total Np concentration. To verify this dependence and to study a possible equilibration between NpO_2^+ and NpO_2(coll, hyd), two additional series of experiments were performed in AQDS/AH_2QDS (3:1) redox buffer solutions at constant pH = 5.7 and pe = - 1.4 and varying initial Np(V) concentration ($[Np(V)]° = 1.6\cdot10^{-7}$ to $1.35\cdot10^{-4}$ M). However, the corresponding Np(V) equilibrium concentration of $\log[NpO_2^+]_{eq} = -\log K°_{V\text{-}IVcoll} - \log\gamma_{NpO2+} + pe = -(5.0 \pm 0.4) + 0.1 - 1.4 = -6.3 \pm 0.4$ is not achieved. The reduction of Np(V) proceeds down to concentrations at or below the detection limit of $10^{-8.3}$ M, even for initial Np(V) concentration below the NpO_2^+ concentration expected in equilibrium with NpO_2(coll, hyd) (Fig. 3). The reduction of Np(V) is probably a more complex process including consecutive and/or parallel reactions:

$$NpO_2^+ + 2\,H_2O + e^- \Leftrightarrow \{Np(OH)_4(aq)\} \rightarrow Np_m(OH)_{4m}(aq)$$
$$\rightarrow Np_m(OH)_{4m}(sorbed), NpO_2(coll, hyd)$$

For initial Np(V) concentrations of 10^{-7} - 10^{-4} M the reduction of NpO_2^+(aq) to mononuclear $Np(OH)_4$(aq) is followed by spontaneous polymerization to $Np_m(OH)_{4m}$(aq), further agglomeration and sorption on the container walls or on solid phases present in the system.

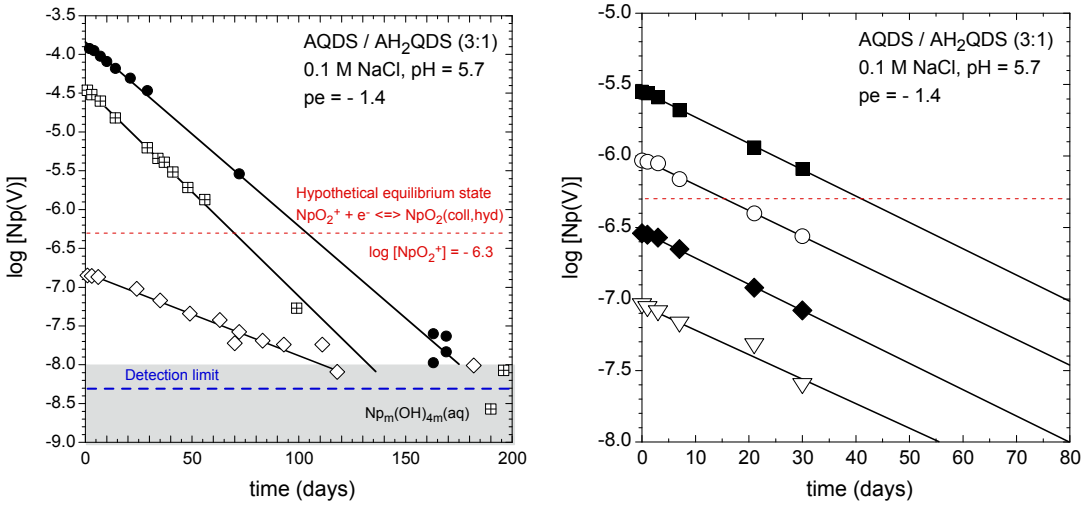

Figure 3: *Reduction of Np(V) in AQDS/AH$_2$QDS redox buffer solutions in 0.1 M NaCl at constant pH = 5.7 and pe = - 1.4 and varying initial Np(V) concentration ([Np(V)]° = 1.6·10^{-7} to 1.35·10^{-4} M). The dotted line indicates the Np(V) concentration expected for an equilibrium state between NpO$_2^+$(aq) and NpO$_2$(coll, hyd).*

Conclusions

The present results indicate that the redox potential in solution is the decisive parameter for the reduction of Np(V) at pH 5 - 10 in non-complexing aqueous media. Independent of the reducing agent and whether the system is homogeneous or heterogeneous, Np(V) is found to be stable at pe ≥ 0.5 ($E_h \geq 0.03$ V) and reduced to Np(IV) at pe ≤ - 0.2 ($E_h \leq -0.01$ V). The observed reduction rates depend also strongly on pe. The question whether the borderline at pe = 0.15 ± 0.35 ($E_h = 0.01 \pm 0.02$ V) corresponds to a redox equilibrium between NpO$_2^+$(aq) and intermediate mono- or polynuclear Np(IV) hydrolysis species and the mechanism for the reduction of NpO$_2^+$(aq) to Np(IV) polymers Np$_m$O$_p$(OH)$_{4m-2p}$(coll) are not yet clear and deserve further investigations. One may assume that the initial step in the reduction process leads to mononuclear Np(OH)$_4$(aq) species which immediately form polymers with a high tendency towards sorption on the container walls or solid phases present in heterogeneous systems.

References

Artinger, R., Marquardt, C.M., Kim, J.I., Seibert, A., Trautmann, N., Kratz, J.V. (2000). Humic colloid-borne Np migration: Influence of the oxidation state. Radiochim. Acta 88, 609-612.

Cui, D., Eriksen, T.E. (1996). Reduction of Tc(VII) and Np(V) in solution by ferrous iron. A laboratory study of homogeneous and heterogeneous redox processes. SKB Technical Report 96-03, Stockholm, Sweden.

Guillaumont, R., Fanghänel, Th., Fuger, J., Grenthe, I., Neck, V., Palmer, D.A., Rand, M.H. (2003), OECD, NEA-TDB. Update on the Chemical Thermodynamics of Uranium, Neptunium, Plutonium, Americium and Technetium. Elsevier, Amsterdam.

Lieser, K.H., Mühlenweg, U. (1988). Neptunium in the Hydrosphere and Geosphere. I. Chemistry of Neptunium in the Hydrosphere and Sorption of Neptunium from Groundwaters on Sediments under Aerobic and Anaerobic Conditions. Radiochim. Acta 43, 27-35.

Nakata, K., Nagasaki, S., Tanaka, S., Sakamoto, Y., Tanaka, T., Ogawa, H. (2002). Sorption and reduction of neptunium(V) on the surface of iron oxides. Radiochim. Acta 90, 665-669.

Nakata, K., Nagasaki, S., Tanaka, S., Sakamoto, Y., Tanaka, T., Ogawa, H. (2004). Reduction rate of neptunium(V) in heterogeneous solution with magnetite. Radiochim. Acta 92, 145-149.

Neck, V., Altmaier, M., Seibert, A., Yun, J.I., Marquardt, C.M., Fanghänel, Th. (2007). Solubility and redox reactions of Pu(IV) hydrous oxide: Evidence for the formation of $PuO_{2+x}(s, hyd)$. Radiochim. Acta 95, 193-207.

Neck, V., Kim, J.I. (2001). Solubility and hydrolysis of tetravalent actinides. Radiochim. Acta 89, 1-16.

Rai, D., Strickert, R.G., McVay, G.L. (1982). Neptunium Concentrations in Solutions Containing Acinide-Doped Glass. Nucl. Technology 58, 69-76.

Zeh, P., Kim, J.I., Marquardt, C.M., Artinger, R. (1999). The Reduction of Np(V) in Groundwater Rich in Humic Substances. Radiochim. Acta 87, 23-28.

REDOX STATE DETERMINATION IN HYPERALKALINE SOLUTIONS BY SPECIATION OF SELENIUM

B. Grambow[1*], C. Bailly[1], V. Baty[1], C. Landesman[1], S. Ribet[1]

[1] SUBATECH (Ecole des Mines, University of Nantes, IN2P3/CNRS (FRANCE)

*Corresponding author: grambow@subatech.in2p3.fr

Abstract

In order to account for potential redox state desequilibrium in hyperalkaline solutions, it is necessary to supplement EH measurements by Pt electrodes with measurement of solution speciation of redox sensitive elements. In the present communication preparatory work for using Selenium speciation as indicator for redox states is described.

Introduction

Selenium has wide ranging interest due to its important role in the nutrition of animals and plants, to it chemical toxicity and the radiotoxicity of the nuclear fission product selenium 79. It is a redox sensitive element existing in aqueous solutions in the redox states –II(organic and inorganic), IV and VI and in the solid state as well as Se(0). It is of large radiological concern, due to the relative high mobility of both Se(IV) and Se(VI) in natural water environments. In the present work, only preparatory work is described. Detailed measurements will be reported in the next project year.

State of the art

Laboratory experiments show that even at high Se concentrations over a wide range of pH the Pt electrode is completely insensitive to the relative abundance of dissolved Se(VI) and Se(IV) (Runnells and Lindberg 1990). Hence, Se speciation cannot be deduced directly form Eh measurements with Pt electrodes and geochemical equilibrium calculations. This indicates that under certain conditions the Pt electrode measured Eh does not correspond to a “master variable” of the redox system. It is for example often observed that dissolved oxygen and organic carbon are together present in a groundwater system even though they are not in mutual thermodynamic equilibrium (Washington, Endale et al. 2004). This clearly points to the need of direct measurement of solution speciation to assess the redox state relevant for Se speciation.

Assessment of the thermodynamics of Selenium in hyperalkaline solutions

Thermodynamic database

A full review of the chemical thermodynamics of selenium in aqueous/solid systems has recently been presented by the NEA-TDB project (Olin, Noläng et al. 2005). However, no thermodynamic data were proposed for ion pairs of the form $X(SeO_3)$ where X could be Ca or Mg. Thermodynamic data were proposed by (Liu and N. 1994) . For $CaSeO_3$ a formation constant of log K=3.17 was proposed. It recently has been observed that the effect of Ca concentrations on the sorption behaviour of Se(IV) on bentonite could only be explained by the assuming the presence of a neutral $CaSeO_3$ complex(Alhajji 2007). A formation constant of log K = 4 provided a good representation of the experimental data. Similarily, in hyperalcaline solutions in contact with cement pastes, adsorption behaviour of Se(IV) could only be explained by assuming presence of a $CaSeO_3$ complex (Macé 2006). However, a detailed study of the formation constant of the $CaSeO_3$ complex is still missing. Therefore, the effect of this complex in hyperalkaline solutions will be assessed by a sensitivity study.

Eh/pH diagrammes

Using the thermodynamic database recommended by NEA, calculations of Eh/pH diagrams in the relevant pH range were performed using the geochemical code Chess (Van der Lee 1993). Comparison is made for inclusion or omission of the above mentioned ion pair $CaSeO_3$. using a formation constant log K = 3. The calculation results are included in the figures 1a and b for a total Se concentration of 10^{-6} M and Ca concentrations relevant for cement systems of 0.01 M.

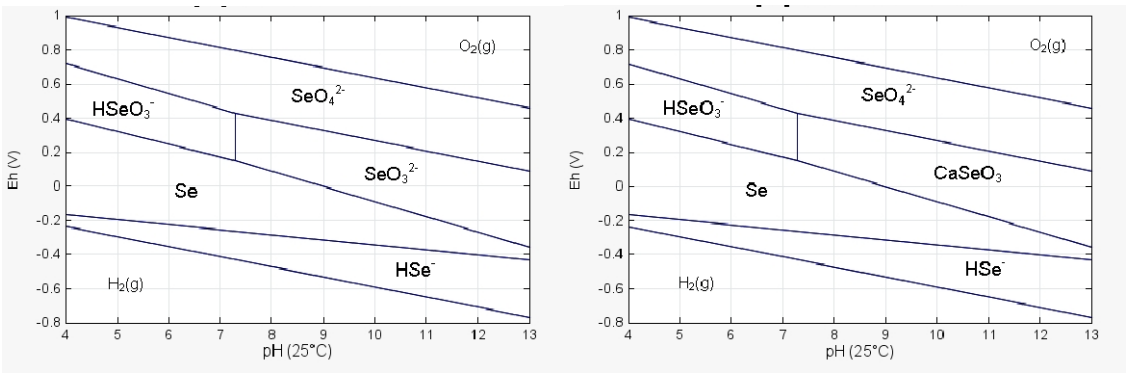

Figure 1a and b: *Eh/Ph diagram for Se in the absence (a) and presence (b) of $CaSeO_3$ complexes. Total Se and Ca concentrations are 10^{-6}M and 10^{-2} M respectively. Complex formation constant log K = 3*

The Figures 1a and b show that the stability fields of SeO_3^{-2} and $CaSeO_3$ are about overlapping for the selected conditions. Considering that the stability constant for the ion pair is rather uncertain, it is important to assess, to which degree these uncertainties affect the ability to use solution speciation methods to deduce the redox state of the solution. Figure 3 shows the effect of varying the formation constant for $CaSeO_3$ on the calculated stability field boundary between Se(0) and Se(IV). In the range studied the uncertainty in log K values amount to an uncertainty of 30 mV in the the stability field boundary.

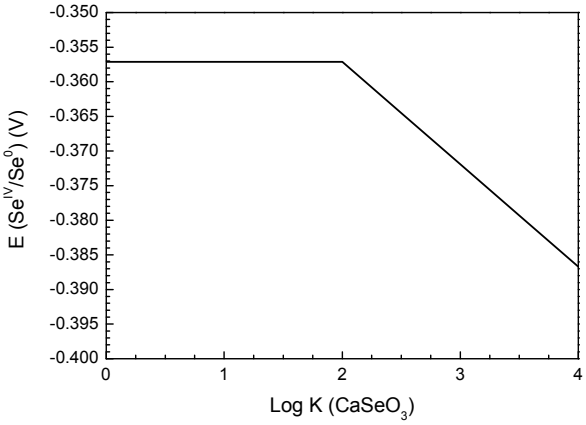

Figure 2: *Effect of variations in the formation constant of $CaSeO_3(aq)$ on the equilibrium potential Se(IV)/Se(0)*

Solution speciation in hyperalkaline solution will further be complicated by the formation of polyselenide species such as Se_2^{-2} Se_3^{-2}, Se_4^{-2} with stability fields indicated in the following two Eh/pH diagrams, calculated with Chess on the base of the thermodynamic data of Olin et al. 2005.. These ions have formal oxidation states between 0 and –II. Obviously, polymer formation depends on total Se concentration in solution, hence experiments of redox state determination needs to be done as a function of total Se concentration to assess the influence of these species.

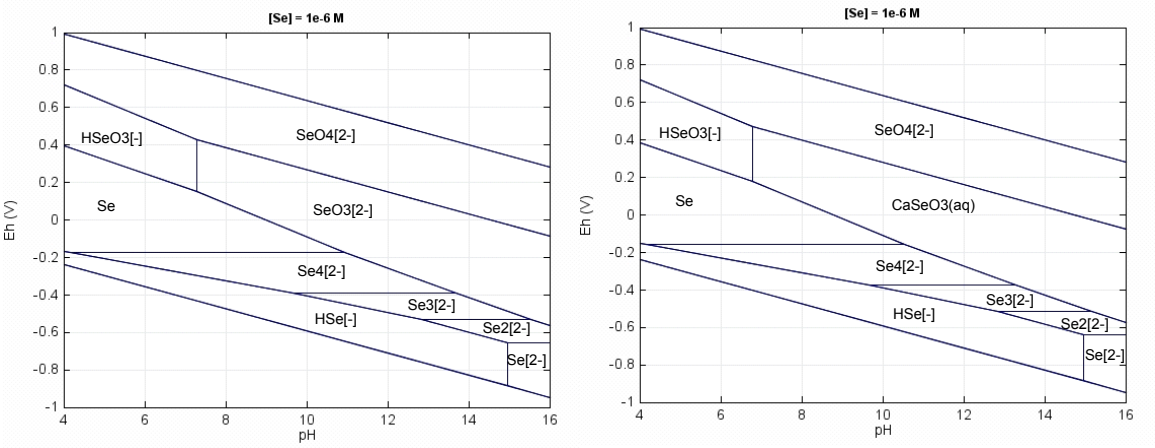

Figure 3: *Effect of polymer species on the Eh/Ph diagram in absence (a) and (b) presence (b) of $CaSeO_3(aq)$ (formation constant log K=2.5)*

It becomes obvious that polymer species play a large role under alkaline conditions and the presence of polymer species will strongly reduce the stability field for Se(0, triclinic). Essentially, in the interesting hyperalkaline pH range between pH 11 and 13, no Se(0, triclinic) will be formed. Even further reduced is the probability to form monoclinic Se(0).

Analytics allowing Se speciation

Solution analyses

Solution species for Se(IV) and Se(VI) can easily be distinguished simultaneously using ion chromatography. Quantifications limits in our laboratory were smaller than 10^{-6} M. The validity of the method has been tested (Macé 2006) for two anoxic hyperalkaline solutions, one in equilibrium with Ettringite, the other with a CEM1 cement paste. After one month of contact Se(IV) was found to be the dominant species with Se(VI) concentrations being less than 1%.

Technique	*DPV*
Mechanism	$HSe^- + Hg \Leftrightarrow HgHSe + 2e^-$ $Se^{2-} + Hg \Leftrightarrow HgSe + 2e^-$
Reactants	NH_4Cl 1 M, pH 8,0 Gélatine 0,003%
Detection limit	**10^{-7} M**
Deoxygenation time	3 min
potential of deposite	-0,2 V
Deposition time	30 s
Equilibrium time	2 s
Petential scan	-0,2 ? - 1,2 V
grade : amplitude/length	5 mV / 0,1 s
Impulse amplitude/length	25 mV / 40 ms

Table 1: *Parameters for analysis of Se(-II) by a mecury drop electrode (Liu 2007)*

In contrast, Se(-II) can best be analysed using polarographic techniques, using a hanging mercury drop electrode. The analytical parameters for Se(-II) analyses are summarized in table I. The detection limit is 10^{-7} M. Methods for analysing polyselenides in solution have not yet been developed in our laboratory. This will be done in the next year . The idea is to use in a first stepUV identification at large total Se concentration (about 10^{-4}M) concentration, calibrate in a second step the ion chromatography with this identified species and couple finally ion chromatography with a fraction collector and analyse of collected fractions by collision cell ICP/MS. This should allow detection limits as low as $5 \cdot 10^{-8}$ M.

It becomes obvious from these observations that Se speciation in solution can currently only be determined in our laboratory for reliable direct redox state measurements if total Se concentrations are higher than 10^{-6} M. about 20 times lower detection limits can be achieved by coupling ion chromatography ICP-MS. Upper limits of total Se concentrations in hyperalkaline solutions are in the range of 10^{-3} M governed by the potential formation of $CaSeO_3$(s). In this concentration range Se(0) is present under certain redox conditions and Se(0)/Se(-II) or Se(0)/Se(IV) might be encountered as redox couple indicating the solution redox state.

Solid state analyses

Se(0) cannot be detected in solution but requires redox sensitive solid state analytical techniques such as XPS. This technique works in presence of solid phases (ciment phases) but it might as well work, if Se(0) is present in colloidal form. In the latter case, colloids must be separated by ultrafiltration and the Se-redox state on the filter residues shall be analysed. Ultrafiltration will be done in the inert gas box and transfer of the sample from the inert gas box to the XPS will be done in specially designed transfer-equipment, allowing no access of air to the samples. Of course, since Se(0) is a solid, we do not need to know the quantity of Se(0) but we need to know whether it is there. In case of equilibrium, it does not matter for redox state determination whether other redox

states of Se are present in the solid phase as well. If there is no equilibrium, even the observation of Se(0) is meaningless for redox state determination.

Some further uncertainties in the determined redox potential arise from the contribution of surface energy as a function of particle size to the gibbs free energy of formation of Se(0). Indeed, in the literature, various stability constants for solid Se(0) are given. Indeed, Se(0) exists in trigonal ($\Delta°G_f$=0) or monoclinic form ($\Delta°G_f$=1.281±0.184 kJ/mol, thermodynamic data from Olin et al. 2005). These uncertainties can be estimated for the Se(0)/Se(-II) couple in the following way:

$$E = E° + \frac{RT \cdot \ln(10)}{2 \cdot F} \log_{10} \frac{[Se(0)]}{[Se(-II)]}$$

with

$$E° = \frac{-\Delta°G_{reac}}{n \cdot F}$$

From the thermodynamic data base of Olin et al. (2005) we obtain for the reaction

$$Se(0) + 2e^- = Se^{-2}$$

in case of trigonal Se(0) a value of $\Delta°G_{reac}$ = 128.6±3 kJ/mol or E°= -0.666±0.01 V and in case of metastable monoclinic Se(0) we have $\Delta°G_{reac}$ = 127.3±3 kJ/mol or E°= -0.660±0.01 V. The difference between both solids has only a very small effect of 6 mV on the expected equilibrium potential.

First experimental observations

A first series of hyperalkaline solutions have been prepared with total Se concentration of $2 \cdot 10^{-4}$ M. Fresh cement water was simulated by mixing $6.5 \cdot 10^{-2}$ mol/L of NaOH with $2.2 \cdot 10^{-3}$ mol/L $Ca(OH)_2$ and 0.11 mol/L KOH. The solution had a pH of 13.2, which stayed about constant in the experiment. No solid phase was present. The initial Se(IV)/(VI) ratio was varied from 100% Se(IV) to 100% Se(VI) by adding either or both Na_2SeO_3 or Na_2SeO_4.One series of experiments was performed in presence of H_2O_2 ($2 \cdot 10^{-3}$ M) as oxidant the other without H_2O_2. The experiments were performed in an inert-gas box at O_2<1 ppm. Eh was measured by a platinum electrode, Se(IV) and Se(VI) concentrations by ion chromatography after having filtered the solutions by membranes of 0.45µm average pore diameter. Prior to IC analyses solutions samples were stored in an N2 filled desiccator to avoid air oxidation. The experiment was followed as a function of time for 3 days.

Initial total Se concentrations and initial Se(IV)/(VI) ratios were without any influence on solution Eh. In the absence of H_2O_2 an Eh value of 15±5 mV was achieved both in blank and Se containing solutions. The presence of H_2O_2 increased the Eh to a value of 82±1 mV again both in blank and Se containing solutions. Comparison to the above described Eh/pH diagram (Figure 4) shows that all experiments were performed within the stability field of Se(IV) or at the Se(IV)/(VI) interface. Hence it might be expected

that Se(IV) concentrations remain stable in the experiment whereas Se(VI) becomes reduced. However, this is not observed. IC analyses show that the final Se(VI)/(IV) measured after 3 days was equal to the initial ratio. This shows also for hyperalkaline solutions that Se(VI) is entirely non-reactive for the duration of the experiment, and this observation explains as well the absence of any effect of Se(IV)/(VI) ratio on the solution Eh.

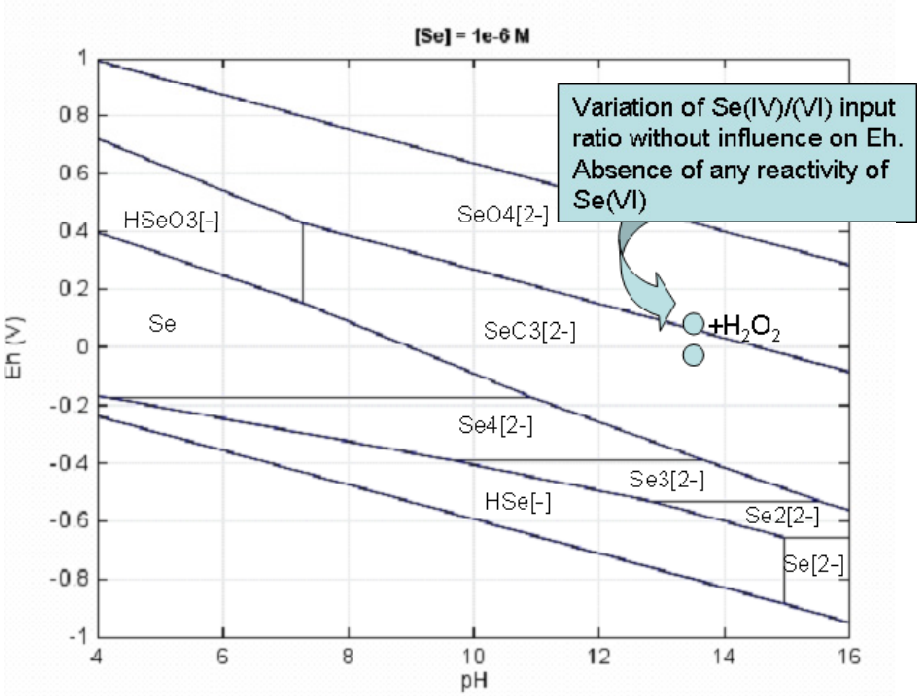

Figure 4: *Positioning of experiments in the Eh/pH space (the experiments are obtained for 10^{-4} M, the calculated diagram for 10^{-6} M Se(tot) but this is without significance for location of the Se(IV)/(VI) boundary which might be contraining here.*

Summary and conclusions

A strategy has been developed for using Se speciation for redox state determination in hyperalkaline solutions. Until now, work was concentrated on theoretical calculations. These calculations show an overlap in the stability fields of $CaSeO_3$(aq) and of SeO_3^{-2} and it points to a large effect of polyselenide formation on the location of redox stability field boundaries, even at rather low total Se concentrations. It is likely that polyselenide formation will strongly depend on kinetic constraints and on total Se concentration. In particular at low concentrations, formation kinetics will be extremely slow.

Only first experiments were performed. These first experiments confirm that Eh measurements by Pt electrodes are also in hyperalkaline solutions not useful to infer the redox state of dissolved Selenium. Hence direct solution speciation is necessary. Detailed experimental data on systems with and without solide phases will be collected over a much larger Eh range in the next project phase.

References

Alhajji, E. (2007). Etude des propriétés de sorption de la bentonite MX-80 vis-à-vis de Se(IV), Ni(II), et Cs(I). Du système disperse au système compacte. Orsay, Université de Paris Sud Orsay. Ph.D.: 151.

Licht S, Forouzan F, (1995) "Speciation analysis of aqueous polyselenide solutions", Journal of the Electrochemical Society, vol 142, 5, pp 1546-4551

Liu, C. W. and N. T. N. (1994). Modeling of selenium transport at the Kesterson reservoir, California, U.S.A. Journal of Contaminant Hydrology 15: 345-366.

Liu, X. (2007). Rétention du Séléniure sur la Pyrite en Milieu Réducteur. Nantes, University of Nantes. PhD.

Macé, N. (2006). Influence de la température sur la rétention de sélenite par une pate cimentaire alterée et par ses phases pures constitutives. Orsay, Université d'Orsay Paris XI: 247.

Olin, A., B. Noläng, et al. (2005). Chemical thermodynamics of selenium. Amsterdam, Elsevier.

Runnells, D. D. and R. D. Lindberg (1990). Selenium in aqueous solutions: the impossibility of obtaining a meaningful Eh using a platinum electrode, with implications for modeling of natural waters. Geology 18,: 212-215.

Van der Lee, J. (1993). CHESS, another speciation and surface complexation computer code. Fontainebleau, France, CIG-École des Mines de Paris: 86.

Washington, J. W., D. M. Endale, et al. (2004). "Kinetic control of oxidation state at thermodynamically buffered potentials in subsurface waters." Geochimica et Cosmochimica Acta 68, 4831.

INFLUENCE OF CHLORIDE CONCENTRATIONS ON THE SIGNAL OF REDOX ELECTRODE AND ON UV-SPECTROSCOPIC DETERMINATION OF FE SPECIES

Barbara P. Bischofer [1*], Sven Hagemann [1], Cathrin Hühne [2], Dagmar Schönwiese [2], Tina Scharge [1]

[1] Gesellschaft für Anlagen und Reaktorsicherheit (GRS) mbH, (GER)

[2] Technische Universität Braunschweig (TU BS), (GER)

* Corresponding author: Barbara.Bischofer@grs.de

Abstract

The oxidation state of heavy metals and radionuclides has a considerable impact on their mobility. Provided an existing thermodynamic equilibrium, the oxidation state is imposed by chemical composition and physical parameters, especially like pH and redox potential (Eh).

For nuclear repositories in salt formations, potentially intruding solutions always exhibit a high ionic strength. Measurement of Eh with a normal platinum electrode is problematic in such environments because half cell potentials of reference electrodes are altered by variable liquid junction potentials. In order to maintain a relation between electrode signal and Eh, a model for the calculation of the medium induced bias is experimentally investigated. Since Fe^{2+}/Fe^{3+} is believed to be the most important redox couple in aqueous solutions, we have chosen this redox couple as subject of our investigations.

Species analysis is another method of identifying an element specific redox potential. But there are only insufficient data on the speciation of iron in saline solutions. To set up a suitable speciation model for Fe(II)/Fe(III), the speciation of iron is measured using UV/VIS spectroscopy. For this purpose the influence of saline solutions on the detection of Fe(II) and Fe(III) has to be analyzed.

The measurements with the redox electrode in saline chloride solutions resulted in a deviation of 30 to 43 mV near saturation. An increasing Fe(II)/Fe(III) ratio led to a lower linear decline in the measured redox potential than expected according to Nernst equation. An increase in H^+-concentrations showed rising measured redox potentials of about 7 mV per measured pH unit. By application of UV/VIS spectroscopy, no salinity effect is found for detection of Fe(II) and Fe_{tot} with the phenanthroline method, for determination of Fe(III) a concentration of at least 0.5 mol/l thiocyanate is necessary in saline solutions.

Introduction

Redox potentials in aqueous media are most commonly measured by determining the electric potential between a platinum electrode and a reference electrode (e.g. Ag|AgCl). In natural systems, generally more than one redox couple is present and most of the redox couples are in disequilibrium. Hence, an aqueous system has not only one redox potential but several potentials specific for each redox couple present. Unfortunately a redox electrode can only measure one potential that consequently must be regarded as a somehow mixed product of the individual redox couple potentials.
Measurements in natural media showed that the apparent electrode potential is more closely to the Fe^{2+}/Fe^{3+} redox couple potential than to any other. This probably results from the relatively fast electron exchange between the two species. Other researchers discovered that the platinum electrode acts as an iron specific electrode after Fe^{2+} has been oxidized to Fe^{3+} and subsequently precipitated as $Fe(OH)_3$ on the platinum surface (Doyle, 1968; Lindberg and Runnels, 1984; Runnels und Lindberg, 1990).

There is no information if and how the measured potential of the platinum electrode and the reference electrode is altered by the presence of high concentration of inorganic salts. In principle both electrodes could be affected. The reference electrode could be impacted by altered liquid junction potentials at the interface between reference solution (e.g. 3 M KCl) and sample solution as it is been observed in pH measurements. On the other hand the platinum electrode could be affected by influencing or even inhibiting the electrochemical surface reactions.

A method for accessing element specific redox potentials is by species analysis. A large number of different analytical approaches exist (Cornelis et al., 2005), but in our study we concentrate on spectrophotometric methods with UV-VIS complexing active agents like phenanthroline, ferrozine or thiocyanate. Methods like these are well established in water analysis but it is less well known whether these methods are also suitable for highly saline solutions.

Having the species of the redox sensitive components in its concentrations determined, the redox potential of a redox buffered aquatic system can be calculated by geochemical modelling tools. But the reliability of such calculations depends on availability and quality of the thermodynamic data of the redox sensitive species. Iron is a very important element in this context, because it contributes very significantly with its solid phases containing Fe^{2+} and Fe^{3+} to the redox potential of aquatic systems. The speciation of Fe in brines differs from the speciation in non-saline systems. In brines other chloro- and sulfato-complexes are formed, , mixed chlorohydroxo, and chlorosulfato complexes.

In this first part of the study the influence of different chloride salts and of different Fe(II)/Fe(III) ratios as well as H^+ concentration on the Fe redox potential in brines are investigated. Furthermore the influence of saline solutions on the detection of Fe(II) and Fe(III) with UV/VIS-spectroscopy is examined.

Materials and Methods

Determination of the Fe Redox Potential

The Eh-Measurements were carried out at 25.0°C with a combined Pt ring electrode (Metrohm 6.0451.100) in an inert argon atmosphere. The iron containing solutions were prepared with CO_2-free water in a glove box flushed with argon. Measurements were conducted as titrations varying the salt concentrations (NaCl, KCl and $MgCl_2$) till near saturation with 3 and 5 repetitions, respectively. In general, experiments were conducted in 0.01 M $HClO_4$-solution, thus ensuring a constant H^+-concentration. The Fe(II)/Fe(III) concentration ratio was kept constant at 1 with $c(Fe_{tot}) = 10^{-4}$M. Some additional measurements were conducted with varying H^+-concentrations but constant Fe(II)/Fe(III) ratio and constant salt concentration or with a varying Fe(II)/Fe(III) ratio but constant salt and H^+ concentration.

Eh-Measurements were conducted after 2 minutes time of stirring and up to 6 additional minutes equilibration time. Readings were only accepted, if the signal during the measurement were within 0.1 mV in 120 sec. An exception was made by variation of the H^+concentration. Here readings were taken if the signal during the measurement differed no more than 0.3 mV in 120 sec.

Additionally the pH was measured with an Orion Ross-electrode (Pt/I_2, I^- electrode, Orion Nr. 8102SC).

All used salts (NaCl, KCl and $MgCl_2$) were purchased from Merck (Germany). NaCl and KCl had the grade suprapur, $MgCl_2$ (purchased as hexahydrate) had the grade p.a. For the preparation of Fe(II) and Fe(III) containing solutions $FeCl_2$ and $FeCl_3$ (purity of 99,99%, respectively 99,99+%) from Sigma Aldrich were used.

UV/VIS-Spectroscopy of Fe Species

The German DIN-method (DIN 38406 Part 1, 1983) using phenanthroline was selected for the quantitative detection of Fe(II). The advantages of this method are its fast sample preparation and the high stability of the Fe(II)-phenanthroline complex. Preliminary tests in non-saline solutions with varying mixtures of Fe(II) and Fe(III) showed, that phenanthroline also forms a complex with Fe(III). But the peak of this complex is detected at lower wavelengths. At the absorption maximum of the Fe(II)-phenanthroline complex (510 nm), this complex has an approximately 60fold lower extinction coefficient. Herrera et al. (1989) found, that the detection of Fe(II) is not disturbed as long as the ratio Fe(II)/Fe(III) is greater than 0.1. If not, a masking with fluoride is necessary.

For the quantitative determination of Fe(III) the complexation with potassium thiocyanate (KSCN) was chosen. The absorption maximum of the Fe(III)-thiocyanate complex is observed at 478 nm. The advantages of this method are again the fast sample preparation and that there is no disturbance due to Fe(II). One disadvantage of the thiocyanate method is the quick decomposition of the complex. Therefore the samples have to be prepared directly before the measurement. Another disadvantage is the relatively low sensitivity of the thiocyanate complex. But this is insubstantial since it is planned that in natural systems Fe(II) and Fe(III) concentrations will be detected with a

spectrometer including a 5 m long flow cell. This should result in a 5000fold increase of absorption compared to the use of normal 1cm quartz cuvettes.

The absorption band of the Fe(III)-thiocyanate complex is completely superimposed by the absorption band of the Fe(II)-phenanthroline complex. Therefore analysis of Fe(III) is not simultaneously possible with the detection of Fe(II) with phenanthroline.

For the analysis of total Fe, hydroxylammoniumchloride as reducing agent is added and the total Fe is detected as Fe(II) using the phenanthroline method.

All three methods (total Fe and Fe(II) with phenanthroline, Fe(III) with thiocyanate) were successful tested in non saline solutions. In case solutions contain Fe(II), solutions were prepared with CO_2-free water and dealt with in an inert argon atmosphere.

The UV/VIS spectrometer worked with is the model Lambda 20 from Perkin Elmer.

Normal 1 cm quartz cuvettes were used for detection.

Results and Discussions

Determination of the Fe Redox Potential

Response of the electrode in different saline media

Titrations in metal chloride solutions showed, that the apparent Eh decreases with increasing chloride concentration reaching a maximum deviation of about 30 to 43 mV near saturation (cf. Fig. 1). A comparison of the different saline solutions reveals a good consistency of the measured Eh by low chloride concentrations. However from about 1.2 mol/kg chloride, the measured voltage shows salt specific deviations. In solutions of KCl the Eh decreases more strongly with the chloride concentration than in NaCl solutions. In solutions of $MgCl_2$ the Eh is even higher than in NaCl solutions with equal chloride concentrations. For chloride concentrations of about 2-5 mol/kg the slope is very small, but with still higher chloride concentrations the measured Eh in $MgCl_2$ solutions declines significantly.

Two phenomena contribute to this effect. Firstly, formation of Fe(III)chloro complexes leads to a decline in free Fe^{3+} concentration. Analogue chloro complexes of Fe(II) are much weaker. Secondly, the activity coefficients of Fe^{3+} tend to be much smaller than those of Fe^{2+}, as expressed in the quadratic term in the Debye-Hückel expression. Both effects cause the ratio Fe(II)/Fe(III) in the Nernst equation (cf. equation 1) to rise and therefore the measured Eh to decline.

$$E_h = E_h^0 - 0{,}05916 \log \frac{a_{Fe^{2+}}}{a_{Fe^{3+}}} \qquad (1)$$

In order to quantify this effect in greater detail, additional measurements are being undertaken to develop a consistent set of chloride complex formation constants and Pitzer ion interaction coefficients, which will allow a calculation of free Fe^{2+} and Fe^{3+} activities in the investigated media. Only then the additional effect of the medium on the electrodes themselves can be assessed with sufficient precision.

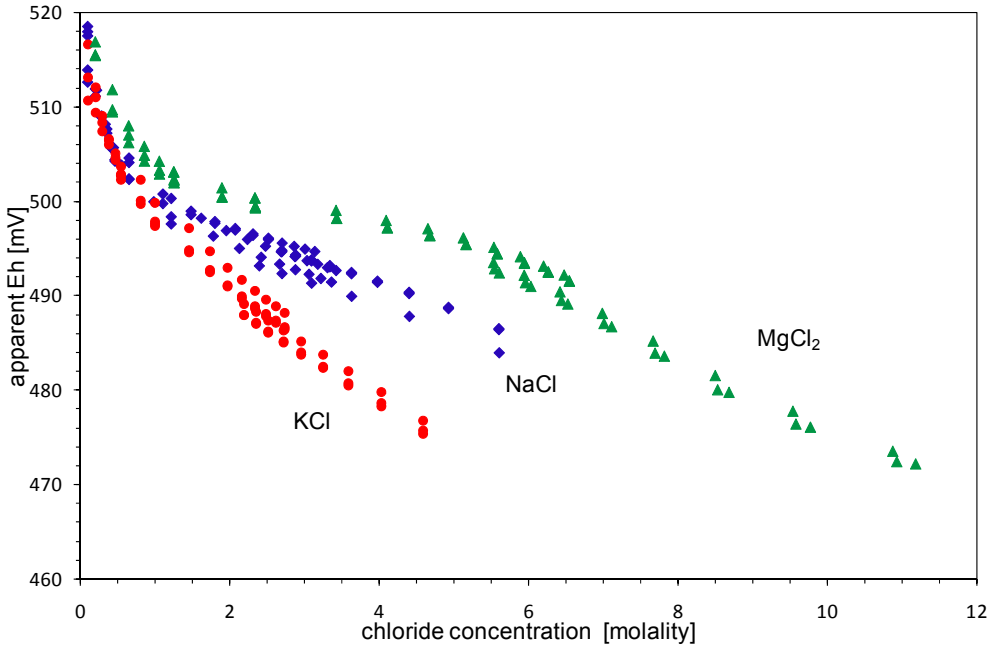

***Figure 1**: Eh in relation to chloride concentration of an redox defined system by concentration of Fe(II)/Fe(III) = 1 in 0.01 m $HClO_4$, c(Fe_{tot}) = 10^{-4}.*

Behaviour in constant saline media

Eh measurements by varying H^+-concentrations were conducted in a concentrated NaCl solution (5.65 m) and at a constant Fe(II)/Fe(III) concentration ratio. Figure 2 shows that the measured Eh increases steadily with decreasing of the apparent pH. An increase of 2.6 pH units (H^+-concentration $9 \cdot 10^{-5}$ till $5 \cdot 10^{-2}$ mol/l) denotes in a decrease of up to 18.5 mV. The difference of the two repetitions, reflecting the uncertainty of the measurements, amounts to 3.1 mV at maximum.

This behaviour can be qualitatively explained as a result of increasing complex formation of Fe(III) with OH^-. Again a more detailed analysis will be possible after a consistent thermodynamic speciation and activity model has been developed.

Response of the electrode to changing Fe(II)/Fe(III) ratios

Another important task was to check in high concentrated media whether the redox electrode responds to a variation of the Fe(II)/Fe(III) ratio in the expected way. According to (eq. 1) a change of the ratio

$$\log \frac{a_{Fe^{2+}}}{a_{Fe^{3+}}}$$

by one log unit should result in a linear change of Eh by -59,16 mV. We have made a titration resulting in solutions of same salt concentration (5.65 m NaCl), same H^+ concentration (0.01 M) but varying Fe(II)/Fe(III) concentration ratios ranging from 1/15 to 13/1 (Fe_{tot} = 1.5*10^{-4} – 4.7* 10^{-4}M). In the constant ionic media, and the constant salt and H^+-concentration used for these measurements the activity coefficients of all iron species remain constant. Then, the change in the activity ratio ($a_{Fe^{2+}}/a_{Fe^{3+}}$) is the same

as the change in the concentration ratio ($c_{Fe^{2+}}/c_{Fe^{3+}}$). Figure 3 illustrates that a linear relation is indeed found. But the slope of the regression line is -50.79 which corresponds not very well with the theoretical prediction. This deviation will have to be investigated further.

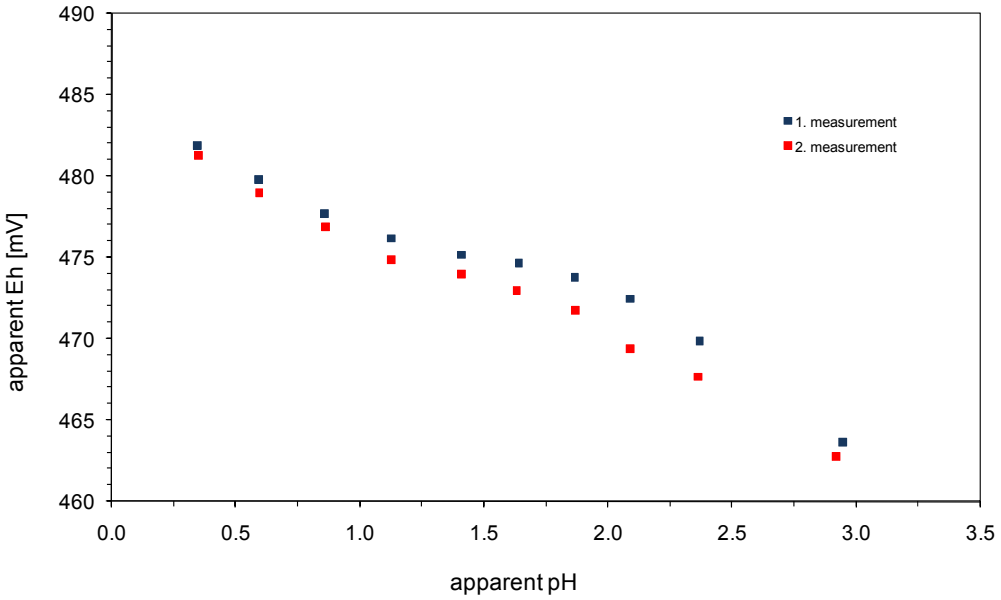

Figure 2: *Eh in relation to measured pH of a redox defined system by ratio Fe(II)/Fe(III) = 1, c(Fe_{tot}) = 10^{-4} M in a concentrated sodium chloride solution (c_{NaCl} = 5.65 mol/kg)*

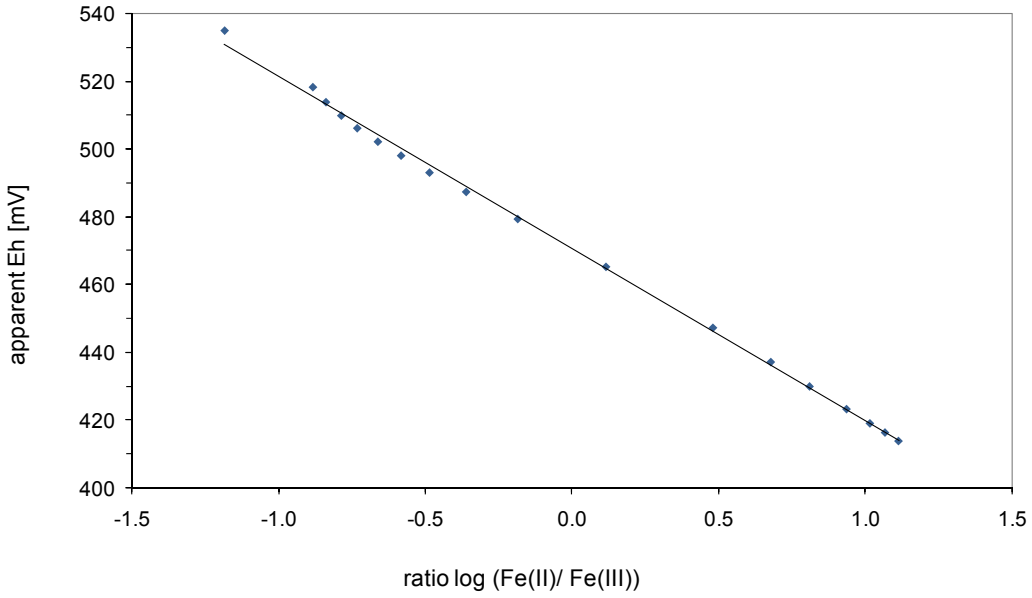

Figure 3: *Eh in relation to the Fe(II)/Fe(III) ratio, with c(Fe_{tot}) = 1.5* 10^{-4} - 4.7* 10^{-4}M, c_{NaCl} = 5.61 mol/kg, 0.01 M $HClO_4$.*

UV/VIS-Spectroscopy of Fe Species

For the determination of the detection of Fe with phenanthroline, we have prepared a series of solutions with known content of Fe(II) and increasing NaCl concentrations ranging from 0.005 to 5.0 mol/kg. The concentration of Fe as total iron was then determined using ammoniumhydroxylchloride and phenanthroline. Figure 4 shows the apparent Fe_{tot} concentrations found in the samples. There was little deviation from the actual added concentration of $3.581 \cdot 10^{-5}$ mol Fe/l (2 mg Fe/l). Overall the measured variation lies within 2.3 % (with one outlier at 4 %) of the added concentration.

A similar analysis was performed for the thiocyanate method that is used for the determination of Fe(III). Here, the concentration of Fe(III) was always $7.162 * 10^{-5}$ mol/l (4 mg/l). In the first series of experiments 0.1 mol/l SCN was used as ligand concentration. Figure 5 shows a strong impact of NaCl content on the determined Fe concentration by this concentration of SCN. Up to 25% less than the added Fe concentration was analyzed. Formation of mixed chloro thiocyanato complexes with lower spectral absorbance might be suspected as the reason.

It was possible to outweigh this effect by increasing the thiocyanate concentration to 0.5 and 1 mol/l, respectively. After that deviations where found to be within the ranges of the usual uncertainty of the method.

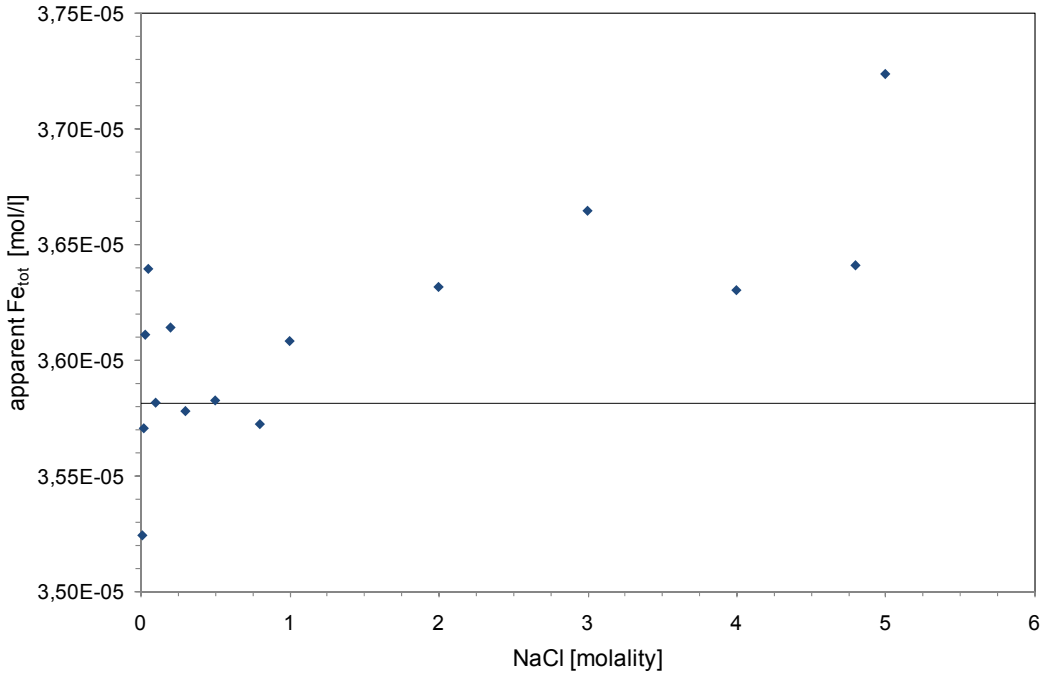

Figure 4: *Measured Fe_{tot} concentration with phenanthroline depending on the NaCl concentration; added Fe(II) concentration always $3.581 * 10^{-5}$ mol/l.*

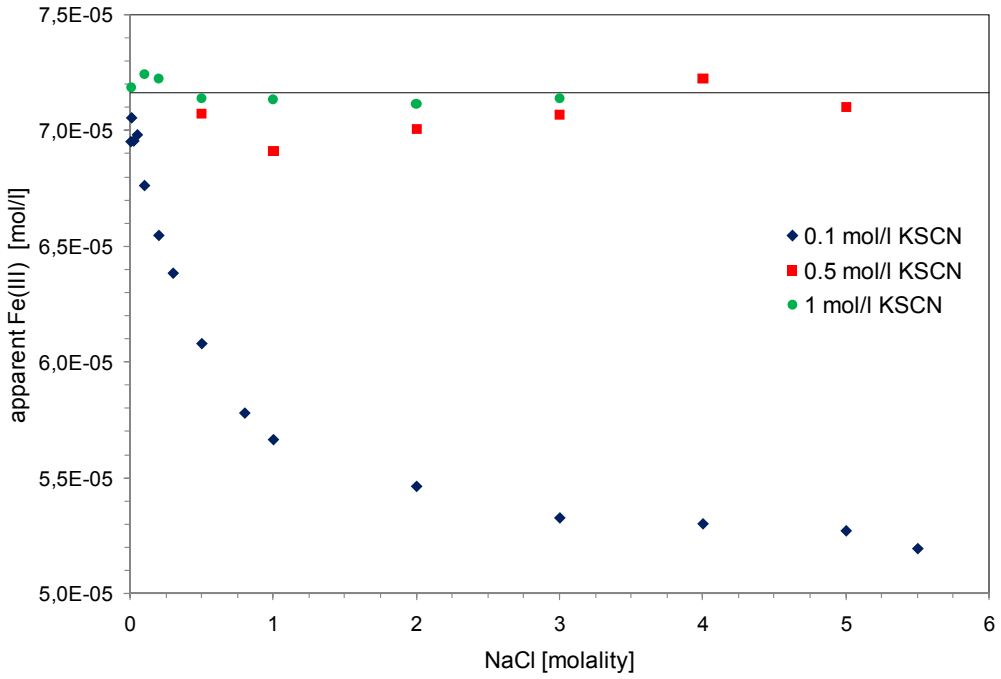

Figure 5: *Apparent Fe(III) concentration determined as thiocyanato complex depending on the NaCl concentration; cFe(III) always at 7.162 *10^{-5} mol/l.*

Summary and Conclusions

Several series of experiments have been conducted in order to assess the performance of the platinum redox electrode in saline solutions.

The measurements of the redox potential in concentrated chloride solutions show that there is a salinity effect. The measurements revealed a rather small but existent deviation of 30 to 43 mV near saturation. Depending on the regarded system or whether the equilibrium of the regarded system is located near a boundary of an important Eh/pH-stability field of aqueous species this small deviation can be very significant.

In accordance with theoretical predictions, a change of the Fe(II)/Fe(III) concentration ratio leads to a linear decline with increasing Fe(II)/Fe(III) ratio. But compared to the theoretical slope of 59.16 mV a reduced slope about approximately 15 % was observed.

Eh measurements with varying H^+-concentrations in concentrated NaCl solutions resulted in an increasing redox potential of about 7 mV per decreasing measured pH unit.

No salinity effect is observed for the determination of Fe(II) and Fe_{tot} with phenanthroline in NaCl solutions. For the analysis of Fe(III) with thiocyanate a complex dependence on the salinity was found for 0.1 mol/l SCN, but for higher thiocyanate concentrations (0.5 and 1.0 mol/l SCN) only a scattering around the true value was seen.

Accounting for the salinity effect by measuring the redox potential are probably both, the reference electrode and a change in speciation.

For a detailed explanation of all observed effects and for the calculation of the Fe^{2+}/Fe^{3+} activities, further Pitzer ion interaction parameters and a consistent set of chloride

complex formation constants valid in high saline systems have to be developed. Therefore further measurements are planned.

For analyzation of Fe in highly saline solutions with UV/VIS spectroscopy, the phenanthroline method according to the German DIN-method (DIN 38406 Part 1, 1983) can be used to determine Fe(II) and Fe_{tot}. For quantification of Fe(III) with thiocyanate concentrations of at least 0.5 mol/l KSCN are necessary.

Acknowledgement

We kindly acknowledge the funding of the European Commission and of the German Federal Ministry of Economics and Technology (BMWi).

References

Cornelis R, Caruso J, Crews H, Heumann K (2005): Handbook of elemental speciation II – species in the environment, food, medicine and occupational health, Wiley 768 S.

DIN 38406 Part 1 (1983): German standard methods for the examination of water, waste water and sludge; cations (group E); determination of iron (E 1)), WILEY-VCH, Weinheim.

Doyle R W (1968): The origin of the ferrous ion-ferric oxide nernst potential in environments containing dissolved ferrous iron, Am. J. Sci. (266), 840-859.

Herrera L, Ruiz P, Aguillon J C and Fehrmann A (1989): A New Spectrophotometric Method for the Determination of Ferrous Iron in the Presence of Ferric Iron, J. Chem. Tech. Biotechnol. (44), 171-181.

Lindberg R D, Runnells D D (1984): Ground Water Redox Reactions: An Analysis of Equilibrium State Applied to Eh Measurements and Geochemical Modeling, Science (225), 925-927.

Runnels D R, Lindberg R D (1990): Selenium in aqueous solutions: The impossibility of obtaining a meaningful Eh using a platinum electrode, with implications for modeling of natural waters, Geology (18), 212-215.

THE EFFECT OF IRON CORROSION ON CONDITIONS INSIDE WASTE PACKAGES

David Dobrev, Petr Brůha, Antonín Vokál *

Nuclear Research Institute Řež plc (Czech Republic)

* Corresponding author: voa@ujv.cz

Abstract

This paper describes the results of experiments investigating the effect of iron corrosion on conditions that could develop after the ingression of water in failed disposal canisters with spent fuel assemblies. In the experiments, which were performed at various temperatures in closed vessels with and without addition of iron powder or carbon steel plates in synthetic bentonite water, Eh, pH, iron corrosion potentials and the rate of the evolution of hydrogen were measured. Primarily Eh was significantly decreased by the addition of iron in reaction vessels. pH was also slightly decreased. A comparison of continuous and discontinuous measurements of Eh in a closed vessel with iron confirmed that iron corrosion products affect the long-term continuous measurements of Eh both with Pt or Au electrodes. The results of long-term experiments with carbon steel plates also suggest that reactions in closed vessels under normal laboratory conditions are affected by the diffusion of oxygen in the reaction vessels.

Introduction

Conditions inside waste packages will be determined primarily by the reactions of thermodynamically unstable iron with groundwater penetrating into waste packages and by the nature of the iron corrosion products formed. The main corrosion products of iron corrosion are Fe (II) ions, hydrogen and products of reactions of these species with species presented in water flowing into waste packages. The composition of water will correspond to the composition of ground water affected by other engineered barriers (in the Czech concept of DGR mainly by compacted bentonite).

An equilibrium or long-term steady state cannot be expected to form inside waste packages, because they are already open to the flow of water to and from waste packages. The maximum pressure of hydrogen achieved in waste packages will depend on the transport properties of compacted bentonite. After achieving the maximum, breakthrough pressure, hydrogen will break through bentonite and the pressure will be reduced. This process will be repeated until all the iron in waste packages is consumed or the sealing properties of bentonite are lost (formation of a preferential path for hydrogen release) after which hydrogen pressure will decrease to a steady state level.

Both iron species and hydrogen have a strong influence on fuel corrosion rates (e.g. Shoesmith et al., 2004, Spahiu et al., 2000, Loida et al., 2004). It was found that hydrogen can reduce the uranium matrix dissolution rate, but the main reasons underlying this decrease have not been sufficiently explained. No detailed effort was devoted to the effect of iron species on conditions that will evolve inside waste packages with spent fuel assemblies, primarily on the effect of iron corrosion on Eh development, which to a great extent controls spent fuel dissolution.

According to Grenthe et al., 1992, the Eh in deep groundwater systems is governed by the following reaction:

$$Fe(OH)_{3(s)} + 3H^+ + e^- = Fe^{2+} + 3H_2O \quad (1)$$

This half-cell reaction is affected mainly by very low values of solubility product of $Fe(OH)_{3(s)}$. This is, however, valid only for groundwater in contact with rock containing a sufficient amount of this product. It can be expected that inside waste packages, iron precipitation products will not be hydrous ferric oxide, but rather iron hydroxide, magnetite or possibly some green rusts depending on the composition of groundwater (Arcos et al., 2008). The rate of the corrosion reaction, the rate of oxidation and hydrolysis of Fe^{2+} and the rate of the formation of precipitation products will govern the development of Eh inside waste packages. One possibility of estimating chemical conditions in such complex systems is to use advanced geochemical models (Domski, 2000, Pan et al., 2002). A great disadvantage of these models is that a lot of important input data must be estimated. This can lead to great uncertainty about the real conditions inside waste packages.

The main aim of this work is therefore to measure Eh in simplified systems simulating the conditions inside waste packages and the effect of iron corrosion on Eh development inside waste packages after ingressions of groundwater. The results can then be used to validate geochemical models.

Experimental

The first system that simulated the environment inside a waste package after the ingression of water consisted of a closed vessel with synthetic bentonite porewater and electrodes and with and without 5 g of iron powder (Fe ≥ 99,5 %, Riedel-de Haën Cat.: 12311, Lot.:S19452). Synthetic bentonite pore water corresponding to the composition of sodium bentonite Volclay KWK 20-80 of a density of 1600 $kg.m^{-3}$ (table 1) was prepared according to the recipe prepared on the basis of the calculations carried out in the NF-PRO project (Bayens, 2005). Pt, Au and standard commercial silver chloride RE 403 (Theta 90) electrodes were used for Eh measurements. An electrochemical noise measurement system with home-made three electrodes, two steel working electrodes (carbon steel rod of diameter 3 mm, Czech standard 11321, mechanically polished by 320 grit SiC paper) and one reference electrode was used to measure corrosion potentials. Before the electrodes were immersed in the corrosion cell, the cell was purged by nitrogen for 30 minutes. An ECM 8 Electrochemical Multiplexer Analyser with evaluation software ESA 400 Electrochemical Signal Analyser version 2.01 from Gamry Instruments was used to evaluate the results. The experiments were carried at various temperatures controlled by a TDC 2 Temperature Controller with a Watlow series 988 PID control unit.

Table 1: *Composition of the synthetic bentonite pore water (Bayens, 2005)*

pH	8
Ionic strength [mol.l^{-1}]	0.29
c(Na) [mol.l^{-1}]	$2.07.10^{-1}$
c(K) [mol.l^{-1}]	$3.1.10^{-3}$
c(Mg) [mol.l^{-1}]	$1.2.10^{-2}$
c(Ca) [mol.l^{-1}]	$9.8.10^{-3}$
c(Sr) [mol.l^{-1}]	$8.6.10^{-5}$
c(Cl) [mol.l^{-1}]	$6.18.10^{-2}$
c(SO_4) [mol.l^{-1}]	$9.5.10^{-2}$
c($C_{anor.}$) [mol.l^{-1}]	8.10^{-4}
c(F) [mol.l^{-1}]	$2.2.10^{-4}$
c(Si) [mol.l^{-1}]	$1.8.10^{-4}$

In the second system, instead of iron powder, 8 carbon steel plates (Czech standard 11321, mechanically polished by 600 grit SiC paper) were immersed in approximately 2 l of synthetic bentonite water solution. Composition of carbon steel samples is given in Table 2. The corrosion rates were continuously measured by measuring hydrogen evolution through volume changes (Vokal et al., 2007) and by measuring the weight of the carbon steel plates after the experiments. Eh was measured by Pt and Au electrodes. The experiments lasted 30 days. Under these conditions, commercial reference electrodes could not be used because of the significant changes of electrolytes inside the electrodes. A special reference electrode had to be prepared by coating Ag wire with silver chloride.

Table 2: *Composition of carbon steel used in experiments*

No. of Steel	C [%] - max	Mn [%] - max	P [%] - max	S [%] - max
11 321	0.10	0.45	0.035	0.035

Results and Discussion

Experiments with iron powder

A comparison of the results of Eh measurements (recalculated against standard hydrogen electrode) in bentonite water with and without iron powder is given in Fig. 1. It can be seen that the Eh of bentonite water decreased firstly by the effect of nitrogen bubbling through the water for 30 minutes in both systems with and without the addition of iron, but the decrease of Eh in a system with iron powder was considerable after a very short time. These low values of Eh in a system with iron did not change over time.

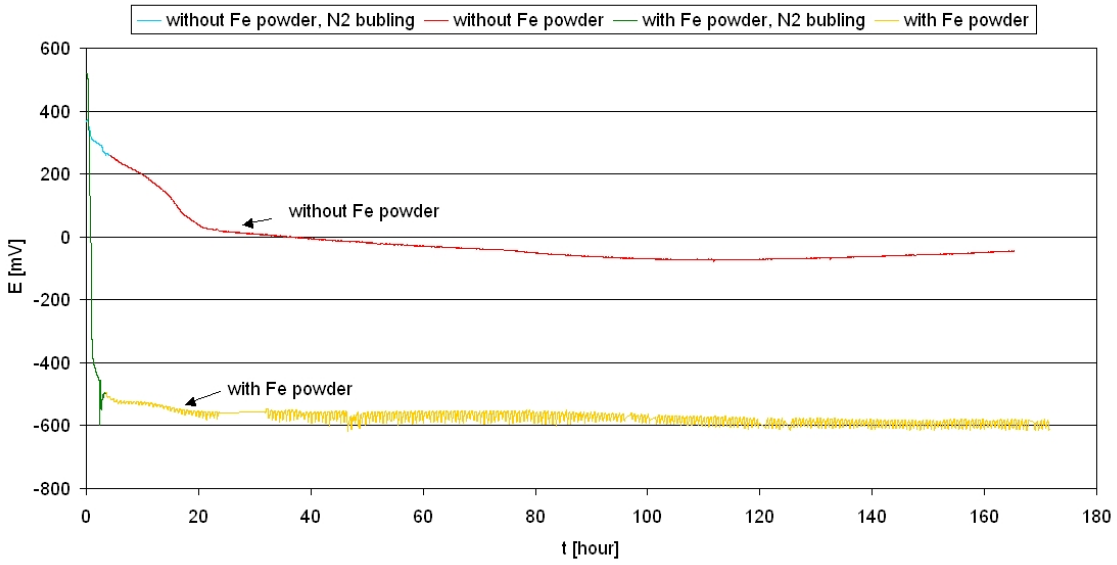

Figure 1: *Redox potentials of bentonite water with and without addition of iron powder*

The results of the measurements of the corrosion potentials of iron, which represent potentials at which the rates of anodic half-cell reaction of iron corrosion (reaction (2)) and cathodic half-cell reaction of water reduction (reaction (3)) will be equal, are given in Figs. 2 and 3.

$$Fe \rightarrow Fe^{2+} + 2e^{-} \qquad (2)$$

$$2H_2O + 2e \rightarrow H_2 + 2\,OH^{-} \qquad (3)$$

It can be seen that the addition of iron changes the Eh and the corrosion potentials of iron. The results of the corrosion potential change will depend on the corrosion temperature. At 50 °C (and also at 60 °C not shown in the paper) the corrosion potentials of iron are increased significantly in the presence of iron powder, but at 70 °C the corrosion potentials of iron decrease in a system with iron powder over time and increase in the system without iron powder. The decrease of Eh at 50 and 60 °C by adding iron to the system led presumably to a decrease in the rate of anodic reaction (2) so that the corrosion potential settled at a higher value at which the rates of reaction (2) and (3) will be equal.

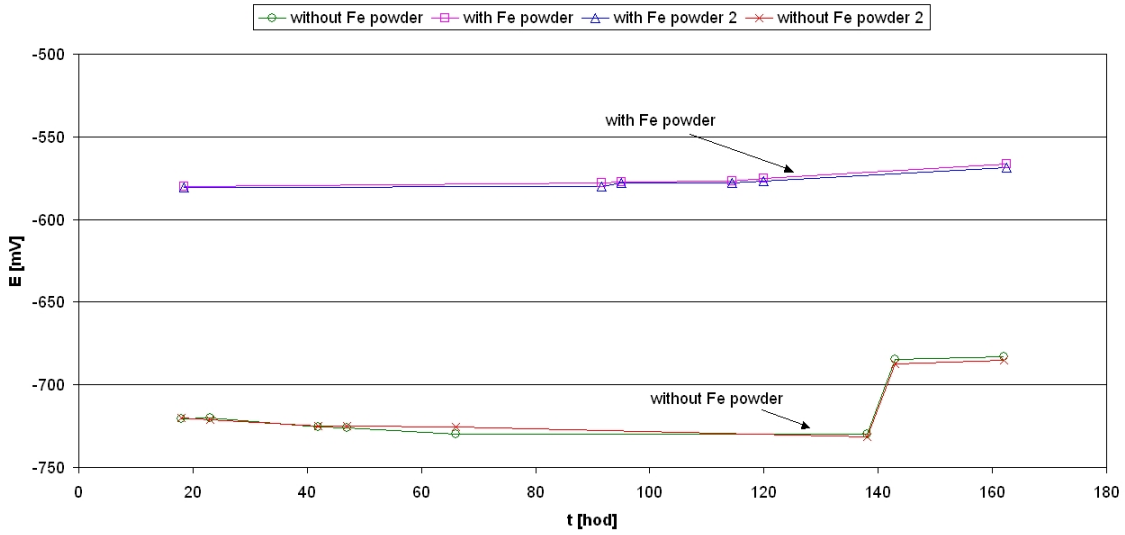

Figure 2: *Corrosion potentials of bentonite water with and without addition of iron powder measured at 50 °C*

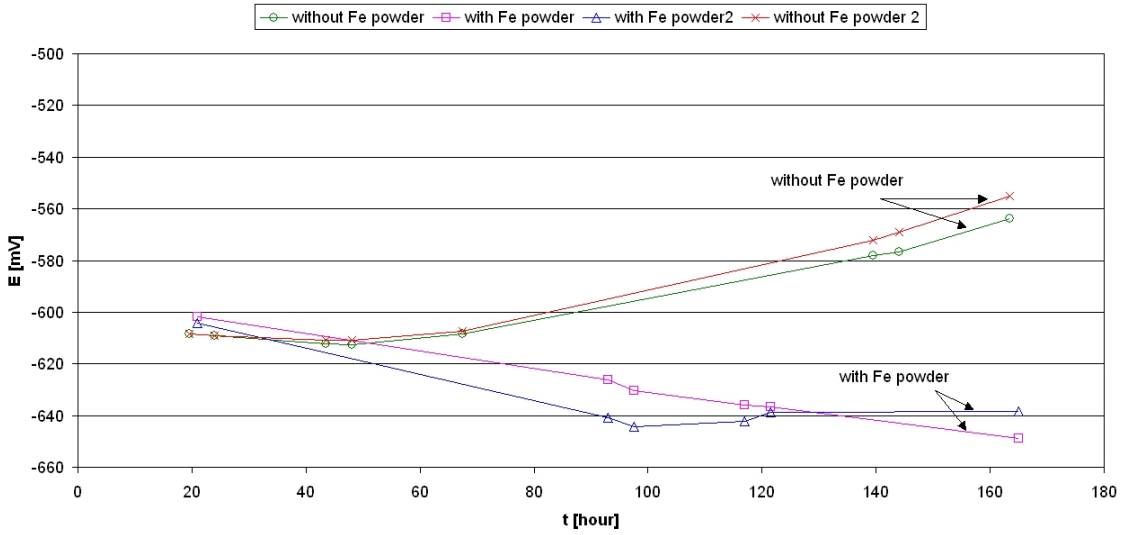

Figure 3: *Corrosion potentials of bentonite water with and without addition of iron powder at 70 °C*

It appears that at 70 °C an increase of corrosion potentials of electrodes in water without iron is caused by the fact that at this temperature oxygen penetrates more easily to the vessel, what causes that in addition to cathodic reaction (3), a more efficient reaction with oxygen (4) is also applied. The rate of anodic reaction (2) is then increased accordingly.

$$\tfrac{1}{2}\, O_2 + H_2O + 2e^- \rightarrow 2\, OH^- \qquad (4)$$

A decrease of corrosion potentials in the system with iron powder suggests that at 70 °C the rate of anodic reaction (2) increases with temperature and accordingly increases the rate of cathodic reaction (3).

Experiments with carbon steel plates

In the second experimental system 8 carbon steel plates were added in reaction vessel instead of iron powder. In these experiments, the corrosion rates of carbon steel plates were continuously measured using measurements of the amount of hydrogen evolution generated through the cathodic reaction (3) (Vokal et al., 2007). The results of the measurements of hydrogen accumulation and the changes of Eh measured with Pt and Au electrodes are given in Fig. 4. It can be seen that the rate of hydrogen evolution decreases over time, probably due to the formation of corrosion products. The rate of hydrogen evolution corresponds to a decrease of the corrosion rate from initial values of approximately 25 μm/yr to values of approximately 1 μm/yr after 10 days of corrosion. The average corrosion rate from the measurements of the weight loss of 8 carbon steel plates after 30 days was 3.7 ±0.5 μm/yr. Eh decreased during first day of the experiment to values lower than –400 mV, but then started to increase and after several days stabilized at positive values of approximately 200 mV. We assumed in agreement with Appelo and Postma, 1999 that corrosion products covering the electrodes caused this increase. Therefore a special device enabling Eh to be measured discontinuously by pumping a small amount of water from the reaction vessel for measurement with a clean Pt electrode was developed for a second experiment under otherwise the same conditions as in the first experiment. After the Eh was measured the water was put back into the reaction vessel. The results from the second experiment with discontinuous measurements are plotted in Fig. 5. The corrosion rate from hydrogen evolution decreased in this experiment from 32 μm/yr to about 1 μm/yr. The average corrosion rate from the measurements of the weight loss of 8 carbon steel plates after 30 days was 5.2 ± 0.7 μm/yr. It can be seen that the Eh values obtained by discontinuous measurements with clean electrodes measured after some time of corrosion were much lower than the values obtained with electrodes immersed in the solution. Nevertheless, the results of Eh measured with clean electrodes after some time were higher than the initial values of Eh after measuring in the first days of corrosion. This could be caused by the penetration of oxygen in the closed reaction vessel despite an overpressure of hydrogen in the vessel.

The discontinuous measurements also enabled pH to be measured (Fig. 6). It was observed that pH decreased from the initial values of approximately 8.6 to values of approximately 7.3 after 15 days of corrosion despite the formation of OH^- ions in reaction (3).

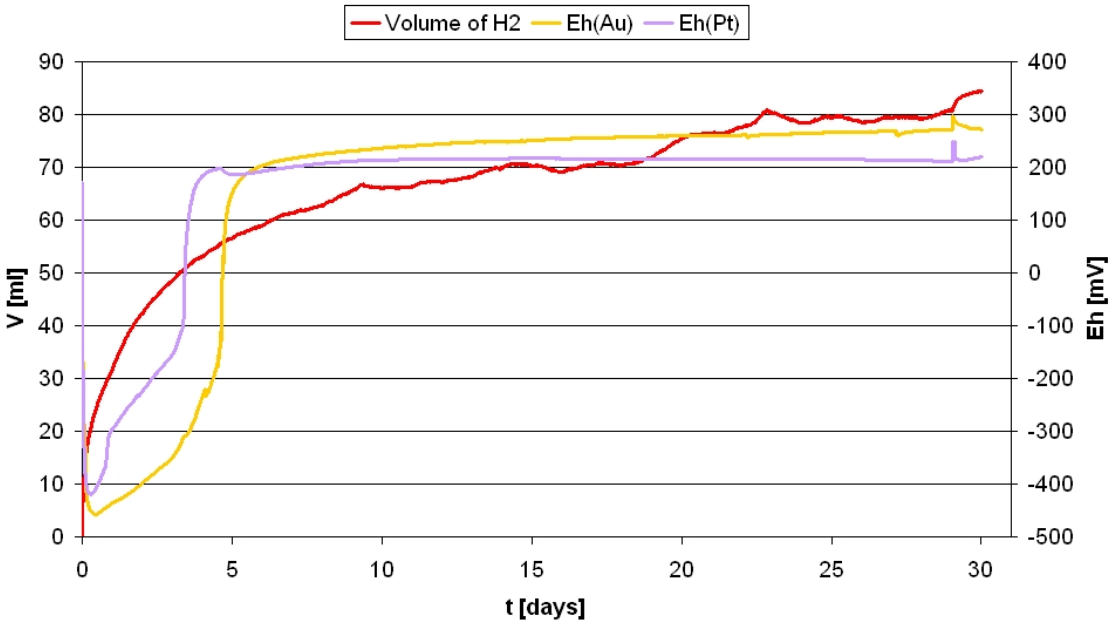

Figure 4: *Change of Eh potentials of bentonite water due to corrosion of carbon steel plates at 70 °C (1st experiment)*

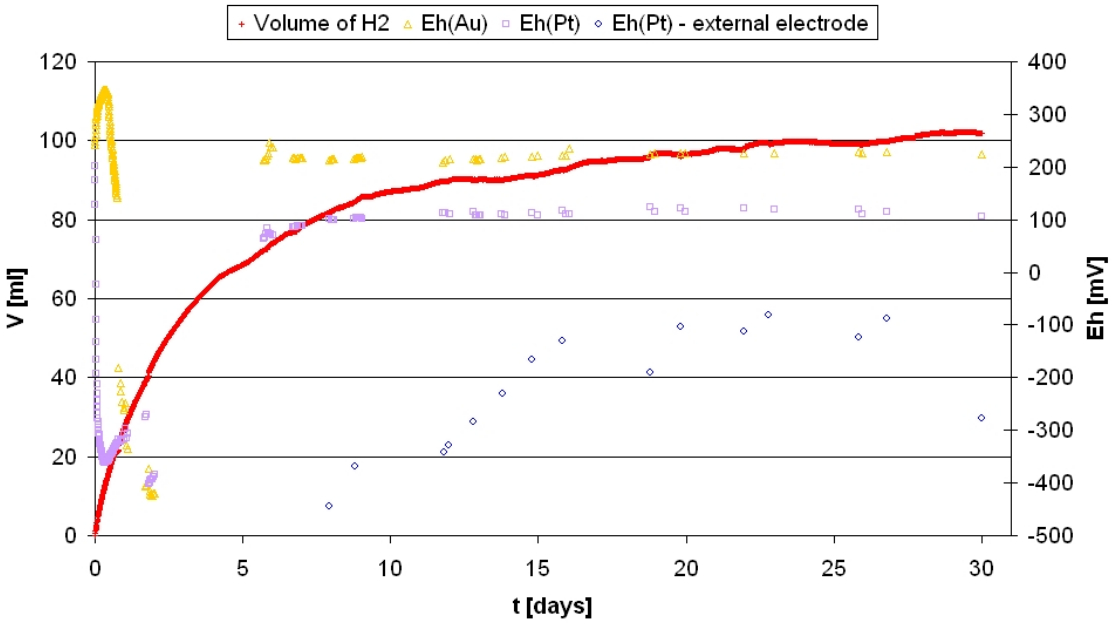

Figure 5: *Change of Eh potentials of bentonite water due to corrosion of carbon steel plates at 70 °C (2nd experiment)*

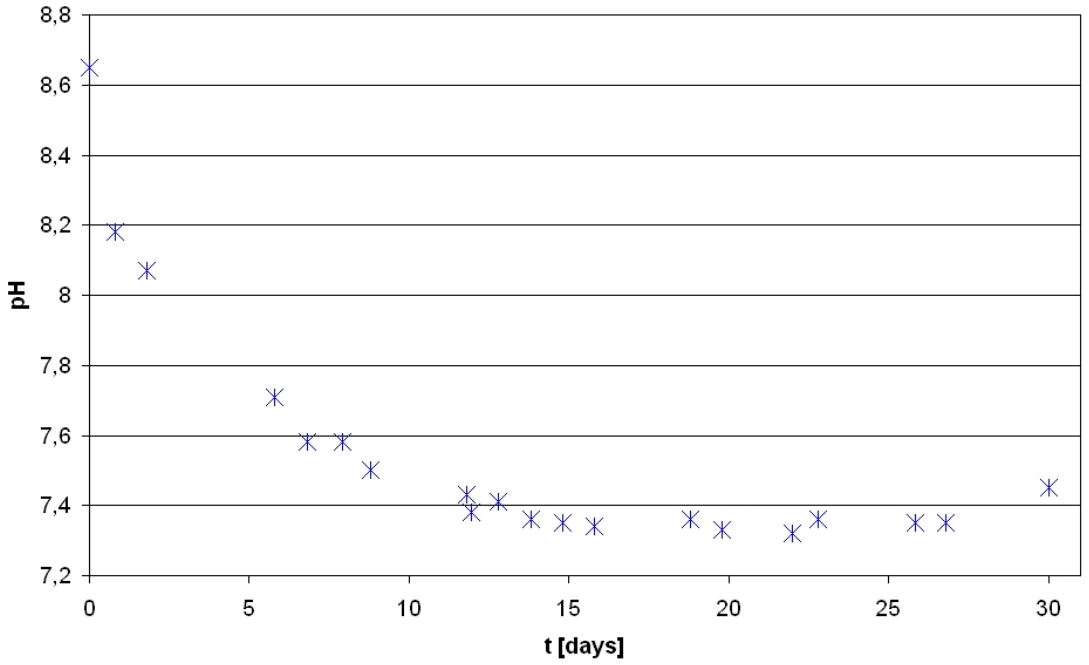

Figure 6: *Change of pH due to corrosion of carbon steel plates at 70 °C (2nd experiment)*

Conclusions

It was shown that the corrosion of iron significantly decreases the Eh of water. Also, surprisingly, a pH decrease was measured in the synthetic bentonite water system with corroding carbon steel plates. Reason for the decrease in pH has not yet been elucidated. It was confirmed that in long-term experiments, iron corrosion products affect continuous measurements of Eh with Pt or Au electrodes in a system with iron, which is manifested by an apparent increase of Eh after the first days of corrosion. But this increase in Eh did not disappear completely if the measurements were performed discontinuously with clean electrodes. This indicates that oxygen could diffuse slowly in reaction vessels. Therefore further experiments are now being prepared using an anaerobic box with a concentration of oxygen below 0.1 ppm.
In addition to uncertainty about the effect of the diffusion of oxygen in long-term experiments, there are also other factors that can affect conditions inside waste packages after their failure, such as radiation or the presence of other inner waste package materials. Consequently there is still rather great uncertainty about the conditions under which radionuclides will be leached from spent fuel matrix and spent fuel structure materials. This uncertainty will have to be reduced by systematic research.

Acknowledgement

This work was partly funded from EC-EURATOM 7th Framework Integrated project RECOSY No.230357, Ministry of Trade and Industry of the Czech Republic under project 1H-PK25 and Radioactive Waste Repository Authority.

References

Appelo C.A.J., Postma D., Geochemistry, groundwater and pollution, A.A. Balkema/Rotterdam/Brookfield, 1999

Arcos D et al (editor), Deliverable D2.6.4, RTDC-2 Synthesis Report, NF-PRO project, 2008

Baeyens B.: Information from WP 2.5 of 6th EC integrated project NF-PRO, 2005

Domski P.S., In-Package Chemistry Abstraction, OCRWM Analysis, ANL-EBS-MD-000037. 2000

Grenthe I., Stumm W., Laaksuharju M., Nilsson A.C., Wikberg P.: Redox Potentials and Redox Reactions in Groundwater Systems, Chemical Geology, Vol. 98, Issues 1-2, July 1992

Loida A., Metz V., Kienzler B., Geckeis H., Impact of Hydrogen Overpressure on Spent Fuel Alteration Behaviour in Salt Brine During a Three-Year Long Corrosion Test, Mat. Res. Soc., Symp. Proc., Vol 824, p. 95, MRS, 2004

Pan Y.-M., Brossia C.S., Cragnolino G.A., Dunn D.S., Jain V., Sridhar N., Evolution of Solution Chemistry through Intercations with Waste Package Internal Structural Components, Mat. Res. Soc. Symp.Proc.Vol. 713, 2002, MRS, p. JJ1.10

Shoesmith D.W., Noel J.J., Garisto F., An Experimental Basis for a Mixed Potential Model for Nuclear Fuel Corrosion within a Failed Waste Canister, Mat. Res. Soc., Symp. Proc., Vol 824, p. 81, MRS, 2004

Spahiu K., Werme L., Eklund U.,The Influence of Near Field Hydrogen on Actinide Solubilities and Spent Fuel Leaching, Radiochimica Acta 88, 507, 2000

Vokál A., Brůha P., Dobrev D., Polívka P., Silber R., A Study of Anaerobic Corrosion of Carbon Steel, Deliverable 2.3.8, NF-PRO project, August 2007

DEVELOPMENT OF MULTIPARAMETRIC OPTICAL SENSING FOR ENVIROMENTAL APPLICATIONS

Dörte Steinbrück and Michael U. Kumke*

Institut of Chemistry, University of Potsdam, Germany

* Corresponding author: kumke@chem.uni-potsdam.de

Abstract

For the determination of fundamental redox parameters, such as proton (pH) or oxygen concentration, innovative fiber-optical chemical sensing (FOCS) is being developed. Different fluorescence probes for fiber-based pH monitoring were tested with respect to the accessible pH range, the selectivity, and the sensitivity, respectively. Furthermore, for the implementation of FOCS-based pH measurements the immobilisation of fluorescence probes in different polymer materials is the crucial step. In the present study, the spectroscopic properties of the promising pH fluorescence probe 2',7'-Bis(2-carboxyethyl)-5(6)-carboxyfluorescein (BCECF). BCECF showed a good fluorescence response to the proton activity in the pH range < 8. For the implementation into a fiber-based sensor scheme the immobilisation in different proton permeable polymers was tested.

Introduction

FOCS has been proven a powerful alternative to electrochemical-based techniques for oxygen sensing. While standard electrochemical techniques are based on a Clark-type electrode design, which inherently consumes part of the analyte during the measurement, FOCS are based on luminescence measurements and are free of analyte consumption. Compared to electrochemical approaches FOCS has further advantages with respect to miniaturization, durability of the sensors, response time, and costs. Successful FOCS-based oxygen sensing in such divers systems like salivary glands of flies or inside noodles has been reported (Schmälzlin et al., 2006, Schmälzlin et al., 2005, Löhmannsröben et al., 2006). Recently, a joint collaborative for depths profiling of oxygen concentrations in biofilms was initiated. The detection scheme is based on the luminescence quenching of a Pt-complex by molecular oxygen. Using dual-phase modulation (or dual lifetime referencing) the often encounter problems arising from strong unwanted background signals (e.g., in biological matrices often chlorophyll is present in the sample) are effectively circumvented. While the FOCS-based oxygen measurements are in a very advanced state-of-the-art, the determination of other physico-chemical parameter such as pH or E_h using FOCS is less developed.

Although suitable probes for the detection of many chemical parameter are commercially available (driven by bioanalytical very often microscopy-based applications), the integration in fiber-optical sensing schemes is at its infancy. The difficulties to overcome in the future are i) related to the integration of the chemical probe in a suitable polymer matrix that is permeable for the analyte molecules but at the same time sufficiently retarding the probe molecules, ii) the combination of polymer and fiber with respect to fixation and signal transduction, iii) cross-sensitivity to other compounds present in the sample, and iv) the adaptation of detection electronics (e.g., MHz to GHz modulation frequencies).

In the present paper we are reporting on recent progress in the development of a FOCS-based pH sensor for environmental monitoring, e.g., in mines or deep underground repositories. A fairly large number of fluorescence-based pH indicator dyes are well characterized for homogeneous solution applications (Draxler and Lippitsch, 1995, Lin et al., 1999, Draxler et al., 1993, de Marcos and Wolfbeis, 1996). However, for luminescence-based sensing applications in complex matrices cross sensitivities to other parameters such as ionic strength in general, the presence of specific ions, or the oxygen concentrations need to be known and, if possible, suppressed in an adapted experimental set up. A promising fluorescence probe for pH sensing is 2',7'-Bis(2-carboxyethyl)-5(6)-carboxyfluorescein (BCECF) because the spectral distribution of the emission spectrum, the fluorescence efficiency as well as the fluorescence decay time are dependent on pH (Boens et al., 2006, Hille et al., 2008).

Experimental

BCECF was purchased from Sigma-Aldrich ($\geq$ 98%) and used as received. The sample solutions were prepared in Millipore water. For the pH adjustment of the solutions HCl and NaOH (both purchased from Carl Roth, Karlsruhe) were added.

The absorption measurements were carried out using a Lambda 750 UV/Vis Spectrometer (Perkin Elmer). The steady-state fluorescence measurements were performed on a FluoroMax3-P spectrometer (Jobin Yvon). An FLS920 Spectrofluorometer (Edingburgh Instruments) was employed in the time-resolved fluorescence measurements and operated in the time-correlated single photon counting (TCSPC) mode. For excitation a SuperContinuum Source SC400 pp-2 (20 MHz, pulse duration 400 fs, Fianium) was used.

Characterisation of BCECF

In Figure 1 the chemical structure of BCECF is depicted together with different polymers tested in the search of a suitable polymer for the design of a FOCS-based pH sensor. A special requirement for the polymers is sufficient water permeability (Borisov et al., 2008, Davies et al., 1992, Bobacka et al. 2002).

From the chemical structure of BCECF it can be seen, that various carboxylic and phenolic functional groups are present, which will respond to the pH of the environment and subsequently influence the spectroscopic properties of the probe.

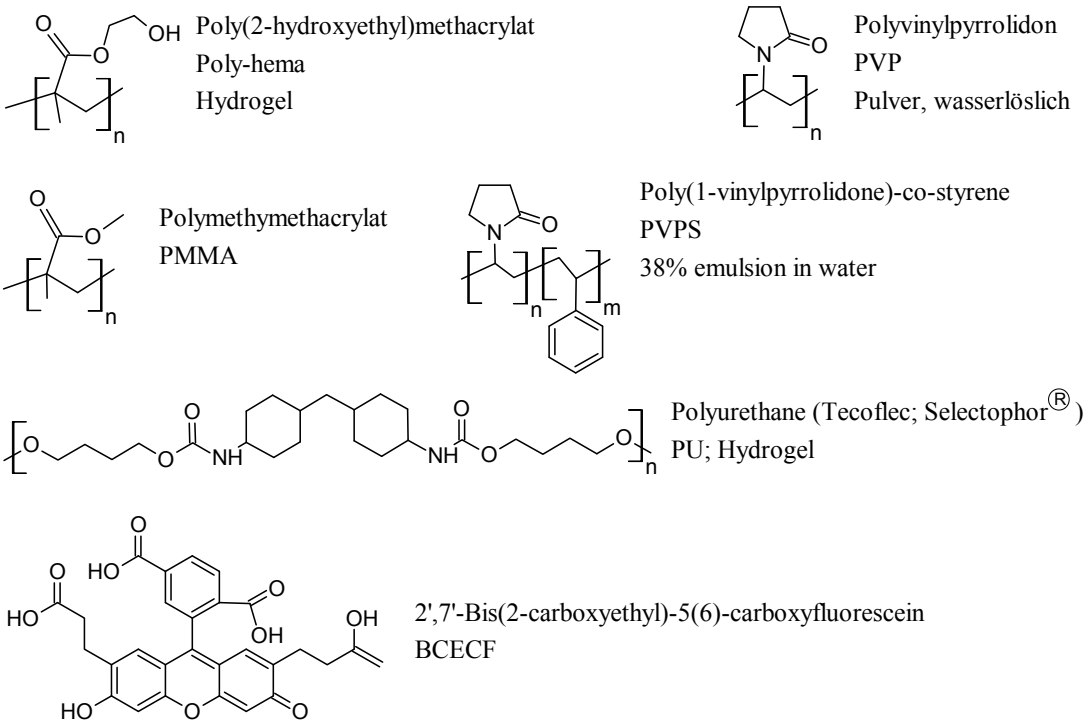

Figure 1: *Structures of water-permeable polymers and the pH-sensitive dye BCECF.*

Absorption spectra of BCECF

In Figure 2 the absorption spectra of BCECF at different pH are shown. Upon increasing the pH a bathochromic shift of the absorption is observed, which can be attributed to alterations of the electronic structure of BCECF due to deprotonation of carboxylic and phenolic groups directly attached to the chromophore. On the right hand side of Figure 2 the extinction at λ = 490 nm as function of pH is shown. Two inflection points are observed, the first one is located around pH ~ 3.6 and can be attributed to the deprotonation / protonation of the carboxylic groups of BCECF (see Figure 1 for structure). At higher pH (~7.3) a second inflection point is observed, which is tentatively attributed to the deprotonation of the phenolic group.

Excitation and Emission spectra

Figure 3 (right side) shows the observed changes of the excitation spectra (at λ_{em}= 550 nm) and of the respective alteration found in the emission spectra (at λ_{ex} = 480 nm) upon variation of the pH.

In contrast to the trends found for the absorption maximum, the emission maximum is shifted to higher energies (smaller wavelength) with increased pH. While the protonated BCECF (present at very low pH) has two emission maxima at λ_{em} = 520 nm and λ_{em} = 550 nm, the deprotonated BCECF species shows only one maximum at λ_{em} = 520 nm. This strongly suggests the presence of an excited state proton transfer reaction. While at low pH in the absorption as well as in the excitation spectra only one absorption band is observed (absorption and excitation spectra contain information on the molecular species in its electronic ground state), in the emission already fluorescence contributions

from protonated and deprotonated species are found (the fluorescence emission spectrum contains information on the reactivity in the electronically excited state of a species). It is tempting to attribute the observed spectral features to a strong change in the acidity of the phenolic groups of BCECF. From similar molecules such as isocoumarins a very comparable behaviour has been reported (Steinbrück et al., 2008).

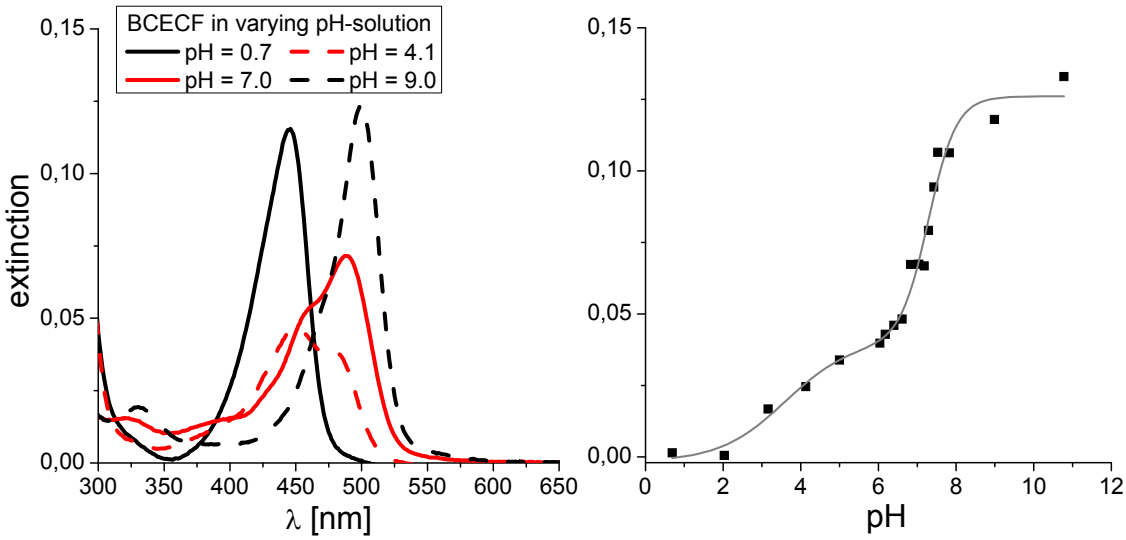

Figure 2: *Absorption of BCECF in aqueous solution at different pH-values.*

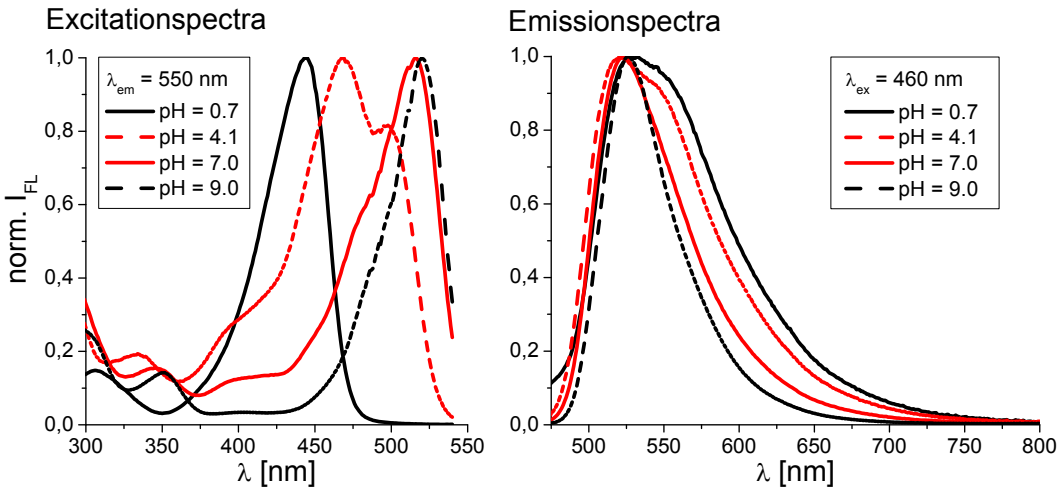

Figure 3: *Excitaion and Emissionsspectra of BCECF at different pH-values.*

In Figure 4 (left side) the dependence of the fluorescence intensity at different emission wavelengths with excitaion at 470 nm on the pH is shown. The sensitivity of the fluorescence depends on the emission wavelength. At λ_{em}= 520 nm the change in fluorecence intensity is much higher than at λ_{em}= 550 nm.

The plot of the emission intensity over pH at different excitation wavelengths illustrates that the sensibility depends also on the excition wavelength. The best matched wavelength pairs are: excitaion at 470 nm and emission at 520 nm.

Compared to absorption (see Figure 2) the second inflection point is in the same range. Particular the step by λ_{em}= 520 nm is found to be very steep and sharp around pH 7 (pK_A ~ 7.1).

The first pK_A derived from the fluorescence spectra is located around four. The small difference compared to the absorption spectra is a consequence of the excited state proton transfer reaction and the fact, that the corresponding fluorescence spectra of the protonated and deprotonated form are broad and subsequently overlapping. In the emission spectra always the sum of both species is observed and can not be adequately separated.

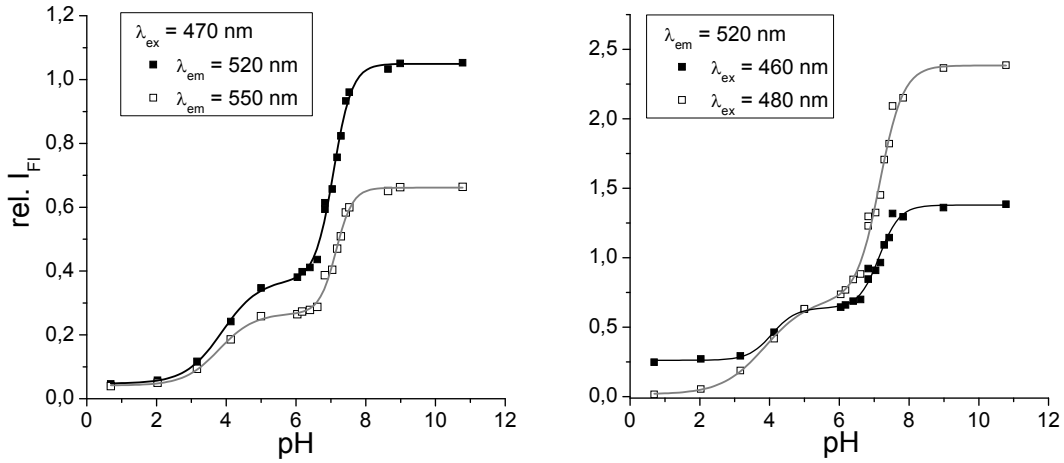

Figure 4*: Intensity of fluorescence from excitation (left) and emission (right) spectra of BCECF as function of the pH.*

Fluorescence-Lifetime

In time-correlated single photon counting experiments the fluorescence decays at different emission and excitation wavelengths pairs were recorded. In Figure 5 the fluorescence decays at two different pH values are presented (left) and the dependence of the calculated monoexponential fluorescence decay time on the pH is shown (right). Here, the emission wavelength has no influence to the decay time and therefore, it is possible to cumulate the whole emission yielding high sensitivity.

The observed dependence of the fluorescence on the pH adds further evidence to the proposed presence of an excited state proton transfer. In very good agreement with the results obtained from absorption and steady-state emission experiments, the evaluation of the time-resolved data also yielded a pK_A ~ 7.2 and a second, however, much lower pK_A at 1.5.

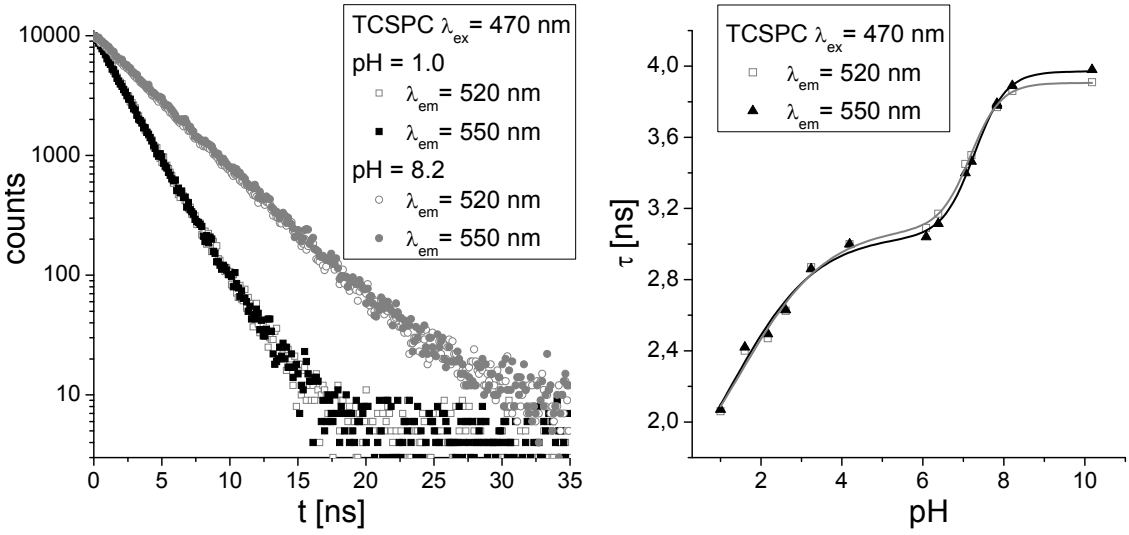

Figure 5: *Fluorescence decays of BCECF at λ_{ex} = 470 nm at different pH and λ_{em} (left). Fluorescence lifetime λ_{em} = 520 nm and 550 nm of BCECF as function of the pH (right).*

Summary/Conclusion

The pH influence on the spectroscopic properties of BCECF was investigated in steady-state and time-resolved emission as well as in absorption. Due to the intrinsic properties of BCECF three different pK_A were found, one of which is attributed to a proton transfer reaction in the electronically excited state. It is better referred to as pK_A*. Based on these findings, BCECF is a promising pH probe for FOCS. Especially, because it is still sensitive in highly acidic pH range (below pH 2), which is very attractive for sensing applications in mining environments. However, in order to access the low pH interval, a time-resolved detection scheme is required.

From the comparison of absorption and fluorescence measurements it can be concluded that for applications with a requirement for high selectivity and sensitivity fluorescence based detection is preferential because of a much larger dynamic range and higher sensitivity. First successful experiments were carried out, in which BCECF was immobilized in a water permeable polymer. BCECF doped polymer beads were subsequently used in pH measurements. After such proof of principle the next step is the combination of the doped polymer and fibers and the improvement of the response time of such senors. Currently, a MHz modulation technique is implemented in order to use the pH dependence of the BCECF fluorescence decay time for pH sensing.

Due to the spectroscopic properties reported, BCECF seems to be a promising candidate for a combined optical senor for pH and oxygen determination using similar set-ups. A miniaturized multiparameter FOCS can be envisaged using different time windows (ns- and µs- timescales) for the detection of chemical parameters in environmental matrices (e.g., simultaneous measurement of oxygen and pH at same location in sample).

In the future, further chemical parameters, such as specific ions (e.g., iron) or the E_h value, are planned for implementation in an optical fiber-based sensor, therefore, making full use of the advantages of this technique with respect to miniaturisation,

sensitivity and selectivity, multiparameter as well as distributed sensing capabilities. To reach this goal, redox-sensitive dyes will be tested in terms of accessible E_h and dynamic range, immobilization in polymer materials, and cross-sensitivities.

Acknowledgements

The authors are thankful to Dr. E. Schmälzlin for his support in sensor preparation and carrying out FOCS measurements. For financial support the authors wish to thank the European Commission (FP7-212287).

References

Bobacka J., Ivaska A., Lewenstam A. (2002): Potentiometric Ion Sensors Based on Conducting Polymers, Electroanalysis 15 366-374.

Boens N., Qin W., Basaric N., Orte A., Talavera E. M., Alvarez-Pez J. M. (2006): Photophysics of the fluorescent pH indicator BCECF, J. Phys. Chem. A 110 9334–9343.

Borisov S. M.,. Herrod D. L, Klimant I. (2008): Fluorescent poly(styrene-block-vinylpyrrolidone) nanobeads for optical sensing of pH, Sensors and Actuators B

Davies M.L., Hamilton C.J, Murphy S.M., Tighe B.J. (1992): Polymer membranes in clinical sensor applications, Biomaterials 13 971-978.

de Marcos S., Wolfbeis O.S. (1996) Optical sensing of pH based on polypyrrole films, Anal. Chimica Acta 334 149–153.

Draxler S., Lippitsch M. E. (1995): pH sensors using fluorescence decay time, Sensors and Actuators B 29 199–203.

Draxler S., Lippitsch M. E, Leiner M. J.-P. (1993) Optical pH sensors using fluorescence decay time, Sensors and Actuators B 11 421–424.

Hille C., Berg M., Bressel L., Munzke D., Primus P., Löhmannsröben H.-G., Dosche C. (2008): Time-domain fluorescence lifetime imaging for intracellular pH sensing in living tissues, Anal Bioanal Chem 391 1871–1879.

Lin H.-J., Szmacinski H.,. Lakowicz J.R (1999): Lifetime-based pH sensors: Indicators for acidic environments, Anal. Biochemistry 269 162–167.

Löhmannsröben H.-G., Beck M., Hildebrandt N., Schmälzlin E., van Dongen J. T. (2006): New Challenges in Biophotonics Laser-based Fluoroimmuno Analysis and in-vivo Optical Oxygen Monitoring, Congrès: Laser applications in Europe : Workshop on Laser Applications in Europe, Dresden , ALLEMAGN, 6157, pp. 61570E.1-61570E.6

Schmälzlin E., van Dongen J. T., Klimant I., Marmodee B., Steup M., Fisahn J., Geigenberger P., Löhmannsröben H.-G. (2005): An optical multifrequency phase-modulation method using microbeads for measuring intracellular oxygen concentrations in plants, Biophysical Journal 89 1339–1345.

Schmälzlin, E., Walz, B., Klimant I., Scheweb B., Löhmannsröben H.-G (2006): Monitoring hormone-induced oxygen consumption in the salivary glands of the blowfly,

calliphora vicina, by use of luminescent microbeads, Sensors and Actuators B 119 251–254.

Steinbrück D., Rasch C., Kumke M.U. (2008): Photophysics of Ochratoxin A in aqueous solution, Zeitschrift für Naturforschung B, 63b 1321–1326.

GENERAL CHARACTERISATION OF THE REDOX SYSTEMS IN THE SWEDISH CANDIDATE SITES FOR DEEP DISPOSAL OF NUCLEAR WASTE

Maria Jose Gimeno[1*], Luis Auque [1], Javier Gomez [1], Patricia Acero [1], Marcus Laaksoharju [2]

[1] University of Zaragoza (SP)

[2] GEOPOINT AB (SW)

* Corresponding author: mjgimeno@unizar.es

Abstract

Two sites in Sweden are being characterised as possible candidates for hosting the proposed repository: Forsmark and Laxemar-Simpevarp, in the eastern coast of Sweden. The Swedish repository system consists of copper canisters, with a cast iron insert containing spent nuclear fuel, which are surrounded by bentonite clay and deposited at approximately 500 m depth in saturated, granitic rock. The main geologic, hydrologic and hydrogeochemical features in both candidate sites are presented in this work, especially in relation to their redox characteristics. Moreover, the methodology for quality assurance of the hydrochemical data and for the measurement of potentiometric Eh values is briefly explained in order to evaluate the uncertainties and to build confidence on the interpretation of Eh data and on the results for redox species..

With regard to the redox parameters and indicators, Eh values range from –143 to –281 mV in Forsmark and from -210 to -310 mV in Laxemar-Simpevarp. All these values are clearly reducing, which indicates the good redox-buffering ability of microbial or water-rock interaction processes. This is consistent with the detected presence of Fe(II)-bearing minerals (mainly chlorite and pyrite) in the fracture fillings at all depths in Laxemar-Simpevarp and Forsmark areas. These mineral occurrences prove that oxidising episodes have not exhausted the reducing capacity of fracture filling minerals even in the shallowest part of the studied systems.

Another typical redox feature of both studied systems is that neither Eh values nor concentrations of redox-sensitive elements (iron, sulphur, manganese and carbon) nor calculated potentials from redox couples nor microbiological populations show any clear trend with depth. This could be a consequence of their complex hydrological setting and palaeohydrogeological evolution.

The findings from this work set the necessary basis for the development for each of these systems of a general conceptual model in which the results from mineral phases,

raw hydrochemical data and potentiometric Eh measurements can be combined with different types of geochemical modelling calculations in order to identify the origin of waters and the main geochemical processes determining their redox evolution as well as to evaluate the significance of potentiometric redox measurements.

General description of the two Swedish candidate sites; Forsmark and Laxemar

The general description of the Swedish candidate sites for underground deep disposal of nuclear waste has been extensively provided elsewhere (Ström *et al.*, 2008; Laaksoharju, 2008; Laaksoharju *et al.*, 2008a,b). Thus, only the main features of both sites are presented in this section.

The Forsmark site (Figure 1) is located in the municipality of Östhammar, in the vicinity of the Forsmark power plant and the offshore repository for reactor waste (SFR). The topography of the area is relatively flat and the dominant rock types are metamorphosed medium-grained granites and granodiorites (Ström *et al.* .2008).

The Laxemar-Simpevarp area is located close to the shoreline of the Baltic Sea (Figure 1), in the municipality of Oskarshamn. The investigated area is located immediately adjacent to the Oskarshamn nuclear power plant and the Central Interim Storage Facility for Spent Nuclear Fuel (Clab), were all the Swedish spent nuclear fuel is provisionally being stored. The predominant rock-types in this area are granite and quartz-monzodiorite (Ström *et al.* .2008).

Figure 1*: Map of Sweden with the locations of the two candidate sites for hosting the deep repository for nuclear waste disposal, Forsmark and Laxemar-Simpevarp.*

Most of the bedrock in both sites was formed between 1900 and 1800 Ma ago and it has suffered both ductile and brittle deformation. The majority of the fracture systems that are water conducting today were activated or reactivated during the Palaeozoic and have probably been water pathways ever since (Tullborg *et al.*, 2008).

The present hydrochemistry of groundwaters in the Forsmark and Laxemar-Simpevarp areas is the result of a complex mixing process driven by the input of different recharge waters at least since the last glaciation. Mixing can be considered the prime irreversible process responsible for the chemical evolution of the Forsmark and Laxemar-Simpevarp groundwater systems. Then, the successive disequilibrium states resulting from mixing conditioned the subsequent water-rock interaction processes and, hence, the re-equilibration pathways of the mixed groundwaters.

As a general trend in both Forsmark and Laxemar-Simpevarp, the deepest groundwaters (> 600-900 m.b.s.l.) are saline (> 10 g L^{-1} TDS, with a maximum around 70 g L^{-1} at Laxemar) and Na-Ca-Cl to Ca-Na-Cl types, whereas the shallowest groundwaters (< 200-500 m.b.s.l.) are mainly meteoric, Na-HCO_3-type and dilute (< 3.5 g L^{-1} TDS). The groundwaters at intermediate depths are generally brackish (3.5-18.5 g L^{-1}) with more or less marine influence and Ca-Na(Mg)-Cl(SO_4) (Laaksoharju, 2008; Laaksoharju *et al.*, 2008a,b, and references therein). pH values are between 7.2 and 8.6 in the groundwaters of both sites and do not show any clear variation trend with depth. pH is mainly controlled by calcite dissolution-precipitation reactions and, probably, microbial activities, being of secondary importance the influence of other common chemical processes, such as aluminosilicate dissolution-precipitation or cation exchange. Although it will be treated with much detail in the following sections, it is worth to make clear here that groundwater redox conditions are clearly reducing in both sites. Eh values in Forsmark range from -143 to -281 mV, whereas in Laxemar-Simpevarp all the potentiometrically measured values range from -210 and -310 mV (Auque *et al.*, 2008, Gimeno *et al.*, 2008a, b).

Data selected for explorative analysis and modelling activities

Three types of data are considered for the explorative analysis and for the modelling of the redox systems in Forsmark and Laxemar; 1) potentiometrically measured Eh by using the sophisticated methodology developed by SKB; 2) hydrochemical data from water samples, including microbiological determinations and; 3) chemical and mineralogical study of rock samples, including both bulk rock and fracture fillings.

Since the calculations, interpretations and conceptual model implementations for the studied underground systems are based on combining the results from these three types of data, their measurement, selection and the procedures for ensuring their quality and representativeness are a major concern. Therefore, a description of these procedures for each type of data is presented below

Potentiometric Eh measurements

The potentiometric Eh measurement can have both technical and interpretative problems (Auque *et al.*, 2008 and references therein). These problems are, among others, the existence of mixed-potentials, the presence of non-electroactive species, problems of electrode poisoning, presence of low concentrations of redox species or lack of electrochemical equilibrium between the two redox species forming a redox pair.

SKB has developed over the last 25 years one of the best available methodologies for the measurement of this parameter (e.g. Grenthe *et al.*, 1992; Christensen *et al.*, 2000; Auque *et al.*, 2008 and references therein) and its careful use is, at the very least,

extremely helpful information for the study of something as complex as the redox system. The SKB methodology for the potentiometric measurement of Eh in deep groundwaters is based on an integrated system for: (1) sealing off a borehole section by inflatable packers and pumping of groundwater from the section; (2) sampling of pumped groundwater as well as sampling *in situ* in the section to obtain groundwater samples at maintained pressure and (3) on-line long-term measurements (weeks or months; in this last case, usually with several logging periods) of chemical and physical parameters in the unbroken sample water line both at the surface and at depth downhole. Eh is measured and logged simultaneously by three different electrodes (gold, platinum and glassy carbon electrodes) downhole as well as at the surface, against Ag/AgCl double junction gel-filled reference electrodes in both cases. Together with Eh, each probe measures pH and water temperature and the cell at the surface measures also electrical conductivity and dissolved oxygen. This allows checking whether Eh variability is related to variations in the chemical composition of the waters, which makes easier the selection of Eh-values.

From a careful analysis of these logs an Eh value for the groundwaters from the borehole section can be determined. The continuous logging of the redox potential during weeks allows the attainment of stable readings in waters with low concentrations of the redox active species. Moreover, coincident measurements obtained by different electrodes corroborate the existence of electrochemical equilibrium. Hence, those values can be used as reference in geochemical modelling.

In order to ensure the quality and representativeness of the potentiometrically measured Eh values, these values are only accepted for explorative or modelling purposes when corresponding to logs longer than 3 days that produce stable and coincident readings (in a range smaller than 50 mV) by at least two electrodes in the long term and that have simultaneous and stabilised pH logging (to minimize the uncertainty associated with the pH).

Selection of water samples for hydrochemical determinations

The studied water samples are representative of the surface and hydrochemical conditions present in the two candidate sites. Samples reflecting the near-surface conditions (shallow soil pipe waters) and underground conditions (percussion drilled boreholes and core drilled boreholes) are included here.

The hydrochemical data sets from the groundwaters in the studied sites include several hundred groundwater samples from drilled boreholes. The deepest fracture groundwater samples with sufficient analytical data reflect depths down to 1.5 km (Laaksoharju *et al.*, 2008a). The methodology for hydrochemical data screening has been presented elsewhere (eg. Smellie *et al.*, 2008a,b and references therein). Hydrochemical data are compiled in the SICADA database, which form the basis to the hydrochemical evaluation. These data have already undergone an initial screening process by field and laboratory personnel based on sampling, sample preparation and analytical criteria before being included in the database. The next stage in the hydrogeochemical site descriptive process is to assess these screened data in more detail to derive a standard set of representative groundwater data for hydrogeochemical modelling purposes.

The final selection of data which best represents the sampled borehole section is based on identifying as near as possible a complete set of major ion analytical data. In order to achieve an adequate dataset to work with, the following criteria have also been applied:

- A charge balance of ± 5% was considered to select adequate groundwater samples.
- In most cases the drilling water content was recorded and, as a general rule, less than 1% drilling water was considered acceptable. In some cases, as a trade-off between quality and quantity, samples with larger drilling water contents (<10%) have been included.

Selection of rock samples for chemical and mineralogical analysis

Rock samples are also frequently included in the study and interpretations carried out. The main rock sample types include sediments and soil samples, representative from near surface conditions, and fracture filling mineral associations, borehole sections and bulk hosting rock (mainly granitic rock forming the wall rock adjacent to fractures), representative from deep underground conditions closer to repository depths.

The sampling methodology for rocks and mineral has been widely described by Tullborg *et al.* (2008) and references therein. For the rock samples representative from underground conditions, investigations are based on sampling associated to drill cores from boreholes. In the case of fracture filling sampling, it is important to judge whether a fracture was open or sealed in situ, because many fractures open up during drilling. Within the site investigation this difficulty is partly overcome by using a down-hole imaging system.

General characterisation of the redox systems in Forsmark and Laxemar-Simpevarp

There are 12 sets of logs in the Forsmark area that passed the selection criteria, ranging in depth from 110 to 950 m (Gimeno *et al.*, 2008a). For the Laxemar-Simpevarp area, there were 22 sets of logs that passed the selection criteria and they range between 122 and 914 m in depth (Gimeno *et al.*, 2008b).

Eh values range from –143 to –281 mV in Forsmark and from -210 to -310 mV in Laxemar-Simpevarp (Figure 2). Even though Eh-pH plots (Figure 2) show a general trend of decreasing Eh values as the pH increases, no clear trend with depth is observed (Figure 3). This behaviour was already noticed by Nordstrom and Puigdomenech (1986) in their work on different Swedish groundwaters down to 600 m depth but it is clearly different to the observed evolution in Palmottu, Finland (where a similar measurement methodology has been applied) and in most aquifers elsewhere, where a marked decrease of redox potential is observed as the residence time and depth of the waters increase (e.g. Drever, 1997; Blomqvist *et al.*, 2000).

All the Eh values from both studied sites are located in a clearly reducing zone, even for the samples located in the shallowest parts of the systems, where possible perturbations of the original redox environment may have taken place during the measurements. This

would indicate the redox-buffering ability of microbial or water-rock interaction processes. Moreover, most of the measured Eh values are in the range defined by Drever (1997) for groundwaters buffered by sulphate-reduction.

An examination of Figure 3 allows appreciating the strong heterogenegeneity in the distribution of Eh data with depth both in Forsmark and in Laxemar-Simpevarp. This behaviour could be the result of a modification in the original redox state in some groundwaters (perturbation of the system). But, most probably, it can be the consequence of the complex hydrological setting and palaeohydrogeological evolution of the Laxemar-Simpevarp area, where the redox-sensitive elements, the potentials calculated from redox couples or the microbiological populations do not show a clear trend with depth either.

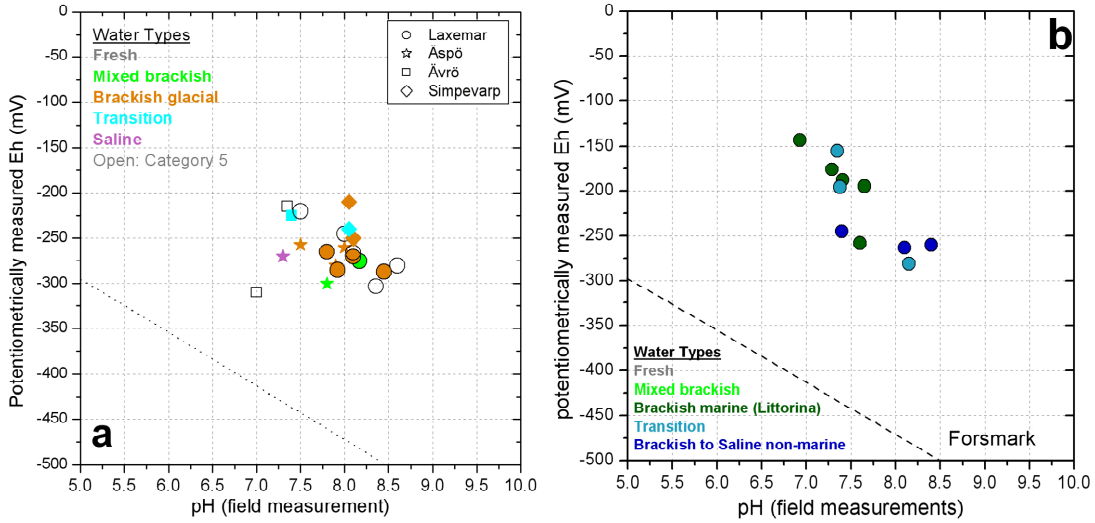

***Figure 2**: Eh-pH plot for the groundwaters from Laxemar-Simpevarp (a) and Forsmark (b) areas respectively.*

With regard to the redox-sensitive elements, these are mainly iron, sulphur, manganese and carbon (e.g. CH_4) in the studied systems. None of these elements show a clear variation trend of the concentrations with depth (Gimeno *et al.*, 2008a and b). For Fe^{2+}, most values below 200 m are below 2 mg/L, whereas S^{2-} is usually low (probably related to sampling problems; Gimeno *et al.*, 2008b) although meaningful values have been measured both in Forsmark (up to 0.84 mg/L) and Laxemar-Simpevarp areas (up to 2.5 mg/L). In the case of manganese, the concentrations of this element in the deep groundwaters from Forsmark and Laxemar vary from very low (even below the detection limit) to more than 2.5 mg/l.

During the microbiological investigations a wide variety of metabolic groups has been cultured in the groundwater samples from both areas. Acetogens represent the most abundant group, but also NRB , MRB, IRB SRB (nitrogen, manganese, iron and sulphate reducing bacteria, respectively) and methanogens have been identified (Hallbeck and Pedersen, 2008, a, b, c).

As regards the mineral phases present in the bulk rock and in the fracture fillings, both Fe(II) and Fe(III) minerals have been widely detected in the studied systems. In the shallowest part of the systems (upper 80-100 m), clay minerals and goethite are

especially abundant in fracture fillings, whereas at greater depths the main iron phase is hematite in both studied systems (Tullborg *et al.*, 2008). Besides the presence of hematite, the occurrence of Fe(II)-bearing minerals (mainly chlorite and pyrite) has been described in the fracture fillings at all depths in Laxemar-Simpevarp and Forsmark areas (Drake and Tullborg, 2008; Sandström *et al.*, 2008). These mineral occurrences prove that oxidising episodes have not exhausted the reducing capacity of fracture filling minerals even in the shallowest part of the studied systems. In the case of manganese minerals, even though the presence of manganese oxyhydroxides has recently been identified in the fracture fillings of the more superficial part (at 10 m depth), they have not been found deeper either in Laxemar-Simpevarp or in Forsmark. This is consistent with the existence of reducing conditions and with the presence of dissolved Fe^{2+} and S^{2-}, which are known to diminish the stability of manganese oxyhydroxides (Appelo and Postma, 2005).

In order to develop a general conceptual model for each of these systems, the results from mineral phases, raw hydrochemical data and potentiometric Eh measurements will be combined in the next work phases with different types of geochemical modelling calculations, including redox pair and saturation index calculations with respect to key minerals as well as some thermodynamic calculations related to some Terminal Electron Acceptor Processes (TEAP) and bioenergetics. This integrated approach must allow to identify the origin of waters and the main geochemical processes determining their redox evolution in both target sites and to evaluate the significance of potentiometric redox measurements. The redox pairs taken into account are the dissolved SO_4^{2-}/HS^- and CO_2/CH_4 redox pairs, and the heterogeneous couples $Fe^{2+}/Fe(OH)_3$, $HS^-/S_{(c)}$, SO_4^{2-}/FeS_{am} and SO_4^{2-}/ pyrite. These are the redox pairs that, apparently, have performed better in similar systems elsewhere in the Scandinavian Shield (see Gimeno *et al.*, 2008a,b and references therein).

Acknowledgements

This study forms part of the SKB site investigation programme, managed and supported by the Swedish Nuclear Fuel and Waste Management Company (SKB), Stockholm. We gratefully acknowledge the careful revision and suggestions of an anonymous reviewer, which have considerably improved the original manuscript.

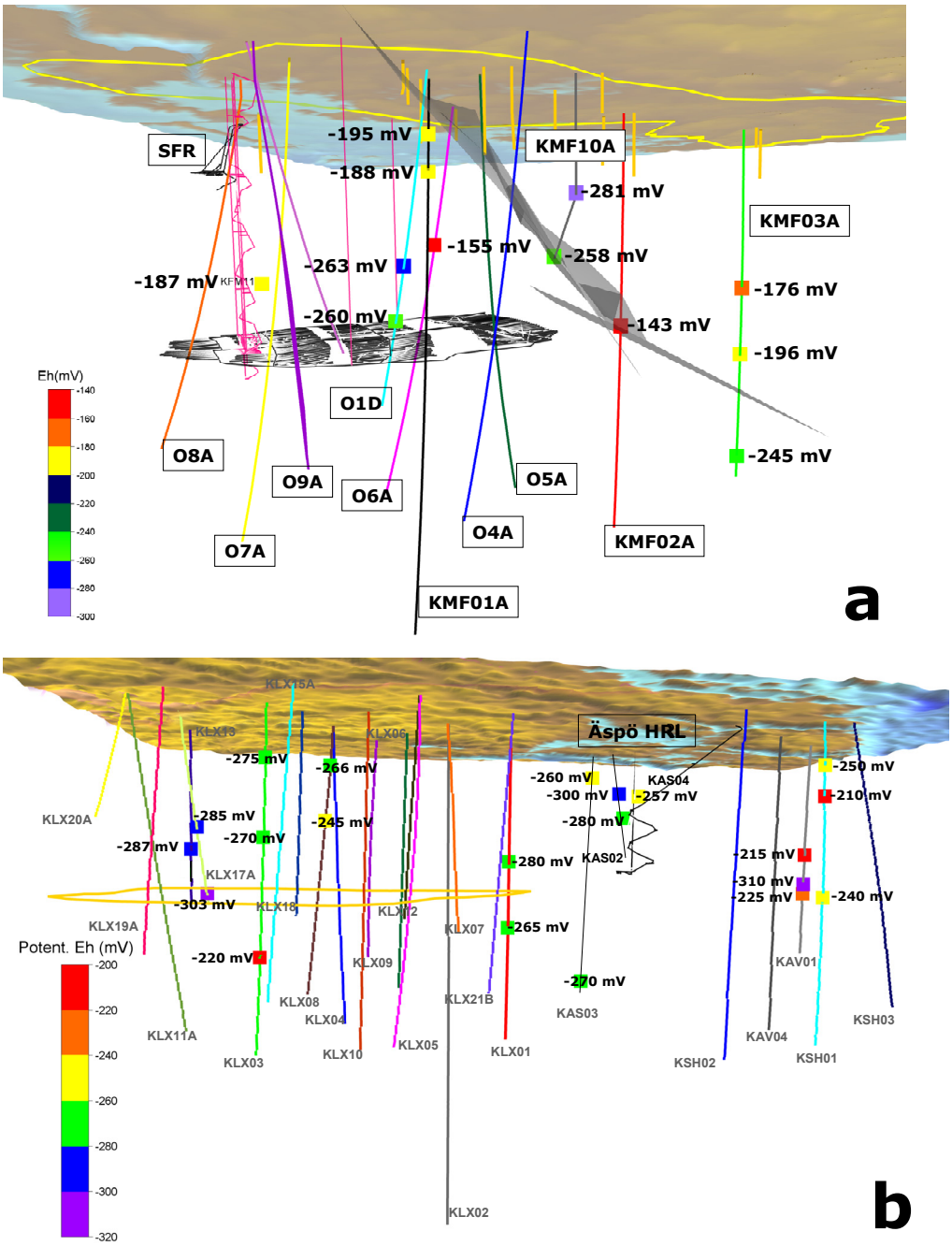

***Figure 3**: 3D plots of Forsmark (a) and Laxemar (b) with the available Eh values superimposed on a simplified sketch of the system showing the position of the boreholes. Vertical scale for some of the objects in the figure is exaggerated and, therefore, some observations may not be placed at the exact depth. For visual reference, preliminary-selected repository candidate areas (not definitive) are marked in black and white (Forsmark) and in yellow (Laxemar) and correspond to 450-500 m depth. Grey-shaded areas in panel (a) correspond to fracture zones separating domains with different hydrogeologic and hydrogeochemical behaviour.*

References

Appelo CAJ and Postma D (2005): *Geochemistry, Groundwater & Pollution.* Balkema, Rotterdam, The Netherlands, 2nd edition, 649 p.

Auque LF, Gimeno MJ, Gomez J and Nilsson A-C (2008): Potentiometrically measured Eh in groundwaters from the Scandinavian Shield. *Applied Geochemistry*, 23 (7): 1820-1833.

Blomqvist R, Ruskeeniemi T, Kaija J, Ahonen L, Paananen M, Smellie J, Grundfelt G, Pedersen K, Bruno J, Pérez del Villar L, Cera E, Rasilainen K, Pitkänen P, Suksi J, Casanova J, Read D and Frape S (2000): *The Palmottu Natural Analogue Project. Phase II: transport of radionuclides in a natural flow system.* European Commission, Final Report, Phase II, EUR-19611, 171 p.

Christensen TH, Bjerg PL, Banwart SA, Jakobsen R, Heron G and Albrechtsen H-J (2000): Characterization of redox conditions in groundwater contaminant plumes. *Journal of Contaminant Hydrology*, 45, 165–241.

Drake H and Tullborg E-L (2008): *Fracture mineralogy of the Laxemar site. Final report.* SKB-R-08-99, Svensk Kärnbränslehantering AB, Stockholm, Sweden.

Drever JI (1997): *The Geochemistry of Natural Waters: Surface and Groundwater Environments*. 3rd ed., Prentice Hall, New York, USA, 436 p.

Gimeno MJ, Auqué LF, Gómez J and Acero P (2008a): *Water-rock interaction modelling and uncertainties of mixing modelling.* SDM-Site Forsmark. SKB-R-08-86, 212 pp.

Gimeno MJ, Auqué LF, Gómez J and Acero P (2008b): *Water-rock interaction modelling and uncertainties of mixing modelling.* SDM-Site Laxemar. SKB-R-08-113, Svensk Kärnbränslehantering AB, Stockholm, Sweden.

Grenthe I, Stumm W, Laaksoharju M, Nilsson A-C and Wikberg P (1992): Redox potentials and redox reactions in deep groundwater systems. *Chemical Geology,* 98, 131-150.

Hallbeck L and Pedersen K (2008a): *Explorative analysis of microbes, colloids and gases. SDM-Site Forsmark.* SKB-R-08-85, Svensk Kärnbränslehantering AB, Stockholm, Sweden.

Hallbeck L and Pedersen K (2008b): *Explorative analysis of microbes, colloids and gases. SDM-Site Laxemar.* SKB-R-08-109, Svensk Kärnbränslehantering AB, Stockholm, Sweden.

Hallbeck L and Pedersen K (2008c): Characterization of microbial processes in deep aquifers of the Fennoscandian Shield. *Applied Geochemistry*, 23(7), 1796-1819.

Laaksoharju M (Ed.) (2008): *Bedrock hydrogeochemistry, Laxemar. Site descriptive modelling. SDM-Site Laxemar.* SKB R-08-93, Svensk Kärnbränslehantering AB, Stockholm, Sweden.

Laaksoharju M, Smellie J, Tullborg E-L, Gimeno M, Molinero J, Gurban I, Hallbeck L (2008a): Hydrogeochemical evaluation and modelling performed within the Swedish site investigation programme. *Applied Geochemistry*, 23 (7), 1761-1795.

Laaksoharju M, Smellie J, Tullborg E-L, Gimeno M, Hallbeck L, Molinero J and Waber N (2008b): *Bedrock hydrogeochemistry, Forsmark. Site descriptive modelling. SDM-Site Forsmark.* SKB R-08-47, Svensk Kärnbränslehantering AB, Stockholm, Sweden.

Nordstrom DK and Puigdomènech I (1986): Redox chemistry of deep ground-waters in Sweden. SKB TR 86-03, Svensk Kärnbränslehantering AB, Stockholm, Sweden; 30 p.

Sandström B, Tullborg E-L, Smellie J, MacKenzie AB and Suksi J (2008): Fracture mineralogy of the Forsmark site. SKB R-08-102, Svensk Kärnbränslehantering AB, Stockholm, Sweden; 113 p.

Smellie J, Tullborg E–L, Nilsson A-C, Sandström B, Weber N, Gimeno M and Gascoyne M (2008a): Explorative analysis of major components and isotopes. SDM-Site Forsmark. SKB R-08-84, Svensk Kärnbränslehantering AB, Stockholm, Sweden; 287 p.

Smellie J, Tullborg E-L and Nilsson A-C (2008b): Explorative analysis and expert judgement of major components and isotopes. Site descriptive modelling SDM-Site Laxemar. SKB R-08-108, Svensk Kärnbränslehantering AB, Stockholm, Sweden.

Ström A, Andersson J, Skagius K and Winberg A (2008): Site descriptive modelling during characterization for a geological repository for nuclear waste in Sweden. *Applied Geochemistry*, 23 (7):1747–1760.

Tullborg EL, Drake H and Sandstrom B (2008): Palaeohydrogeology: A methodology based on fracture mineral studies. *Applied Geochemistry*, 23 (7): 1881-1897.

THE REDUCTIVE IMMOBILIZATION OF ^{237}Np AND ^{239}Pu ON IRON CANISTER UNDER REPOSITORY CONDITIONS

D. Cui[1*], V.Rondinella[2], C. Kütahyali[2,3], M. Amme[2,4], T. Wiss[2], D. Grolimund[5], D, E. Wieland[5] C. Borca[5] and K. Spahiu[6]

[1.]Studsvik AB, 611 82 Nyköping, Sweden

[2.]Inst. for Transuranum Elements, JRC, European Commission, 76125 Karlsruhe, Germany

[3.]Ege University, Inst. of Nuclear Sc., 35100 Bornova-Izmir, Turkey

[4.]Nuclear Decommissioning Authority (NDA), Harwell OX11 0RH, United Kingdom

[5.]Paul Scherrer Institut, CH 5232 Villigen PSI, Switzerland

[6.]SKB, SE-10240 Stockholm, Sweden

*Corresponding author: daqing.cui@studsvik.se)

Abstract

The fates of ^{237}Np and ^{239}Pu under near field repository conditions around iron canister have been investigated. The polished and pre-corroded iron coupons were interacted for 120 days in a deoxygenated solution containing 0.1mM ^{237}Np(V), 0.1 μM ^{239}Pu(VI), 10 mM NaCl and 2 mM $NaHCO_3$. The concentrations of Np and Pu in solution were analyzed and it was observed that the pre-oxidized iron with 40μm Fe_3O_4 layer is more reactive than the newly polished iron to immobilized Np(V) and Pu(VI). The iron corrosion products and immobilized ^{237}Np were characterized by SEM, EDS and μ - XRF, and XANES. It is observed that even 7-8 μm Np rich (>50%Np 10% Si and 20%Fe) layer precipitated on the Fe_3O_4 layer. The evidences provided from this work are useful for the performance assessment of deep repository.

Introduction

In most concepts of deep geological nuclear waste repository, particularly in the case of direct disposal of spent fuel, reducing conditions in the near field of the repository are essential for the stability of the waste and to attenuate the migration of radionuclides (RNs). Such reducing conditions may be offset by radiolysis at the surface of spent fuel and potentially lead to oxidative dissolution of oxidized and negatively charged species such as U(VI), Np(V), Pu(V/VI), Se(IV-VI) and Tc(VII) from spent fuel. Long lived ^{237}Np and ^{239}Pu are two of the most toxic and important nuclides considered in the safety assessment. At the interface groundwater-iron canister material at the near field

of a repository, the reducing effect of iron is expected to dominate over the oxidizing effect of gamma-radiolysis in a damaged canister (Loida et al., 1995). Thus a reducing environment will prevail at the interface of groundwater and iron canisters, and therefore, Np(V) and Pu(VI) dissolved from spent fuel should be reduced to their sparingly soluble reduced forms. The rates and mechanisms of redox reactions between iron (including iron corrosion products) and Np(V) - Pu(VI) are not well known. Effective experimental procedures have been elaborated within to study relevant processes under repository- conditions, such as U(VI) interaction with iron and iron corrosion products (Cui and Spahiu, 2002).

The main objectives of this research work are to study the role of iron canister / iron corrosion products in the reductive immobilization of carbonate complexed 0.1mM Np(V) and 0.1 μ M Pu(VI) under near-field repository conditions and to characterize the reductively immobilized Np. Solution samples were analyzed by the method of Inductively Coupled Plasma Mass Spectroscopy (ICP-MS) analysis. Scanning Electron Microscopy Energy Dispersive Spectrometer (SEM-EDS), micro X-ray Fluorescence (μ-XRF) and X-ray Absorption Near Edge Structure (XANES) were used to characterize of the chemical form of immobilized Np and its distribution in iron corrosion products on iron surface.

Experimental

Solutions

To study the redox chemistry under simulated near field conditions, oxidized forms of redox sensitive radionuclides $^{237}Np(V)$, $^{239}Pu(VI)$ were used. The oxidative NO_3^- anions do not exist in deep groundwater system, therefore, particular care was adopted to remove traces of nitrate from the stock solution for the experiment. Concentrated HNO_3 is often used to dissolve AnO_2 and could involve 100-1000 times more nitrate (NO_3^-) than redox sensitive radionuclides in the batch experiments. The iron surface could be oxidized by nitrate (Su and Robert, 2004) and become less reactive as reductant, thus strongly affecting the outcome of the experiment. Effective methods for making nitrate free Np(V) and Pu(VI) solutions with neutral pH were investigated.

The Np(V) stock solution was prepared from $^{237}NpO_2$ solid material. It was first tested to dissolve the material in concentrated HCl, which lead only to partial dissolution. Afterwards, about 0.11 g of the oxide was dissolved in boiling $HClO_4$. The resulting deep red solution of Np(VI) was evaporated to dryness and the perchloric acid was fumed away. Subsequently the brown residual was dissolved in 0.1 M HCl and reduced to Np(V) using a stoichoimetric amount of $NaNO_2$ and thus resulting in an emerald-green solution. From this solution, the solid sodium neptunium (V) carbonate was precipitated with $NaHCO_3$ and NaOH. The solid was filtered, washed three times with water, and dissolved in 0.1 M HCl, yielding a stock solution of 4400 ppm. From this stock solution, the solution with 9.29×10^{-5} M Np(V), 10 mM NaCl, 2 mM $NaHCO_3$, pH 8.5 was made.

The preparation of the Pu(VI) stock solution was started using solid plutonium(IV) sulphate hydrate ($Pu(SO_4)_2 \cdot H_2O$) of high isotopic purity (^{239}Pu NIST isotopic standard). About 0.3 g of the solid was dissolved in boiling $HClO_4$. The oxidative digestion was continued for 4 h and about 50 mg of $K_2S_2O_8$ were added to ensure oxidation to Pu(VI). After cooling, the solution had an intense yellow color and was then diluted to approximately 0.5 M $HClO_4$. From this solution, Pu(VI) hydroxide was

precipitated using concentrated NH_4OH. The resulting voluminous solid was filtered, washed 3 times with water, and dried for 48 h. Some of the resulting grains were collected and dissolved in HCl, yielding a stock solution of 3.13 mM. Using this stock solution, the solution b) with 9.62×10^{-8} M Pu(VI), 10 mM NaCl, 2 mM $NaHCO_3$, pH 8.5 was made.

Due to the difficulties of handling fissile nuclide ^{239}Pu during transportation and analysis and keeping high concentration Pu(VI) stable in pH 8.5 solution, and to avoid possible disturbance of Pu(VI) to the redox behavior of Np, only 10^{-7}M Pu(IV) (0.1% of Np) was employed in the initial solution.

Iron coupons

Iron coupons with 99.98 % purity were polished by 0.6 μm (4000 mesh) sand papers and cut to pieces with 0.3 cm^2 outer surfaces. Some of them were then stored in acetone in refrigerator while other samples were pre-corroded for six months corrosion in a distilled water at 80°C. A thick black colored corrosion layer formed on the coupons. The fact that corrosion product particles fell down to the bottom of the vessel could be moved by magnetic stirring confirms that magnetite was the dominant corrosion product. The formation of Fe_3O_4 layer on pre-corroded iron pieces was also confirmed by the peak position 668 cm^{-1} of Laser-Raman spectroscopic analysis, as shown in Fig. 1 and by X-ray diffraction analysis on the black powder scrapped off from the corroded iron surface.

Arrangement of batch experiments

Four reaction bottles were located in a big vessel where an in.-situ oxygen trap (an open beaker containing 30 mL solution with 3g $FeCO_3$ + 3g $CaCO_3$) was also placed, as that described elsewhere (Cui and Spahiu, 2002). The large vessel was slowly and continually purged with Ar+0.03%CO_2. 30 mL deoxygenated solution with 0.1mM Np(V), 0.1μM Pu(VI) were pre-filtered by using 0.2 μm filters immediately before adding 0.3 cm^2 sized newly polished iron samples and pre-corroded iron samples into the solutions. After different reaction times, solution samples were taken through the rubber septa screw-caps by using a syringe. The samples were acidified to avoid Fe(III) precipitation and/or sorption of Np-Pu on the precipitate and then analyzed by ICP-MS.

Microscopic analysis of iron corrosion products and immobilized Np

Using a procedures described elsewhere (Cui et al., 2008), after four months reaction time, the reacted iron coupons were dried in Ar atmosphere and in vacuum, and embedded in Epoxy. The cross sections of the iron coupons were polished and analyzed by SEM-EDS and the distribution of Np on outer corroded iron surface was analyzed by μ-XRF and the oxidation state of the immobilized Np at a Np rich points was preliminarily analyzed by XANES.

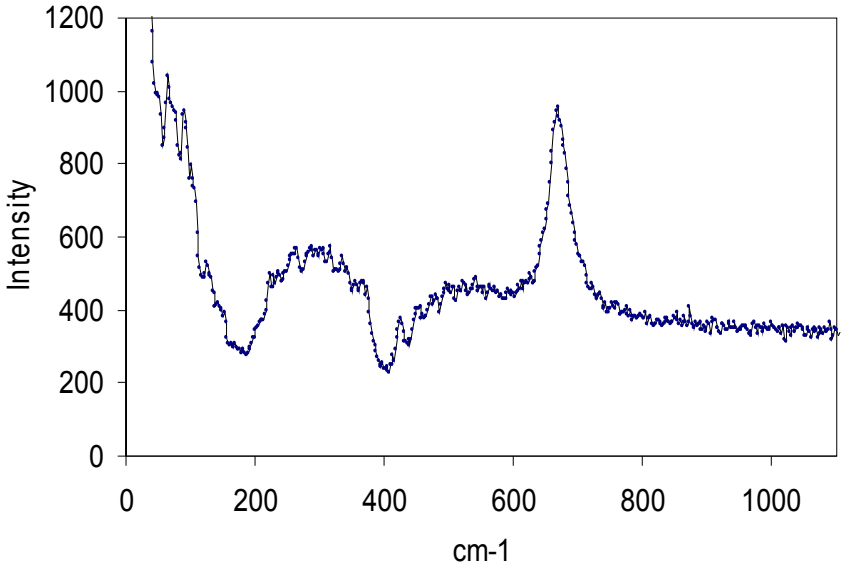

Figure 1. *Raman spectroscopic analysis of corrosion layer formed on the pre-corroded iron sample, the peak position (668 cm^{-1}) matches that for magnetite.*

Result and discussion

Maintaining anoxic conditions

At the end of the experiments after 120 days, the pH and Eh of the solutions in the four batch experiments were measured using pre-calibrated electrodes. pH values were in the range 8.71 to 8.80 and Eh ranged between -257 to –265 mV (against standard hydrogen electrode). This confirmed that the anoxic conditions were well maintained during the experiments.

The reaction rates of Np(V) - Pu(VI) immobilization on iron surfaces

The concentrations of Np and Pu in the four batch-type experiments at different reaction times are potted as shown in Fig. 2. The factors of evaporation and sorption on the glass vessel wall were corrected on the basis of data from blank experiments.

The results shown in Fig.2 indicate that the metallic iron can significantly remove Np(V) (0.1mM) and Pu(VI) (0.1 μM) from solutions. The pre-corroded iron surfaces with Fe_3O_4 layer is much more effective than the polished iron surface in removing Np(V) and Pu(VI) from solution. After four months reaction time, small pieces of polished iron (0.3cm^2) can immobilize 27% (0.7mg) of 0.1mM Np(V) or 84% of total 0.1 μM Pu(VI) from 30 mL solution. The Fe_3O_4 coated iron pieces at the same solution conditions can immobilize 97% of 0.1mM Np(V) or 95% 0.1 μ M Pu(VI) from the corresponding solutions. The possible explanation is that the Fe_3O_4 coated iron surface contains more reaction sites to adsorb carbonate complexed Np(V) and Pu(VI) anions than the freshly polished iron surface. The adsorption should be the first step of reductive immobilization process. It should noted that Np(V) concentration was 1000 times higher than that of Pu(V), therefore, the rate of concentration changes shown in Fig. 2 can not be used for directly comparing the reaction rates of these two radionuclides.

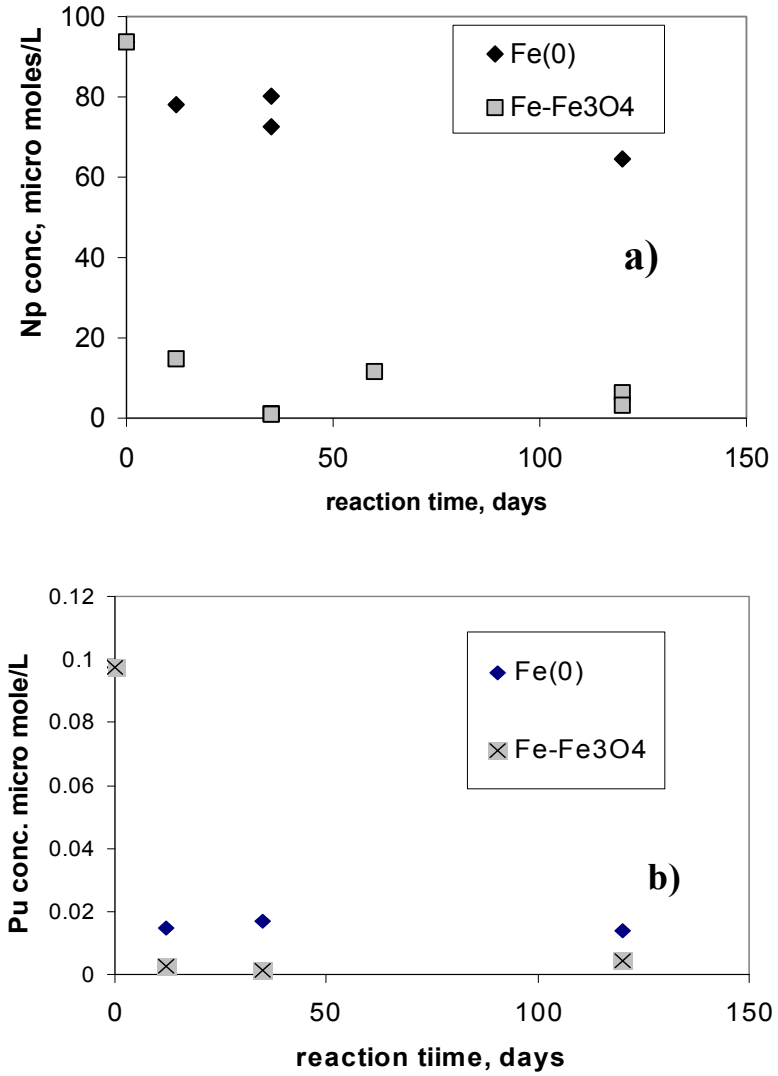

Figure 2. *The evolution of the concentrations of Np(a) and Pu(b) with time in batch experiments with newly polished iron samples and Fe_3O_4 coated iron samples.*

Characterization of iron corrosion layer and immobilized Np

SEM EDS analysis

The SEM image of the cross section of Fe_3O_4 coated iron surface with immobilized Np is shown in Fig. 3a and the composition of the Np rich layer as analyzed by SEM-EDS is shown in Fig 3b. The figures supply information on the distribution of the immobilized Np and of Fe_3O_4 iron corrosion products along the iron surfaces. It shows that an uneven 20-40 μm thick layer of Fe_3O_4 was formed on iron surface after six months pre- corrosion in distilled water at 80°C and four months interaction in deoxygenated solution. Micrometer sized pores and cracks can be observed on the Fe_3O_4 corrosion layer and Np was immobilized on the top of Fe_3O_4 layer with a relatively even thickness.

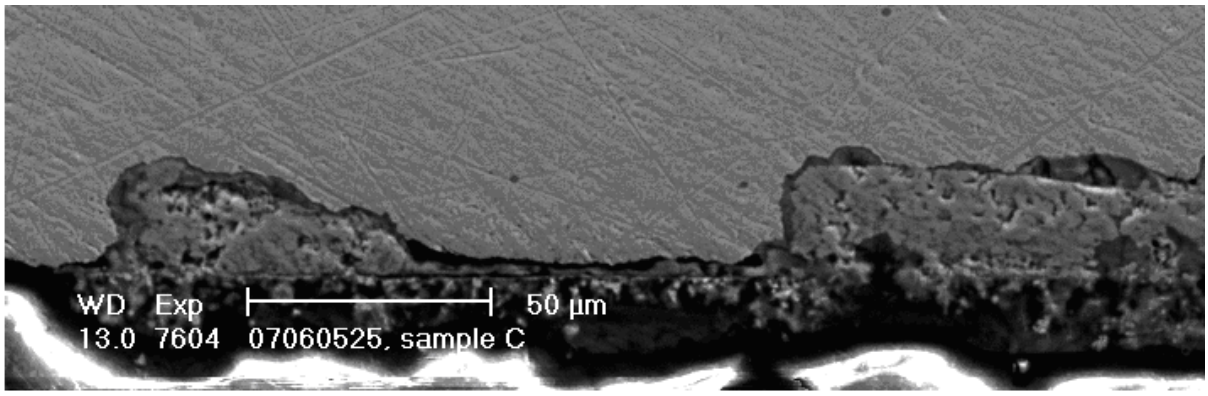

a)

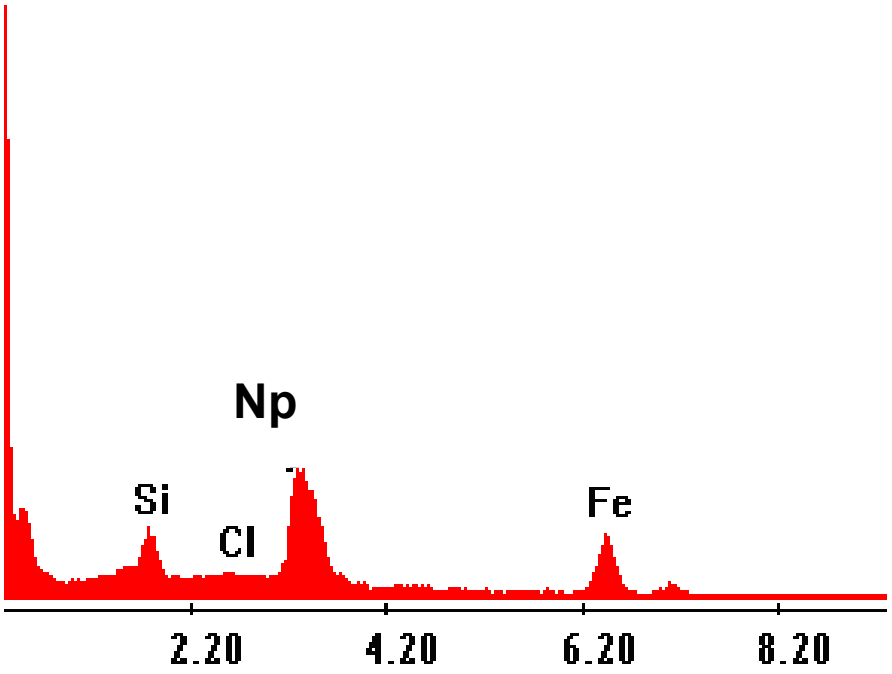

b)

Figure 3. *The result of SEM-EDS analysis on the cross section of a 0.3 cm^2 sized iron sample. The iron sample was first pre-corroded and coated with Fe_3O_4, and then reacted in 30 mL 0.1 mM Np(V) solution for 4 months.*

a) SEM–image. The upper light grey part is iron metal matrix and the dark grey part is a 25-40 µm thick corrosion product, porous Fe_3O_4. The 7-8 µm thick white colored layer below the corrosion product is the layer containing 50% immobilized Np.

b) SEM-EDS analysis of the composition of the white colored layer with immobilized Np: (wt%) 9.43Si : 1.59Cl : 54.23Np : 34.75Fe

(7-8 µm). SEM-EDS analysis (Fig. 3b) shows that the 7-8 µm thick Np rich layer contains *(wt%) 9.43Si : 1.59Cl : 54.23Np : 34.75Fe and (atom%) 27.25Si : 3.64 Cl : 18.58 Np and 50.52 Fe.* The coordination of Si, Fe and Np on the iron corrosion layer observed in this work is similar with that of Si, Fe and Np observed in a previous work (Cui and Spahiu, 2002), an even layer of immobilized U contained about 30% Si (atom%) were observed. In this work and the previous one (Cui and Spahiu, 2002), all

Si was dissolved from glass vessel wall during 3- 4 months reaction. The coordination of 30 % Si in the reduced actinides (U and Np) suggests two possibilities, a) the co-precipitation of An(IV) with some Fe-Si phases and/or b)formation of the less soluble tetra valence An-SiO_4 phases under the reducing conditions (Robit et al., 2006). Further characterization work to identify the phase of the immobilized Np, such as Laser Raman, XRD and/or TEM-EDS-diffraction has been planned. The immobilized Np on the polished iron piece is not as intensive as that on the Fe_3O_4 coated iron pieces.

μ -XRF analysis

The results of μ -XRF elemental mapping are shown in Fig. 4a for Fe mapping and Fig. 4b for Np mapping. μ-XRF is more sensitive than SEM-EDS. More immobilized Np is found on the vertical edge area. At this area most XRF counts are from outer surface, where most Np was immobilized.

XANES analysis

The oxidation state of the immobilized Np at a Np rich point in Fig 4b was preliminarily analyzed by XANES. The peak position of the X-ray Absorption Near Edge Structure (XANES) spectra of immobilized Np was found at 17.625 keV. According to the observations of previous work (Denecke et al., 2005) and preliminary data from this work, it can be interpreted that Np(V) is, at least partially, reduced to Np(IV) and precipitated on the top of corrosion product (Fe_3O_4) layer under the experimental conditions. The oxidation of a part of the immobilized Np during the solid sample treatment, transportation and analysis can not excluded. Detailed analysis of the spectroscopic data collected at different spots on the Np layer is ongoing.

Conclusions

- 0.1mM Np(V) and 0.1μM Pu(VI) in anaerobic carbonate containing solution can be effectively immobilized by iron canister material.
- Pre-corroded iron surface coated with Fe_3O_4 layer is more reactive to immobilize Np(V) and Pu(VI).

Acknowledgements

The batch experiments were conducted at Instutute for Transuranium Elements, Joint Research Centre, European Commission by D. Cui during his stay as a visiting scientist. μ -XRF and XANES analysis were done at SLS/PSI, Switzerland. The data treatment and report writing at Studsvik AB, Sweden, was coordinated and supported by the European 7th frame work, RECOSY project and SKB, Sweden. The authors wish to thank J. Cobos and M. Cardinate for their helps in the experiments, and B. Lynch and S. V. Winckel for the ICP-MS analysis.

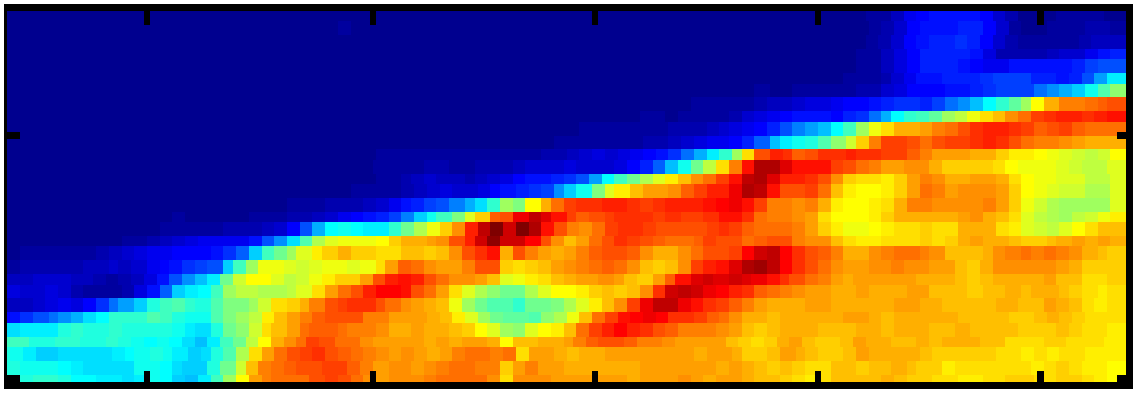

a)

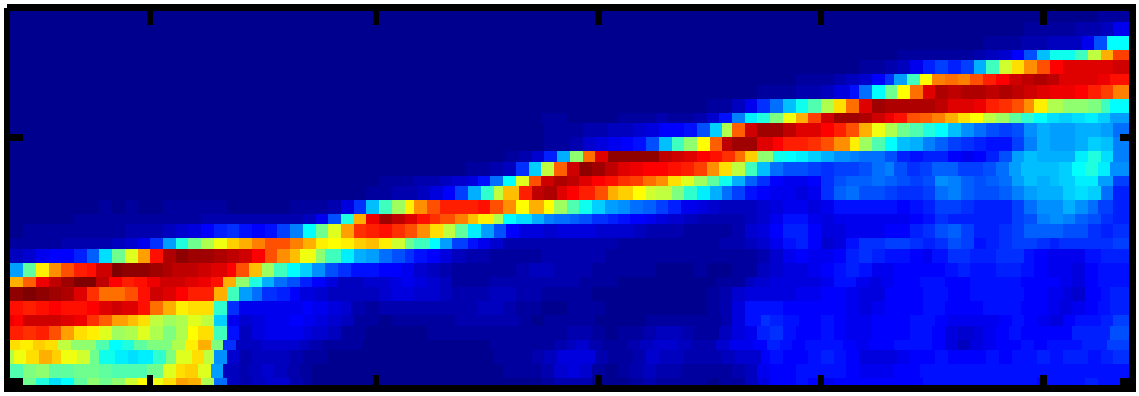

b)

Figure 4. *The result of μ -XRF elemental mapping a) Fe mapping b) Np Mapping on the Np rich edge of outer surface of Fe_3O_4 coated iron coupon.*

References

Cui, D., Schderger, A., Erich W., Spahiu, K. and Wersin, P. On the interactions between iron canister material and fission product ^{79}Se and ^{99}Tc under simulated deep repository conditions NF-PRO –WP2.5 Final report, 2008

Cui, D., Spahiu, K., The reduction of U(VI) on a corrosion product of metallic iron under anoxic groundwater conditions, Radiochimica Acta **90**, p 623-628, 2002

Denecke, M. A. Dardenne, K., and Marquardt, C.M., Np(IV)/Np(V) valence determinations from Np L3 edge XANES/EXAFS. Talanta, Vol. **65**, Issue 4, 28 February 2005, Pages 1008-1014.

Loida, J., Grambow, B., Geckeis, H., Dressler, P.: Processes controlling radionuclide release from spent fuel. Mat. Res. Soc Symp. Proc. **353**, 577 (1995).

Robit V., Poinssot, C., Grambow, B., Catalette, H., Cui, D. and Spahiu, K., Assessment of the relevance of coffinite formation within the near-field environment of spent nuclear fuel geological disposal, Mat. Res. Soc. Symp Proc. Scientific basis for nuclear waste management. XXIX (2006).

Su,C. and Robert; P.W. Nitrate reduction by zerovalent iron: Effects of formate, oxalate, citrate, chloride, sulfate, borate, and phosphate, Environmental Science & Technology **38**, °9, 2715-2720(2004)

REDOX TRANSITIONS IN BODA ALBITIC CLAYSTONE UNDER NATURAL CONDITIONS: VARIATIONS IN THE Fe^{2+}/Fe^{3+} RATIO OF CLAY MINERALS

Károly Lázár [1*], Zoltán Máthé [2], Mária Földvári [3]

[1] Institute of Isotopes, HAS (HU)

[2] Mecsekérc Environmental (HU)

[3] Geological Institute of Hungary (HU)

* Corresponding author: lazar@iki.kfki.hu

Abstract

Fe^{2+} and Fe^{3+} species in layered clay minerals are analysed in samples obtained from two boreholes in Boda Siltstone Formation. In the first series occurrence of Fe^{2+} components and Fe^{2+} => Fe^{3+} oxidation is demonstrated in upper layers of a strata near to the surface. In the second series minerals are identified with iron present exclusively in ferrous form in a thin strata found in a borehole at 1050 m depth. Thus, in cases when the related clay minerals are in equilibrium with the pore water, the Fe^{2+} => Fe^{3+} process can probably be considered as a counterpart of a coupled redox process which may influence the migration of redox sensitive species of multivalent radionuclei.

Introduction

Redox processes may influence the migration of certain radionuclides which are able to change their valency, and as a consequence, to change the charge of the migrating species. For example, reduction may proceed in the following processes: UO_2^{2+} <=> UO_2, $^{79}SeO_3^{2-}$ <=> ^{79}Se (0), $^{237}NpO_2^{+}$ <=> $^{237}NpO(OH)_2$, $^{99}TcO_4^{-}$ <=> $^{99}TcO_2$. As shown, the complexes are charged when the central radionuclides are in higher valency state, thus, they are hydrated and are able to migrate in aqueous media. In contrast, these complexes are neutral in their reduced forms, and in accordance, they may precipitate.

In turn, the opposite process of the previous reduction should also proceed in the neighbouring media, first in the pore water, then, in second stage, in the host rock. In several cases the Fe^{2+} => Fe^{3+} oxidation is considered as the possible counterpart of the previously mentioned reductions.

Boda Siltstone Formation (BSF, with albitic claystone as the main lithotype) is considered as a perspective media for disposal of nuclear waste in Hungary. Thus, the ability of the constituting mineral components to participate in the redox processes may also be evaluated. In general, overwhelming part of the Boda Formation was formed

under strong oxidation conditions in strong alkaline media at arid/semi-arid conditions. In correspondence, dominant part of the iron is present as hematite [Árkai et al., 2000]. Thus, further oxidation can hardly be expected.

In the present study Fe^{2+} and Fe^{3+} components are studied with Mössbauer spectroscopy in BSF samples. Two examples are discussed in detail. In the first one the oxidation of Fe^{2+} to Fe^{3+} is demonstrated in layered minerals in regions close to the upper boundary of the Boda Formation in a borehole driven from the ground. In the second example samples obtained from a deep drill crossing a reductive zone below the surface at 1050 m are analysed, and the iron containing minerals are identified.

With the present study we would like to demonstrate that minor amounts of iron can be present in ferrous form in spite of the predominance of the oxidative conditions in Boda Formation controlling the genesis of the formation. Furthermore, it is also shown that Fe^{2+} ions in layered clay minerals are accessible to $Fe^{2+} \rightarrow Fe^{3+}$ oxidation in natural environment. In addition, it is shown with the second case that regions may occur in the formation where iron exists exclusively in ferrous state. Finally, the present study provides a characterization also on the redox state of our samples intended to use for radioisotope migration studies.

Experimental

Samples

The studied samples were obtained from two different parts of the Boda Siltstone Formation. Oxidation processes are demonstrated in samples collected from the BAT-14 drill. This vertical drill was bored from the ground. The claystone strata commences in 22.3 m depth, it is covered with Quaternary sediments (loess, redeposited loess and marl). Changes reflected in the mineral composition and oxidation state of iron in a borehole crossing a reduction zone are demonstrated by comparing samples from Delta-9 drill. This borehole was drilled in horizontal direction in a roadway at 1050 m depth below ground level.

Methods

The mineral compositions of samples were analysed either by X-ray diffraction or by thermogravimetry (TG) and differential thermal analysis. Only those minerals can be analysed with the latter methods which exhibit weight changes or thermal effects upon heating. The respective amounts of these thermally responding minerals can also be estimated as well.

Oxidation and coordination states of iron in iron-bearing minerals were analysed by Mössbauer spectroscopy. This method identifies the state of only one element – in the recent case that of iron. Thus, information is provided only on iron bearing minerals.

Results

Measurement of the Fe^{2+} and Fe^{3+} species in samples from the top layers of BSF strata

The relative amounts of the thermally active minerals present in the studied samples are shown in Table 1.

Mössbauer spectra were collected in two velocity ranges on the samples. The spectra recorded in the wider velocity range (± 12 mm/s) contain the contributions of all the iron bearing components, namely the whole sextet of hematite. The spectra recorded in the narrower range (± 4 mm/s) provide better resolution for identifying the respective components, however they show only the two inner lines of the hematite sextet. The corresponding spectra are shown in Fig. 1, and data are collected in Table 2.

Table 1. *Mineral composition of the samples determined by thermal analysis (%)*

mineral / depth*	1.1 m	2.4 m	6.1 m	11.5 m	57.8 m
Chlorite	0.5	33**	8**	13	27
illite-muscovite	24	10	10	13	25
Montmorillonite	7	15	10	5	1
Calcite	35	8	12	7	5

* depth measured from the upper boundary of the claystone strata
** chlorite and/or some kaolinite

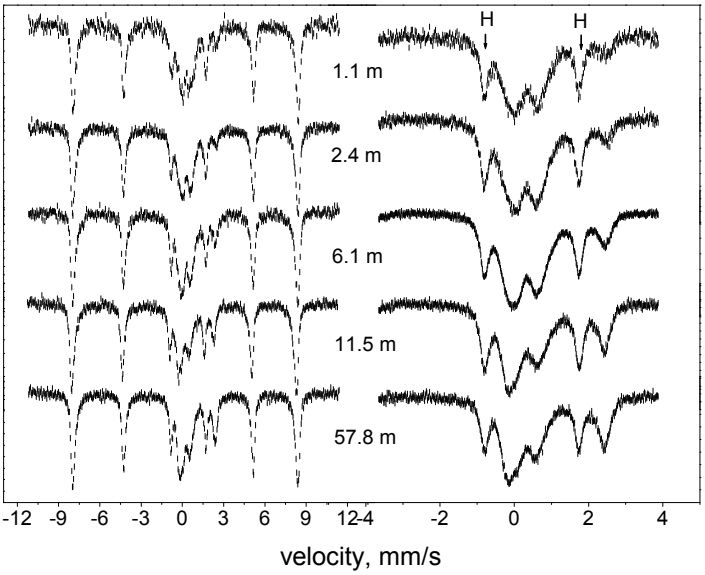

Figure 1: *Mössbauer spectra of samples taken from different depths of BAT-14 borehole. Spectra are collected in two velocity ranges. (H marks the positions of the two central peaks of the sextet of hematite)*

The assignment of the hematite, amounting to 64 – 66 % of iron, is unambigous. Data published in the Mössbauer Mineral Handbook [Stevens et al., 1998] can be considered

for the identification of the components filling in the remaining 34 – 36 % spectral area. The IS = 1.1 and QS = 2.6 mm/s pair of data is reported for the characteristic Fe^{2+} positions in chlorite in most of cases. However, in several studies IS = 1.2 and QS = 2.4 pair of data is also specified. These data are also characteristic for some other layered clay minerals (illite, montmorrilonite). Thus, adopting these values, the Fe^{2+} doublet can probably be attributed to ferrous ions located in chlorite or in other clay minerals. Several positions are available for iron in chlorite – both Fe^{2+} and Fe^{3+} may be located in it [Zazzi et al., 2006]. The assignment of the Fe^{3+} components is similar – the Fe^{3+} (a) and Fe^{3+} (b) doublets may attest either the presence of chlorite or the illite-muscovite as well [Stevens et al., 1998].

Table 2. *Mössbauer data extracted from the spectra of Fig. 1. (IS: isomer shift, relative to metallic iron, mm/s; QS: quadrupole splitting, mm/s; MHF: magnetic hyperfine field, Tesla; RI: relative intensity, %)*

Depth (m) *	Component	IS	QS	MHF	RI
1.1	Fe^{2+}	1.26	2.39		4.0
	Fe^{3+} (a)	0.19	0.85		3.2
	Fe^{3+} (b)	0.33	0.73		27.0
	Fe^{3+} (hematite)	0.40	0.22	50.7	65.7
2.4	Fe^{2+}	1.30	2.37		3.9
	Fe^{3+} (a)	0.12	0.81		2.3
	Fe^{3+} (b)	0.32	0.72		28.0
	Fe^{3+} (hematite)	0.37	0.22	50.7	65.6
6.1	Fe^{2+}	1.27	2.36		7.7
	Fe^{3+} (a)	0.21	0.79		15.1
	Fe^{3+} (b)	0.43	0.78		13.6
	Fe^{3+} (hematite)	0.37	0.23	50.6	63.6
11.5	Fe^{2+}	1.26	2.35		10.5
	Fe^{3+} (a)	0.19	0.76		8.5
	Fe^{3+} (b)	0.33	0.98		12.5
	Fe^{3+} (hematite)	0.38	0.22	50.6	68.5
57.8	Fe^{2+}	1.27	2.32		14.1
	Fe^{3+} (a)	0.18	0.76		12.9
	Fe^{3+} (b)	0.32	0.95		8.5
	Fe^{3+} (hematite)	0.38	0.22	50.7	63.6

* The depth is measured from the upper boundary of Boda Claystone, which is covered with loess and marl in thickness amounting together to 22.3 m.

Thus, in short, it can be concluded from the relevant RI data that the Fe^{2+} portion decreases in the clay minerals from 14 % to c.a. 4 % as approaching the top few meters of the Boda Formation. This can probably be attributed to a secondary oxidation in the layered clay mineral (the amount of the other main constituing mineral, hematite, practically does not vary). This phenomena demonstrates that $Fe^{2+} \rightarrow Fe^{3+}$ oxidation may proceed under natural conditions in Boda Claystone which may influence occasional migration processes as well.

Crossing a reductive zone

More expressed differences can be demonstrated in the deeper regions of the Boda Claystone by analysing the state of iron in the minerals present. Reductive conditions were prevailing during the genesis of the formation in exceptional periods. This is clearly reflected in the state of the iron in the respective samples collected from a horizontal bore drilled in a depth at 1050 m. The occurrence of the reductive zone is estimated in a layer positioned in between the 83 – 85 m distance from the commencement of the drill.

The mineral compositions of samples collected from the close vicinity of this zone were analysed by X-ray diffraction and by thermal analysis (Table 3). Additionally, the state of iron in samples taken from the zone was analysed by Mössbauer spectroscopy.

Table 3. *Mineral compositions in samples obtained in Delta-9 bore in depth at 1050 m*

Distance (m)	79.6	83.2	85.1 – 85.2	86.6 – 86.8
Method	X-ray	diffraction	thermal	analysis
Mineral				
quartz	8	12		
albite	30	27		
illite/sericite/muscovite	38	25	27	17
chlorite	6	18	22	14
kaolinite	~ 0	10		
montmorillonite			2	~ 0
calcite	4	3	5	7
dolomite	5	1		
hematite	9	~ 0		

Data shown in Tables 3 and 4 and spectra of Fig. 2 attest that the Delta-9 boring crossed a zone which was primarily formed under reducing conditions. Hematite is not found by XRD at all in the sample taken from 83.2 m, and in correspondence, only ferrous iron is detected in the spectra of the sample taken from 83.7 m. (Reduction of hematite to form chlorite and pyrite in secondary diagenetic processes could hardly be assumed.) The IS, QS data in this sample are exactly the same as reported for chlorite [Stevens, 1998], thus in this sample the presence of chlorite is specified. The general Fe^{3+} / Fe^{2+} ratio characterizing the Boda Claystone is reversed in average by departing from this reductive layer located at 83 – 85 m, since the 60 % portion of ferric iron in hematite is restored in the sample taken at the ~ 92 m distance.

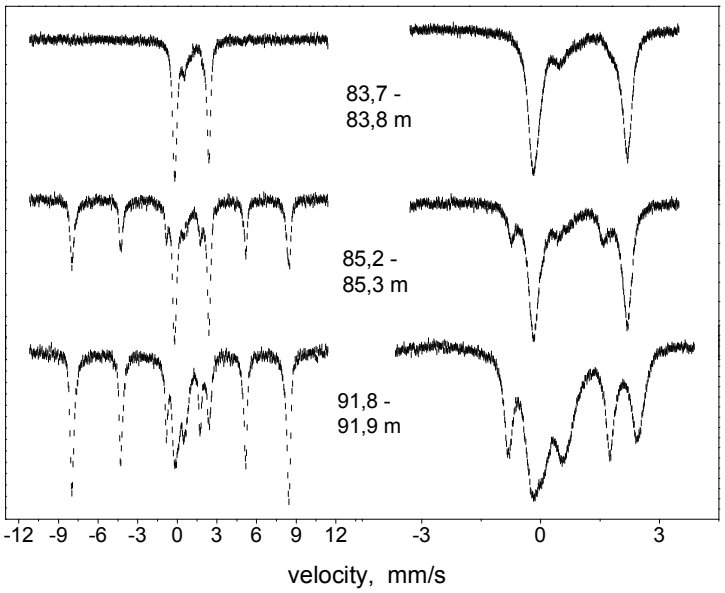

Figure 2. *Mössbauer spectra of samples taken from different distances in the Delta-9 borehole drilled horizontally in 1050 m depth. Spectra are collected in two velocity ranges.*

Table 4. *Mössbauer data extracted from spectra of Figure. 2. (IS: isomer shift, relative to metallic iron, mm/s; QS: quadrupole splitting, mm/s; MHF: magnetic hyperfine field, Tesla; RI: relative intensity, %)*

Distance*	**Component**	**IS**	**QS**	**MHF**	**RI**
83.7 – 83.8	Fe^{2+} (chlorite)	1.13	2.62	-	70
	Fe^{2+}	0.87	2.34	-	7
	Fe^{2+} (pyrite)	0.34	0.63	-	23
85.2 – 85.3	Fe^{2+} (chlorite)	1.13	2.62	-	40
	Fe^{2+} (pyrite ?)**	0.37	0.59	-	14
	Fe^{3+} (hematite)	0.38	0.22	50.9	45
91.8 – 91.9	Fe^{2+} (chlorite)	1.12	2.67	-	15
	Fe^{2+}/Fe^{3+} **	0.35	0.58	-	24
	Fe^{3+} (hematite)	0.38	0.22	50.9	60

* The distance is measured from the commencement of the horizontal drill (in meters)

** The IS, QS parameters of Fe^{2+} in the pyrite (low spin state) and Fe^{3+} (high spin state) in silicate minerals can hardly be distinguished.

Summary and Conclusions

Two examples are presented to prove and analyse the occurence of Fe^{2+} ions in minerals of Boda Claystone. In the first case presence of the Fe^{2+} is demonstrated in a vertical borehole driven near to the ground level. In this instance, Fe^{2+} is present in minor amounts beside the preponderance of the hematite. $Fe^{2+} \rightarrow Fe^{3+}$ oxidation in the topmost region is also evidenced. In the second case an example is shown to demonstrate the occasional occurrence of a strata formed under reducing conditions. In this region – similarly to the previous example - most of the ferrous iron is present in layered clay mineral (chlorite). Thus, it can be assumed that the $Fe^{2+} \rightarrow Fe^{3+}$ oxidation may provide the counterpart process for reduction of certain migrating radionuclides, provided the redox equilibrium is mediated by the pore water.

Acknowledgement

The kind consent of PURAM for providing the samples for characterisation is thankfully acknowledged.

References

Árkai P., Balogh K., Demény A., Fórizs I., Nagy G., Máthé Z., (2000) Acta geologica Hungarica, Vol 43. p. 351.

Stevens J.G., Khasanov A.M., Miller J.W., Pollak H., Li Z. (Editors) (1998) Mössbauer Mineral Handbook, Mössbauer Effect Data Center, Asheville, North Carolina

Zazzi A., Hirsch T.K., Leonova E., Kaikkonen A., Grins J., Annersten H., Edén M. (2006) Clays and Clay Minerals, Vol. 54. p. 252.

SOIL MICROORGANISM TOLERANCE TOWARDS HEAVY METALS AND THEIR ACCUMULATION ABILITIES

Loreta Levinskaitė[1*], Alexey Smirnov[1], Benedikta Lukšienė[2], Ruta Druteikienė[2] and Dalis Baltrūnas[2]

[1]Institute of Botany, LT

[2]Institute of Physics, LT

*Corresponding author: loreta.levinskaite@botanika.lt

Abstract

The work was aimed at studying abilities of soil microorganisms to participate in metal/radionuclide mobility processes by accumulating them. Soil microorganisms were treated by a mixture of heavy metals (Cr(III), Ni, Fe(III), Cd, Mn) in order to isolate the most tolerant ones. Among more metal-tolerant microorganisms microscopic fungi dominated. Tests of fungal tolerance towards each metal showed that the most tolerant fungi to almost all metals were *Aspergillus niger*, *Penicillium oxalicum* and *Paecilomyces lilacinus*.

Accumulation ability of metal-tolerant fungi was tested using Fe(III) and ^{242}Pu. All the fungi showed high Fe-accumulation capacity. While growing in the medium with 1mM iron, most fungi accumulated over 90% of Fe in their biomass. Very good accumulation and growth abilities in Fe-supplemented medium were demonstrated by *Paecilomyces lilacinus*. Preliminary investigation of ^{242}Pu accumulation by fungal biomass showed that all the fungi accumulated ^{242}Pu, and among the most effective radionuclide accumulators *Eupenicillium sp., Penicillium oxalicum* and *Aspergillus niger* could be mentioned.

Introduction

It is well known that microorganisms show a multiplicity of interactions with metals in soil and can contribute to metal mobility or immobilization. The balance between mobilization and immobilization depends on the microorganisms involved, their environment and associated physico-chemical conditions (Luptakova et al., 2007). The microbial reduction/oxidation of metals play an important role in the cycling of both inorganic and organic species. Reduction of higher-valency species of metals can lead to mobilization, e.g Mn(IV) to Mn(II), or immobilization, e.g. Cr(VI) to Cr(III) (Fomina, Gadd, 2007).Microorganism immobilization of heavy metals can result from sorption, transport and intracellular sequestration or precipitation as organic and inorganic compounds (Ehrlich, 1997; Gadd, 2005; White et al.,1995). Interaction of

microorganisms with radionuclides also affects radionuclide geochemical processes, in particular radionuclide migration (Keith-Roach, 2002; Pedersen, 2005; Ehrlich, 2006; Fomina, Gadd, 2007, Dighton et al., 2008). Ability of microorganisms to immobilize heavy metals and radionuclides has drawn attention of investigators. Investigations are performed searching of microorganisms as effective metal- and radionuclide-accumulators and for their application in removal of heavy metals from polluted substrata (Ravikumar Patil et. al., 2007; Parekh et al, 2008 ; Sar et al., 2004).

Our study within the project is focused on investigation of microorganism capabilities of participating in metal/radionuclide mobility processes with special emphasis on their involvement in redox processes. The aim of the current work was to find out ability of soil microorganisms to survive in metal-polluted environment and influence metal mobility by accumulating them. The model experiments involved screening of metal-tolerant soil microorganisms, testing their tolerance level and investigation of their metal- and radionuclide-accumulation abilities as the first step for further investigation of redox phenomena.

Materials and methods

Isolation of microorganisms

Grassland soil (400 mg) was treated with the mixture of heavy metals: $MnCl_2 \cdot 4H_2O$ – 22 g, $Cr(NO_3)_3 \cdot 5H_2O$ – 2.2g, $NiCl_2 \cdot 6H_2O$ – 1,4g, $Cd(NO_3)_2 \cdot H_2O$ – 0.02g, $FeCl_3 \cdot 6H_2O$ – 30g. Metal salts were added as a sterile water solution. The soil was treated for 6 weeks. The control sample was without metal addition, but treated with sterile water of the same amount as the previous one. Microorganisms were isolated on the nutrition agar media (MEA for fungi and NA for bacteria).

Identification of fungi

Fungi were isolated into pure cultures. For culture isolation and identification, media MEA, Czapek, CYA, PDA, YES were used. Fungi were identified following the handbooks (Bridžiuvienė et al.,1997; Domsch et al., 1980; Ellis, 1971; Lugauskas et al., 1987; Klich, 2002; Kozakiewicz, 1989; Pitt, 1979; Samson, 1974; Samson, Frisvad , 2004; Samson, Hoekstra , 2000).

Tests of metal-tolerance of fungi

Fungi were grownt on CYA agar supplemented with heavy metals as salts mentioned above at concentrations of 0.1–20 mM. The tests were done in triplicates. Fungi were incubated for 7 days at 26 ± 2 ^{o}C. The metal effect on fungal growth was evaluated as differences in size of grown fungal colonies on heavy metal-containing media and metal-free media (control), and calculated in %.

Investigation of Fe-accumulation in fungal biomass

Fungi were grown in liquid CYA medium. 1ml of spore suspension (10^6/ml) was added to 50 ml growth medium with 1 mM Fe as $FeCl_3$. Cultures were grown on a rotary shaker at 26 ± 2 ^oC. After 3-day cultivation fungal biomass was harvested, dried at 105 ^oC and weighed. Fe remaining in the growth sollution was detected by the AAS method using the PERKIN ELMER Zeeman 3030 spectrophotometer.

Evaluation of ^{242}Pu sorbed by fungal biomass

To determine sorbtion ability of plutonium by fungi, each 3-day fungal culture in the growing medium (100 ml) was treated with 0.0206 Bq of ^{242}Pu for 1 h. After the treatment, fungal biomass was dried, dry biomass was weighed and burnt in a muffle furnace at 550 ^oC overnight. Plutonium was extracted from the ashes by digestion with 8 $mol \cdot L^{-1}$ HNO_3. Plutonium purification was carried out using a strong basic anion exchange resin DOWEX 1x8. The thin layer samples for alpha-spectrometry were prepared by electrodeposition on stainless steel discs from the Na_2SO_4/H_2SO_4 electrolyte solution for 1 hour using the current density of 0.6 $A \cdot cm^{-2}$. Plutonium isotope was determined by alpha-spectrometry using a Canberra PD type detector (area 450 mm^2, resolution 17 keV (FWHM) at 4-6 MeV).

Results and discussion

The experiment of heavy metal effect on microorganisms showed that after 6 weeks the mixture of heavy metals evidently influenced microbial counts and their community structures. Especially severe effect of the metals was exerted against bacteria. Only ~ 0.1% of the total count of bacteria remained in comparison with the control. Fungi showed significantly higher tolerance to heavy metals. About 61% of the total count of fungi survived in the metal-treated soil were detected. Reduction in microbial counts indicates that essential functions of microorganisms have been affected or cells have been damaged (Chaterjee et al., 1990; Gorbunova, Terekhova, 1995). Evidently, the species composition of fungi in soil affected by metals was poorer than the control sample. Among the best survived fungi were *Aspergillus niger, Fusarium sp., Eupenicillium sp., Penicillium oxalicum, Paecilomyces lilacinus* and *Phoma sp.,* which were further investigated for their metal-tolerance and accumulation abilities. These fungi are common in soil and could be expected to be distributed in repository sites. Additionally, it is reported that fungi of these taxonomical groups, such as *Aspergillus niger, Penicillium, Paecilomyces, Fusarium*, were spread in locations with radioactive contamination (Zdanova et al., 2000).

Some other studies also showed a change in microbial community structure in metal polluted environment indicating bacterial population decrease and shift towards fungi (Kools et al, 2005; Chander, Dyckmans, 2001, Wainwright, Gadd, 1997; Lugauskas et al., 2005). Rather high metal-tolerance of fungi, determining their survival in polluted substrata, can be related to the fungal intrinsic peculiarities including cell wall composition, extracellular polysaccharide and metabolite excretion that lead to binding or precipitation of metals (Caesar-Tonthat et al., 1995; De Groot, Woodward, 1999).

Tests of metal-tolerance showed that these fungi differed in their tolerance reaction towards each metal of the mixture. The most negative influence on fungal growth was exerted by cadmium and nickel, while manganese was the least harmful to most of cultures (Fig. 1). Growing in the medium with Cd, all fungi were able to develop at 1mM Cd, and 2.5 mM of the metal was lethal for the fungi. Tolerance to nickel was rather similar, however *Penicillium oxalicum* was able to grow at 2.5 mM of Ni. *Aspergillus niger* also showed rather high tolerance at 1 mM concentration – its growth was only insignificantly slower than the control. The most tolerant fungi to Cr were *Penicillium oxalicum* and *Paecilomyces lilacinus*, which grew at 20 mM in the medium. Chromium exhibited the most negative effect on *Phoma sp*. – 10 mM Cr absolutely inhibited growth of the fungus. Evident differences in tolerance were noticed, when Fe was added to the medium. The most sensitive fungus was *Fusarium sp.,* which was unable to develop at 3.5 mM Fe, whereas *Penicillium oxalicum* and *Aspergillus niger* developed even at 20 mM of Fe in the medium. Manganese showed the weakest negative effect on the fungi. Most of the microorganisms grew very well even with 20 mM manganese in the medium, only two of them *Phoma sp.* and *Fusarium sp.* were much more susceptible to the metal. High tolerance of fungi of *Penicillium, Aspergillus and Paecilomyces* genera was also shown by other studies (Gadd, 2005; Zafar et al. 2007; Wainwright, Gadd, 1997; Valix, Loon, 2003).

The metal-tolerant fungi were investigated for their heavy metal (Fe) and radionuclide (^{242}Pu) accumulation abilities. Iron and plutonium have chemical and biochemical similarities, and microorganisms participating in Fe mobility regulation could be important in Pu solubility and bioavailability (Francis et al, 2007). Fungal accumulation of metals includes metal binding onto cell walls and intracellular uptake. Iron uptake by fungi involves reduction from Fe (III) to Fe(II) before intracellular uptake or after uptake (De Luca, Wood, 2000).The results showed that while growing in the medium, the fungi were able to accumulate significantly big amounts of Fe by their biomass. (Table 1). Fungi *Phoma sp*. and *Paecilomyces lilacinus* removed the highest Fe amount from the media – 99.7 and 98.7 % respectively. However, the biomass amount of these two fungi differed greatly. Growth of *P. lilacinus* was even stimulated by added Fe (compared to the control growth in Fe-free medium), while growth of *Phoma sp.* was affected negatively. When calculating Fe amount accumulated in the biomass, the highest accumulation capacity was demonstrated by *Fusarium sp.* (51 mg/g dry biomass). However, the growth of this fungus was suppressed by Fe.

Rather high Fe accumulation capacity was shown by *P. lilacinus* and *Eupenicillium sp*. It should be mentioned that 1 mM Fe had no negative effect on the biomass growth; on the contrary, slight growth stimulation was noticed. The least Fe amount removed from the medium was detected in *Aspergillus niger* case. The fungus grew very well in Fe-supplemented medium, whereas its accumulation capacity was much weaker as compared to the other fungi. The pH of the growth medium was shifted to the acidic side by all the fungi and most evidently by *A. niger,* known as a producer of acidic metabolites (Mandal, Banerjee, 2006). Thus, summarizing the most efficient Fe accumulators, which also tolerated the metal added well, were *Paecilomyces lilacinus* and *Eupenicillium sp*.

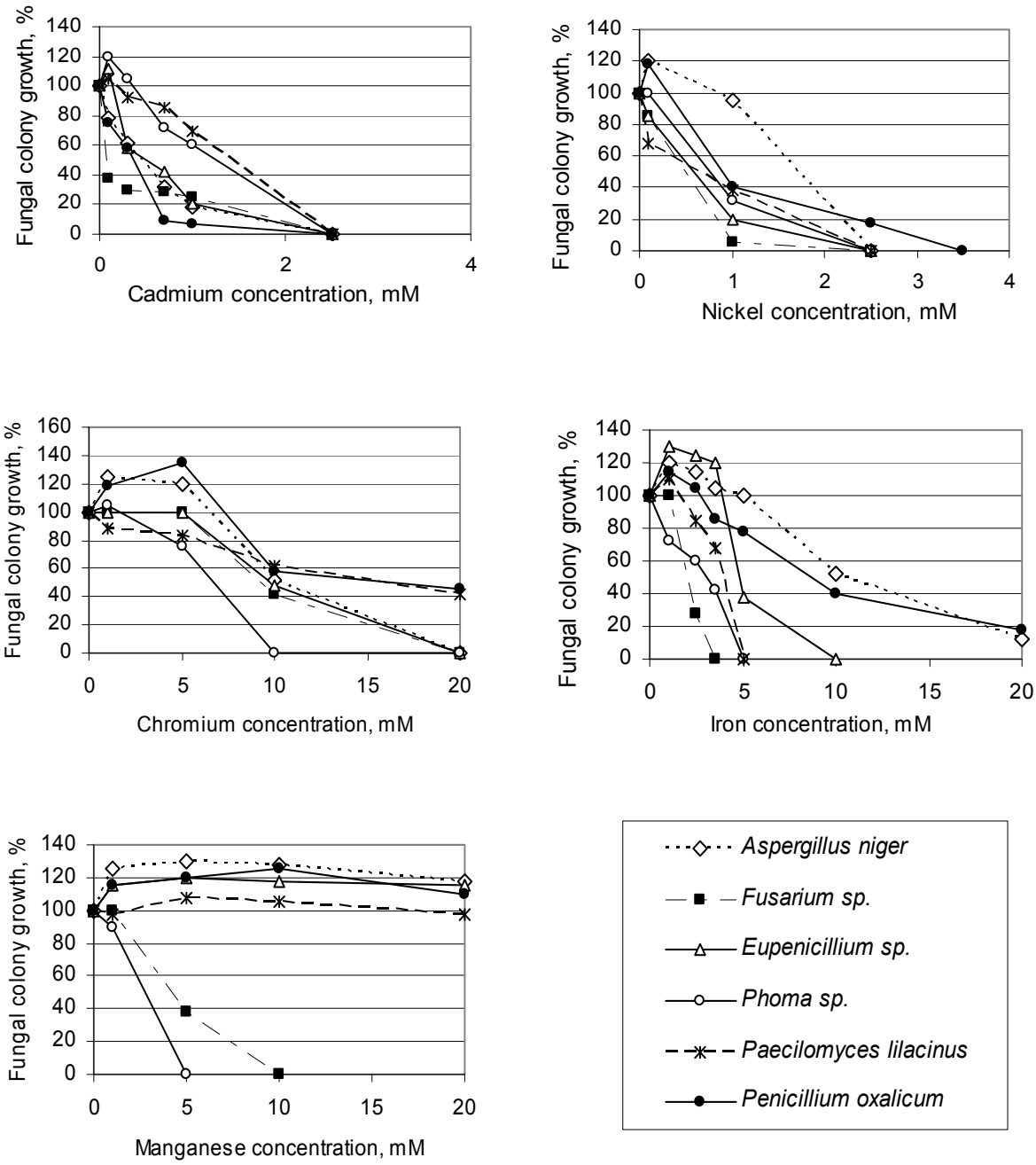

Figure 1: *Growth of fungi on the metal-containing media, represented as fungal colony diameter after 7-day growth compared to fungal colonies on metal free-media*

***Table 1**. Fe removal from growth medium by growing fungal biomass (Fe added to the medium - 1 mM)*

Fungi	P^H change (decrease), $P^H_{initial}$=7,15	Accumulated Fe (mg/1 g dry biomass)	Fe removed from the growth medium, (%)	Biomass growth (%)*
Aspergillus niger	-3.48	16.7	82.8	107
Eupenicillium sp.	-2.74	30.7	93.0	104
Fusarium sp.	-1.31	51.0	96.0	77
Paecilomyces lilacinus	-0.92	38.7	98.7	113
Phoma sp.	-0.84	29.4	99.7	76
Penicillium oxalicum	-0.92	20.6	94.8	98

* (%, compared to the control growth without iron addition)

The experiment of ^{242}Pu accumulation by metal-tolerant fungi showed that all the fungi were able to sorb radionuclide ^{242}Pu by their living biomass (Table 2). The least radionuclide amount sorbed during 1 hour-treatment was 0.0093 and 0.0099 Bq/g dry biomass of *Paecilomyces lilacinus* and *Phoma sp*., respectively. The highest radionuclide sorption capacity was detected in *Eupenicillium sp.* biomass (0.0514 Bq/g). Fungi *Aspergillus niger* and *Penicillium oxalicum* also showed good sorption abilities – 0.0249 and 0.0325 Bq/g of ^{242}Pu were detected in their biomass.

***Table 2:** Plutonium sorbed by fungal biomass during 1 h from the liquid medium supplemented with ^{242}Pu*

Fungi	^{242}Pu, Bq/g dry biomass
Aspergillus niger	0.0325
Eupenicillium sp	0.0514
Fusarium sp.	0.0165
Paecilomyces lilacinus	0.0093
Phoma sp.	0.0099
Penicillium oxalicum	0.0249

High plutonium sorption capacity by biomass was also demonstrated using fungus *Rhizopus arhizus*, which removed significant amounts of plutonium (Dhami et al., 1998). Microorganisms could adsorb radionuclides on their cell surfaces or accumulate them within cell (Francis, 2000). Sorption as an immobilisation process may inable metals and radionuclides to be transformed *in situ* into insoluble forms and could be applicable to remove them from polluted aqueous solution (Gadd, 2001)

Summary and conclusions

The obtained results show that soil fungi are able to withstand rather high heavy metal concentrations in soil, especially when compared to bacteria. The most tolerant microorganisms towards heavy metals added to the soil were *Aspergillus niger, Fusarium sp., Eupenicillium sp., Penicillium oxalicum, Paecilomyces lilacinus* and *Phoma sp.* Metal-tolerance tests revealed that fungi which were able to survive under heavy metal stress in soil differed in their tolerance towards each metal. The highest growth inhibition effect on the pure fungal cultures was manifested by Cd and Ni, while Mn showed the weakest negative influence. *Penicillium oxalicum* showed high tolerance towards most of the metals: its growth occurred at 20 mM of Cr, Fe and Mn, as well as 2.5 mM of Ni added to the medium. *Aspergillus niger (*Fe, Mn) and *Paecilomyces lilacinus* (Cr,Mn) were also highly tolerant fungi. Fungi *Fusarium sp.* and *Phoma sp.* were the most sensitive among the tested fungi.

Metal-accumulation tests revealed that all metal-tolerant fungi were able to remove Fe from the solution highly efficiently - most fungi accumulated over 90% of Fe in their biomass. Very good accumulation and growth properties in Fe-supplemented medium were demonstrated by *Paecilomyces lilacinus* and *Eupenicillium sp*. Preliminary investigation of ^{242}Pu accumulation by fungal biomass showed that all the metal-tolerant fungi were able to sorb ^{242}Pu in their biomass from 0.0093 to 0.0514 Bq/g of dry biomass. Fungi *Eupenicillium sp., Penicillium oxalicum and Aspergillus niger* showed the most effective radionuclide ^{242}Pu sorption. Abilities to accumulate high amounts of the metal and tolerate it well allow fungi to be active participants in metal migration processes in polluted habitats including repositories. Microbial biosorption capacities of heavy metals and radionuclides could also have potential application in bioremediation of polluted environment.

Acknowledgement

This work was partly supported by the Lithuanian Agency for International Science and Technology Development Programmes (Grant No.31V-138). The authors express their appreciation to Dr. R.Gvozdaite from the Institute of Physics for technical assistance in alpha-spectrometric studies.

References

Caesar-Tonthat TC, van Ommen Kloeke F, Geesey GG, Henson JM (1995): Melanin production by a filamentous fungus in response to copper and localisation in copper sulfide by sulfide-silver staining – Applied and Environmental Microbiology, 61, 1968-1975.

Chander K, Dyckmans J (2001): Different sources of heavy metals and their long-term effects on soil microbial properties. Biol Fertil Soils, 34:241-247.

Chaterjee C, Nautiyal N, Pathak A, (1990): Some enzymatic changes at variable zinc in three Aspergillus species differing in zinc requirement – Mycological Research, 94, 511-513.

De Groot RC, Woodward B (1999): Using copper-tolerant fungi to biodegrade wood treated with copper-based preservatives – International Biodeterioration &Biodegradation, 44, 17-27.

De Luca NG, Wood PM (2000): Iron uptake by fungi: contrasted mechanisms with internal or external reduction – Advances in Microbial Physiology, 43, 39-74.

Dhami PS, Gopalakrishan V, Kannan R, Ramanujam A, Salvi N, Udupa SR (1998): Biosorption of radionuclides by *Rhizopus arhizus* – Biotechnology Letters, 20, 225-228.

Dighton J, Tugay T, and Zhdanova NN,(2008): Interactions of fungi and radionuclides in soil –Microbioogy of Extreme Soils Eds. Dion, P, Nautiyal, CS), Berlin Heidelberg, Springer-Verlag, 333-355.

Ehrlich HL (1997): Microbes and metals – Applied Microbiology and Biotechnology, 48, 687-692.

Ehrlich HL (2006): Geomicrobiology: relative roles of bacteria and fungi as geomicrobial agents – Fungi in Biogeochemical Cycles, (ed. Gadd GM), Cambridge University press.

Fomina M, Gadd GM (2007): Transformation of Metals and Minerals by Microorganisms – Journal of Basic Microbiology, 36(4), 269-282.

Francis Aj (2000): Microbial transformations of plutonium and implications for its mobility. www.pubs.bnl.gov/documents/21140.pdf`

Francis AJ, Dodge CJ, Ohnuki T (2007) Microbial transformation of plutonium – Journal of Nuclear Radiochemical Sciences, 8(9), 121-126.

Gadd GM (2001): Microbial metal transformations – The Journal of Microbiology, 39(2): 83–88.

Gadd GM (2005}: Microorganisms in toxic metal polluted soils – Microorganisms in soils: Roles and Functions (ed. by F. Buscot , A. Varma). Soil biology, 3, 325-3 349.

Gadd GM (2007): Roles of micro-organisms in the environmental fate of radionuclides – Health Impacts of Large Releases of Radionuclides, Ciba Foundation, 94-108.

Gorbunova EA, Terekhova BA (1995): Heavy metals as a stress factor towards fungi manifestation of their action on the cell and organism level – Mycologia and phytopathologia, 29, 63-69.

Keith-Roach M.J (2002): Interactions of microorganisms with radionuclides – Radioactivity in the environment, 2, Elsevier: London.

Kools SAE, Ferwerda B, Gestel CAM, and Straalen NM (2005): microbial responses to zinc in soil microcosms with and without a natural assemblage of enchytraeids. Environmental Toxicology and Chemistry, 24(9): 2178–2184.

Lugauskas A, Levinskaitė L, Pečiulytė D, Repečkienė J, Motuzas A, Vaisvalavičius R, Procyčevas I (2005): Effect of copper, zinc and lead acetates on microorganisms in soil – Ekologija, 1, 61-69.

Luptakova A, Macingova E, Slesarova A, Ubaldini S, Abbruzzese C (2007): Solubilization and immobilization of toxic metals by bacteria. IMWA Symposium 2007, Water in Mining Environments, May 2007, Cagliari, Italy.

Mandal SK, Banerjee PC (2006): Oxalic acid production by *Aspergillus niger*: influence of hydrogen ion concentration and nitrogen source – Research Journal of Microbiology, 1(2), 190-197.

Parekh NR, Poskitt JM, Dodd BA, Potter ED, Sanchez A (2008): Soil microorganism determine the sorption of radionuclides within organic soil systems – Journal of Environmental Radioctivity, 99(5), 841-852.

Pedersen K, (2005): Microorganisms and their influence on radionuclide migration in igneous rock environments – Journal of Nuclear and Radiochemical Sciences, 6(1),11-15.

Ravikumar Patil HS, Makari HK, Gurumurthy H (2007): In-vitro biosorption of lead and zinc by using living biomass of *Aspergillus oryza* – www.eco-web.com.

Sar P, Kazy SK, Souza D (2004): Radionuclide remediation using a bacterial biosorbent. International Biodeterioration & Biodegradation, 54(2-3), 193-202.

Valix M, Loon LO (2003): Adaptive tolerance behaviour of fungi in heavy metals – www.sciencedirect/com.

White C, Wilkinson SC, Gadd GM (1995): The role of Microorganisms in biosorption of toxic metals and radionuclides – International Biodeterioration & Biodegradation. 35(1-3), 17–40.

Zafar S, Aqil F, Ahmad I (2007): Metal tolerance and biosorption potential of filamentous fungi isolated from metal contaminated agricultural soil – Bioresource Technology, 98, 2557-2561.

Zdanova NN, Zakharchenko VA, Vember VV, Nakonechnaya LT (2000): Fungi from Chernobyl: mycota of the inner regions of the containment structures of the damaged nuclear reactor – Mycological research, 104(12), 1421-1426.

THE EFFECT FROM MICROORGANISMS ON THE REDOX STATE OF LABORATORY AND NATURAL SYSTEMS

Karsten Pedersen, Johanna Arlinger, Sara Eriksson, Lisa Rabe, Lotta Hallbeck

Microbial Analytics Sweden AB, Mölnlycke Fabriker 9 SE-435 35 Mölnlycke, Sweden

* Corresponding author: karsten.pedersen@micans.se

Abstract

Understanding the effect of microorganisms on the redox state of natural systems require basic knowledge about microbial processes. This is because many redox reactions, such as sulphate reduction, only proceed if bacteria are present and active. Observations of natural groundwater from surface and tunnel boreholes in hard rock have revealed elevated concentrations of sulphide. Investigations of the effect from drainage of a borehole on microbes and dissolved sulphide and ferrous iron have been performed. It was found that the number of sulphate reducing bacteria was positively correlated with the concentration of sulphide and negatively with redox potential. During the site investigations for a nuclear waste repository in Forsmark and Laxemar, significant correlations have been found between the measured redox with the so called Chemmac redox electrodes and the number of sulphate reducing bacteria and the concentration of manganese. The results demonstrate that the measurement of the concentration of single variables such as sulphide or manganese will not allow indication of the redox state of a natural system. Rather than focus on a single parameter, it will be more meaningful to analyse reactants such as the sulphide, sulphate, organic carbon and hydrogen and their biological turnover rates. Such work will be performed in the laboratory under controlled conditions.

Introduction

The reliable measurement of redox potential requires that equilibrium is established at the electrode and among the various redox couples in solution. However, most redox reactions in natural waters occur only under the conditions of microbial processes, which involve the exchange of several electrons and the presence of complex biochemical pathways (e.g. Figure 1). Biogeochemical systems are, therefore, non-equilibrium systems and in most cases, they will never reach equilibrium. This is important for life processes because the maintenance of non-equilibrium conditions is a pre-requisite of life. A good example of a kinetically hindered redox reaction is the microbial reduction of sulphate to sulphide. Here, we will focus on this process, because sulphate reducing bacteria are common in deep, natural groundwater, and in marine systems, and sulphide has a significant effect on the potential of redox electrodes.

The reduction of sulphate to sulphide during the oxidation of organic carbon to carbon dioxide is kinetically hindered at room temperature and atmospheric pressure (Goldstein and Aizenshtat 1994). The calculated half life for thermochemical sulphate reduction in the presence of acetate and elemental sulphur at 100 °C was 372 000 years (Cross et al. 2004). It is, consequently, not possible that sulphate reduction to sulphide occurs in most natural systems without microorganisms.

The reduction of sulphate to sulphide can be represented by a general stoichiometric summary reaction:

$$2CH_3CHOHCOOH + SO_4^{2-} \rightarrow 2CH_3COOH + 2CO_2 + 2H_2O + S^{2-} \quad \text{(Eq. 1)}$$

However, the actual biochemical reaction pathway is much more complicated, and includes a cascade of biochemical enzyme-catalysed reactions inside the living cells that are strictly controlled by the genetic code (i.e., DNA) of the individual cells. In addition, feedback and substrate-level control mechanisms may also be active. It is important to understand the biochemistry underlying summary reactions such as the one above; otherwise the modeling of biological redox processes may come out wrong.

Consider the summary equation above for sulphate reduction with lactate as the electron donor. The reaction would seem to indicate that lactate reacts directly with sulphate resulting in the formation of acetate, carbon dioxide, and sulphide. This, however, is very far from what actually happens. In fact, lactate and sulphate never make contact, but rather are dealt with by the bacterium in two separate biochemical pathways inside the cell (Figure 1). Lactate is split into acetate and formate via pyruvate and the formate is then oxidized to carbon dioxide and hydrogen. This process involves three enzymes (i.e., lactate dehydrogenase, pyruvate formate lyase, and formate hydrogenolyase) and an oxidized proton–electron transport molecule denoted nicotinamid adenine nucleotide (NAD^+). The electrons released are used as electron donors in the reduction of sulphate via a membrane-bound respiration chain. Consequently, the oxidation of the organic carbon is not directly connected to the reduction of the sulphate. Sulphate reduction will occur only when the cell needs to get rid of electrons that have generated a proton gradient across the cell membrane. From this, it should be clear that the rate of sulphate reduction cannot be determined solely from concentrations of sulphate, lactate or acetate and sulphide. Rather, the needs of the cell are what determines whether sulphate reduction will occur and at what rate. It is important to understand that sulphate reduction is possible with hydrogen only, without concurrent cell growth on organic carbon sources.

Turning to other processes, such as iron, manganese, and nitrate reduction with organic carbon as the reducant, and acetate formation and methanogenesis, both with hydrogen and carbon dioxide, will reveal other biochemical pathways, each of which is unique to the respective redox process. An endless array of more or less intricately linked processes can be found by anyone looking into a microbiology textbook, such as *Brock Biology of Microorganisms* (Madigan and Martinko 2006). A full understanding of microbial oxidation–reduction processes is thus very complex. It becomes necessary to develop model approximations and simplifications that do not violate the rules of microbial biochemistry, otherwise the model output may be wrong.

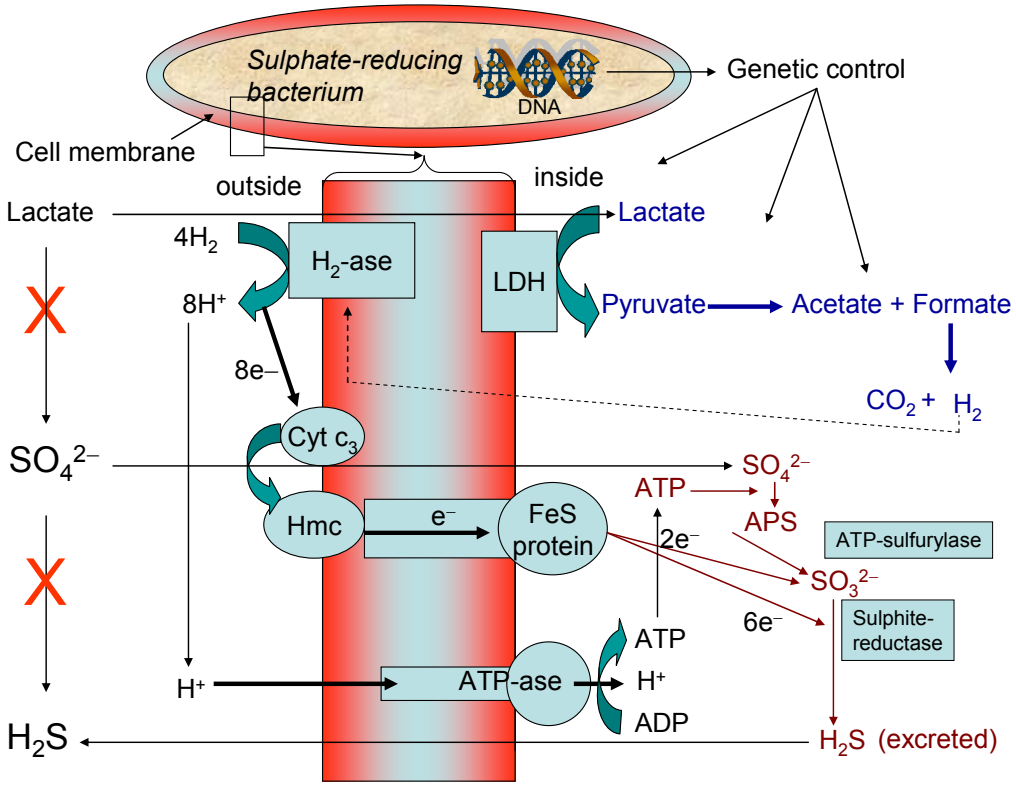

Figure 1: *Electron transport and energy conservation in sulphate-reducing bacteria. In addition to external hydrogen (H_2), H_2 originating from the catabolism of organic compounds such as lactate and pyruvate can fuel hydrogenase with electrons via enzymes such as lactate dehydrogenase (LDH). The protons released by the hydrogenase feed the proton gradient across the cell membrane, and this gradient phosphorylates ADP to ATP via ATP-ase. The enzymes hydrogenase (H_2-ase), cytochrome c_3 (cyt c_3), and a cytochrome complex (Hmc) are periplasmic proteins located between the outer and inner membranes of the cell. A separate protein functions to shuttle electrons across the cytoplasmic cell membrane to a cytoplasmic iron-sulphur protein (FeS) that supplies the adenosine 5′-phosphosulphate (APS) reductase (forming SO_3^{2-}) and sulphite reductase (forming H_2S) with electrons. The process of sulphate reduction is controlled by the genetic code (i.e., DNA) of the bacterium. Environmental conditions are scanned by bacterial sensors that send messages to the DNA, which turns the sulphate reduction on and off under favourable and unfavourable conditions, respectively.*

Materials and Methods

The Äspö Hard Rock Laboratory

Several boreholes in the Äspö hard rock laboratory show high concentrations of sulphide that rapidly decreases when the boreholes are opened. Two of these boreholes, denoted KA3110A at 414 m depth and KA3510A at 450 m depth were used in this work. Details about the tunnel boreholes in the Äspö can be found elsewhere (Pedersen et al. 1996, 1997; Kotelnikova and Pedersen 1998). Pressure resistant platinum micro-electrodes (0.5 mm tip) from Unisense A/S were used. As reference, pressure resistant microelectrodes, also from Unisense A/S, with Ag/AgCl in gelstabilized electrolyte were used. See www.unisense.com for details. The boreholes were drained of up to 1000 L groundwater and sulphide, ferrous iron, redox potential and the number of

sulphate reducing bacteria plus some basic chemistry were analysed. This experiment was repeated twice, in April and October 2008. Details about the methods can be found elsewhere (Hallbeck and Pedersen 2008a).

The sites Forsmark and Laxemar

The investigation candidate sites for a possible future repository for high level radioactive waste are situated on the east coast of Sweden. A total of 23 samples were analysed for microbial numbers, geochemistry and redox potential. The redox was analysed with the so called Chemmac redox electrode system that is installed down in the borehole (Grenthe et al. 1992; Auqué et al. 2008). The geochemical constituents were analysed on samples collected on the ground from pumped out groundwater. Microbial numbers were analysed on samples collected with a pressure container that was opened and closed at the depth of the sampled fracture as described elsewhere (Pedersen 1997).

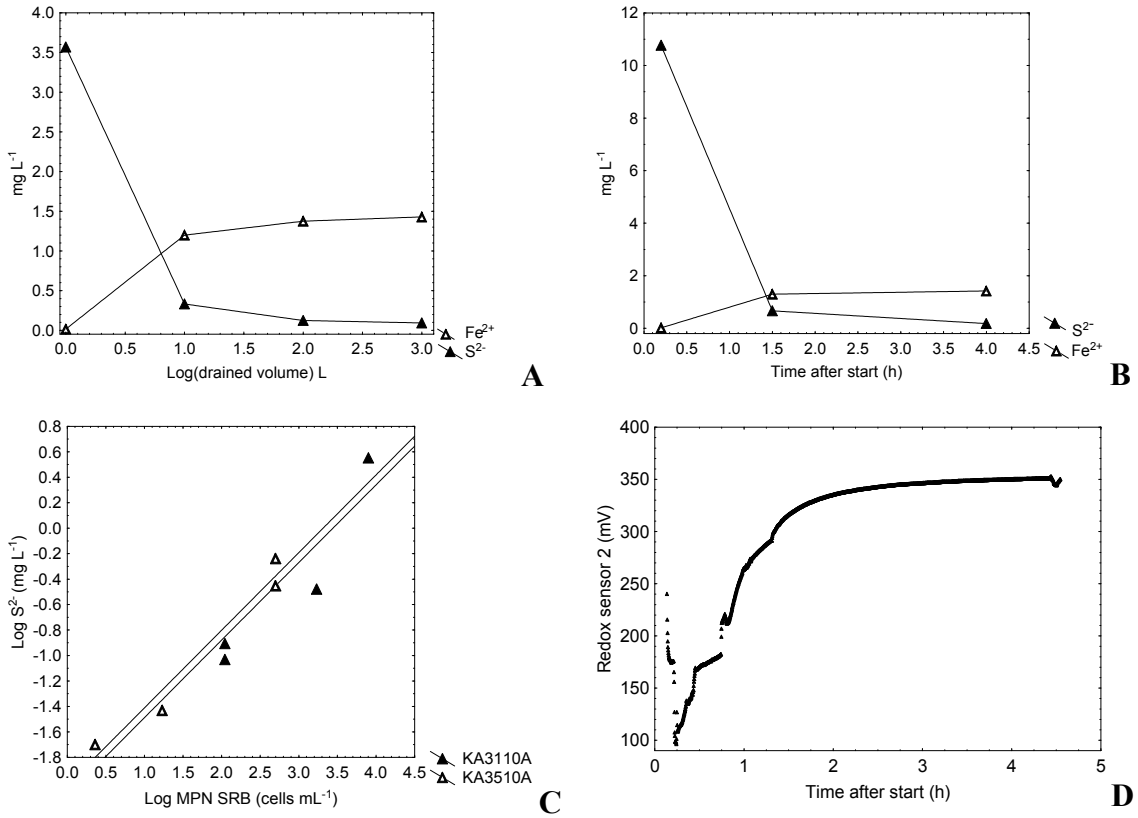

***Figure 2**, A-B. The concentrations of ferrous iron and sulphide during drainage of borehole KA3110A in the Äspö Hard Rock Laboratory tunnel in April (A) and October (B). C. The relation between sulphide and the number of cultivable sulphate reducing bacteria. D. The development of redox potential during drainage in October.*

Results

The Äspö Hard Rock Laboratory

The amount of sulphide rapidly decreased during draining of KA3110A in both experiments and ferrous iron appeared. Ferrous iron was absent in the borehole at start of drainage (Fig 2A and B). The number of cultivable sulphate reducing bacteria correlated positively with the sulphide concentration in both boreholes (Fig. 2C). When the redox potential was measured in the second experiment in KA3110A, there was an increase in the redox potential of about 200 mV (Fig. 2D), which corresponded to a decrease in sulphide from about 10 mg L^{-1} to 0.2 mg L^{-1}. However, the basic chemistry of the groundwater remained constant and did not change during drainage or between the two sampling occasions (Table 1). It was only parameters related to microbial processes that were influenced by the drainage process.

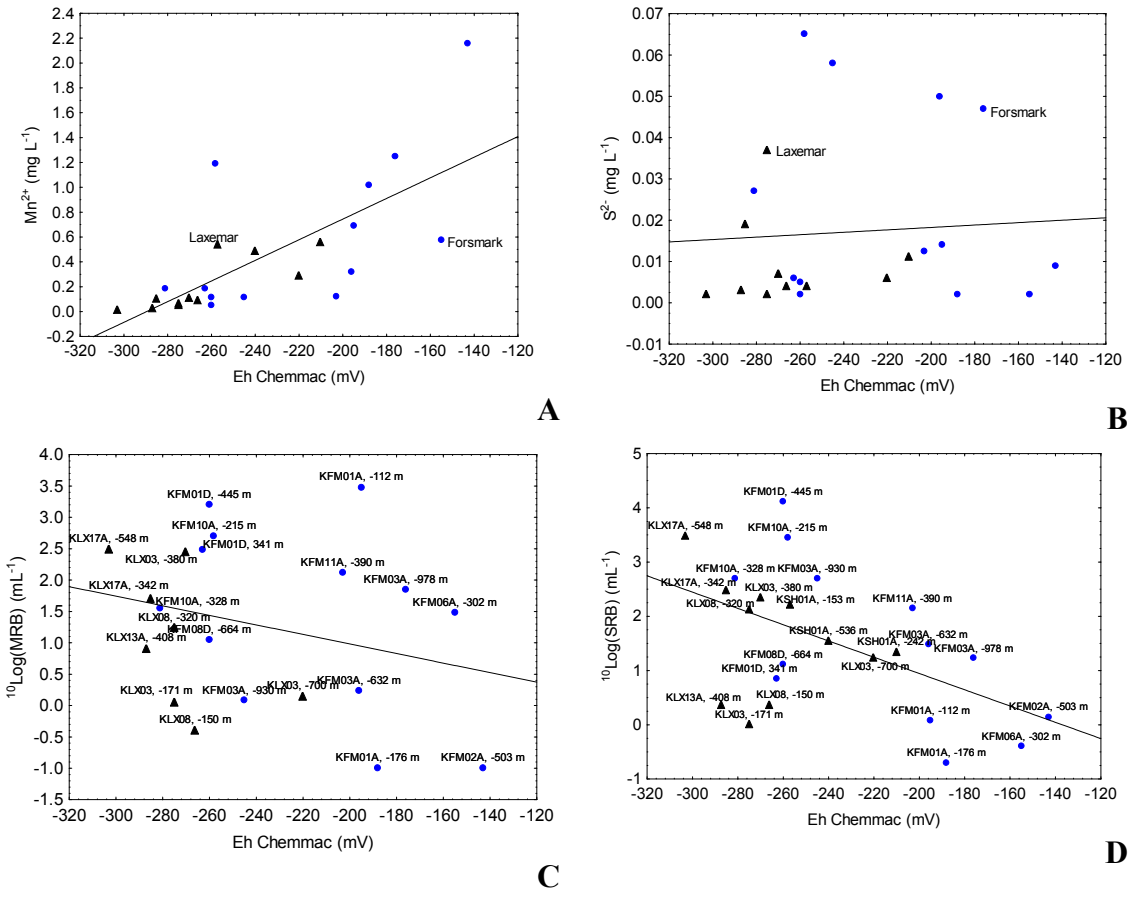

Figure 3. *The relation between dissolved manganese(II) (A) and sulphide (B) and redox in Laxemar and Forsmark groundwater. The relation between the numbers of manganese reducing bacteria (C) and sulphate reducing bacteria (D) and redox in Laxemar and Forsmark groundwater. The correlation lines have the following equations, correlation coefficients (r) and probability of r (p).*

A: y=2.40	*+0.008x*	*r=0.711*	*p=0.0001*
B: y=0.0241	*+0.0000292x*	*r=0.0669*	*p=0.7617*
C: y=0.541	*-0.0076x*	*r=-0.273*	*p=0.23*
D: y=2.054	*-0.015x*	*r=-0.519*	*p=0.0093*

Table 1. *Chemistry of groundwater during draining of the borehole KA3110 as shown in Figure 2.*

Borehole	Date of sampling (y-m-d)	Drained volume (Litre)	Time after start (hours)	pH	Cl^- (mg/L)	SO_4^{2-} (mg/L)	HCO_3^- (mg/L)
KA3110	08-04-06	1	0.2	8.01	3045	295	177
KA3110	08-04-06	10	1.5	7.58	3048	320	188
KA3110	08-04-06	100	4.0	7.52	3058	322	186
KA3110	08-04-06	1000	15.0	7.48	3057	320	187
KA3110	08-10-14	1	0.2	7.78	3221	323	174
KA3110	08-10-14	10	1.5	7.54	3246	324	185
KA3110	08-10-14	100	4.0	7.47	3242	311	184
KA3110	08-10-14	1000	15.0	7.48	3262	296	183

Discussion

Two different types of redox measurement systems (Unisense and Chemmac) were used in Äspö and the site investigations. The Unisense system was not calibrated against the Chemmac. Therefore, the Äspö redox results should only be interpreted relative to the change in chemistry of the Äspö groundwater.

The Äspö tunnel experiments clearly demonstrated that the redox active components sulphide and iron were strongly influenced by the drainage process, while the salinity (represented as chloride) was constant. To some extent, sulphate, pH and HCO_3^- were initially influenced (Table 1). The drainage experiments then illustrated the relation between microbial processes and redox as discussed next.

The drainage experiments showed that the concentration of sulphide correlated with the numbers of sulphate reducing bacteria. This is reasonable, because sulphate reducing bacteria must be active and reduce sulphate to sulphide when present. However, if ferrous iron is also present, iron sulphide may form, which will decrease the measured concentration of dissolved sulphide. This was the case in the drainage experiment where sulphide and ferrous iron were inversely related. Consequently, if microbial sulphate reduction to sulphide and microbial ferric iron reduction to ferrous iron are on-going simultaneously, analysis of concentrations will not reveal the rates of reduction. Molecular methods that analyse DNA expressions of key enzymes for these microbial redox processes are needed. Such methods are available and in use in this Recosy project.

There was very little sulphide in all of the 23 Forsmark and Laxemar site investigation samples despite the fact that there were high numbers of sulphate reducing bacteria is several samples. As judged from the Äspö tunnel experiments (Fig 2C), a correlation between the sulphide concentration and the number of sulphate reducing bacteria was expected for the site investigation samples. One possible reason for the absence of such a correlation may be that an artifact was introduced during the pumping from the sampled depth to the ground where samples for geochemistry were taken. There is a drop in pressure of the pumped groundwater that corresponds with the depth, which, together with the large tube surface in the used 4 mm inner diameter tubing may have triggered precipitation of sulphide with ferrous on the tube walls. Typically, rinsing the

tube after a sample period resulted in rinsing water stained black by iron sulphide, suggesting that sulphide was removed from solution with iron during pumping. As manganese(II) is more stable in solution with iron than sulphide, manganese will not be affected in a similar way. This is yet a hypothesis that requires more research, but it could explain why sulphate reducing bacteria correlated with the measured redox potential at the sample depth, as sulphide did with sulphate reducing bacteria in the Äspö tunnel experiments (Fig 2C). The absence of correlation between manganese reducing bacteria and Chemmac redox potential may be due to a lag in time between microbial manganese(II) production and the analysis of their numbers.

Summary and Conclusions

The results presented here demonstrated that the measurement of the concentration of single variables such as sulphide, ferrous iron or manganese only, will not allow indication of the redox state of a natural system. This is because the measured redox value is a mixed potential that do not resolve participating redox couples. This is similar to the difficulty in pH calculations; it is not possible to calculate or model the concentrations of participating acids and bases from the measured pH value only. Most of the redox reactions in groundwater are not reversible and therefore the Eh-values from these complex redox reactions cannot be calculated. Experience shows that measuring the redox active species is complicated due to especially the reactivity of ferrous iron and sulphide. A combination of microbial and chemical analyses will give a more correct view of the main redox reactions in a natural system.

Organic matter should not likely exist in the presence of sulphate, ferric iron, nitrate or other electron acceptors in natural waters as far as thermodynamics are concerned. This is because these systems are non-equilibrium systems due to the fact that the oxidation of organic material with these electron acceptors is kinetically hindered. It becomes important to measure the rates of biological redox processes that influence the potential of redox electrodes. Rather than focusing on or a few single parameters, it will be more meaningful to analyse reactants and rates such as the sulphide, sulphate, organic carbon and hydrogen and their turnover rates. Such work is best performed in the laboratory under controlled conditions. Pure cultures of different microorganism, such as nitrate, iron, manganese and sulphate reducing bacteria can be studied one by one with one active redox couple at the time. Successively, mixed cultures and mixed redox couples can be introduced. This strategy may allow the detailed characterization of how the measured redox potential depends on different microbial processes and the rate of the respective process.

Acknowledgement

This work was performed under the Recosy program with co-funding from the Swedish Nuclear Fuel and Waste management Co.

References

Auqué, L.F., Gimeno, M.J., Gómez, J.B. and Nilsson, A.-C. 2008, Potentiometrically measured Eh in groundwater from the Scandinavian Shield, Applied Geochemistry, 23 no. 7, 1820-1833.

Cross, M.M., Manning, D.A.C., Bottrell, S.H. and Worden, R.H. 2004, Thermochemical sulphate reduction (TSR): experimental determination of reaction kinetics and implications of the observed reaction rates for petroleum reservoirs, Organic Geochemistry, 35 393-404.

Goldstein, T.P. and Aizenshtat, Z. 1994, Thermochemical sulfate reduction. A review, Journal of Thermal Analysis, 42 241-290.

Grenthe, I., Stumm, W., Laaksoharju, M., Nilsson, A.-C. and Wikberg, P. 1992, Redox potentials and redox reactions in deep ground water systems, Chemical Geology, 98 131-150.

Hallbeck, L. and Pedersen, K. 2008a, Characterization of microbial processes in deep aquifers of the Fennoscandian Shield, Applied Geochemistry, 23 1796-1819.

Hallbeck, L. and Pedersen, K. 2008b, Explorative analysis of microbes, colloids and gases together with microbial modelling. Site description model. SDM-Site Laxemar, R-08-209, Swedish Nuclear Fuel and Waste Management Co, Stockholm Sweden, 1-72.

Hallbeck, L. and Pedersen, K. 2008c, Explorative analysis of microbes, colloids and gases. SDM-Site Forsmark, R-08-85, Swedish Nuclear Fuel and Waste Management Co, Stockholm Sweden, 1-76.

Kotelnikova, S. and Pedersen, K. 1998, Distribution and activity of methanogens and homoacetogens in deep granitic aquifers at Äspö Hard Rock Laboratory, Sweden, FEMS Microbiology Ecology, 26 121-134.

Madigan, M.T. and Martinko, J.M. 2006, *Brock Biology of Microorganisms, 11th edition*, Prentice Hall, London UK

Pedersen, K. 1997, Microbial life in granitic rock, FEMS Microbiology Reviews, 20 no. 3-4, 399-414.

Pedersen, K., Arlinger, J., Ekendahl, S. and Hallbeck, L. 1996, 16S rRNA gene diversity of attached and unattached groundwater bacteria along the access tunnel to the Äspö Hard Rock Laboratory, Sweden, FEMS Microbiology Ecology, 19 249-262.

Pedersen, K., Hallbeck, L., Arlinger, J., Erlandson, A.-C. and Jahromi, N. 1997, Investigation of the potential for microbial contamination of deep granitic aquifers during drilling using 16S rRNA gene sequencing and culturing methods, Journal of Microbiological Methods, 30 no. 3, 179-192.

THE COMPLEXATION OF Tc(IV) WITH GLUCONIC ACID AT HIGH pH

N. Evans[1], R. Hallam[1], S. Aldridge[1],P. Warwick[1] and N. Bryan[2]

[1]Department of Chemistry, Loughborough University, Loughborough, Leics, LE11 3TU, UK

[2]Centre for Radiochemistry Research, School of Chemistry, The University of Manchester, Oxford Road, Manchester, M13 9PL, UK

*Corresponding author: N.D.M.Evans@lboro.ac.uk

Abstract

In the UK, a technetium containing floc may be disposed of in a high pH, low Eh cementitious repository, whereupon the floc would degrade by alkaline hydrolysis and/or radiolysis releasing the Tc into the porewater. Its chemistry would then be dominated by TcO_4^-, in aerobic waters and the sparingly soluble TcO_2(s) in anaerobic. Repository heterogeneity could mean that both Tc(VII) and Tc(IV) are present simultaneously. If TcO_4^- migrates into reducing conditions, organic ligands in the waste may complex with Tc during reduction to form water-soluble complexes. Also possible, is increased Tc solubility when organic ligands react with TcO_2(s). For gluconic acid the Tc aqueous concentration starting from TcO_4^- and reducing the mixture was higher than in systems with TcO_2 as the starting point. This suggests that the pertechnetate was not reduced to TcO_2, but an intermediate oxidation state complex was formed, e.g. Tc(V). The conditional stability constant for the Tc(IV)-gluconic acid complex has been determined to be $\log \beta = 26.6 \pm 0.2$.

Introduction

The currently preferred UK option for the management of intermediate-level radioactive waste (ILW) is to store it in a deep underground repository. This may then be backfilled with a cementitious material. Once closed, the repository will become saturated with groundwater, and highly alkaline porewater would develop with an initial pH of around 13.4. However, this will decrease to 12.5 as the groundwater flow dissolves, and removes, any NaOH and KOH present. The mineral phases in the cement will act as a buffer and maintain the pH at 12.5 for *ca*. 10^5 years. Corrosion of waste-containing steel canisters will lead to the gradual formation of reducing conditions. Thus, the behaviour of radionuclides likely to be in the waste must be understood in the context of this chemistry (Warwick et al., 2003).

^{99}Tc, a low energy β emitter, present in some nuclear waste streams as TcO_4^-, is an important species for performance assessment of any proposed repository, due to its high yield (6% of fission products) and long half-life (2.1×10^5 years). The aqueous chemistry of technetium is likely to be dominated by the highly mobile pertechnetate anion (TcO_4^-) in aerobic waters, and by Tc(IV), as TcO_2 (am) solid, in anaerobic (Cui et al., 1996). Under reducing conditions, TcO_4^- in non-complexing aqueous solutions initially undergoes a one-electron reduction to the unstable $TcVIO_4^{2-}$ species (Heller-Grossman et al., 1981). Subsequent 2- or 3-electron reductions to Tc(V) or Tc(IV) species then readily occur. However, the Tc(V) and Tc(VI) species are unstable and disproportionate into more stable Tc(IV) and Tc(VII) species. This leads to the formation of four significant technetium aqueous species (Fig. 1), although in a repository only TcO_2(s) and TcO_4^- are likely to be present.

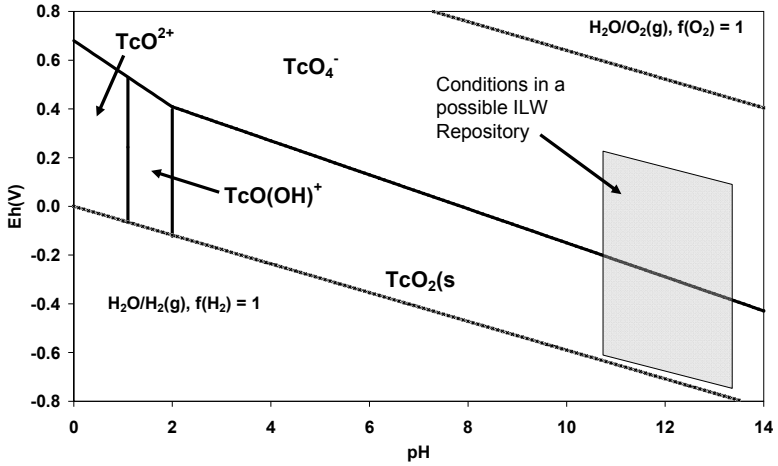

Figure 1. *Predominance diagram for technetium*

The solubility of Tc(IV) in anaerobic conditions at high pH above amorphous TcO_2(s), the phase most likely to be present in a repository, has been a matter of debate for some time. A recent study by Warwick et al. (Warwick et al., 2007) showed that, from pH 11 to 13.5, the aqueous Tc concentration appeared to be independent of pH. However, at pH values greater than 13.5, the aqueous concentration of technetium increased with increasing pH. This increase in solubility can be explained by the equilibrium in equation 1. Log K for the species $TcO(OH)_3^-$ was determined to be log K_2 = -14.2 (Aldridge et al., 2007), but this anionic Tc(IV) species is only likely to be formed in significant quantities above the highest pH likely to be found in a cementitious repository, and hence should be of little interest to performance assessment.

$$TcO_2 \cdot nH_2O \leftrightarrow TcO(OH)_3^- + H^+ + (n-2)H_2O \qquad (1)$$

In the past in the UK, small amounts of technetium were discharged into the Irish Sea. It was originally thought to disperse widely, but was discovered to concentrate in seaweed (Copplestone et al., 2004). Hence, treatment with tetraphenylphosphonium bromide (TPPB) is now used to precipitate out the technetium as TPPTc, to prevent more marine discharges. This leads to the possibility that the floc may be sent to a cementitious repository for disposal. However, TPPB degrades by alkaline hydrolysis at high pH. It is also prone to radiolytic degradation.

Organic complexing agents will be present as inherent components of the waste, especially those like isosaccharinic acid (ISA), gluconic acid and similar polyhydroxylated carboxylic acids which will be formed by the anaerobic, alkaline degradation of cellulose. These are highly complexing and can cause significant increases in radionuclide solubility at high pH (Warwick et al., 2003). The repository will not be homogenous and there are likely to be areas of reducing and oxidising potential. This heterogeneity could mean that both Tc(VII) and Tc(IV) are present within the repository. If TcO_4^- migrates into an area in which reducing conditions exist, the organics may complex with technetium during reduction to form water-soluble complexes. This approach to complex formation, i.e. reduction in the presence of complexing ligands, is widely used to produce ^{99m}Tc radiopharmaceuticals. However, such investigations have been carried out at near-neutral pH and little has been reported on technetium complexation in the highly alkaline conditions to be expected in a cementitious repository.

Also of relevance to technetium mobility, is the possibility of increased solubility when organics are in contact with reduced technetium (TcO_2(s)). In other words, does the presence of organics affect the reduction of Tc(VII) to Tc(IV)? With these considerations in mind, studies were undertaken in which TcO_4^- was reduced electrochemically, and by use of Sn(II) and Fe(II), in the presence and absence of gluconic acid, to determine whether there was an increase in technetium solubility when TcO_2 was contacted with the organic ligands, TcO_2 was prepared by the reduction of TcO_4^- and then contacted with anaerobic solutions of the ligands.

Experimental

All experiments were conducted in a Unilab MBraun Nitrogen Glove Box with O_2 levels kept below 1 ppm. All solutions were boiled, N_2 sparged and kept in the presence of iron filings to maintain reducing conditions. Solid sodium gluconate was added to NaOH(aq) at pH 13.3, to give concentrations between 0.4 and 0.001 mol dm^{-3}. Ammonium pertechnetate was added and the pH and Eh measured. Reduction was achieved by 3 methods, the addition of 0.7 g of $SnCl_2$ or $FeCl_2$ and the solutions were left for 14 days, or electrochemically. The activity in solution was measured by liquid scintillation counting using Canberra Packard TRI-Carb 2750TR/LL, indicating an aqueous concentration of Tc(IV) of around 4 x 10^{-9} mol dm^{-3}. 5 replicates were used. Control experiments without sodium gluconate showed that reducing conditions were maintained for the requite periods of time. Control experiments with gluconate showed that 14 days was sufficient for steady state to be established. To measure the stability constant for the reaction of Tc(IV) with gluconic acid, the solubility product approach was used, as discussed by Warwick et al. (2004).

Results and discussion

The solubility product for the TcO_2(am) phase formed in these experiments was determined to be log K_{sp} = -33.6 ± 0.32 (Evans et al., 2008).

Complexation of Tc(IV)

Fig. 2 shows the effect of increasing gluconic acid concentration on technetium(IV) solubility. The slope of close to unity indicates that the increase in solubility of Tc is being controlled by the formation of a 1:1 Tc(IV)-gluconate complex. This relationship allows the calculation of a conditional stability constant for this complex using the solubility product approach.

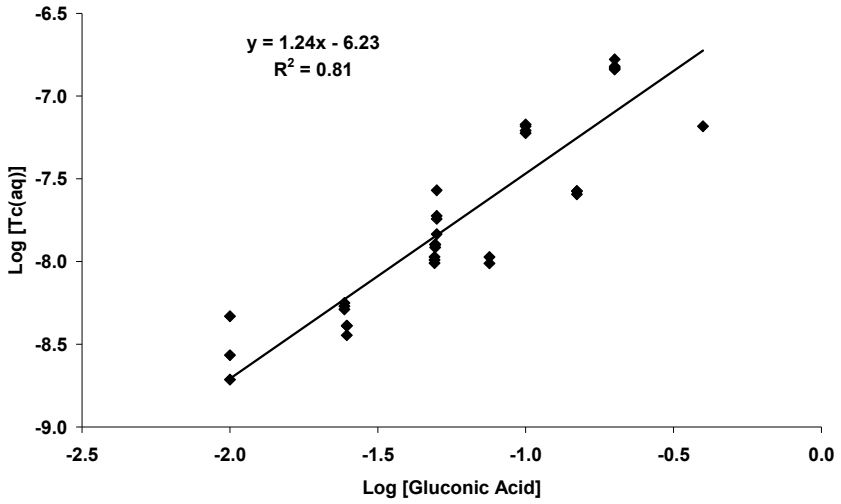

Figure 2. *Effect of concentration of gluconic acid on aqueous technetium concentration above TcO_2(am) at pH 13.3.*

The dissolution of TcO_2 can be written as:

$$TcO_2.2H_2O(am) \leftrightarrow TcO_2{+}(aq) + 2OH^-(aq) + H_2O \qquad (2)$$

Therefore, the solubility product $K_{sp} = [TcO^{2+}][OH^-]$. In the absence of gluconate, dissolved Tc(IV) will consist of the $TcO(OH)^+$ ion and its major hydrolysis products, equation 3.

$$[Tc]_{solution} = [TcO^{2+}] + [TcO(OH)^+] + [TcO(OH)_2]^0 + \text{etc.} \quad (3)$$

Or $[Tc]_{solution} = [TcO^{2+}]A$, where $A = 1 + \sum\beta_x[OH]^x$ (the side reaction coefficient) (Maes et al., 1988), which is constant at a given pH. Addition of gluconic acid caused the following reaction to occur, equation 4.

$$TcO^{2+} + Gl^{y-} \leftrightarrow TcOGl^{(2-y)+} \qquad (3)$$

The concentration of dissolved Tc(IV) will be increased by the formation of the gluconate complex, equation 5:

$$[Tc]_{solution} = [TcO^{2+}]A + [TcOGl^{(2-y)+}] \quad (4)$$

Following the derivation in (Warwick et al., 2004), the conditional stability constant of the complex is given by:

$$\beta = \frac{[Tc]_{solution} - \left(\frac{K'_{SP}}{[OH^-]}\right)A}{\left(\frac{K'_{SP}}{[OH^-]}\right)\left([Gl^{y-}]_{total} - \left\{[Tc]_{solution} - \left(\frac{K'_{SP}}{[OH^-]}\right)A\right\}\right)} \quad (5)$$

The conditional stability constant was calculated using equation (8) and was determined to be; $\beta = 4.0 \times 10^{26}$ or $\log \beta = 26.6 \pm 0.2$.

Reduction of Tc(VII) in the presence of sodium gluconate.

In the presence of gluconate a lowering of the aqueous technetium concentration took place upon reduction, showing that the ligand did not prevent reduction taking place. If this reduction was to Tc(IV), then the final aqueous concentration of technetium should be the same as that produced by the addition of the same ligands to Tc(IV) solution, i.e. the Tc(IV)-ligand complexes would again be formed, but by two different routes, assuming steady state had been obtained. However, the final Tc solubility in the system where reduction took place in the presence of gluconate was higher than when TcO_2 was the starting point (Fig. 4). This indicates that Tc(VII) may not have been reduced to Tc(IV) but an intermediate oxidation state such as Tc(V) complex may have been formed. This idea is well known in the formation of ^{99m}Tc radiopharmaceuticals (Johannsen et al., 1996). It is known that polyhydric complexes of Tc(V) can be formed by the reduction of pertechnetate in aqueous solution of the excess O-donor ligand (Huber et al., 1987), although in pharmaceuticals this is not carried out at high pH. Apart from a few cases, the complexes have not been structurally characterised, because of the difficulty of obtaining pure compounds in crystalline form. The Tc-glycolato complex (Huber et al., 1987) has been identified as $[TcO(OCH_2CH_2O)_2]^-$.

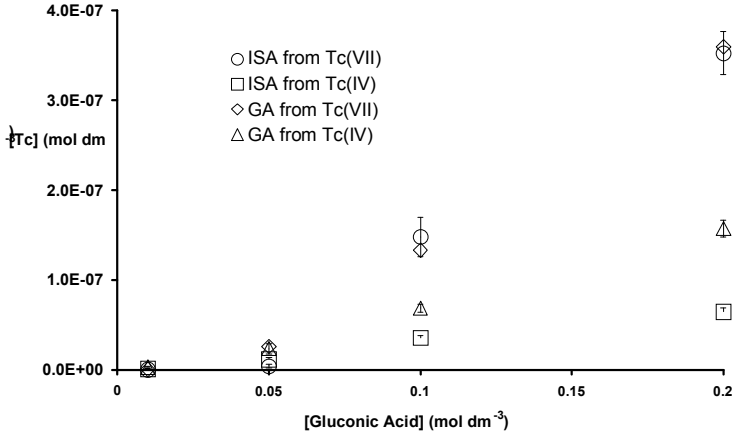

Figure 3*. Comparison of final Tc concentrations in the presence gluconic acid at pH 13.3, starting from TcO4- and Tc(IV).*

Conclusions

The presence of gluconic acid caused an increase in Tc(IV) solubility, indicating the formation of a Tc(IV)-Gluconate complex with a 1:1 stoichiometry. The conditional stability constant was calculated using equation (8) and was determined to be; log β = 26.6 ± 0.2. In the presence of gluconate a lowering of aqueous Tc concentration took place upon reduction. The aqueous Tc concentration in systems starting from Tc(VII) was higher than when TcO_2 was the starting point, suggesting that Tc(VII) was not fully reduced to Tc(IV), but that an intermediate oxidation state complex may have been formed. These results indicate that a detailed understanding of the effect of organic ligands on the reduction of technetium will be required for performance assessment if technetium is to be disposed of in a cementitious repository.

References

Aldridge S, Warwick P, Evans N, Vines S, Degradation of tetraphenylphosphonium bromide at high pH and its effect on radionuclide solubility, Chemosphere, 66, 672-676, 2007

Copplestone D, Jackson D, Hartnoll R, Johnson M, McDonald P, Wood N, Seasonal variations in activity concentrations of Tc-99 and Cs-137 in the edible meat fraction of crabs and lobsters from the central Irish Sea. J Environ. Radio., 3, 29-48, 2004

Cui D, Eriksen T, Reduction of Pertechnetate by Ferrous Iron in Solution: Influence of Sorbed and Precipitated Fe(II), Environ. Sci. Tech., 30, 2259-2262, 1996

Evans N, Hallam R, Aldridge S, Warwick P, The fate of Tc in a UK intermediate-level nuclear waste repository, Waste Manage. Environ. IV, 579-588, 2008

Heller-Grossman L, Abrashkin S, Shafferman A, Davis M, Taube R, Tc-99m Generators. 2. Physicochemical Factors in the Radiolytic Reduction of Pertechnetate, App. Rad. Iso., 32, 501-506, 1981

Huber G, Anderegg G, May K, Synthesis and characterization of a technetium(V) glycolato complex. Poly., 6(8), 1707-8, 1987

Johannsen J, Spies H, Technetium (V) chemistry as relevant to nuclear medicine. Top. Cur. Chem., 176, 77-121, 1996

Maes A, De Brabandere J, Cremers A, A Modified Schubert Method for the Measurement of the Stability of Europium Humic Acid Complexes in Alkaline Conditions, Radiochim. Acta., 44/45, 51-56, 1988

Warwick P, Evans N, Hall A, Vines S, Complexation of Ni(II) by α-Isosaccharinic Acid and Gluconic Acid from pH 7 to pH 13. Radiochim. Acta, 91, 233-240, 2003

Warwick P, Aldridge S, Evans N, Vines S, The Solubility of Technetium(IV) at High pH, Radiochim. Acta, 95, 709-716, 2007

Warwick P, Evans N, Hall A, Vines S, Stability Constants of Uranium (IV)-α-isosaccharinic and Gluconic Acid Complexes, Radiochim. Acta, 92, 1-6, 2004

ACTINIDE BEAHIOUR IN HUMIC ACID BENTONITE TERNARY SYSTEMS

P.I. Ivanov[1], T. Griffiths[1], L.G. Abrahamsen[1], N.D Bryan*[1], N.V. Aksenov[2], G.A. Bozhikov[2], O.D. Maslov[2], S.N. Dmitriev[2], N.D.M. Evans[3] and P. Warwick[3]

[1]Centre for Radiochemistry Research, School of Chemistry, University of Manchester, Manchester M13 9PL, (UK)

[2]Flerov Laboratory of Nuclear Reactions, JINR, 141980 Dubna, (Russia)

[3]Deapartment of Chemistry, Loughborough University, Loughborugh, (UK)

* Corresponding author: nick.bryan@manchester.ac.uk

Abstract

The effect of humic acid (HA) on U(VI) sorption on bentonite was studied in batch experiments at room temperature and ambient atmosphere at a ^{237}U(VI) concentration of 8.4×10^{-11} M and HA concentration of 100 mg·L^{-1}. The distribution of U(VI) between the liquid and solid phase was studied as a function of pH and ionic strength both in the absence and presence of HA. It was shown that the uranyl sorption on bentonite is strongly dependant on pH and the presence of humic, and indifferent to the addition order. In the absence of HA, an enhancement in the uptake with increasing pH was observed, and a sharp sorption edge was found to take place between pH 3.2 and 4.2. The presence of HA slightly increases uranium(VI) sorption at low pH and curtails it at moderate pH. In the basic pH range for both the presence and absence of HA, the sorption of uranium is significantly reduced, which could be attributed to the formation of soluble uranyl carbonate complexes. Experiments at higher uranium concentration (10^{-4} M) revealed significant differences at high pH, although there was less difference at moderate and low pH. The influence of ionic strength on U(VI) and HA uptake by bentonite was investigated in the range 0.01 – 1.0 M, and while there was an enhancement in the sorption of humic acid with increasing ionic strength, U(VI) sorption was found to be indifferent to ionic strength both in the absence and presence of HA at $I < 1$ M. In the Pu(III) ternary system, there is evidence of significant irreversibility on a timescale of a few months. When the Pu is added to the bentonite as a humate complex, the extent of sorption is reduced, compared to systems where the Pu has been added to the bentonite first, and the humic added later. On a timescale of a few days, the length of time that the Pu is in contact with the bentonite prior to the addition of the humic appears to make little difference to the result.

Introduction

For its appropriate physicochemical and mechanical properties, bentonite is widely proposed as a backfill and barrier material in nuclear waste repository designs, as it has high radionuclide sorption capacity, high swelling potential, high plasticity and very low hydraulic conductivity. Many studies investigating the influence of humic acids on U(VI) sorption on various other minerals have been reported in the literature, however most experiments have been performed at a relatively high uranium concentration, above 10^{-7} M, while the concentration range in which the actinides may exist in nature is reported to be below 10^{-10} M (Montavon et al, 2000).

The aim of the current work is to demonstrate a methodology for the study of humic ternary systems using short-lived γ-emitting isotopes, i.e., ^{237}U and ^{237}Pu, which allow experiments at very low concentrations (U: 8.4×10^{-11} M, Pu: 3.7×10^{-11} M), close to the concentrations expected in environmental systems for uranium and representative of the Pu concentrations that might be expected in the near vicinity of a waste repository. As an example, these isotopes have been used to study the effect of humic acid on radionuclide sorption on bentonite and the distribution of uranium in the U(VI)-humic acid-bentonite ternary system as a function of the order of addition, equilibration time, ionic strength and pH. The effect of order of addition in the ternary system was examined in order to test the reversibility of sorption on bentonite in the presence of humics. In the case of the Pu experiments, reversibility in systems of changing E_h was studied. Although the system components are those that might be expected in or near a repository, for experimental reasons, the solid:solution ratios studied here are not those that would be expected inside a waste repository. Redox and oxidation state changes might be expected during repository evolution, but the changes here are necessarily on a faster timescale. Clearly, the exact changes in E_h and oxidation states will be highly repository specific and may not be the same as those measured here.

Experimental

There follows a summary of the experimental procedures. The full details will appear in the full paper when this work is completed and published.

Materials

Commercially available humic acid from the Aldrich Chemical Company (Germany) was used in the experiments. Natural bentonite (obtained from Aldrich also) was used without pretreatment: SiO_2 (68.40 %); Al_2O_3 (18.86 %); Fe_2O_3 (5.35 %); CaO (2.59 %); MgO (2.51 %); Na_2O (1.14 %); K_2O (0.15 %). The specific surface area was found to be 30.98 $m^2 \cdot g^{-1}$ (B.E.T.), and the bulk density is 1.85 $g \cdot cm^{-3}$. The point of zero charge (pHzcp) of bentonite (not for our specific sample) is reported to be at pH=7.8 ± 0.1 (Yu et al., 2006). All reagents used in the experiments were of analytical grade. Fresh Millipore de-ionized water (18 MΩ) was used in the preparation of all solutions. The trace concentration sorption experiments used the isotopes ^{237}U ($T_{1/2}$ = 6.75 d, Eγ = 59.54 keV (34.5 %); 208.00 keV (21.2 %)) and ^{237}Pu ($T_{1/2}$ = 45.3 d, Eγ = 97.1 keV (12.5%), 101.1 keV (20.1%), 113.9 keV (7.6%)), which were produced by the ^{238}U(γ,n)^{237}U and ^{235}U(^{4}He,2n)^{237}Pu reactions, respectively. In these experiments, the ^{237}U and ^{237}Pu concentrations were measured by γ- spectrometry. Higher concentration

uranium experiments used depleted uranium measured by Liquid Scintillation Counting (LSC).

Batch Experiments

A series of batch experiments were performed at room temperature and ambient atmosphere ($pCO_2 = 10^{-3.5}$ atm) in order to study the effect of HA on uranyl sorption on bentonite. In all experiments the solid to solution ratio was 1 $g \cdot L^{-1}$. The amounts of HA and U adsorbed onto bentonite were determined from the difference between the concentrations in the suspension and supernatant after the equilibration time. The solutions were adjusted to the required pH by adding appropriate quantities of KOH or HNO_3. In order to ensure equilibrium with the atmosphere, the samples of bentonite and electrolyte were prepared and left exposed to the atmosphere for a few days before the radionuclides were added. The pH was readjusted during this period with KOH or HNO_3. In all experiments, the ionic strength was maintained at the necessary value using $NaClO_4$, added as a small volume of a concentrated stock solution. It was assumed that the contributions of bentonite and humic counterions to the ionic strength were negligible. The final concentration of uranium(VI) in the solution was $8.4x10^{-11}$ M. After 5 days, 1 mL aliquots were taken and analysed, and the ^{237}U(VI) activity in the supernatant was measured after centrifugation at 4000 rpm for 10 min. The concentration of HA in the supernatant was determined by UV (253 nm).

A set of parallel experiments measured the behaviour of uranium at higher concentration (10^{-4} M) using depleted uranium (added as uranyl nitrate). The concentration of U in the higher concentration samples was determined by LSC on a Wallac Quantulus 1220 ultra low level LSC spectrometer using 20 mL polyethylene vials and OptiPhase HiSafe 3 cocktail (Perkin Elmer).

In another series of experiments at the trace concentrations, the effect of the order of addition of the components in the ternary system on the kinetics of metal ion distribution between the mineral and supernatant was investigated. The solid/solution ratio was 1 $g \cdot L^{-1}$. In the first set of experiments, Pu(III) or U(VI), HA and bentonite were mixed together without any pre-equilibration, while in the second and third sets, the metal ions were put in contact with bentonite, and after that HA was added after 1 and 7 days for the U systems and 1 and 5 days for the Pu experiments. Periodically, aliquots were taken and the ^{237}U or ^{237}Pu concentration in the supernatant was measured. As part of the separation procedure following the production of ^{237}Pu, the plutonium is produced in the Pu(III) oxidation state by elution with HCl 9 M/NH_4I 0.1 M. However, the oxidation state was not controlled following addition of the Pu to the ternary system, and indeed, since the system is in equilibrium with the atmosphere, oxidation would be expected.

Results and discussion

The effect of addition order and contact time

The effect of the addition order of the uranyl ternary system components was investigated at pH=5.0 and ionic strength 0.01, and the results are given in Fig. 1. In the system where the uranyl was added to the humic prior to contact with the bentonite, it takes approximately 2-4 days for equilibrium to be established (50 and 60 % sorbed in the presence of HA).

In the U(VI)/bentonite binary systems (squares and triangles in Fig. 1, before addition of HA). It takes approximately 1 h to reach the point of 50% sorption, but the equilibrium value of 80 – 85 % retention is reached after 2-3 days. For both the 1 and 7 day systems, the sorption of U(VI) on bentonite appears to be reversible in the presence of HA. In both cases, there was a gradual decrease in the uranyl uptake to the equilibrium level of 50 – 60 %, identical to that in the 0 day system. It took approximately 2 and 1 days for the 1 and 7 day aged systems to reach the new equilibrium, respectively. The indifference of the U(VI) sorption to the addition order and the reversibility of the uranyl sorption on bentonite, observed under the current experimental conditions is consistent with the previously reported results for other mineral phases and higher uranium concentrations (Krepelova et al., 2006; Ho et al., 1985).

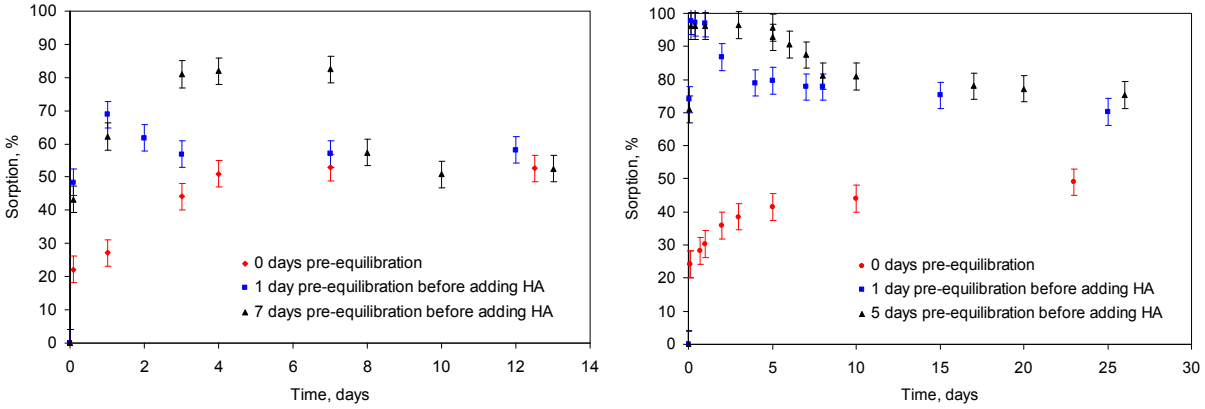

Figures 1 (left) and 2 (right): *Effect of the addition order and pre-equilibration time on sorption onto 1 g·L^{-1} bentonite at pH=5.0 and I=0.01 M for Fig. 1 - U(VI) (8.4x10^{-11} M) and Fig. 2 – Pu(III) (3.7x10^{-11} M). 100 mg·L^{-1} HA added after: 0 days (●), 1 day (■) and 7 (U) or 5 (Pu) days (▲) after the actinide was put in contact with the bentonite.*

Figure 2 shows the results of an equivalent set of experiments to those in Figure 1, but using ^{237}Pu instead of ^{237}U. This time, the ^{237}Pu was added as Pu(III), but the oxidation state was not controlled after addition, and the behaviour is very different. For the system where metal ion and humic were mixed prior to contact with the mineral phase, there is a rapid, initial increase as for the U system, but whereas the U data show equilibrium after a few days, this time the amount bound continues to increase.

In work with non-redox active ions, the slow sorption over the first few days after contact has been attributed to the formation of humic ternary complexes and slow humic sorption (Bryan et al., 2005). However, given that the U data show no kinetics beyond a few days, it seems unlikely that the steady increase in Pu sorption beyond 5 days can be attributed simply to slow humic sorption. For the binary ^{237}Pu/bentonite reaction (before addition of HA), sorption is very rapid, with 70-75% sorption within a few minutes and apparent equilibrium (95% sorbed) within a few hours.

The U systems were relatively insensitive to the order of addition, but this is not the case for Pu. Following addition of the humic, there is a reduction in the amount of Pu bound, but in both systems the amount sorbed only falls to approximately 75%, significantly higher than for the 0 day system. Hence, on the timescale of a few months, and under these particular conditions, there is significant (pseudo-)irreversibility. It is

interesting that the 1 and 5 day pre-equilibration systems behave in the same way following the addition of the humic, i.e., in both cases it takes 2-3 days for the amount sorbed to fall to approximately 75%. Given that the amount of Pu sorbed in the 0 day system still appears to be increasing at the end of the experiment, and indeed the other systems may not have reached complete equilibrium (overall, there may be a slight downward trend in the data, particularly for the 1 day system, but given the size of the error bars, this is not certain), it is possible/likely that at some point in the future, the 0 day and 1 and 5 day plots will converge, but this would take a significant amount of time, and certainly a few months at least. Kinetic effects with half-times of this order can have a significant effect upon transport in the real world.
Given that the solid phase and humic are the same for the U and Pu systems, and that both use very low, trace concentrations, it seems likely that it is some difference in the metal ion chemistry that is responsible for the effect, and it is tempting to think that the difference is due to the redox properties of Pu(III) (very likely to be oxidised) and U(VI) (unlikely to change oxidation state). Alternatively, under these conditions, Pu(III) would be expected to show significantly more hydrolysis than U(VI), and this too could be the cause of the difference.

The effect of pH

Uranyl sorption on $1 g \cdot L^{-1}$ bentonite was studied as a function of pH at ionic strength 0.01, both in the absence and presence of HA, and the results are given in Figure 3. The data were recorded after 5 days equilibration. The kinetic experiments suggest that equilibrium in the uranyl system (apparent at least) is achieved after this time. The sorption of humic acid on bentonite was also studied and the general trend is of decreasing uptake with increasing pH (also shown in Figure 3). At pH higher than 7.8 (pHzcp of bentonite), the uptake is very low, due to the electrostatic repulsion between the negatively charged HA and the charged bentonite surface.

For the low uranium concentration system, at low pH (<4) there is increased sorption of U compared to the HA free system due to the formation of ternary complexes (UO_2^{2+}-HA-bentonite). Schmeide et al. studied the effect of HA on uranyl retention on phyllite and reported that the uranium uptake is enhanced, compared to the uranium uptake in the absence of humic acid, due to the high sorption of HA onto the solids in the acidic pH range (Schmeide, et al., 2000). Murphy et al. found that in the acidic pH region the addition of HA enhances U(VI) sorption on hematite, relative to the HA-free system (Murphy et al., 1999). At higher pH (> 4), there is less U sorbed compared to the HA-free system, because the sorption of the HA itself decreases and so the competition of the HA in solution with the bentonite dominates the behaviour. At higher pH, the amount sorbed falls as carbonate sorption dominates. At pH between 6 and 9, the uranyl uptake is slightly enhanced in the presence of HA compared to the retention on bentonite in the absence of humics. Such a phenomenon has been already observed in the U(VI)-humic-kaolin ternary system (Krepelova et al., 2008). Krepelova et al.(2008) explained the enhanced U(VI) sorption on kaolinite at high pH in the presence of HA and CO_2, compared to the HA free system, with the possible formation of uranyl-carbonato-humate complexes and their interaction with the kaolinite surface (Krepelova et al., 2006). However, the reason for the promotion of uranyl sorption on the solid in the presence of HA is still unclear and additional research is needed.

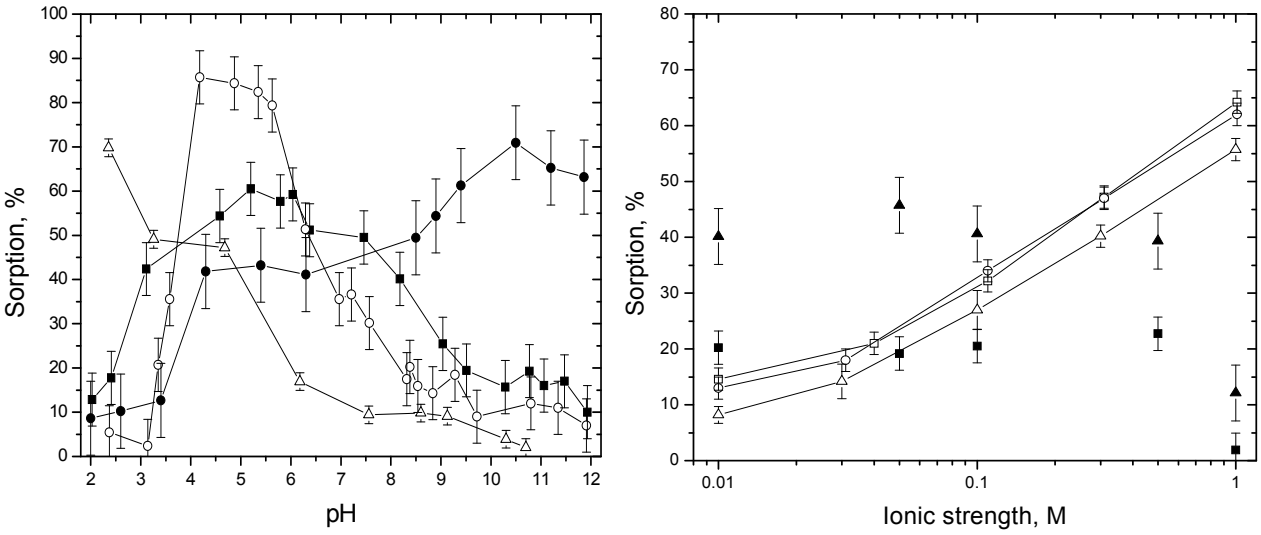

Figures 3 *(left) and 4 (right): Fig. 3 - Effect of pH on U(VI) ($8.4x10^{-11}$ M) sorption onto 1 g·L^{-1} bentonite in the absence of HA (○) and in the presence of 100 mg·L^{-1} HA (■) and the sorption of HA on bentonite alone (Δ). Filled circles (●) represent the sorption of U(VI) at a concentration of $1x10^{-4}$ M on bentonite in the presence of 100 mg·L^{-1} HA. Fig. 4 - The effect of ionic strength on U(VI) sorption on 1 g·L^{-1} bentonite at pH=8.0 ± 0.1 in the absence of HA (■) and in the presence of 100 mg·L^{-1} HA (▲) and the sorption of HA on bentonite alone at pH=7.6 (□), 8.0 (Δ) and 8.8 (○).*

At higher uranium concentrations, the behaviour is modified. The increased sorption at low pH, compared to the HA-free system that was observed in the low U concentration system is not observed. Instead, the increase in sorption appears at the same pH as for the HA-free system. This is expected, since the U:HA ratio is much higher and so ternary complexes could be less significant at low pH. However, at higher pH the uranium sorption is still suppressed. The most significant change in behaviour is at pH > 8: instead of falling, the amount sorbed actually increases. This is either due to the different U:carbonate ratio affecting the competition between the bentonite surface and carbonate, or it could be due to a change in the behaviour of the uranyl with the surface, perhaps due to the formation of a (surface) precipitate due to the higher U concentration. Precipitate formation seems more likely than simple competition, since competition effects would be expected to be significant at all uranium concentrations, whereas there would be a threshold concentration for precipitate formation.

On the whole, the two U ternary systems show broadly similar behaviour below pH 8, in the region where HA speciation dominates, but the plots diverge once the carbonate dominates. It has been suggested that humic substances could have small concentrations of very strong binding sites and so might show radically different effects upon metal ion behaviour as a function of total metal ion concentration, but although there are differences below pH 8, these differences are only what we might expect for a system with a single equilibrium constant, given a change in U:ligand ratio of 7 orders of magnitude. Previous work with the ^{237}U tracer has shown that the equilibrium constant for UO_2^{2+} binding is insensitive to concentration (Ivanov et al., 2008), and the results here are consistent with that. This is important, because virtually all U data are

determined at high concentrations, but will be used to predict behaviour at low concentrations. In the case of the bentonite system in Figure 3 for pH < 8, a prediction of trace behaviour based on the high uranium concentration results would reproduce the general trends, but more importantly would give a conservative prediction, since U sorption is higher for the lower concentration system. Further work is required with other systems to determine whether this is generally true.

The effect of ionic strength

The effect of ionic strength on the U(VI) distribution between the solid and liquid phase in the ternary system at pH=8.0 ± 0.1, a humic acid concentration of 100 $mg \cdot L^{-1}$ and 1 g/l bentonite was examined, and the results are presented in Figure 4. The results were recorded after 5 days equilibration.

The retention of HA on bentonite was found to increase with increasing ionic strength from 0.01 M to 1.0 M. Such an effect is commonly observed, and is generally explained by the decrease of HA molecular size at higher salt concentrations, which leads to a greater sorption capacity of the mineral surface, as well as screening of the lateral repulsion of the HA (Hoogeveen et al., 1996, Reiller et al, 2002; Wang et al., 2000). At pH = 8.0, the effect of ionic strength on U(VI) (10^{-10} M) uptake on bentonite was found to be negligible within the interval 0.01 – 0.5 M, both in presence and absence of HA. A further increase of the salt concentration leads to a decrease in the retention at ionic strength 1.0 M, perhaps due to the non-specific competition between the U(VI) and the background electrolyte ions for the bentonite binding sites.

While the effect of ionic strength on HA uptake is well studied in the literature, there have been fewer studies of the impact of ionic strength on uranyl sorption in ternary systems. The trend in the current experiments is consistent with those of Thakur *et al.*, who examined the effect of ionic strength on UO_2^{2+} sorption on hydroxyapatite and found that the amount sorbed on the surface decreases with increasing ionic strength (Thakur et al., 2005). The observed indifference of sorption behaviour to the ionic strength within the broad range of salt concentration is commonly interpreted as a suggestion of a surface complexation sorption type.

Conclusions

The uranyl/bentonite/humic ternary system is insensitive to the order of addition of the ternary system components. It takes a few days for equilibrium to be established when all three components are put in contact and only a few days for the reestablishment of equilibrium when humic acid is added to the binary bentonite/uranyl binary system. Further, under the correct conditions (pH < 8), the behaviour at environmental concentrations (10^{-10} M) may be inferred from experiments at higher concentrations, although the behaviour is different at higher pH due to the effects of carbonate. These experiments suggest that the behaviour of uranyl in this ternary system (under oxic conditions at least) may be predictable, although the chemistry is complex. Further, research is required to confirm that this is generally true.

The Pu(III)/bentonite/humic ternary system seems to be more complicated. In the binary Pu(III)/bentonite system, equilibrium is established in a few hours, but longer is

required in the full ternary system. Under the conditions studied here and on a timescale of a few months, this ternary system does show significant (pseudo-)irreversibility, and the amount of Pu sorbed onto the surface depends upon whether humic acid is present when the Pu(III) is first introduced to the bentonite, with sorption after 1 month increased if the Pu(III) sorbs as a humate complex.

Acknowledgement

The authors would like to thank: the United Kingdom Engineering and Physical Sciences Research Council for funding this work as part of the KNOO and DIAMOND consortia; NDA for providing funds for NDB to attend the workshop.

References

Bryan, N.; Abrahamsen, L.G.; Farrelly, D.H.; Warwick, P.; Evans, N.D.M.; Knight, L. (2005) A Provisional Humic Acid Ternary System Model, 1st Funmig workshop.

Ho, C.H., Doern, D.C., The sorption of uranyl species on a hematite sol, *Can. J. Chem,.* **63**, 1100 (1985).

Hoogeveen N.G., Cohen-Stuart M.A., Fleer G.J., Polyelectrolyte adsorption on oxides I. Kinetics and adsorbed amounts, *J. Interf. Coll. Sci ,* **182**, 133 (1996).

Ivanov P., Abrahamsen L., Pitois A., Bryan N., Bozhikov G., Maslov O. and Dmitriev S., New U tracer for the Study of Humic Ternary Systems, *Proceedings of the 3rd FUNMIG workshop, Edinburgh November 2007*, 357 – 364 (2008).

Krepelova, A., Reich, T., Sachs, S., Drebert, J., Bernhard, G, Structural characterization of U(VI) surface complexes on kaolinite in the presence of humic acid using EXAFS spectroscopy, *J. Colloid Interface Sci.,* **319**, 40 (2008).

Krepelova, A., Sachs, S., Bernhard, G., Uranium(VI) sorption onto kaolinite in the presence and absence of humic acid, *Radiochim. Acta,* **94**(12), 825 (2006).

Montavon, G., Mansel, A., Seibert, A., Keller, H., Kratz, J.V., Trautmann, N., Complexation studies of UO_2^{2+} with humic acid at low metal concentrations by indirect speciation methods, *Radiochim. Acta*, **88**, 17 (2000).

Murphy, R.J., Lenhart, J.J., Honeyman, B.D., The sorption of Th(IV) and U(VI) to hematite in the presence of natural organic matter, *Colloids Surf. A*., **157**, 47 (1999).

Reiller P., Moulin V., Casanova F., Dautel C., Retention behaviour of humic substances onto mineral surfaces and consequences upon thorium (IV) mobility: case of iron oxides, *Appl. Geochem*., **17**, 1551 (2002).

Shmeide, K., Pompe, S., Bubner, M., Bernhard, G., Nitsche, H, Uranium(VI) sorption onto phyllite and selected minerals in the presence of humic acid, *Radiochim. Acta* **88**, 723 (2000).

Thakur, P., Moore, R.C., Choppin, G.R., Sorption of U(VI) species on hydroxyapatite, *Radiochim. Acta*, **93**, 385 (2005).

Wang, X.K., Dong, W.M., Dai, X.X., Wang, A.X., Du, J.Z., Tao, Z.Y., Sorption and desorption of Eu and Yb on alumina: Mechanisms and effect of fulvic acid *Appl. Rad. Isot*., **52**, 165 (2000).

Yu, Sh.M., Ren, A.P., Chen, Ch.L., Chen, Y.X., Wang, X., Effect of pH, ionic strength and fulvic acid on the sorption and desorption of cobalt to bentonite, *Appl. Rad. Isot.,* **64**, 455 (2006).

THIN FILMS AS SPENT FUEL MODELS

Silvia Stumpf[1*], Alice Seibert[1], Thomas Gouder[1], Detlef Wegen[1], Thierry Wiss[1], Melissa A. Denecke[2], Eva Soballa[2]

[1] European Commission, JRC, Institute for Transuranium Elements, ITU (D)

[2] Institut für Nukleare Entsorgung, KIT, Campus Nord, Herrmann-von-Helmholtz-Platz 1, 76344 Eggenstein-Leopoldshafen, Germany

* Corresponding author: silvia.stumpf@ec.europa.eu

Abstract

Thin films simulating key aspects of spent fuel can be prepared at ITU by sputter deposition using setups appropriately adjusted to work with radioactive substances.
In this contribution production and characterisation of UO_2 thin films doped with fission product (fp) elements is described. The films are used as model systems for spent nuclear fuel, to investigate the surface reactions of these films in single effect studies (i.e. isolating one single parameter like fp, stoichiometry, etc.).

The thin films are prepared by sputter deposition from an actinide metal target (in the actual case U_{metal}) in the presence of O_2. The fp, in this work Pd, is added by co-deposition from a corresponding metal target. Pd is chosen to simulate the presence of ε-particles in spent fuel. The variation of the respective target currents and of the O_2 partial pressure provides for the control of the Pd-content and the oxidation state of the uranium in the compound films. This technique allowed the production of $UO_{2(+x)}$ films with imbedded Pd. Different U/Pd compositions ranging from 2 -70 % Pd-content were produced at different substrate temperatures. The films were characterised by X-ray Photoemission Spectroscopy (XPS), X-ray Diffraction (XRD), Transmission Electron Microscopy (TEM), Scanning Electron Microscopy with Energy Dispersive X-ray emission analysis (SEM-EDX) and Atomic Force Microscopy (AFM). This investigation allowed us to select production parameters that lead to the desired spent fuel model surfaces (UO_2 + Pd metallic particles). In the future these films will be used in corrosion studies under relevant redox conditions (e.g. aqueous electrolytes in equilibrium with different gas phases including presence of H_2) with electrochemical techniques and gas adsorption experiments to determine the influence of the palladium doping together with the presence or absence of hydrogen on the redox behaviour of these low complexity spent fuel models.

Introduction

The safety assessment of nuclear waste disposal concepts requires a fundamental understanding of the corrosion processes on the spent fuel surface, and in particular the UO_2 chemistry in aqueous systems. The dissolution of the UO_2 fuel matrix would result in the release of radionuclides into the groundwater. The processes controlling the dissolution of spent nuclear fuel under a range of proposed waste repository conditions have been the focus of several extensive studies (Johnson and Shoesmith, 1988; Shoesmith, 2000; Johnson et al., 2005). Due to the redox sensitivity of UO_2, the solution redox potential can be considered to be the critical variable, which determines fuel dissolution and finally influences the release of radionuclides. The solubility of UO_2 increases by many orders of magnitude when UO_2 is further oxidized. The responsible oxidants are primarily provided by the radiolysis of water, since environmental oxidants, e.g. O_2, are quickly scavenged by reaction with container material, oxidizable minerals, and organic material present in the near-field of the repository (King et al, 1999). α-Radiolysis is considered responsible for the generation of oxidants in the long-term, because the γ and β radiation fields will have decayed prior to container failure and contact between the waste form and groundwater (Shoesmith et al., 2000; Sunder, 1995). Main products from α-radiolysis of water are considered to be H_2O_2, radicals like OH·, OOH· and electrons. However the oxidation of the UO_2 fuel matrix may be inhibited by the presence of reducing species, such as hydrogen, generated for example during corrosion of the iron canisters (Broczkowski et al., 2005, Bruno and Ewing 2006, King and Schoesmith, 2004). Anyhow this inhibition is described by several authors, the mechanism is not entirely clear. But for reliable performance assessment the knowledge of underlying mechanisms is an necessary addition to the production of datasets for real systems under very special conditions, which can not be easily used for calculation purposes.

Spent nuclear fuel mainly consists of UO_2 (~95%). The remainder is a mixture of fission products, transuranium elements and activation products that occur in many different forms such as oxide precipitates, solid-solutions or immiscible, micron- to nanometer-sized metallic precipitates of Mo, Tc, Ru, Rh and Pd (ε-particles) (Kleykamp, 1985). This results in heterogeneous surfaces, with many different components. Up to now it is not entirely clear which of them is responsible for the activation of hydrogen and the stopping of the UO_2 surface oxidation.
The higher oxides of uranium ($U_4O_9/U_3O_8/UO_3$) as well as mixed oxides (USb_3O_{10}) and intermetallics (UNi_5) are known catalysts used in different fields of redox chemistry and synthesis (Colmenares, 1984, Diaz-Arocas et al., 1995, Christensen et al., 1990). However, the catalytic activity of UO_2 towards H_2 decomposition is not completely clear as investigations were not made in single effect studies but in mixed matrix systems containing for example Fe and Gd, which can have an influence on the catalytic activity of the matrix even in the trace concentration range (Spahiu et al., 2004, Bunji and Zogovic, 1958). Additionally the 4d-elements and their alloys are known catalysts for redox reactions involving hydrogen. The ε-particles, which consist of these elements, can therefore be considered as good candidates for catalysing the decomposition of H_2 at the fuel surface. Nilsson and Jonsson (2008a, 2008b) and Cui et al. (2004) demonstrate that in solution Pd particles and 4d alloy particles (composed of Mo, Ru, Tc, Pd, Rh and Te) catalyze the homogeneous reaction between UO_2^{2+} and H_2 as well as H_2O_2 decomposition and come to the conclusion that UO_2 is not involved in

the activation process. Indeed, Broczkowski et al. (2005) investigated the influence of hydrogen on the corrosion of SIMFUEL (containing as well rare earth elements) in presence and absence of noble metal incorporations and demonstrated the catalytic activity of the ε-particles.
To investigate the catalytic properties of the noble metal particles in the single effect approach, we proposed to use actinide oxide thin films doped with the various noble metals. In the following the production of UO_2 thin films doped with Pd as simulate for the ε-particles is described. Results from different characterization methods are presented. Investigations of their redox behaviour are currently ongoing or will be started in the near future. Gas adsorption measurements e.g. with H_2 and H_{atom}, monitored by surface sensisitive methods like XPS and UV photoelectron spectroscopy are already started, and electrochemical measurements in different electrolytes (0.01 M NaCl with / without carbonate) and gas atmospheres (as there are air, Ar and Ar/H_2-mixtures) are scheduled tentatively for second half of 2009.

Experimental

Thin films of $U_xO_yPd_z$ were prepared in situ by sputter co-deposition from U (99.9% purity) and Pd (99.9% purity) targets at an O_2 partial pressure of about $1*10^{-6}$ mbar. The pressure of the sputter gas (Ar 99.9999% purity) was $1*10^{-2}$ mbar. In order to obtain an Ar-plasma, the Ar atoms were ionized by electrons (50-100eV) emitted from a hot W cathode. The films were deposited on different substrates: single crystalline Si-wafers, polycrystalline gold discs and TEM Cu-grids coated with carbon.
XPS spectra were recorded with a hemispherical analyzer from Omicron (EA 125 U5). The spectra were taken using MgK_α (1253.6 eV) radiation with an approximate energy resolution of 0.9 eV.
The film crystallinity was investigated by Transmission Electron Microscopy (TEM H700 HST from Hitachi) and X-ray Diffraction (Philips PW3830 X-ray generator fitted with a Philipps PW 2213/20 goniometer, including a 1.5 kW copper anode).
Surface morphology was determined by SEM measurements, performed on an Environmental Scanning Electron Microscope (Philips ESEM XL 30 FEG) equipped with a backscatter electron detector for imaging. As the prepared films were electrically conducting they could be analyzed by ESEM without a conducting surface coating which may impair backscatter diffraction bands.
A commercial AFM (Topometrix, TMX 2000, Explorer, available at INE) was used for the topographic characterization of the thin films. A series of AFM images was recorded in contact-mode using triangular cantilevers with silicon nitride tips (tip radius <50 nm).

Results and discussion

UO_2/Pd films produced at room temperature

First experiments of the co-deposition of U and Pd in presence of oxygen showed that UO_2 films containing different Pd concentrations can be produced. The oxygen content can be varied, allowing to obtain stoichiometric or hyperstoichiometric UO_{2+x}, as confirmed by the XPS-U4f lines (Fig. 1, left graph). The Pd content is controlled by varying the U and Pd deposition rates, via adjustment of the respective target voltages/currents. Fig. 1 (right graph) shows the corresponding Pd-3d lines. For Pd concentrations above 60% the binding energies (BE) are characteristic for Pd metal: 335.4 eV ($3d_{5/2}$) and 340.7 eV ($3d_{3/2}$). The weak satellite at 346.7 eV is also attributed to

Pd metal (Kim et al., 1974). With decreasing palladium concentration the Pd signal intensity decreases and the lines slightly broaden. At concentrations ~ 15 % Pd, new Pd-3d lines appear at 2.8 eV higher BE than found for the metal, indicating the formation of a second Pd species. We attribute this to the formation of a Pd-oxide species in this U/Pd composition range. Although Pd is a noble metal, its oxidation is well known and photoemission data are reported in literature by several authors. The chemical shifts of the Pd $3d_{5/2}$ peak of PdO are quoted between 1.3 eV and 1.9 eV (Kim et al., 1974, Tura et al., 1988) and for PdO_2 between 2.1 eV and 2.9 eV (Wagner, 1978). Even the formation of PdO_3 has been proposed by some authors (shift ~ 3.5 eV) (Bolzan et al., 1984). Based on these references the observed peaks at 338.3 eV (and 343.6 eV respectively) are attributed to the formation of an oxidic compound with mixed stoichiometry (PdO_x/UO_y). The shift of about 2.8 eV indicates PdO_2 to be the most likely species.

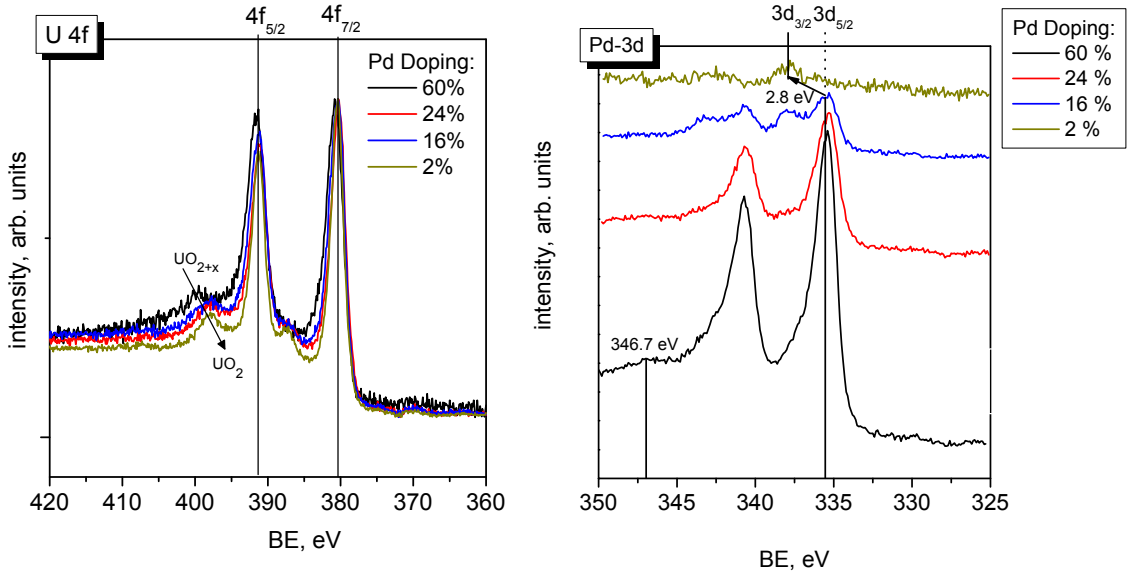

Figure 1: *U-4f spectra (left graph) and Pd-3d spectra (right graph) for different UO_2/Pd compositions.*

With further lowering of the Pd concentration the Pd-3d metal lines further decrease in intensity and only the oxidic signals at higher BEs are observed. The deposition of Pd alone (the potential on the U target being set to 0 V) in the presence of oxygen does not result in any significant oxidation of the noble metal. Figure 2 comprises the Pd-3d and O1-s regions for this set of experiments. The presence of an O-1s signal accounts for some contribution of an oxidic phase. It is due to some residual UO_2, deposited as cross-contamination from the Pd target. Uranium obviously plays an active role in the oxidation of the Pd – which is probably related to the dispersion of Pd in the UO_2 oxide lattice. Further experiments are undertaken to study this in detail.

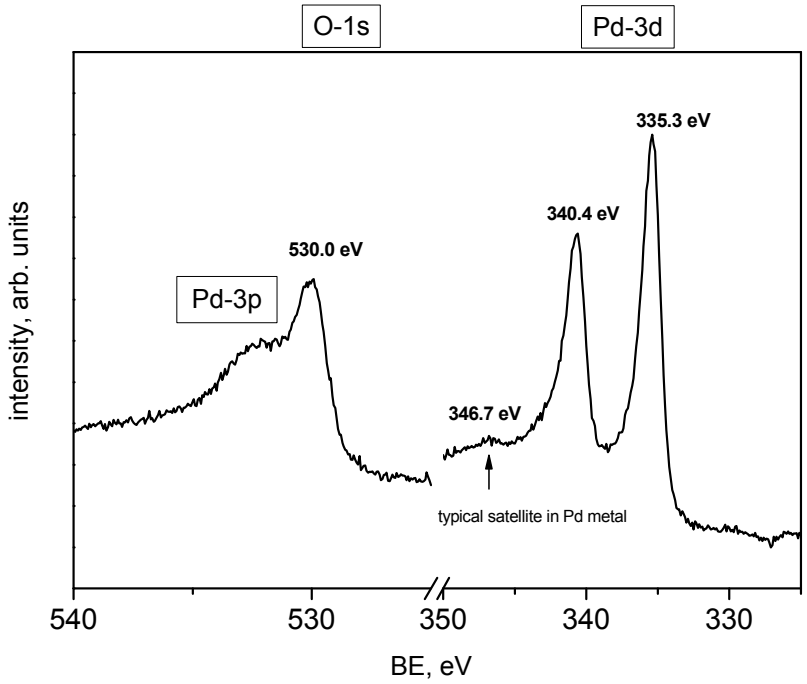

Figure 2: *Pd-3d and O-1s spectra for the sputter deposition of Pd with an Ar/O_2 sputter gas.*

The XRD spectra of thin films with varying Pd concentration support this interpretation. The diffraction peaks for crystalline UO_2 (cubic, fluorite-type lattice) are identified according to Cooper (1982) for the low Pd concentration range up to 30 %. With increasing Pd concentration the UO_2 peak intensities decrease and the lines undergo a slight shift of $\Delta 2\theta \sim 0.2$ °. Diffraction peaks, which could be attributed to a metallic Pd phase (ε-particles), are not detected in this composition range. This indicates the dispersion of small Pd (or PdO_x phase) particles in the UO_2 matrix, or instead the formation of larger, but amorphous particles. The decrease of UO_2 diffraction peak intensity may be explained as concentration effect. Moreover there is the possibility of the loss of crystallinity due to Pd incorporation. This interpretation is corroborated by the observation of a shift of the diffraction peaks to higher 2θ values, indicating a decreased lattice parameter of the crystalline matrix. Such phenomenon has already been observed by Lucuta et al. (1991), who investigated the microstructural features of SIMFUEL by XRD, where a decreased lattice parameter is interpreted in terms of the dissolution of fission product atoms in the fuel matrix. The lack of Pd diffraction peaks was ascribed by the authors to the small amount of Pd as compared to the UO_2 matrix.

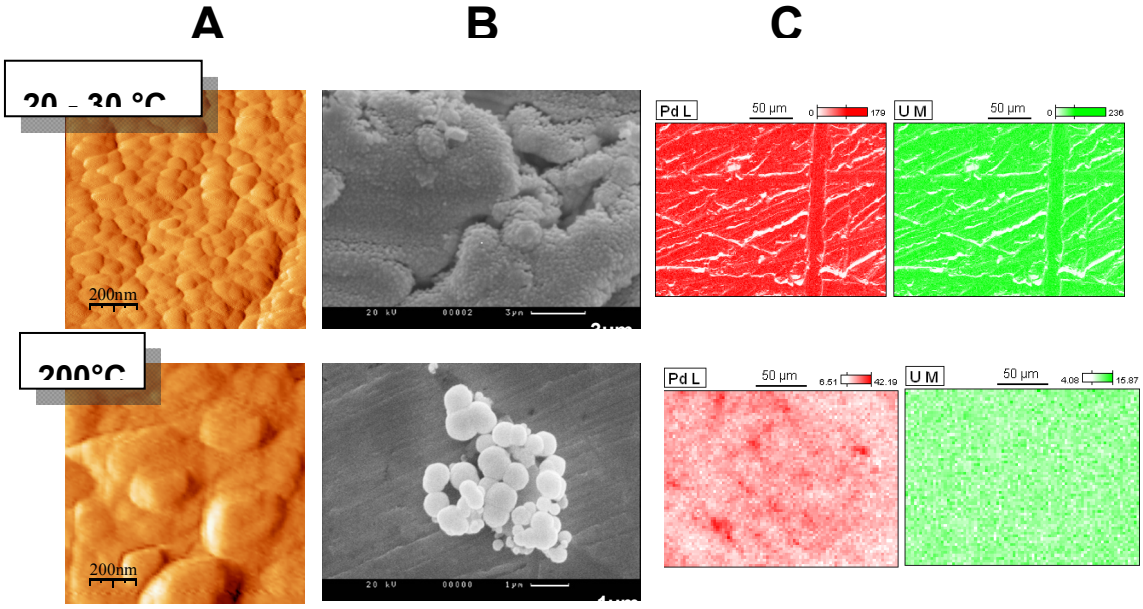

Figure 3: *AFM (A), SEM (B) and EDX (C) measurements of UO_2/Pd thin films (40 % Pd) at different deposition temperatures.* In (C) *the EDX mapping of a 250µm x 200µm surface area for Pd (red trace) and U (green trace) is shown.*

For Pd concentrations above 70 % the UO_2 crystalline phase disappears completely, and new diffraction peaks appears, which can be attributed to metallic Pd (2θ = 40.3 °, according to hkl (420) (Bredig and Allolio, 1927). These XRD results are well confirmed by other methods. TEM measurements at low Pd concentrations (14%) show only diffraction patternscorresponding to crystalline UO_2. The corresponding Bragg circles (instead of points expected for single crystalline material) prove the polycrystalline nature of the UO_2 matrix. Diffraction peaks characteristic of a metallic Pd (ε)-phase are not detectable. SEM/EDX measurements show a homogeneous distribution of Pd and U in the UO_2/Pd films produced at room temperature (Figure 3 C, shown in upper line). No local enrichment or depletion of one element in favour of the other is observed within the resolution of EDX. AFM (A) and SEM (B) pictures show homogeneous deposits with small crystallite sizes (~ 150 nm). The homogeneous dissolution of Pd in UO_2 is interpreted as a result of the method of sputter deposition. Due to the low substrate temperature (~ room temperature) U-Pd-O-clusters from the plasma are instantaneously cooled at the surface and the components are "frozen" in the deposited film. This also explains the lack of crystal order in the Pd phase, in the composition range 16 % to 70 %. Because of the absence of directional bonds in a metallic phase, an amorphous phase is more likely to be observed. UO_2, on the other hand, has more directional bonds (ionic binding with partial covalence) and hence exhibits a higher tendency to form a crystalline compound. The "freezing" of U-Pd-O-clusters in the UO_2 matrix may be as well responsible for the observation of the oxidic Pd phases in the low concentration range (< 16 %). The so produced compounds are maybe the snapshot of an abruptly cooled system and represent a state which is not necessarily thermodynamically stable.

UO_2/Pd films produced at elevated temperature

To favour diffusion of the film components after deposition, and a relaxation of the system into a thermodynamically stable state, the substrate was heated during or after the deposition process (Stumpf et al., submitted). It was hoped, that Pd would segregate into larger metallic particles, more representative of the ε-particles. Some of the sputtered films were repeatedly heated after deposition at moderate conditions (several heating cycles for maximum 2 minutes at temperatures ~ 150°C to 200°C). For the compounds with a Pd concentration of about 16 % the heating process leads to the decomposition of the oxidic Pd, which can be easily followed by XPS from the Pd-3d lines that show an BE shift back to the position characteristic for the metallic Pd and the appearance of the satellite at ~ 346.7 eV. This indicates that even at such low temperatures (compared to the substance melting points) diffusion and rearrangement of the film components is allowed. As a result Pd oxide transforms into a metallic Pd phase. Agglomerates of spherical particles with a diameter of 0.3 µm to 1 µm form on top of the film surface. These are easily detected in the SEM images (Fig. 3 B, lower line). The agglomerates are as well observed in the EDX mappings (Fig. 3 C, lower line) where a Pd accumulation in some regions is significant. The size of these regions of about 10 µm corresponds to the size of the agglomerates seen in the SEM pictures. Indeed these structures resemble very well the results of Cui et al. 2004 who investigated structure, morphology and composition of mixed alloy particles (ε-particles) extracted from spent fuel. In the cited study, the ε-particles are described as agglomerates of micrometer sized spheres (~0.7 µm).

Summary and Conclusions

The investigations showed that the thin film technique is well suitable for the preparation of model systems for spent nuclear fuel. A reproducible production scheme for UO_2/Pd thin films simulating ε-particles in a UO_2-matrix was set up. Investigations of their redox behaviour are currently ongoing: gas adsorption measurements e.g. with H_2 and H_{atom}, monitored by surface sensitive methods like XPS and UV photoelectron spectroscopy. In a next step these films will be deposited on the electrodes of an electrochemical quartz crystal microbalance set-up which was adapted for actinide thin film investigations (Seibert 2006, 2007) and allows surface corrosion processes to be investigated. Electrochemical measurements (e.g. corrosion potential measurements, cyclovoltammetry) in different electrolytes (0.01 M NaCl with / without carbonate) and gas atmospheres (air, Ar and Ar/H_2-mixtures) are planned for the near future.

Acknowledgements

S. Stumpf acknowledges the European Commission for support given in the frame of the program "Training and Mobility of Researchers".

References

L.H. Johnson, D.W. Shoesmith (1988): Spent Fuel. In: Lutze W., Ewing R.C. (eds) Radioactive Waste Forms for the Future. North-Holland, Amsterdam, 635-698

D.W. Shoesmith (2000): Fuel corrosion processes under waste disposal conditions. J.Nucl. Mater. 282, 1

L. Johnson, C. Ferry, C. Poinssot, P. Lovera (2005): Spent fuel radionuclide source-term model for assessing spent fuel performance in geological disposal. Part I: Assessment of the instant release fraction. J. Nucl. Mater. 346, 56

F. King, M. Kolar: Prediction of the effects of α-radiolysis, precipitation and redox reactions with Fe and Fe(II) on the dissolution of UO_2 using the mixed-potential model of fuel dissolution. Ontario Power Generation Report No. 00819-REP-01200-10041-ROO, 1999

S. Sunder: Alpha, beta and gamma dose rates in water in contact with used CANDU UO_2 fuel. Atomic Energy of Canada Limited Report AECL-11380, COG-95-340, 1995

M.E. Broczkowski, J.J. Noel, D.W. Shoesmith (2005): The inhibiting effect of hydrogen on the corrosion of uranium dioxide under nuclear waste disposal conditions. J. Nucl. Mater. 346, 16

J. Bruno, R.C. Ewing (2006): Spent nuclear fuel. Elements 2, 343

F. King, D.W. Shoesmith: Electrochemical studies of the effect of H_2 on UO_2 dissolution.SKB Technical Report TR-04-20, 2004

H. Kleykamp (1985): The chemical state of the fission products in oxide fuels. J. Nucl. Mater. 131, 221

C.A. Colmenares (1984): Oxidation mechanisms and catalytic properties of the actinides. Prog. Solid State Chem. 15, 257

P. Diaz-Arocas, J. Quinones, C. Maffiotte, J. Serano, J. Garcia, J.R. Almazan, J. Esteban (1995): Effect of secondary phases formation in the leaching of UO_2 under simulated radiolytic products. Mater. Res. Soc. Symp. Proc. 353, 641

H. Christensen, R. Forsyth, L. Lundquist, L.O. Werme: Radiation induced dissolution of UO_2. Studsvik Report NS-90/85, Studsvik Energiteknik AB, Nyokoping, Sweden, 1990

K. Spahiu, J. Devoy, D. Cui, M. Lundström (2004): The reduction of U(VI) by near field hydrogen in the presence of UO_2. Radiochim. Acta 92, 597

B. Bunji, B. Zogovic: Reduction of uranium from carbonate solutions with hydrogen using UO_2 as catalyst. Proceedings of the International Symposium on Peaceful Uses of Atomic Energy, Stockholm, 350-355, 1958

S. Nilsson, M. Jonsson (2008): On the catalytic effects of UO_2(s) and Pd(s) on the reaction between H_2O_2 and H_2 in aqueous solution. J. Nucl. Mater. 372, 160

S. Nilsson, M. Jonsson (2008): On the catalytic effect of Pd(s) on the reduction of UO_2^{2+} with H_2 in aqueous solution. J. Nucl. Mater. 374, 290

D. Cui, J. Low, C.J. Sjöstedt, K. Spahiu (2004): On Mo-Ru-Tc-Pd-Rh-Te alloy particles extracted from spent fuel and their leaching behaviour under Ar and H_2 atmosphere. Radiochim. Acta 92, 551

K.S. Kim, A.F. Gossmann, N. Winograd (1974): X-ray photoelectron spectroscopic studies of palladium oxides and the palladium-oxygen electrode. Anal. Chem. 46, 197

J.M. Tura, P. Regull, L. Victori, M. Dolors de Castellar (1988): XPS and IR (ATR) analysis of Pd oxide films obtained by electrochemical methods. Surf. Interf. Anal. 11, 447

C.D. Wagner: Handbook of X-ray Photoelectron Spectroscopy. Perkin Elmer Corporaton, Eden Prairie, 1978

A.E. Bolzan, A.C. Chialvo, A.J. Arvia (1984): Fast faradaic processes observed during the potentiodynamic polarization of polycrystalline palladium in acid electrolyte. J. Electroanal. Chem. 179, 71

M.J. Cooper (1982): The analysis of powder diffraction data. Acta Cryst. B 38, 264

P.G. Lucuta, R.A. Verrall, Hj. Matzke, B.J. Palmer (1991): Microstructural features of SIMFUEL – Simulated high-burnup UO_2-based nuclear fuel. J. Nuc. Mat. 178, 48

G. Bredig, R. Allolio (1927): X-Ray Studies of Catalytically Active Metals. Z. Phys. Chem. 126, 41

S. Stumpf, A. Seibert, T. Gouder, F. Huber, T. Wiss, J. Römer: Development of fuel-model interfaces: Characterization of Pd containing UO_2 thin films. To be submitted to J. Nucl. Mat.

A. Seibert: Fuel Corrosion and radiolysis studies. Report JRC-ITU-TN-2006/78, 2006

A. Seibert: Fuel Corrosion and radiolysis studies. Report JRC-ITU-TN-2007/81, 2007